

# Reliability assessment approach through geospatial mapping for offshore wind energy



**Faryal Khalid**

College of Engineering, Mathematics and Physical Sciences  
University of Exeter

A thesis presented for the degree of  
*Doctor of Philosophy in Renewable Energy*

This thesis is available for Library use on the understanding that it is copyright material and that no quotation from the thesis may be published without proper acknowledgement.

I certify that all material in this thesis which is not my own work has been identified and that no material has previously been submitted and approved for the award of a degree by this University or any other.

---

April 2019



# Abstract

To meet the increased energy demands, uphold commitments made in the Paris agreement and provide energy security to its consumers, the United Kingdom is rapidly expanding its wind energy industry at offshore locations. While harnessing the improved wind resource further offshore, the industry has faced reliability challenges in the dynamic marine environment which contribute to an increase in the cost of energy. This thesis promotes the argument for location - intelligent decisions in the industry by developing a methodology to allocate a combined risk - return performance metric for offshore locations.

In the absence of comprehensive spatially distributed field reliability data for offshore wind turbines, the limit state design methodology is employed to model structural damage. Exposed to stochastic loading from wind and wave regimes, offshore wind turbines are fatigue-critical structures. The aero- and hydro-dynamic loads at representative sites across eight sub-regions in the UK continental shelf are quantified by processing modelled metocean data through established aero-hydro-servo-elastic design tools. These simulated loads and the inherent material fatigue properties provide site-specific lifetime accumulated damage. Normalising this damage based on the potential energy production at each site provides an improved understanding of the feasibility of the sub-region for offshore wind deployment. Results indicate that although sheltered sub-regions display lower resource potential, they have the benefit of the reduced associated structural damage compared to more dynamic locations. A similar observation is made when the methodology is employed on a larger scale incorporating the UK continental shelf and its adjoining areas. Furthermore, not only the energy potential displays an increase with an increase in distance-to-shore, but also the damage per unit energy produced.

The research outcomes of this project are useful for identifying the potential of structural reserves for lifetime extension considerations as more turbines reach their design lifetimes. Additionally, it may be used to inform design parameters, optimise siting of future installations and determine suitable maintenance strategies to improve the economic viability of offshore wind.





## Acknowledgements

Like any project, the initiation and culmination of this doctorate has been facilitated by a remarkable support structure. Foremost, the encouragement of my supervisors has been pivotal; their exemplary dedication to this project and the offshore renewable energy industry has allowed me to develop as a researcher in this four year period. I could not have chosen a better supervision team for my research, therefore, I shall forever be grateful to Dr. Philipp Thies and Professor Lars Johanning.

I have been very lucky to have had incredible mentors throughout my life who cemented the foundations of my academic career including Professor Andreea Koschinsky, Ms. Pinto, Ms. Riffat Minhaj and Ms. Tahmina Mahmood. Dr. Helen Smith is another addition to this list since her well-rounded mentorship during my PhD was an integral part of the experience.

Furthermore, I would like to thank my friends at the Renewable Energy and Mathematics departments, particularly Ajit, JJ and Jon, for addressing the tribulations of my computational misadventures.

This research project was funded by a PhD studentship awarded by the College of Engineering, Mathematics, and Physical Sciences at the University of Exeter. Additional financial support was received from the Institution of Engineering and Technology Travel award, Blue Energy Collaborative Scholarship by INORE and the Global Scholarship Programme for Research Excellence by the Chinese University of Hong Kong.

On a personal note, the friends and family I have found in Cornwall at large have provided me with their undying support, for this I am immensely thankful to them.

Most importantly, I would like to acknowledge the efforts of my mother, who invested her life in me and continuously battled the patriarchy to provide me with the freedom to continue my academic endeavours. I hope I shall continue to make you proud of the daughter you have raised.



# Contents

<b>List of Figures</b>	<b>i</b>
<b>List of Tables</b>	<b>x</b>
<b>Nomenclature</b>	<b>xiii</b>
<b>I Research Context</b>	<b>2</b>
<b>1 Introduction</b>	<b>3</b>
1.1 Role of wind in the renewable energy mix . . . . .	3
1.2 Location-intelligent siting of OWFs . . . . .	5
1.3 Aims and Objectives . . . . .	9
1.4 Contribution to existing knowledge . . . . .	10
1.5 Thesis structure . . . . .	11
<b>2 Conceptual Framework</b>	<b>14</b>
2.1 The UK perspective on offshore wind energy . . . . .	14
2.1.1 UK offshore regional characterisation . . . . .	16
2.1.2 UK Offshore wind lease rounds . . . . .	18
2.1.2.1 Existing rounds . . . . .	18
2.1.2.2 Future rounds . . . . .	18
2.2 Geospatial applications in the OWE industry . . . . .	22
2.2.1 Geographic Information Systems . . . . .	22
2.2.2 Existing applications . . . . .	22
2.2.3 Relevant geographic parameters for offshore wind . . . . .	26
2.3 Wind turbine performance indicators . . . . .	27
2.3.1 Availability . . . . .	27

2.3.2	Capacity factor . . . . .	29
2.3.3	Reliability . . . . .	30
2.4	Stakeholders and technological specification . . . . .	31
2.4.1	Wind turbine manufacturers . . . . .	31
2.4.2	OWT taxonomy . . . . .	32
2.4.3	Foundation Concepts . . . . .	33
2.5	Stochastic processes . . . . .	36
2.5.1	Environmental parameters . . . . .	37
2.5.1.1	Wind . . . . .	38
2.5.1.2	Wave . . . . .	40
2.5.1.3	Relationship between $V_t$ and sea state . . . . .	43
2.5.1.4	Long-term environmental parameters . . . . .	44
2.5.2	Loads . . . . .	46
2.5.2.1	Environmental loads . . . . .	48
2.5.2.2	Combination of environmental loads . . . . .	48
2.6	Design methods and system analysis . . . . .	49
2.6.1	Design standards for offshore wind energy . . . . .	49
2.6.2	Material strength and loading conventions . . . . .	50
2.6.3	Failure theories . . . . .	51
2.6.4	Design methodology and constituent design criteria . . . . .	51
2.6.5	Lifetime extension . . . . .	53
2.7	Structural reliability data . . . . .	54
2.7.1	Adjustment of empirical failure data . . . . .	55
2.7.1.1	Wind industry . . . . .	56
2.7.1.2	Other industries . . . . .	58
2.7.2	Field failure data . . . . .	58
2.7.3	Failure data based on design methodology . . . . .	60
2.8	Research question . . . . .	60
2.8.1	Overarching reliability methodology . . . . .	61
2.8.2	Scope of work . . . . .	63
2.9	Chapter summary . . . . .	64

<b>II</b>	<b>System and Subassembly Reliability Methods</b>	<b>65</b>
<b>3</b>	<b>System Reliability for an OWT</b>	<b>66</b>
3.1	Reliability growth . . . . .	66
3.1.1	Reliability nomenclature . . . . .	69
3.1.2	Lifetime failure distribution . . . . .	70
3.1.3	Reliability and availability . . . . .	73
3.2	Modelling parameters and methodology . . . . .	74
3.2.1	Reliability modelling software . . . . .	74
3.2.2	Failure data mining for a representative OWT . . . . .	75
3.2.3	System reliability model . . . . .	75
3.2.3.1	System configuration . . . . .	77
3.2.3.2	Reliability Block Diagram . . . . .	77
3.2.4	OWT Maintenance characteristics . . . . .	79
3.3	System reliability simulation results . . . . .	80
3.3.1	Reliability statistics and failure rate distribution . . . . .	81
3.3.2	Failures and associated cost . . . . .	83
3.4	Discussion of results . . . . .	88
3.5	Chapter summary . . . . .	89
<b>4</b>	<b>Methodology</b>	<b>91</b>
4.1	Structural Response . . . . .	93
4.1.1	CAE design tools for OWF structural analysis . . . . .	94
4.1.2	Turbine specification . . . . .	95
4.1.2.1	Subssembly properties . . . . .	97
4.1.2.1.1	Blade design and aerofoil properties . . . . .	97
4.1.2.1.2	Tower and Support structure properties . . . . .	98
4.1.3	Site environmental characteristics for illustrative location . .	100
4.1.3.1	Wind . . . . .	101
4.1.3.2	Wave . . . . .	102
4.1.3.3	Tidal currents . . . . .	103
4.1.4	Model set-up guidance . . . . .	103
4.1.5	Choice of variables . . . . .	104
4.1.5.1	Coordinate system definition . . . . .	104

4.1.5.2	Motion degrees of freedom . . . . .	108
4.1.5.3	Directionality . . . . .	109
4.1.6	FAST modules . . . . .	111
4.1.6.1	ServoDyn . . . . .	112
4.1.6.2	TurbSim and InflowWind . . . . .	112
4.1.6.3	AeroDyn . . . . .	114
4.1.6.4	ElastoDyn . . . . .	115
4.1.6.5	HydroDyn . . . . .	116
4.1.6.6	SubDyn . . . . .	117
4.1.7	Validation . . . . .	120
4.2	Accumulated lifetime damage . . . . .	121
4.2.1	Fatigue Nomenclature . . . . .	122
4.2.1.1	Fatigue life prediction methods . . . . .	124
4.2.1.1.1	S-N approach . . . . .	125
4.2.1.2	Cycle counting methods . . . . .	126
4.2.1.3	Miner's Rule . . . . .	128
4.2.2	Post-processing tools . . . . .	129
4.2.2.1	Extreme value generation . . . . .	129
4.2.2.2	Fatigue life calculation software . . . . .	129
4.2.2.3	Post-processing with MLife . . . . .	130
4.2.2.3.1	Damage equivalent loads . . . . .	131
4.2.2.3.2	Wöhler exponent . . . . .	132
4.2.2.3.3	Ultimate design load . . . . .	134
4.2.2.3.4	Goodman correction . . . . .	135
4.3	Chapter summary . . . . .	137
<b>5</b>	<b>Reliability-critical Subassembly Identification</b>	<b>140</b>
5.1	Industrial cost drivers . . . . .	141
5.2	Structural assembly analysis . . . . .	142
5.2.1	CAE simulator inputs . . . . .	142
5.2.1.1	Environmental parameters . . . . .	143
5.2.1.2	Choice of DLCs . . . . .	145
5.2.1.3	FAST initialisation parameters . . . . .	147
5.2.2	Turbine dynamic response to various LLCs . . . . .	148

5.3	Choice of critical subassembly . . . . .	152
5.3.1	Geometric description at support structure nodes . . . . .	153
5.3.1.1	Turbine performance indicators . . . . .	157
5.3.1.2	Relevant response characteristics for lifetime damage	157
5.3.2	Power production per unit damage . . . . .	159
5.4	Sensitivity analysis . . . . .	160
5.4.1	Aero-hydro-servo-elastodynamic sensitivity . . . . .	161
5.4.1.1	Aerodynamic load simulation seeds . . . . .	162
5.4.1.2	Hydrodynamic load simulation seeds . . . . .	164
5.4.1.3	Influence of seed on lifetime damage . . . . .	167
5.4.2	Simulation length discretisation requirements . . . . .	167
5.4.3	Damage equivalent loads at the substructure nodes . . . . .	169
5.4.3.1	Lifetime load extrapolation distribution . . . . .	172
5.4.3.2	Residual cycle counting . . . . .	174
5.4.3.2.1	Goodman correction . . . . .	175
5.4.3.2.2	$L^{Ult}$ methodology . . . . .	177
5.4.3.3	Availability factor . . . . .	182
5.5	Suitable parameters for spatial reliability distribution . . . . .	183
5.6	Chapter summary . . . . .	184

### **III Site-specific Performance Indicators 187**

#### **6 Sub-regional Characterisation for OWE Deployment 188**

6.1	Look-up table approach . . . . .	189
6.1.1	Load cases . . . . .	190
6.1.2	Environmental parameters . . . . .	190
6.1.3	$L^{Ult}$ analysis . . . . .	192
6.1.4	Sample outputs from look-up table . . . . .	194
6.2	Sub-regional characterisation for UKCS . . . . .	196
6.2.1	Environmental data . . . . .	196
6.2.2	Processing metocean data for $D^{life}$ estimates . . . . .	199
6.2.3	Structural fatigue analysis outputs . . . . .	208
6.2.3.1	Sensitivity Analysis . . . . .	208
6.2.3.2	Sub-region fatigue DELs at mudline . . . . .	213

6.2.3.3	Energy production . . . . .	214
6.3	Metocean-centric metric for sub-regions . . . . .	215
6.4	Cost of energy in the UKCS sub-regions . . . . .	219
6.4.1	Interaction between OPEX and revenue . . . . .	222
6.4.2	OPEX adjustments . . . . .	224
6.5	Chapter summary . . . . .	225
<b>7</b>	<b>Geospatial Mapping of Site Characteristics</b>	<b>227</b>
7.1	Site-specific metocean characteristics . . . . .	227
7.1.1	Input environmental parameters . . . . .	228
7.1.2	Comparison of the ECMWF and NEXT databases for site characterisation . . . . .	230
7.2	Characterisation of UKCS and adjoining areas . . . . .	237
7.2.1	Resource characterisation . . . . .	238
7.2.2	Damage characterisation . . . . .	240
7.2.3	Combined power and damage characterisation . . . . .	242
7.2.3.1	Correlation between power and damage . . . . .	242
7.2.3.2	Spatial distribution of the $K^{DP}$ parameter . . . . .	244
7.3	Dependance of $K^{DP}$ on the environmental parameters . . . . .	245
7.4	Chapter summary . . . . .	245
<b>IV</b>	<b>Discussion and Conclusion</b>	<b>248</b>
<b>8</b>	<b>Discussion and Concluding Remarks</b>	<b>249</b>
8.1	Discussion of research outcomes . . . . .	249
8.1.1	Site-specific structural response . . . . .	250
8.1.2	Identification of reliability-critical subassembly . . . . .	251
8.1.3	Sensitivity analysis of turbine response characteristics and fatigue life . . . . .	252
8.1.4	Ideal support structure design . . . . .	255
8.1.5	Look-up table approach for reliability assessment . . . . .	256
8.1.6	Sub-regional characterisation of performance indicators . . . . .	257
8.1.7	Development of a met-ocean centric KPI . . . . .	259



8.1.8	Geospatial mapping of performance metrics for UKCS and adjoining regions . . . . .	261
8.2	Limitations . . . . .	267
8.3	Concluding remarks . . . . .	271
8.3.1	Implication of thesis . . . . .	271
8.3.1.1	Application to manufacturing . . . . .	271
8.3.1.2	Application to wind farm siting . . . . .	272
8.3.1.3	Operation and maintenance companies . . . . .	273
8.3.1.4	Research community/Future work . . . . .	274
	<b>References</b>	<b>275</b>
	<b>A Publications</b>	<b>300</b>
A.1	Conference publications . . . . .	300
A.2	Journal publications . . . . .	300
	<b>B DLCs</b>	<b>301</b>
	<b>C OWT repair times and cost</b>	<b>304</b>
	<b>D Variables of interest</b>	<b>307</b>
	<b>E Damage Sensitivity to Wind and Wave Seeds</b>	<b>310</b>
	<b>F Sensitivity of sub-regional damage</b>	<b>313</b>
	<b>G <math>K^{DP}</math> residuals</b>	<b>315</b>



# List of Figures

1.1	Distribution of power generation capacity in the European Union between 2005 to 2017 based on source. . . . .	4
1.2	Spatial distribution of total and new offshore wind energy installations in the European Union in 2018. . . . .	6
1.3	Average water depth and distance to shore of bottom-fixed OWFs in the EU categorised based on development status. The size of each bubble indicates the farm production capacity. . . . .	7
1.4	Influence of location- and technology-based factors on production - based availability of OWFs in the UK. . . . .	8
1.5	Flowchart outlining the structure of the thesis and the relationship between chapters. . . . .	13
2.1	Offshore wind farm deployment locations in the UKCS differentiated based on lease rounds, indicating the larger scale of Round 3 projects relative to earlier deployments. . . . .	19
2.2	Characterisation areas based on resource and constraints assessment for Round 4 of OWE lease by TCE. . . . .	21
2.3	Average environmental parameters including wind speed, significant wave height and water depth for the UKCS pertinent to OWE. . . . .	25
2.4	Sensitivity of LCOE to main cost drivers with ranges showing the impact of varying wind power density, depth and distance from shore while keeping the other variables constant to calculate the mid-point levelised cost. . . . .	26
2.5	Proportion of turbine numbers in the global market share by various manufacturing companies based on data collected by the Wind Monitor in 2018. . . . .	32

2.6	Wind turbine configuration taxonomy standard followed for the scope of this thesis. . . . .	33
2.7	Illustration of various turbine foundation concepts, left to right: Tension leg platform, Semi-submersible, Tension leg Buoy (with conical and lattice transition pieces), Spar buoy, Tension leg spar, Jacket, Monopile, Onshore reference. . . . .	34
2.8	Depth, distance-to-shore and project size for various foundation concepts of OWFs based on Global Renewable Infrastructure Project database. . . . .	35
2.9	Sources, adjustment and associated uncertainty bands for failure rate databases for use in reliability assessment calculations. . . . .	55
2.10	Comparison of assembly failure rates between databases for onshore and OWT deployments. CARR and EZ are the available offshore failure rates. . . . .	57
2.11	Systematic procedure flowchart that can be implemented for determination of device reliability based on availability and type of data. . . . .	62
3.1	Methodology used to conduct a system reliability assessment using available field failure rate data from the OWE industry and available geospatial and reliability assessment tools, namely ArcGIS and BlockSim. . . . .	67
3.2	Assessment approach for reliability growth management model with the contribution of this study highlighted in green. . . . .	68
3.3	Constituent failure rate distributions for lifetime analysis and the resulting idealised and realistic bathtub curves. . . . .	71
3.4	Correlation plot based on annual OWF data from Egmond aan Zee showing the lack of correlation between failure rate and availability. . . . .	73
3.5	Subsystems and constituent assemblies of a standard OWT categorised into subsystems. . . . .	78
3.6	Reliability block diagram for an OWT system. . . . .	78
3.7	Block states for major replacement simulations . . . . .	81
3.8	Block states for the major and minor repairs. . . . .	82
3.9	Failures and cost for major replacements. . . . .	85

3.10	Failures and cost for major repairs. . . . .	86
3.11	Failures and cost for minor repairs. . . . .	87
4.1	Dual-phase methodology using an aero-elasto-servo-dynamic tool in conjunction with a damage life estimation tool to conduct a spatial system performance analysis using modelled metocean data. . . . .	92
4.2	Average annual OWT rated capacity (MW) for newly installed devices in Europe between 1991-2018. At the conception of this project in 2016, the average rating of a turbine was 5 MW. . . . .	96
4.3	Diagrammatic representation of the modelled NREL 5-MW baseline monopile wind turbine. The tower bottom corresponds to the location of the TP for this research. . . . .	97
4.4	Comparison of load time series for possible variables to inform choice of variable for analysis of OWT dynamic response. . . . .	107
4.5	Downwind rotor wind and wave direction convention . . . . .	110
4.6	Comparison of the directionality of the subassembly loads. . . . .	110
4.7	Dynamic interaction between the offshore environmental conditions, applied loads and wind turbine sub-systems based on the FASTv8 modularisation framework . . . . .	113
4.8	Output time series data for metocean parameters generated by FAST114	
4.9	Structural components of the substructure and analysis nodes of a member in the element and substructure coordinate systems. . . . .	119
4.10	Sequential analysis to predict fatigue life using the S-N approach . . . . .	122
4.11	A representative sinusoidal fatigue cycle with associated nomenclature. . . . .	123
4.12	Simplified symmetric Goodman diagram. . . . .	136
4.13	The dual-phase Stream 2 methodology developed to provide location-specific performance indicators to facilitate informed site selection for OWT deployment. . . . .	138
5.1	$V_t$ and wave elevation statistics for the considered LLCs from the shallow water K13 site in the Upwind project. . . . .	146

5.2	OWT generator speed and pitching moment at the transition piece for LLC01 - LLC17 displaying characteristic difference between time series data for operational (DLC 1.2) and parked (DLC 6.4) conditions represented by solid and dashed lines, respectively. . . . .	149
5.3	Forces and bending moments at various locations on the support structure for multiple LLCs. . . . .	151
5.4	Geometric properties of the OWT at the analysis nodes. . . . .	156
5.5	Diagrammatic representation of the (a) location of and (b) shear forces and (c) bending moments at the analysis nodes of a fixed OWT for LLC16. . . . .	156
5.6	Lifetime damage equivalent loads at various nodes of the support structure. . . . .	158
5.7	Short-term damage equivalent loads at various nodes of the support structure displaying the relative contribution of individual lumped load cases. . . . .	159
5.8	Short-term power production per unit damage equivalent load cases at the mudline of the support structure (J1) for the various LLCs. .	160
5.9	Defining TurbSim seed requirements for simulation robustness of an operating OWT using comparison of mean and average standard deviation values relative to 36 seeds for LLC01, LLC07 and LLC14. The horizontal red line corresponds to the average of 36 seeds. . . .	165
5.10	Defining HydroDyn seed requirements for simulation robustness of an operating OWT using comparison of mean and average standard deviation values relative to 36 seeds for LLC01, LLC07 and LLC14. The horizontal red line corresponds to the average of 36 seeds. . . .	166
5.11	Comparison between the influence of the choice of wind seed on the percentage difference from the mean of the bending moment of 36 seeds and associated fatigue damage for LLC17. Structural failure occurs at $D^{life} = 1$ as denoted by the horizontal red line. . . . .	168
5.12	Comparison between the influence of the choice of wave seed on the percentage difference from the mean of the bending moment of 36 seeds and associated fatigue damage for LLC17. Structural failure occurs at $D^{life} = 1$ as denoted by the horizontal red line. . . . .	168

5.13	Simulation length discretisation requirements for the turbine parked state, DLC 6.4, for $V_t$ below cut-in speed and above cut-out wind speed. . . . .	170
5.14	Simulation length discretisation requirements for the turbine operational state, DLC 1.2, with $V_t$ within the operational range. . . . .	171
5.15	Comparison of lifetime damage calculated using a Weibull wind distribution and user-defined distribution with occurrence probabilities as shown in 5.1 at various analysis nodes using the bending moment of the NREL 5MW turbine. . . . .	174
5.16	Influence of half-cycle counting on the damage rate for various LLCs.	175
5.17	Influence of Goodman correction on damage equivalent loads for the short-term ten minute FAST simulations at the analysis nodes. . . . .	176
5.18	Influence of Goodman correction on lifetime damage equivalent loads at the analysis modes. . . . .	178
5.19	Comparison of the lifetime damage accumulated due to the shear forces and the bending moments at various analysis nodes of the NREL 5-MW wind turbine using a Weibull distribution with $\beta = 1.97$ , $\eta = 11.85$ and mean wind speed of 10.5 m/s. Structure fails at $D^{life} = 1$ . . . . .	179
5.20	Damage life calculated using analytical $L^{Ult}$ for bending moment and shear stress. Structural failure occurs at $D^{life} = 1$ as denoted by the horizontal red line. . . . .	181
5.21	Damage life of an NREL 5MW OWT at the K13 shallow water site based on the analytical and simulated $L^{Ult}$ values. Structural failure occurs at $D^{life} = 1$ as denoted by the horizontal red line. . . . .	182
5.22	Damage life of NREL 5MW OWT based on overturning moment at the mudline based on the $L^{Ult}$ values generated by the $L^{max}$ for onshore and offshore locations. Structural failure occurs at $D^{life} = 1$ as denoted by the horizontal red line. . . . .	183
5.23	Damage life of an NREL 5MW OWT at the K13 shallow water site based on the availability of the turbine. . . . .	184

5.24	Flowchart summarising the analyses conducted for selection of the reliability-critical node in the illustrative assembly and a suitable set of physical, numerical and material parameters to develop the methodology for improved quantification and visualisation of OWT deployment sites. . . . .	185
6.1	Bending moments for all $H_s - T_p$ combinations for $V_t = 11$ m/s . . .	194
6.2	Available and extracted power plots for the NREL 5 MW OWT. . .	195
6.3	Damage rate for all $H_s - T_p$ combinations for $V_t = 11$ m/s . . . . .	196
6.4	Sub-regional division and location of the NEXT data GPs for which comprehensive data is publicly available. . . . .	198
6.5	Methodology flowchart for conducting fatigue analysis at the sites identified in Figure 6.4 for various sub-regions in the UKCS. . . . .	200
6.6	Comparison between the available scatterplot binning of the NEXT data in the FUGRO report to the resampled data for fatigue life analysis. . . . .	202
6.7	Resampled $H_s - T_p$ scatter plot for all wind speeds at GP15571. . .	203
6.8	Weibull fitted wind data from the provided and resampled data. . .	203
6.9	Scatter plots for $0 \leq V_t < 15$ for GP15571 . . . . .	204
6.10	Lifetime accumulated damage within each wind speed bin at GP15571 with $L^{Ult} = 5 \times L^{max}(ReactMxyss)$ , $m = 4$ and $DesLife = 20$ years. An aggregate of all $V_t$ bins at this site yields a $D^{life}$ of 0.202 with the maximum damage at $8 \leq V_t < 10$ m/s. . . . .	205
6.11	Distribution of accumulated lifetime damage for each wind speed bin at the 40 investigated GPs. . . . .	207
6.12	Lifetime fatigue damage envelope for the HornSea site using the NEXT model data. . . . .	209
6.13	Influence of the $L^{Ult}$ values of on calculated damage equivalent load estimates for fatigue life analysis. . . . .	210
6.14	Influence of the design life values of 5, 10, 15, 20, 25 and 30 years on calculated damage equivalent load estimates for fatigue life analysis. . . . .	211
6.15	Influence of the Wöhler exponent values of 3, 4 and 5 on calculated damage equivalent load estimates for fatigue life analysis. . . . .	211



6.16	Distribution of $D^{life}$ categorised based on GP locations across the UKCS with $m = 4$ , $DesLife = 15$ years and $L^{Ult} = 5 \times L^{max}$ . . . . .	213
6.17	Annual energy production at the various sub-regions of the UKCS. .	215
6.18	Theoretical capacity factors at various sub-regions of the UKCS discounting downtime due to factors outside of metocean conditions. .	216
6.19	Relationship between the annual energy production and damage for the 5 MW NREL turbine deployed at various sub-regions in the UKCS. . . . .	217
6.20	$K^{DP}$ performance indicator combining the influence of energy production weighted by accumulated fatigue damage at the various sub-regions of the UKCS. . . . .	218
6.21	Comparison of reported COE with the expected sub-regional COE distribution based on cost estimates for the CAPEX, OPEX and D&D. . . . .	221
6.22	Revenue and CAPEX per unit power weighted by FCR for various sub-regions in the UKCS based on annual energy production and lifetime accumulated damage estimates. . . . .	223
6.23	Sub-regional COE with fatigue-based OPEX costs factored in. . .	225
7.1	Mapped mean metocean parameters for Week 1, 2017 in the UKCS extracted from the ECMWF ERA-Interim dataset with time series at GPs around the HornSea offshore wind farm site. The farm site is marked by a red cross off the east coast of the UK. . . . .	231
7.2	$V_t - H_s$ percentage occurrence scatter plot for $54^\circ\text{N } 1.50^\circ\text{E}$ from ECMWF data from 2008 - 2017 taken as representative for the HornSea site in the UKCS. . . . .	232
7.3	Comparison of the $H_s - V_t$ scatter plot for the percentage occurrence probability of sea states for the HornSea site. . . . .	233
7.4	Comparison of the binned accumulated damage at the mudline for an NREL baseline turbine deployed at the HornSea OWF site with $m = 4$ , $DesLife = 20$ and $L^{Ult} = 5 \times L^{max}$ using the ECMWF-ERA Interim and the NEXT databases. . . . .	235

7.5	$H_s - T_p$ scatter plot for $V_t = 1$ m/s using the NEXT and ECMWF databases for comparing the mudline damage at the HornSea offshore wind site. . . . .	236
7.6	Heat map displaying the spatial distribution of $E^{ann}$ for the NREL 5 MW baseline turbine deployed at the UKCS and its adjoining areas with the east and west coast demarcated at $2.5^\circ\text{W}$ . . . . .	239
7.7	Heat map for the spatial distribution of $D^{life}$ at the OWT mudline for the UKCS and adjoining areas using $m = 4$ , $DesLife = 15$ years and $L^{Ult} = 5 \times L^{max}$ with the east and west coast demarcated at $2.5^\circ\text{W}$ . . . . .	241
7.8	Portfolio analysis for the accumulated lifetime damage at the mudline and annual energy production for the NREL 5 MW turbine deployed at the UKCS and its adjoining areas. The bilinear relationship between $E^{ann}$ and $D^{life}$ is also highlighted. . . . .	243
7.9	Heat map for the spatial distribution of $K^{DP}$ for a 5 MW turbine with design lifetime of 15 years at the UKCS and its adjoining areas with the east and west coast demarcated at $2.5^\circ\text{W}$ . . . . .	244
7.10	Dependance of the damage per unit energy on the annual average $V_t$ and $H_s$ at sites across the UKCS and its adjoining regions. . . . .	246
8.1	Relative influence of the design input parameters such as $m$ , $L^{Ult}$ and $DesLife$ on the lifetime accumulated damage estimates by MLife showing that $D^{life}$ displays the maximum sensitivity to the Wöhler exponent $m$ . . . . .	255
8.2	Mapped and tabulated ranking of sub-regions in the UKCS based on the risk-return metric calculated using the NEXT database. OWTs with higher structural integrity should be deployed at locations with a higher ranking for similar design lifetimes. . . . .	260
8.3	Cumulative OWE installations by sea basin across Europe. . . . .	261
8.4	Map showing the distribution of the UK offshore wind farm lease sites by round within the UKCS boundary. . . . .	262
8.5	Spatial distribution of annual energy production and accumulated lifetime damage at the OWT mudline for the UKCS and adjoining areas with the east and west coast demarcated at $2.5^\circ\text{W}$ . . . . .	264

8.6	Contour map of $K^{DP}$ with the east and west coast demarcated at $2.5^\circ\text{W}$ . . . . .	265
8.7	Lifetime energy production and accumulated damage scatter plot with associated $K^{DP}$ characteristics for an NREL 5 MW turbine deployed at the UKCS and its adjoining regions with a lifetime of 15 years. . . . .	266
E.1	Comparison between the influence of the choice of wind seed on the percentage difference from the mean of the bending moment of 36 seeds and associated fatigue damage for LLC01. . . . .	310
E.2	Comparison between the influence of the choice of wave seed on the percentage difference from the mean of the bending moment of 36 seeds and associated fatigue damage for LLC01. . . . .	311
E.3	Comparison between the influence of the choice of wind seed on the percentage difference from the mean of the bending moment of 36 seeds and associated fatigue damage for LLC01. . . . .	311
E.4	Comparison between the influence of the choice of wave seed on the percentage difference from the mean of the bending moment of 36 seeds and associated fatigue damage for LLC07. . . . .	312
F.1	Comparison of the best-, worst- and mean-case scenario using fatigue-influencing variable inputs from F.1 for all NEXT GPs. . . . .	314
G.1	Residuals for the $K^{DP} - V_t$ model fit. . . . .	316
G.2	Residuals for the $K^{DP} - H_s$ model fit. . . . .	316



# List of Tables

2.1	The Beaufort Force with associated wind speed limits and sea state description. . . . .	44
2.2	Categories of loads experienced by on an OWT shown in the order of decreasing ease of predictability. . . . .	47
3.1	OWT assembly failure rate categorised into subsystems with corresponding repair strategy. . . . .	76
3.2	Summary results for the system reliability assessment for an offshore wind turbine providing estimates for the lifetime failures, downtime and associated costs. The assemblies with the highest failure consequence are listed based on contribution to downtime and restoration costs. . . . .	84
4.1	Summary of specifications for the modelled NREL 5-MW baseline monopile wind turbine. . . . .	98
4.2	Tower properties for the 5MW NREL baseline turbine appended with substructure properties from the OC3 monopile. . . . .	99
4.3	Input metocean parameters for a 5MW monopile OWT deployed at the Hornsea Project One site. . . . .	101
4.4	Relevant coordinate system extensions for the NREL 5 MW turbine. . . . .	105
4.5	FAST output variables at the mudline, transition piece and tower top based on coordinate system selection, nodal reduction and physical formulation. . . . .	106
4.6	Fatigue nomenclature for cycle $i$ and their corresponding calculation method. . . . .	123
4.7	Features of considered fatigue life post-processors. . . . .	131
4.8	Welds in the OWT support structure with associated S-N curve. . . . .	133

5.1	Load case metocean parameters based on the K13 shallow water site from the UpWind Project. . . . .	144
5.2	Appropriate initialisation paramaters for ServoDyn and ElastoDyn modules. . . . .	148
5.3	Rationale and summarised analysis description for structural response sensitivity investigations in FAST. . . . .	161
5.4	Simulation conditions for seed-dependence study for fixed offshore wind monopile structures. . . . .	162
5.5	Computational parameters for investigating simulation length requirements for turbine dynamic response. . . . .	169
5.6	Rationale and summarised analysis description for fatigue life sensitivity investigations in MLife. . . . .	172
5.7	Material properties of the tower and substructure analysis nodes used as MLife input. . . . .	180
5.8	Suitable values of the parameters used for determining spatial reliability distribution for the NREL 5 MW turbine based on loads at the mudline of the substructure. . . . .	186
6.1	Characteristics of the binning parameters of the look-up table data.	191
6.2	Load cases with the largest structural response at the mudline from the 13340 simulations with associated environmental parameters and power output appended. The highlighted cells correspond to the maximum and minimum values for the bending moments and shear forces at the mudline of an NREL 5 MW monopile in the fore-aft and side-to-side directions as well as the combined loads in the two directions. . . . .	193
6.3	Colour-coded MLife input parameters for which the fatigue analysis is performed at the NEXT GPs; a darker colour corresponds to an input value with higher fatigue damage. . . . .	210
6.4	Risk and return portfolio analysis for the 5 MW baseline turbine deployed in the UKCS and adjoining areas. . . . .	216
6.5	Extracted and adjusted LCC model data for the CAPEX, OPEX and D&D of a 500 MW offshore wind farm. . . . .	220

7.1	Comparison of the $H_s - V_t$ scatter plot for the percentage occurrence probability of sea states for the HornSea site. . . . .	234
7.2	Comparison of the accumulated lifetime damage at the HornSea site based on the ECMWF and NEXT metocean datasets for the best-, worst- and mean scenarios generated by the fatigue variables. . . . .	237
B.1	Recommended design load cases for fatigue calculation. . . . .	301
B.1	Recommended design load cases for fatigue calculation. . . . .	302
B.1	Recommended design load cases for fatigue calculation. . . . .	303
C.1	OWT assembly repair times categorised into subsystems with sub-categorisation based on associated material costs. . . . .	304
C.2	OWT assembly material costs for repair categorised into major replacement, major and minor repairs. . . . .	305
D.1	Considered output parameters from the FAST simulation for fatigue calculation of structural subsystems. . . . .	307
F.1	Details of MLife input parameters for which the fatigue analysis is performed at the NEXT GPs. . . . .	313





# Nomenclature

## List of Acronyms

$V_{rated}$	Offshore wind turbine rated speed	m/s
BOS	Balance of system	
CAE	Computer Aided Engineering	
CAPEX	Capital Expenditure	
CF	Capacity Factor	%
CfD	Contract for Difference	
COE	Cost of Energy	
D&D	Decommissioning and disposal	
DECC	Department of Energy and Climate Change	
DELs	Damage Equivalent Loads	
DLC	Design Load Case	
DOWEC	Dutch Offshore Wind Energy Converter	
ECMWF	European Centre for Medium-Range Weather Forecasts	
EEZ	Exclusive Economic Zone	
ERA	ECMWF Re-Analysis	
EU	European Union	
F	Probability distribution function of failure	
FCR	Fixed charge rate	%

## List of Tables

---

FEA	Finite element analysis	
FEM	Finite element method	
GenDOF	Generator degree of freedom	
GIS	Geographic Information System	
GP	Grid Point	
IntfFXss	Transition piece reaction loads in the substructure coordinate system	
JONSWAP	Joint North Sea Wave Project	
KPI	Key Performance Indicators	
LCC	Lifecycle and Cost model	
LCOE	Levelised Cost of Energy	
LLC	Lumped Load Case	
M	Maintainability function	
M1N1ζKXe	Substructure reaction loads in the element coordinate system	
MSL	Mean Sea Level	m
MTBDE	Mean time between downing events	hours
MTBF	Mean time between failures	hours
MTTF	Mean time to failure	hours
MTTR	Mean time to repair	hours
NESS	North European Storm Study	
NEXT	NESS Extension	
NEXTRA	NEXT RE-Analysis	
NOAA	National Oceanic and Atmospheric Administration	
NREL	National Renewable Energy Laboratory	

---

O&G	Oil and Gas	
OPEX	Operational Expenditure	
OREDA	Offshore and Onshore Reliability Data	
OWE	Offshore Wind Energy	
OWT	Offshore Wind Turbine	
P	Turbine rated power	MW
PCMode	Pitch control mode	
PSD	Power Spectral Density	
R	Reliability function	
RAMS	Reliability, Availability, Maintainability, and Safety	
RBD	Reliability Block Diagram	
React $\zeta$ Xss	Mudline reaction loads in the global and substructure coordinate system	
REZ	Renewable Energy Zone	
RNA	Rotor-Nacelle Assembly	
SAR	Synthetic Aperture Radar	
SPARTA	System Performance, Availability and Reliability Trend Analysis	
SWAN	Simulating WAves Nearshore	
TCE	The Crown Estate	
TI	Turbulence intensity	
TLP	Tension Leg Platform	
TotBins	Total number of bins	
TP	Transition piece	
TRL	Technology Readiness Level	

## List of Tables

---

TWh	Terawatt hours
TwHt5ζLxt	Tower reaction loads in the coordinate system fixed in the tower base
TwrBsζxt	Tower base reaction loads in the coordinate system fixed in the tower base
UK	United Kingdom
UKCS	United Kingdom Continental Shelf
UKMO	United Kingdom Met Office
WAFO	Wave Analysis for Fatigue and Oceanography
WAMIT	Wave Analysis At Massachusetts Institute of Technology
YawBrζxn	Tower top reaction loads in the coordinate system translating and rotating with the tower top and yaws with the nacelle
YawBrζxp	Tower top reaction loads in the coordinate system fixed in tower-top or base plate with no translation with nacelle yaw

## List of Symbols

$\beta$	Weibull shape parameter	
$\eta$	Weibull scale parameter	
$T$	Serial number of tower analysis node	
$T_{Ht}$	Tower Height	
$T_{elev}$	Height of tower analysis node	m
$T_{Ht}$	Tower height	m
$V_{max}$	User defined $V_t$ maximum	m/s
$\bar{V}_{thub}$	Wind speed at hub height	m/s
$\Delta t$	Temporal resolution of the metocean database	hours
$\gamma$	Peak shape parameter for the JONSWAP spectrum	

---

$\lambda$	Failure rate	Per annum
$\nu$	Poisson's ratio	
$\rho$	Air density	kg/m <sup>3</sup>
$\sigma_y$	Tensile yield strength	Pa
$\theta_W$	Mean incident wave propagation direction	degrees
$a$	Area	
$A_f$	Availability Factor	
$b$	Width of beam structure	
$C_p$	Betz Limit	%
$C_{ss}$	CAPEX due to substructural BOS	%
$D$	Rotor diameter	m
$d$	Mean water depth	m
$D^{life}$	Lifetime damage equivalent loads	variable
$D^{ST}$	Short term damage equivalent loads	variable
$D_{in}$	Internal diameter	
$D_{out}$	External diameter	
$DEL^{life}$	Uncorrected lifetime DELs	variable
$DEL_{diff}^{life}$	Relative difference between lifetime DELs due to Goodman correction	variable
$DEL_{GM}^{life}$	Goodman corrected lifetime DELs	variable
$DEL^{ST}$	Uncorrected short-term DELs	variable
$DEL_{diff}^{ST}$	Difference between short term DELs	variable
$DEL_{GM}^{ST}$	Goodman corrected short-term DELs	variable
$DesLife$	Design Lifetime	years

## List of Tables

---

$E^{ann}$	Annual energy production	MWh
$f$	Cyclic frequency	Hz
$f_j^{life}$	Mlife time factor	
$G$	Direction indicator for single-sided velocity component	
$H_s$	Significant Wave Height of incident waves	m
$I$	Centroidal moment of inertia	
$j$	Load time series index	
$K$	Y-intercept parameter of the S-N curve	
$K^{DP}$	Damage per unit energy produced	GWh <sup>-1</sup>
$l$	Wind speed bin	
$L^M$	Mean load of a cycle	
$L^R$	Range of a load cycle about mean load	
$L^{max}$	Maximum recorded or modelled load at a node	variable
$L^{MF}$	Fixed load mean	variable
$L^{Ult}$	Ultimate Design Load	variable
$L_G$	Integral scale parameter of the velocity component	
$L_i^{RF}$	Load range of rainflow cycle	variable
$m$	Wöhler exponent	
$n$	Number of cycles in load range	
$N(.)$	Cycles to failure at a load range	
$N_f$	Number of cycles to failure	
$Occ_i^{tot}$	Number of records in cell $i$ of the $H_s - T_p$ scatterplot	
$p_l^v$	Occurrence probability of bin	
$Q$	Statical moment	

---

$r_{in}$	Internal radius	
$r_{out}$	External radius	
$S_f$	Shear force	
$S_G$	Single-sided velocity component spectrum	m/s
$T$	Time to failure	
$t$	Time	
$T^{scat}$	Length of time for each record	
$T_{years}^{scat}$	Time length of the data	years
$T_p$	Peak spectral period of incident waves	s
$T_z$	Zero-crossing period	s
$U_0$	Strain energy density	
$U_d$	Distortion energy	
$U_h$	Dilatational energy	
$UCM_{ult}$	Unclosed cycle count multiplier	
$ULF$	Ultimate Load Factor	
$V$	Shear force	
$V_T$	Turbulence component of wind speed	m/s
$V_t$	Mean wind speed	m/s
$V_{in}$	Turbine cut-in wind speed	m/s
$V_{out}$	Turbine cut-out wind speed	m/s
$Y$	Young's modulus	
$y^{max}$	Perpendicular distance of the point of maximum stress from the neutral axis	
$z$	Elevation	m

## List of Tables

---

$z_0$	Roughness length	m
$z_{ref}$	Reference elevation	m





# Part I

## Research Context



# Chapter 1

## Introduction

### 1.1 Role of wind in the renewable energy mix

Recognising the need for an effective and immediate response to the global threat of climate change, the Paris Agreement (UNFCCC, 2015) aims to achieve climate resilience through adaptation. Signatories to the agreement sought to limit the increase in global average temperature to 1.5°C above pre-industrial levels as well as aimed to address the impacts of climate change.

To cater to the demand of the Paris agreement, the European Commission has identified '*Energy union and climate*' to be one of its key priorities for 2015 - 2019. The 2030 framework for energy and climate under the union aims to reduce greenhouse emissions, increase the share of renewable energy in the energy market, improve energy efficiency as well as increase interconnection (European Commission, 2017b). Incorporating renewable energy into the energy mix contributes to the five mutually reinforcing dimensions of the energy union including energy security, market integration, energy efficiency, decarbonisation and innovation. Additionally, it allows for improvement in economic growth, sustainable job creation, reduction in air quality index and promotion of international development by engagement with developing countries to supply affordable energy.

The Renewable Energy Directive of 2009 specifies an overarching framework to promote the generation of renewable energy for the European Union (EU) member states. It sets an overall binding target for the EU to meet 20% of its energy needs through renewable sources by 2020 through the attainment of individual national targets. Targets for individual member states are fairly distributed and show

## 1.1. Role of wind in the renewable energy mix

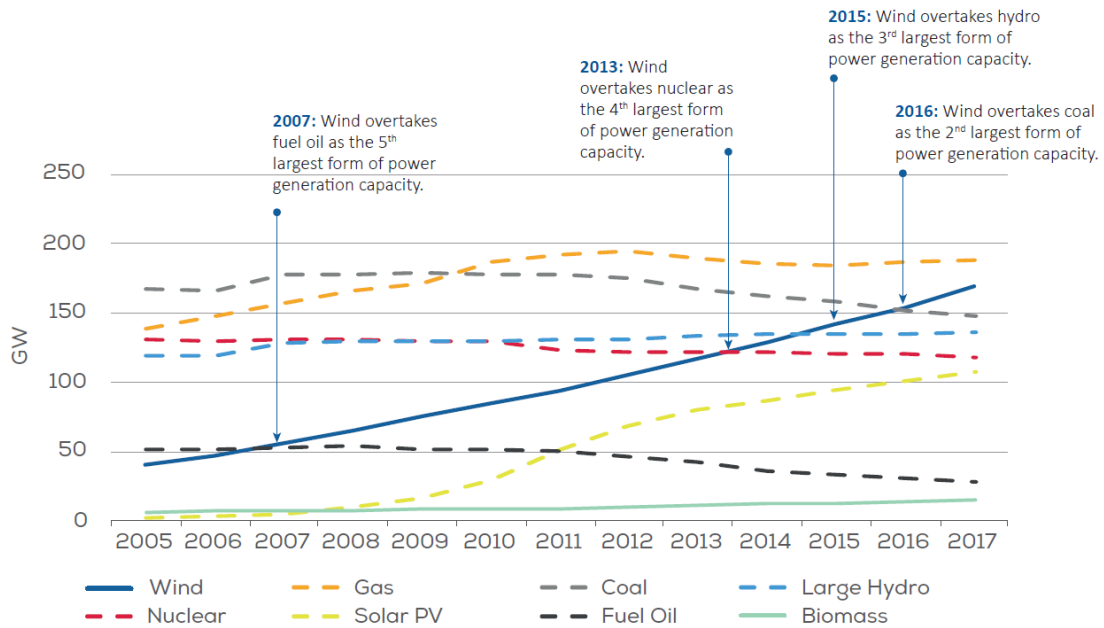


Figure 1.1: Distribution of power generation capacity in the European Union between 2005 to 2017 based on source (WindEurope Business Intelligence, 2018).

considerable variation based on their current production and overall potential, from 10% for Malta to 49% for Sweden (European Parliament, 2009).

As of 2014, the European Council has proposed a collective EU target of 27% for 2030 (European Commission, 2017a) in contrast to the more ambitious 30% target demanded by the European Parliament. To achieve the target renewables share, the need for an improved regulatory framework is stipulated since following the renewable energy trajectory under current policies is expected to increase the share to 24.3% only. A biennial progress report from the member nations allows the EU to keep track of the headway made by the member states as well as provides transparency for investors to favour further deployment.

Of the available renewable sources, wind is the most lucrative technology for addressing the evolving energy requirements in a sustainable manner (DECC, 2011). With a cumulative installed capacity of 168.7 GW in 2017, wind energy in the EU has risen to the second place amongst all conventional and alternative generation sources as seen in Figure 1.1.

Wind farms may be installed to harvest the wind resource on land and offshore. Geographically, of the new wind power deployed within the EU in 2017, 79% is situated in Germany, the United Kingdom (UK) and France. With its abundant resource potential and an expected increase of renewable energy contribution in

the gross final consumption of energy from 1.3% in 2005 to 15% in 2020, the spatial scope of this research is limited to the UK. As of 2018, together onshore and offshore wind have an installed capacity of over 19 gigawatt (GW) in the UK with over 12.5 million homes powered equivalent annually (RenewableUK, 2018) based on annual average consumption for a household estimated at 3.9 MWh. Additionally, CO<sub>2</sub> reductions over 21.5 million tonnes per annum are estimated by using the Department of Business, Energy and Industrial Strategy's static carbon saving factor of 430g/kWh (UK Department of Energy and Climate Change, 2013).

The load factor for offshore and onshore wind are 37.2% and 26.6%, respectively (RenewableUK, 2018), and cost reductions are expected to be 71% and 47% respectively for 2040 (Ernst & Young, 2017). Technosocial advantages associated to Offshore Wind Energy (OWE) have led to an increase of 101% in installations relative to 14.3% for onshore wind during 2017 compared to the previous year (WindEurope Business Intelligence, 2018).

The United Kingdom Continental Shelf (UKCS) is characterised by shallow waters with strong and consistent wind resource, therefore, it provides the ideal conditions for harvesting the offshore wind resource. The spatial distribution of the offshore wind capacity installation in the EU in Figure 1.2 shows that with 1.3 GW, the UK represents 49% of Europe's gross capacity brought online in 2018. Therefore, with its 33 operational projects and a possible generation scenario of 425 TWh (TWh) per annum by 2050 (HM Government, 2010), the UK is the world leader in OWE with ambitious plans for further development.

## 1.2 Location-intelligent siting of OWEs

Economically, the expected increase in the proportion of OWE in the energy mix of the UK cannot be delivered at the cost of a rise in electricity prices for the consumer. Therefore, the UK Renewable Energy Roadmap (DECC, 2011) argued that the OWE industry must reduce its Levelised Cost of Energy (LCOE) from values of £140/MWh in 2011 to £100/MWh by 2020 to become a financially feasible alternative energy source. In practice, quantum leads in investor confidence, policy reforms and electricity market evolution reduced LCOE to £62/MWh (BVGassociates, 2017) in 2017 which is agreement with projections by Mari and Kerr (2018).

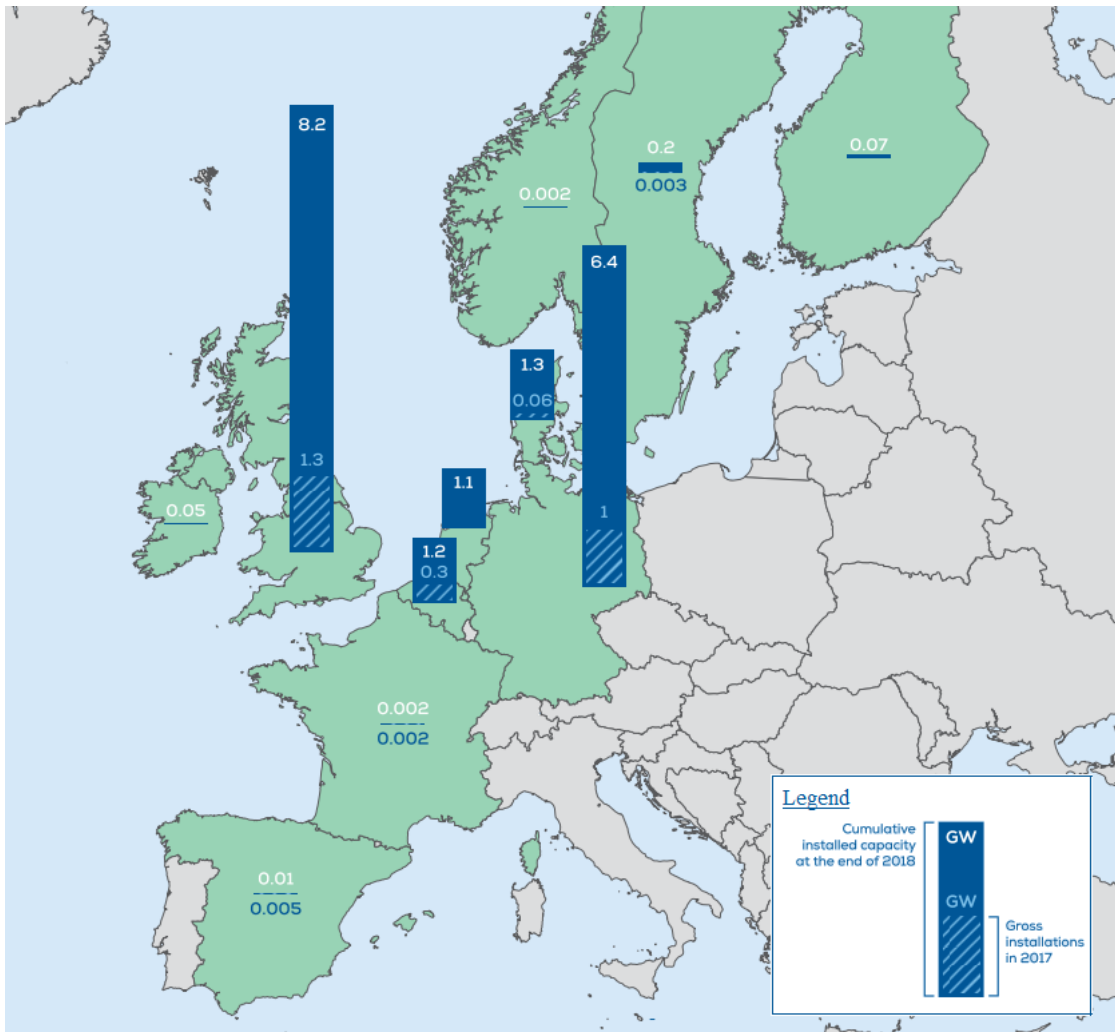


Figure 1.2: Spatial distribution of total and new offshore wind energy installations in the European Union in 2018 (WindEurope Business Intelligence, 2019).

LCOE not only provides information about the cost-effectiveness of various types of energy but may also be used for comparison between individual projects within the same power production stream. The development cost of any OWE project may be split into the capital expenditure (CAPEX) and operational expenditure (OPEX) (Myhr et al., 2014). The relative share of CAPEX and OPEX for offshore wind farms may vary but typically OPEX amounts to 30% of the total expenditure.

Publication by The Crown Estate (2012) states that the increase in LCOE of OWE in the UK may be attributed to ‘sub-optimal reliability’ (The Crown Estate, 2012) amongst other factors. Unscheduled maintenance, due to low reliability and high failure rates, accounts for 70% of OPEX (Crabtree et al., 2015). To reduce the LCOE, a compromise between increase in CAPEX to aim for high reliability and

increase in OPEX due to low reliability must be achieved. Therefore, the influence of reliability must be quantified so as to achieve the targeted system performance.

As discussed, the OWE industry has successfully been able to reduce LCOE to become more competitive with conventional sources of energy. However, as the industry expands, turbines are increasingly being deployed further offshore and in deeper waters to harness the improved wind energy resource as shown in Figure 1.3. It can be seen that while existing projects are predominantly close to shore and at low water depths, projects at the early stage of planning are exploring OWE potential further offshore. Quantification of the system failure behaviour

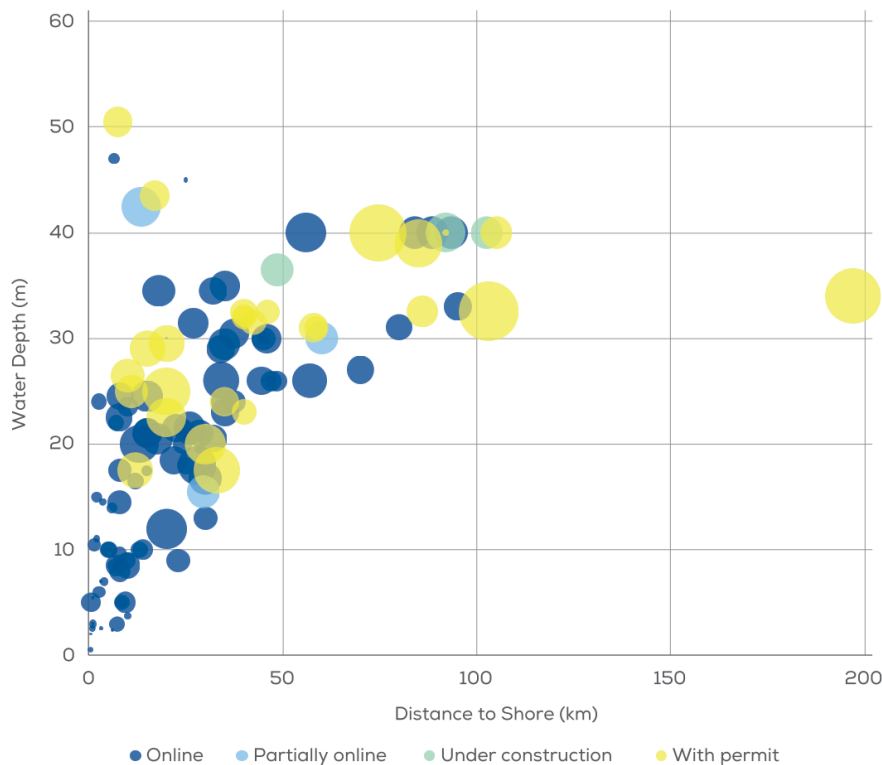


Figure 1.3: Average water depth and distance to shore of bottom-fixed OWEs in the EU categorised based on development status. The size of each bubble indicates the farm production capacity (WindEurope Business Intelligence, 2019).

through reliability assessments provides a robust estimate of device performance. However, there is a lack of sufficient field data for reliability assessments in the OWE industry due to confidentiality to maintain competitive advantage. While reliability data at subsystem level can now be accessed, its usefulness is limited since associated characteristics such as turbine age, configuration, nominal power and deployment location are not accessible (Carroll et al., 2015). While such data can only provide information for the reliability assessment of a generic Offshore



Wind Turbine (OWT), it provides an improved reliability assessment relative to using data from other industries for reliability estimates.

The feasibility of deployment sites can be characterised by a range of geospatial factors, however, it is commonplace to limit this characterisation to the resource potential in the OWE industry. However, an improved location-intelligent decision making process to increase project viability should incorporate the influence of both the risk and return profiles at the proposed deployment location. With the understanding of the significance of site-dependant reliability to the risks associated to a project, its geospatial representation and visualisation is considered integral to take an informed location-intelligent decision.

Key performance indicators for OWE are influenced by location factors such as region of deployment and distance to port. Furthermore, inherent technological parameters such as turbine age, installed capacity as well as the employed maintenance strategy may also be used to predict performance as seen in Figure 1.4. As new projects move further offshore to gain access to higher resource, an

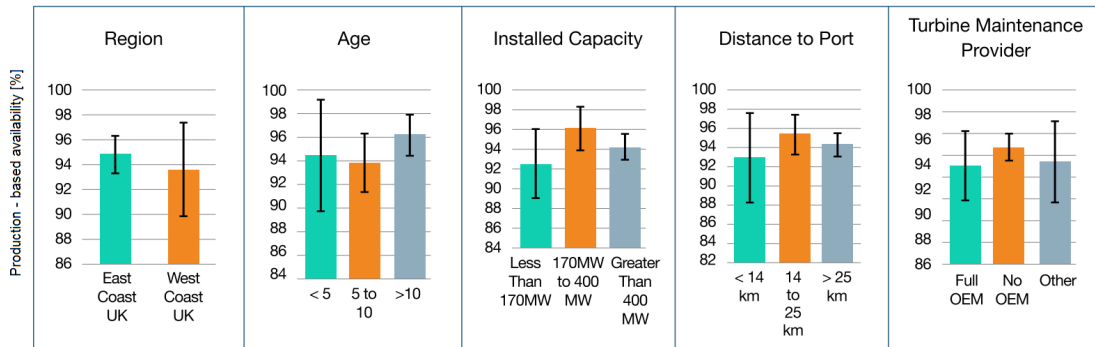


Figure 1.4: Influence of location- and technology-based factors on production - based availability of OWFs in the UK (SPARTA, 2018).

increased focus on the sensitivity of the device to the marine environment for improved siting of the OWE farms is necessary for optimum device performance. Also, an improvement in reliability is expected to be pivotal to improve revenue generation given the reduced weather windows for maintenance operations and the large logistic cost associated to increased distance to shore (Carbon Trust, 2008).

### 1.3 Aims and Objectives

Offshore wind energy devices are fatigue critical machines with unique load spectrums, therefore, adequate quantification of environmental loads on individual assemblies and subassemblies is imperative to conduct robust device reliability assessment. Given the influence of metocean parameters on power production and reliability, this research aims to develop a robust methodology to quantify and visualise expected system performance using a geospatial approach for identification of the best location for large-scale deployment of OWE in the continental shelf of the UK. This is done by combining the risk and return potential at a site, namely subassembly reliability and annual power production estimates, to assess specific project risks and uncertainties regarding the energy supply from OWE.

The proposed methodology will be useful to a spectrum of stakeholders from those at individual farm level to policy making bodies since it advances the understanding of the dependency of LCOE on site conditions. Weighing structural damage on conventional performance metrics such as power production is particularly useful as devices begin to populate lease sites with highly dynamic metocean conditions in search of higher resource. Therefore, the main objectives of this research are:

- Performing system reliability assessment of a generic OWT using industry - specific data
- Identification of the reliability - critical subassembly of an illustrative assembly for the development of the methodology
- Reliability site characterisation to assess the suitability of various sub-regions in the UKCS
- Development and application of a location-specific damage accumulation metric weighed by power production for the feasibility analysis of OWE projects in the UKCS and adjoining regions

It can be observed that the objectives transition from a global system-level reliability to determination of site-specific subassembly-level estimates. The former utilises a probabilistic framework to provide insight into the generic system behaviour and the associated consequence. However, establishing a metocean-centric

metric for OWE site characterisation which draws on outputs of both device generation and structural reliability in order to highlight the significance of metocean parameters to OWE technologies beyond the realm of resource potential calculation is the key aim of this study. To deliver this, the scope of the research is restricted to a single sub-system. After identification of the key environmental factors influencing the reliability assessment of OWE, a computer-aided engineering tool is used to account for varying metocean conditions at deployment sites around the UK for fatigue limit design. For each chosen sea state, a linear damage analysis using a rainflow count algorithm is conducted to quantify fatigue damage by the load cycles of varying stress ranges. An annual/lifetime accumulated fatigue damage prediction is made based on the sum of the extrapolation of the constituent load cycles for individual sites. The resulting accumulated damage is then normalised by the power production to identify optimum siting for OWE deployments.

## 1.4 Contribution to existing knowledge

Bearing in mind the critical role system reliability plays in determining the pace of the development of the offshore wind industry, this thesis contributes to the existing reliability knowledge base. This is done by using available reliability databases and simulated fatigue-induced failure. The contributions of this thesis through its length can be summarised as:

- Critical appraisal of the reliability of OWE with a focus on the influence of metocean parameters;
- Reliability assessment of an OWT using field failure rate data;
- Advancing the argument for a look-up table approach for determining operational fatigue load;
- Performing local sensitivity analysis of lifetime accumulated damage to design parameters;
- Developing a combined accumulated damage-power production metric for characterisation and visualisation of OWE deployment locations in the UKCS; and

- Discussing the dependence of the risk-return metric on environmental parameters.

The developed methodology successfully visualises the damage per unit energy generated at various offshore locations. Further studies may customise this methodology for various devices, deployment conditions and apply it at multiple project stages, from preliminary studies to advanced array design since it can be applied to a range of chart scales with appropriate level of detail.

## 1.5 Thesis structure

The overarching framework followed in this thesis is summarised in Figure 1.5 with all constituent chapters aiming to inform the development of the proposed methodology. The thesis is divided into four sections; the first section puts the research in context, the second section outlines methods used for system and sub-assembly reliability estimates, the third section addresses the aim of this research and the last section concludes the work by discussing the research outcomes.

Additionally, the thesis is divided into eight chapters. By identifying the underlying rationale, defining the objectives and highlighting the unique contribution of the research, Chapter 1 has set the premise for the research project.

Chapter 2 introduces the motivation and status of the offshore wind industry in the UK. It details the current applications of geospatial mapping and existing performance indicators in the OWE industry. Assessing the state-of-the-art turbine technology, it identifies the concept to be used for the scope of the research. An analytical description of the stochastic environmental processes and their consequent influence on system dynamic response is discussed and the range of industrial design methods and available reliability data are reviewed. Finally, the research question is described and an overarching methodology to achieve the aim of the research project is established.

Utilising available OWE failure statistics and suitable distributions, Chapter 3 conducts a reliability assessment for a generic OWT as an attempt to apply Stream 1 of the overarching methodology. It highlights the difference between failure frequency and consequence by including the costs for repairs and replacements. Results of this study show that due to the lack of location-dependant

failure statistics, it is not possible to address the research question using Stream 1.

Therefore, the Stream 2 methodology is discussed in Chapter 4 including a detailed description of the computer aided engineering tools used for dynamic response and fatigue analysis. The turbine of choice is also described along with its associated structural parameters with specific focus on the assembly of choice. Theory relevant to the accumulated damage postprocessing is also covered to provide a basic understanding of the involved methods for fatigue analysis.

Chapter 5 uses the structural model for the support structure of a fixed-bottom turbine to identify the critical node. In order to understand the relative significance of parameters influencing aero-hydro-servo-elastic simulations and post-processing of the loads on the structure, a sensitivity analysis is conducted.

Utilising the reliability-critical node and appropriate values for sensitivity-critical parameters discussed in Chapter 5, a structural dynamic response look-up table is produced and an extreme event analysis is conducted in Chapter 6 to facilitate site damage characterisation. These are then used for an analysis into the regional distribution of power production and accumulated damage metrics. To highlight the economic consequence of the combined damage-power metric, a simplified cost of energy analysis is finally conducted to conclude this chapter.

Chapter 7 expands the methodology developed for regional characterisation of key performance indicators such as power production, lifetime damage accumulation and damage per unit energy produced to the UKCS.

The thesis concludes with a discussion of the outputs in Chapter 8 whilst highlighting the usefulness of the proposed methodology to various stakeholders and its inherent limitations to identify avenues for further improvement.

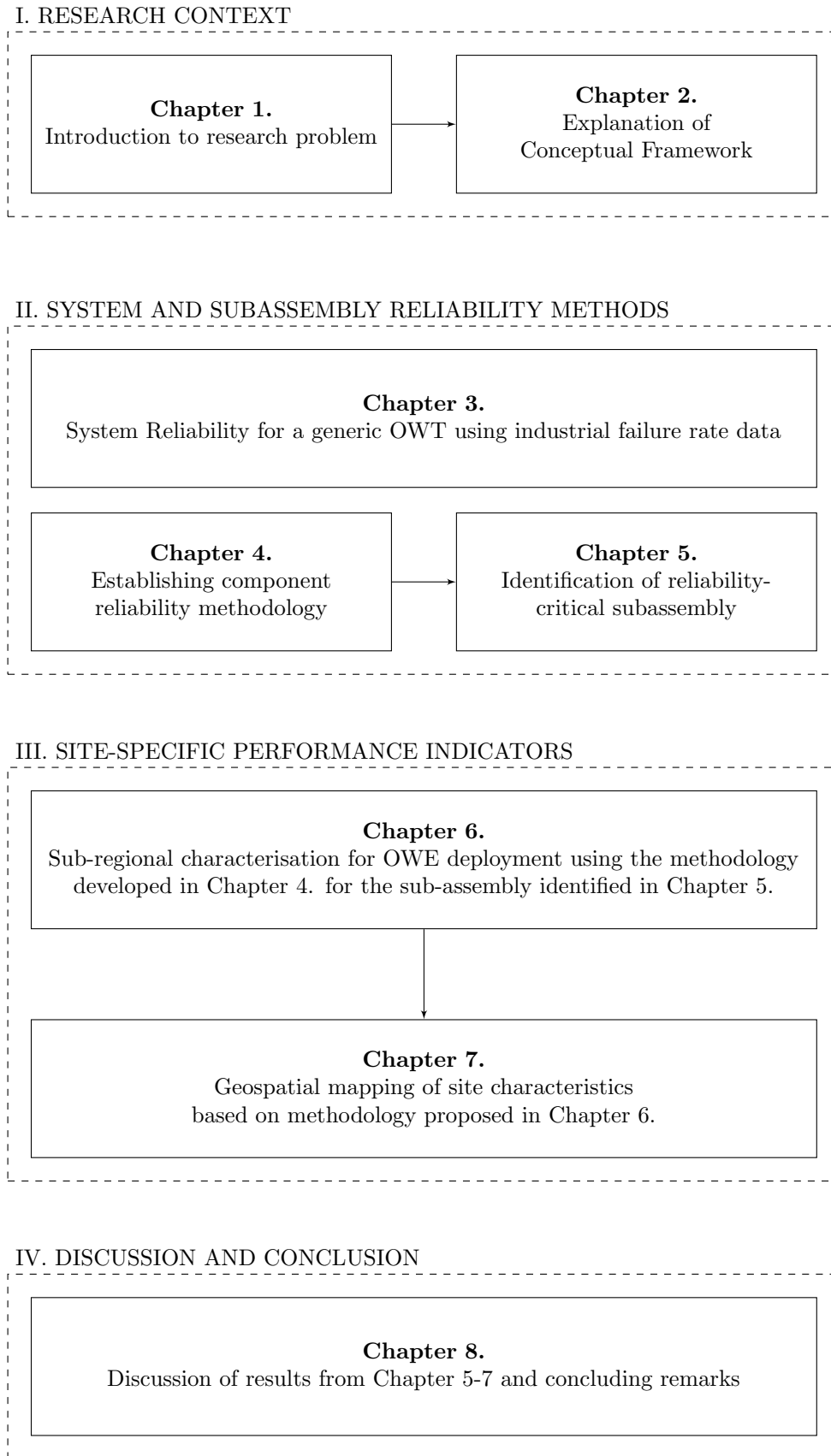


Figure 1.5: Flowchart outlining the structure of the thesis and the relationship between chapters.



# Chapter 2

## Conceptual Framework

### 2.1 The UK perspective on offshore wind energy

The UK has established itself as the global leader in the maturing OWE technology with 33 operational projects with a total of 1832 devices and an installed capacity of 7.11 GW (RenewableUK, 2018). In addition to low-cost decarbonisation, increase of renewable energy in the UK energy market provides security of supply to insulate consumers from volatility in the fossil fuel price. It also provides potential for attracting investment and producing local manufacturing jobs to rebalance the economy. Since 2013, the offshore wind sector has claimed its place as one of the UK's largest infrastructure investment pipeline with investments forecasted at £11.5bn from 2017 to 2021 (Infrastructure and Projects Authority, 2017).

Numerous financial, regulatory and innovation support initiatives have been set up to capitalise on the opportunity that offshore wind provides for the UK. This includes the world's first dedicated offshore wind fund for green infrastructure development, namely the UK Green Investment Bank Offshore Wind Fund. Together with its managed co-investment entities, it attracts new capital and creates a liquid market for operating assets to facilitate industrial growth through reduction in long-term financing costs as well as attracting new investors. The fund has interests in six operational wind farms with a collective capacity of 1.45 GW producing 4500 GWh of electricity per annum.

To fully unlock the UK's offshore wind potential, it is key to bring costs down by lowering the associated risks and increase deployment. The UK Renewable Energy Roadmap (DECC, 2011) analysed the state of the industry in 2011 and



gauged the offshore wind potential to identify possible trajectories the industry could follow up to 2020. LCOE for offshore wind was estimated at £149/MWh to £191/MWh in 2010 and was projected to reduce to between £102/MWh and £176/MWh for expected deployments of 18GW by 2020 to contribute to an overall 15% annual growth of renewable electricity. Further deployment potential was identified beyond 2020 with the possibility of having an offshore capacity of 40GW by 2030. The roadmap suggests that addressing engineering challenges to improve reliability will lead to a decrease in overall costs.

Based on the recommendation of the UK Renewable Energy Roadmap (DECC, 2011), in 2012 The Offshore Wind Cost Reduction Task Force was given the responsibility to build alliances, strengthen supply chain and foster innovation to reduce the cost by 30% to £100/MWh by 2020 (DECC, 2012). Financial support from the government, setting up a developers' forum to improve supply-chain management, managing conflicts with the oil and gas (O&G) industry, increase in offshore wind manufacturing facilities at the ports, risk reduction and coordinated grid development were identified as potential cost-reducing pathways. The overarching premise of these measures was to cement the UK's reputation as the leader in offshore wind to eventually export essential services in all stages of OWF lifecycle, development, construction and operation, to developing global markets.

Additionally, on the recommendation of the Task Force, an Offshore Wind Programme Board was established in 2012 based on successful models in other sectors like aerospace and O&G. This board brings together representatives from industry, The Crown Estate (TCE), UK government, Statutory Nature Conservation Bodies and other stakeholders to increase transparency and coordination within the industry to drive cost-reduction measures.

To support the renewables sector, the UK government introduced a reform in 2015 providing a guaranteed strike price for electricity produced from low-carbon energy projects. Competitive contract awards have undercut the support required by over a half within two years of the reform (Infrastructure and Projects Authority, 2017) thereby signalling effective cost-reduction. For OWE installations within the EU, tender-based support schemes from 2010 to 2015 resulted in a final contract cost in the range of €103.2 /MWh at Horns Rev III in Denmark and €186.1 /MWh at Dudgeon in the UK (European Commission, 2017b). By 2017, three of the four winning projects for the bidding round in Germany were auctioned with-

out a subsidy (Bloomberg, 2018). However, these subsidy-free bids by Orsted and Energie Baden-Württemberg AG were enabled by the extended project realisation window of 2024 which would allow the developers to deploy next generation of larger, cost-effective wind turbines of 13-15MW.

In the UK, as of 2017, the second Contract for Difference (CfD) auctioned 3GW of offshore wind at half the contract cost of the first CfD auction in early 2015 in the UK. With low prices of £57.50/MWh (McCrone et al., 2018) the contracted projects, namely HornSea Project 2 and Moray Offshore Windfarm (East) (BEIS, 2017), are to be delivered in 2022-23. At the next scheduled CfD auction, due to take place in the second quarter of 2019, a subsidy of less than £2/MWh is expected (Department for Business Energy & Industrial Strategy, 2019). Therefore, further cost-reduction through improvements in reliability, maintenance and power capture are expected to deliver these projects. While such subsidy-free deals for OWE have already been concluded internationally (Bloomberg, 2018), being on the verge of near-zero contracts is a breakthrough moment in the UK due to higher contract costs since the cost of grid connection is also included at the auctions.

Using macro vitals, energy imperatives, policy enablement, project delivery and technology potential as markers, Ernst and Young determine renewable energy country attractiveness indices. In 2015, the UK topped the attractiveness index for offshore wind based on this analysis and currently, the UK has climbed up three places to achieve the seventh place in the biannual top 40 ranking in 2018 for all renewable energy generation (Energy Voice, 2018). Despite being derided for its exorbitant costs, the steep learning curve of the industry has allowed it to become financially competitive with new nuclear energy (Harrabin, 2017) as well as new gas-fired power stations (Evans, 2017) in a relatively short period of time.

### 2.1.1 UK offshore regional characterisation

The UK government provides robust and stable policy backdrop for the OWE industry growth in the UKCS complimented by the proactive involvement of the landowner, namely TCE. Since the enforcement of a statutory Transfer Scheme in April 2017, the management of Crown Estate assets in Scotland was devolved from the UK level to a public corporation, namely Crown Estate Scotland for the interim period until new legislation sets out a permanent arrangement. TCE

continues to manage the marine assets in England, Wales and Northern Ireland.

To identify the region where OWTs can be deployed in the UK, it is important to distinguish between marine regions, namely, the UKCS, Exclusive Economic Zone (EEZ), Renewable Energy Zone (REZ) and the territorial waters. The territorial waters, as defined by the United Nations Convention on the Law of the Sea (United Nations, 2001), is a 12 nautical mile belt around the coast where the country can exercise its jurisdiction.

Beyond the territorial waters exist the EEZ and UKCS which differ in geographic and legal terms. The continental shelf of a coastal state is the part of the continental margin with shallow waters of up to 200 m extending beyond the territorial sea and demarcated by the shelf break. While this may geographically lead to shelf regions of up to 400 nm, the maritime EEZ is limited to a distance of 200 nm. Updated UKCS and EEZ boundaries along with the territorial sea limits and renewable energy zones can be found on the UK government website (UK Hydrographic Office, 2015).

A truly maritime nation with a 7,723 mile coastline, the UK has sovereign rights over the fifth largest EEZ (188 nm beyond territorial sea) when the 14 Crown Dependencies and Overseas Territories are included. With exploration and exploitation rights to all subsea and energy resources, the ultimate limit for wind and wave resource exploitation by the UK is marked by the EEZ (UKNDA, 2016).

While Round 1 and 2 lease rounds provided access to wind resource within the territorial waters, the introduction of the Energy Act (Parliament of the United Kingdom, 2004) established an REZ adjacent to the territorial waters allowing Round 3 lease sites to explore resource further away from shore. The REZ, EEZ and UKCS are repeatedly used as interchangeable terms in literature, this thesis considers the largest of the three, namely, the UKCS as the potential deployment region to incorporate any future extension of the REZ.

Regional categorisation of the UKCS based on characteristic wind speed and wave height (Fugro GEOS, 2001) yields eight major sub-regions with the more dynamic West Shetland Shelf, Hebrides Shelf and Northern North Sea and the benign Irish Sea and Southern North Sea. Also included are the Central North Sea, English Channel and the Celtic Sea.

### 2.1.2 UK Offshore wind lease rounds

Currently, three lease rounds and their respective extensions have awarded 62 projects with a combined capacity of 12.97 GW (RenewableUK, 2017), whereas, Round 4 is expected to start in early 2019 after gathering feedback from potential leasing process partners.

#### 2.1.2.1 Existing rounds

Since 2011, the TCE has awarded lease rights to 77 projects through six cycles providing an initial five-year agreement to allow offshore wind developers to acquire necessary consent, appropriate engineering support and gather financial resources (The Crown Estate, 2014). Once successful, the stakeholders are awarded a fifty year lease of the site for the operational stage of the project.

The first established site for offshore wind deployment was at Blyth in 2000 for testing of devices with a total capacity of 4 GW, whereas, in October 2018, Walney 3 Extension, a project rated at 657 MW in the Irish Sea (WindEurope Business Intelligence, 2019), was officially inaugurated as the largest existing offshore wind project globally.

Figure 2.1 shows the distribution of existing sites based on the cycles of project awards. It can be observed that Round 3 lease sites are further offshore due to the current constraints on sea space due to competition with shipping lanes, fishing grounds and environmental conservation. Additionally, the first two rounds were sited in the territorial waters with a distance to shore less than 12 nm and water depths of up to 20 m (Carbon Trust, 2008). However, the 32 GW Round 3 (RenewableUK, 2010) and successive rounds move further offshore with increased water depths. This is expected to cause an increase in engineering challenges, increase associated risk and make projects more capital intensive than earlier lease rounds.

#### 2.1.2.2 Future rounds

Applying the current coastal buffer zone of 7 nautical miles and eliminating UKCS use by competing industries leaves 5,900 km<sup>2</sup> of available seabed for OWE deployment. 88% of this area is over 60 nautical miles away from the shore and 80% at depths of between 40-60m (Carbon Trust, 2008), therefore, future lease rounds are

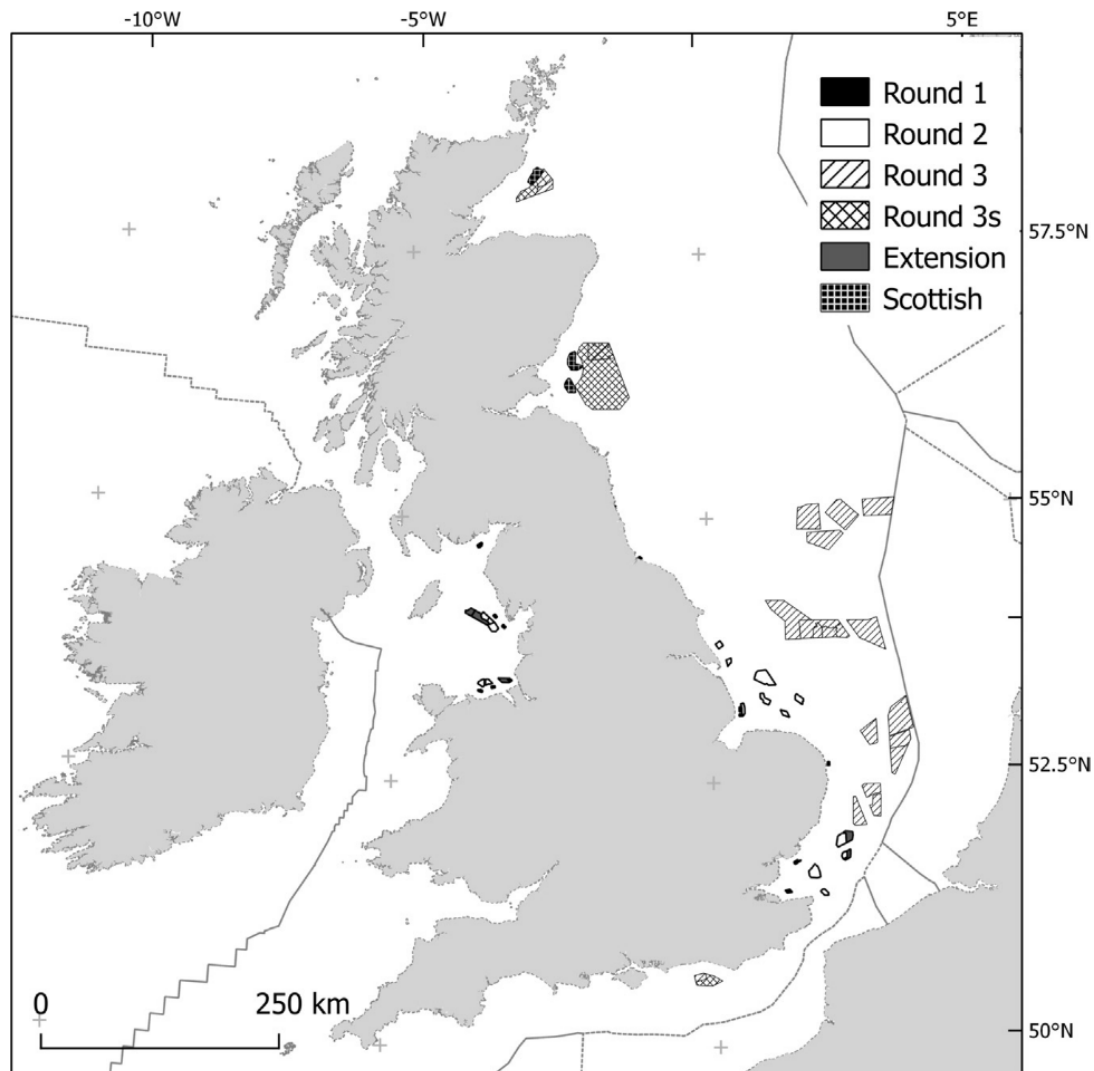


Figure 2.1: Offshore wind farm deployment locations in the UKCS differentiated based on lease rounds, indicating the larger scale of Round 3 projects relative to earlier deployments (Willstead et al., 2017).

likely to be based in these locations.

The existing practice (The Crown Estate, 2018c) in TCE utilises the following four step process for the characterisation of the areas of the seabed to inform future lease site allocation:

1. Technical resource model - Identification of regions in the UKCS based on two key aspects affecting OWE development, namely, depth and accessibility. This reduces the considered regions to those with water depth between five and 50 m and suitable weather windows to conduct maintenance interventions for 80 percent of the time.
2. Exclusions model - Hard constraints precluding the development of OWE projects such as O&G infrastructure, shipping routes and traffic separation schemes (The Crown Estate, 2018b).
3. Restrictions model - Soft constraints such as disposal sites, commercial fisheries and conservation regions.
4. Characterisation areas - Choice of 50 percent of the area of the least constrained regions after the combination of the results of the first three steps. This area is then divided into 18 characterisation areas which are further investigated for the feasibility of inclusion in Round 4 of the leasing process.

While Step 1 identifies suitable locations based on technical feasibility, Step 2 and 3 eliminate exclusion zones to produce the characterisation regions as shown in The Crown Estate (2018a). The resulting 18 characterisation regions can be distinguished in Figure 2.2.

Of the 18 characterisation areas, five have been proposed to be included in the Round 4 tender process including Dogger Bank, Southern North Sea, East Anglia, North Wales and Irish Sea (The Crown Estate, 2018c). An additional four regions are under consideration due to higher uncertainty associated to the development opportunity and will be included subject to further feedback from stakeholders. These include the Yorkshire Coast, The Wash, South East and Anglesey. The remaining nine regions have been excluded based on the spatial constraints assessment and feedback from statutory stakeholders.

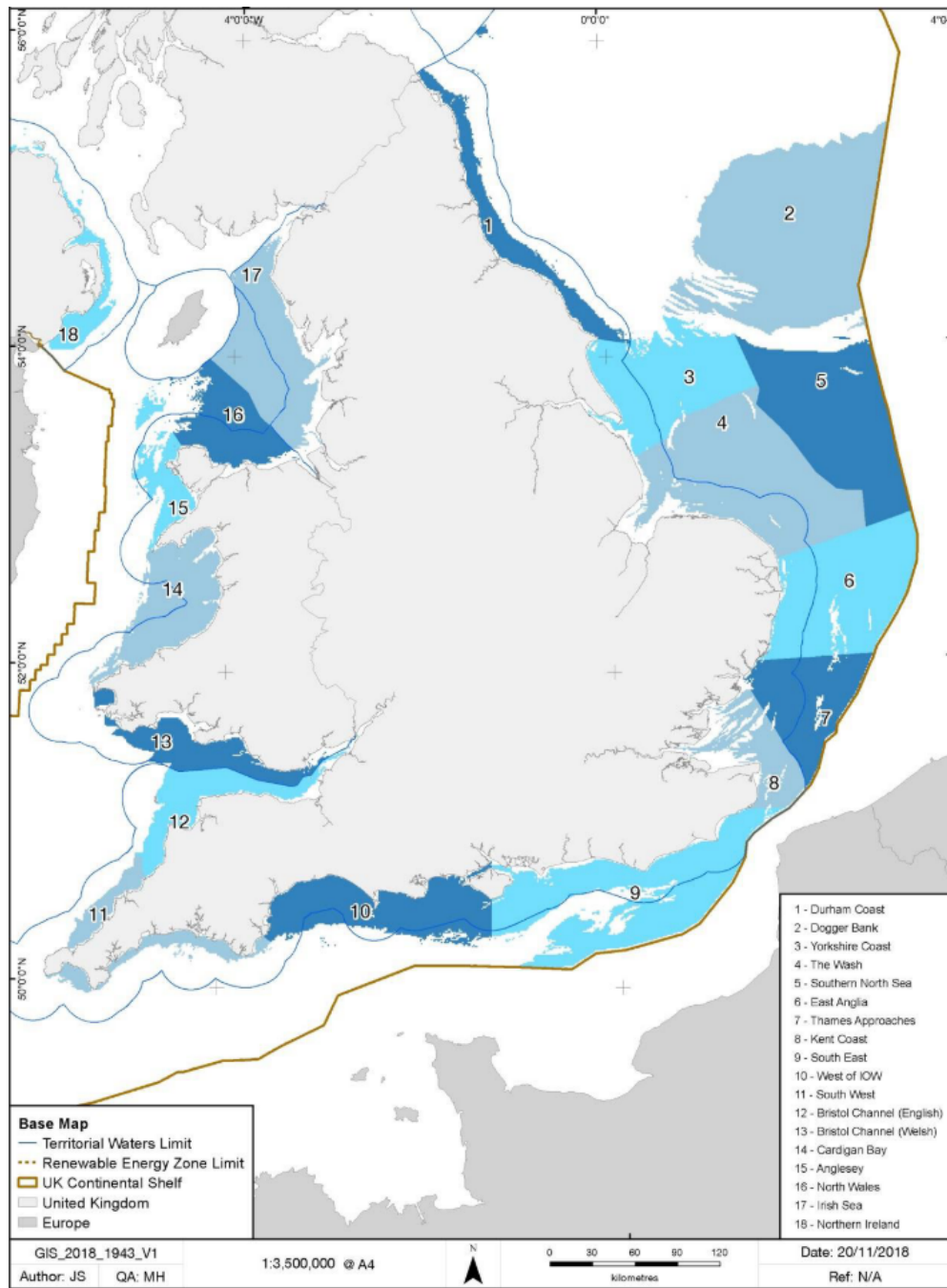


Figure 2.2: Characterisation areas based on resource and constraints assessment for Round 4 of OWE lease by The Crown Estate (2018c).

## 2.2 Geospatial applications in the OWE industry

Site selection for OWE devices requires the consideration of a comprehensive set of geographical factors including wind profile, wave regime, depth and distance to shore through a Geographic Information System (GIS) by suitable supporting framework for the geospatial analysis.

### 2.2.1 Geographic Information Systems

GIS is a computational tool which allows for flexible data description and manipulation at different levels of spatial analysis to explore and identify the interrelations between digital data for multi-level planning and decision making. The results of the analytical spatial analysis may be stored as a geographic database or compiled into spatial data maps.

Based on the premise that a digital map is an organised set of numbers, location of map features can be represented numerically. Similar to graphics design, data in GIS may broadly be divided in two different data models, namely, vector and raster. In a vector data model, geographic features are represented geometrically by elementary entities of points, lines or polygons in a chosen projected coordinate system. In a raster data model, the geographic space is divided into a grid of cells and the location of a feature is implied by its position in the matrix.

With their associated strengths and weaknesses, it is important to identify the data format most suitable for the needs of the project. While raster datasets are suitable for performing geospatial algebraic calculations, vector datasets are appropriate for storing features with a set of attributes that characterize them and improve cartographic representation. Due to the structure of available GIS data and significance of extracting the environmental characteristics for OWE, the geodatabase of this project deals in raster representation.

### 2.2.2 Existing applications

Existing applications of geospatial tools in the OWE industry provide information for various purposes including:

**Extent of exclusion zones due to competing activities and conservation regions.** The significant spatial limitation for OWE deployment due to



hard and soft constraints is analysed by The Crown Estate (2018b) using a multi-criteria GIS analysis tool. Exclusion zones could be allocated due to potential disruption to existing hotspots on major commercial shipping routes, the vicinity to subsea cables, fishing and offshore mining activities. Protected areas based on the World Marine Heritage sites and World Database on Protected Areas could provide an indicator of limitations on OWF siting based on environmental conservation factors (Bosch et al., 2018; The Royal Society for the Protection of Birds, 2010).

Discussion of the aforementioned and additional factors for determining exclusion zones for OWF deployment are discussed in detail for Hong Kong in the existing screening for proposed development sites (Hong Kong Offshore Wind Limited, 2006).

**OWF lease site and project locations.** Available basemap layers of the UKCS produced by the Department of Energy and Climate Change (DECC) (The Crown Estate, 2017) provide shape files for the OWE lease sites as well as planned and installed OWFs in the UKCS. Based on Figure 2.1, it can be seen that most installations are off the east coast with a particularly high density in the Southern North Sea. The Irish Sea boasts additional projects, whilst, planned installations in the English Channel and Celtic Sea have been delayed or cancelled.

**Dominant environmental parameters and bathymetric characterisation.** Numerous available metocean databases provide information regarding the environmental parameters in the UKCS. The ABP Marine Environmental Research Ltd (2008), commonly referred to as the Renewables Atlas, has established itself as the primary tool for identification of potential offshore renewable deployment sites based on a single parameter: the resource potential. Once the usefulness of the Atlas was discovered after its initial publication in 2004, an enhanced version with a larger underlying dataset, finer data resolution and improved statistical outputs was published in 2007. The Atlas provides numerous parameters for wind, wave and bathymetric conditions using meteorological and oceanographic models. Figure 2.3 shows the geospatial distribution of the average annual wind speed, significant wave height and water depth for the UKCS based on the ABP Marine Environmental Research Ltd (2008).

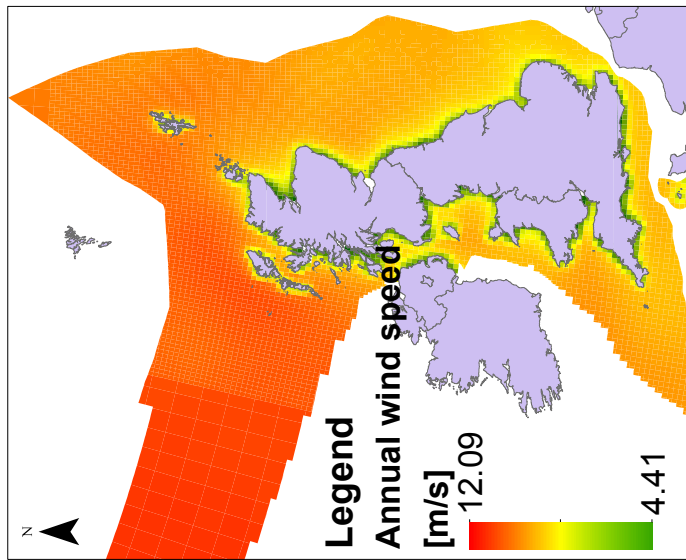
Peak wind speeds across all sub-regions in the UKCS are predominantly in the range of 24.5 m/s - 32.7 m/s, with a south-westerly and westerly wind di-

rection. The wave direction and peak wave height show more variation with the former generally in agreement with the wind direction except when storm tracks and bathymetric conditions influence the wave growth. The peak wave heights are in the range of 6.0 - 16.5 m and show little correlation with the wind speed, therefore, it may be said that additional oceanographic factors are at play as further discussed by DECC (2009). Bathymetric considerations for tethered and fixed installations are mapped in the non-technical summary of the Offshore Energy Strategic Environmental Assessment by DECC (2016).

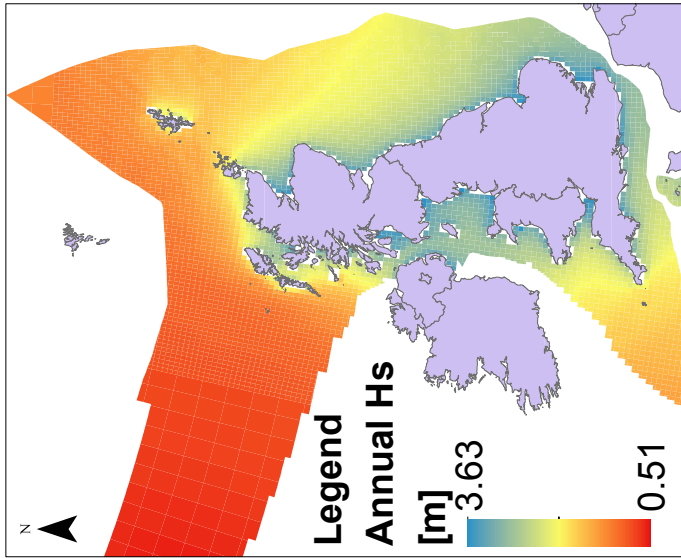
**Identification of the offshore wind resource potential.** Bosch et al. (2018) calculates the seasonal generation potential of 157 countries accounting for exclusion zones due to submarine cables, water depths greater than 1000 m and protected areas based on the appropriate turbine class deployment. The NASA MERRA-2 reanalysis data (Gelaro et al., 2017) with 35 years of hourly global wind speed estimates is used for the global country-level energy potential at a spatial resolution of  $0.5^\circ \times 0.625^\circ$ .

While comparison with previous studies (Lu et al., 2009; Arent et al., 2012; Dupont et al., 2018) shows that this study overestimates the global energy potential due to the increase in spatial scope of OWF deployment up to water depths of 1000 m. On the contrary, the potential for Europe (European Environmental Agency, 2009), USA (Walter Musial et al., 2016), UK (Cavazzi and Dutton, 2016) and India (Nagababu et al., 2016) is underestimated due to the use of lower energy density estimate and reduced spatial feasibility.

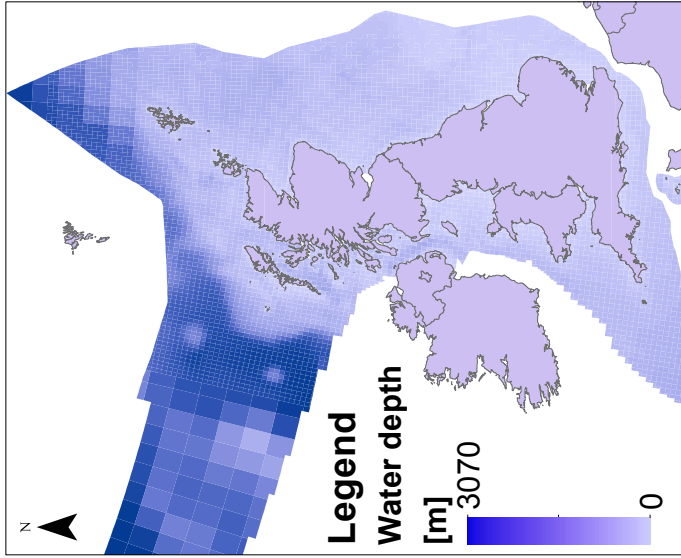
**Decision of turbine type.** Existing research (Bosch et al., 2018) utilises the annual wind speed class characterisation, based on the International Electrotechnical Commission (2005) categorisation, to identify suitable wind turbine classes to be deployed at the EEZ of European countries. Based on this, it is recommended that the offshore regions within the UKCS characterised by average annual wind speed  $\geq 10$  m/s and power density  $\geq 450$  W/m<sup>2</sup> should be populated with Class I turbines to ensure higher device reliability. However, use of annual average wind speed data leads to loss of details of temporal variability which provide significant information about the structural loads experienced by the structure.



(a) Annual average wind speed at 80 m height from mean sea level



(b) Annual average significant wave height



(c) Water depth

Figure 2.3: Average environmental parameters including wind speed, significant wave height and water depth for the UKCS pertinent to OWE based on data from ABPmer (2008).

### 2.2.3 Relevant geographic parameters for offshore wind

Existing cost driver analysis of OWE argues that site characteristics and industrial evolution are at the heart of LCOE which also displays sensitivity to technological assumptions and exogenous factors (The Crown Estate, 2012).

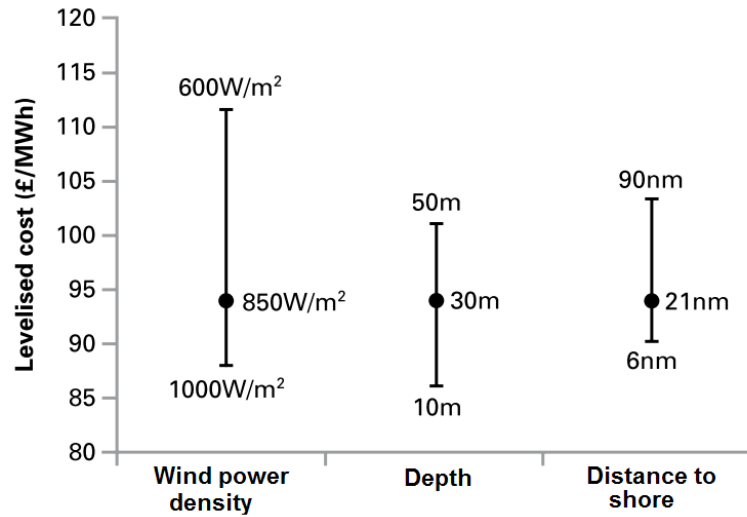


Figure 2.4: Sensitivity of LCOE to main cost drivers with ranges showing the impact of varying wind power density, depth and distance from shore while keeping the other variables constant to calculate the mid-point levelised cost (Carbon Trust, 2008).

The increase in risk and return associated to future OWE projects deployed at locations further offshore may directly translate into a variation in farm performance. Currently explored physical parameters influencing LCOE are displayed in Figure 2.4, however, an ideal metric for OWE performance should incorporate the influence of multiple parameters to provide sufficient insight into the risk and return associated to installations at various sites.

Based on Figure 2.4, location-intelligent siting for improved LCOE may be achieved by harvesting the improved wind resource at locations further offshore whilst minimising the associated increase in CAPEX due to increased depth and OPEX due to increased distance-to-shore.

However, a cost reduction pathways study for the UKCS argues against the popular belief of increased LCOE for OWF projects in deeper waters further offshore (The Crown Estate, 2012) since the benefits of higher energy production may be sufficient to counter the increased structural risk. This is supported by a study

showing the influence of the technological advancements on four sites representative of OWFs deployed at Round II and III lease sites in the UKCS (The Crown Estate, 2012). Furthermore, an analysis of early offshore installations (Feng et al., 2010) have shown little correlation between availability and distance to shore with Kentish Flats exhibiting a lower availability than deployments further offshore such as North Hoyle.

Therefore, optimal siting in the OWE industry should be based on inclusion of all site-dependent factors contributing to power output, CAPEX, OPEX and decommissioning and disposal (D&D), thus, overall LCOE. Ideally, high resolution spatial and temporal environmental data should be processed to inform the power production, optimum turbine design, weather windows and reliability prediction for O&M activities as well as life extension decisions. To this purpose, a metric which combines site-specific risk and return parameters using long-term representative data may prove to be useful to improve available geospatial information for location-intelligent siting of future projects.

### 2.3 Wind turbine performance indicators

There is a broad range of existing Key Performance Indicators (KPIs) for comparison of turbines located in different regions covering aspects of performance, reliability, maintenance, finance and safety (Gonzalez et al., 2017). Industrial stakeholders have expressed the need for the KPIs to be relevant, specific, measurable, comparable, standard and finally traceable for various timescales. This section discusses relevant metrics for the turbine power production which can be used for a wider comparative location-based analysis.

#### 2.3.1 Availability

Availability is predominantly used in the OWT industry to indicate the potential of a turbine to generate power. This performance indicator has applications for energy estimates, design performance evaluation and warranties. Due to its widespread use in divergent disciplines, a broad spectrum of calculation methodologies exist for describing the availability parameter. A comprehensive understanding regarding the the distinctions between various availability descriptions

can be attained through the DNV GL white paper (2017). In the absence of an internationally accepted standard definition of availability (Harman et al., 2008), the industry generally converges at the adoption of two main definitions:

- System availability - Technical availability of an OWT expressed as the percentage of time a device is available to generate electricity relative to its theoretical maximum
- Turbine availability - Commercial availability for performance assessment of an OWT, whereby, downtime for selective parked conditions may be ignored for cross-industrial comparison

Whilst the former definition is largely significant for the academic community, the latter is highly discussed between wind farm owners and manufacturers. With the understanding that system availability is always lower than turbine availability since the latter may exclude influences from severe weather, requested stops, scheduled repairs etc, only the system availability is used to characterise this performance metric for the scope of this thesis. This is because weather variables are the investigated parameters for farm siting in this research and the effects of these are excluded for the latter definition.

Given a set of operational data, availability may broadly be described as a ratio of time or energy. A generic time-based description of availability can be seen in Equation. 2.1.

$$\text{Time - based availability} = \frac{\text{Time available [h]}}{\text{Total time in consideration [h]}} \quad (2.1)$$

With the associated ease of calculation, the time-based availability does not capture the temporal wind speed variation, therefore, does not provide the weighted benefit of turbine availability during high wind speeds.

Time-based availability may be further characterised based on the total time considered. The full-period availability allocates the entire period for which availability is calculated to the total time in consideration, whereas, the wind-in-limits availability attributes only the period of time where the wind speed is within operational range. Therefore, the wind-in-limits availability provides a more meaningful representation of the performance of the turbine and is used for DNV GL full-fleet availability audits (DNV GL, 2017).

The production-based availability provides an improved estimate of the loss factors by quantifying the ratio of energy as seen in Equation. 2.2 which has a direct impact on the cost of energy.

$$\text{Production - based availability} = \frac{\text{Energy produced [kWh]}}{\text{Energy potentially expected [kWh]}} \quad (2.2)$$

By accounting for the wind speed, the production-based availability encapsulates the influence of turbine reliability and is the performance indicator of choice for the System Performance, Availability and Reliability Trend Analysis (SPARTA) project (discussed in Chapter 2.7.2).

While production-based availability provides an improved estimate of availability displaying variation of up to 2% from time-based estimates, it requires a high fidelity data set and is more computationally intensive. For most cases, the wind-in-limits availability provides statistically equivalent estimates to the production-based availability, therefore, can be used as a viable alternative with its associated benefit of reduced data requirement.

### 2.3.2 Capacity factor

Wind turbine performance is widely represented by the Capacity Factor (CF) which is a measure of the ratio between the energy generated and the energy which would be generated if the installation was generating at its rated capacity. Described as a function of energy yield and rated annual power production (Equation. 2.3), it is generally higher for offshore installations relative to onshore turbines (Kaldellis and Kapsali, 2013).

$$\text{CF} = \frac{E^{ann}}{P \cdot 8760} \times 100\% \quad (2.3)$$

Where, CF is the annual capacity factor,  $E^{ann}$  is the actual annual energy production and P is the turbine rated power.

OWTs are expected to have a higher power production forecast than onshore installations (Lynn, 2012). Fleet-wide average capacity factors for OWTs have demonstrated an increase from 30% in 2005 to almost 40% in 2018 with some individual projects achieving up to 50% (The Crown Estate, 2019).

Comparative analysis of annual capacity factors based on three year experience with the Round I offshore wind installations reported under the *Offshore wind capital grants scheme* by the UK government (Feng et al., 2010) shows that it

varies between 24.1% to 35% between four wind farms in the Irish Sea and Southern North Sea. The mean monthly capacity factors for the Round 1 farms is at 33.6% which is 8% larger than onshore farms with installed capacities in excess of 100 MW (Crabtree et al., 2015). For Round 2 installations, a further increase in the mean monthly capacity factor to 38.3% is observed with peak monthly capacity factor at 75.8%.

A wind farm with higher capacity factor also exhibits high availability and contributes to the reduction in cost of energy. Therefore, the above studies imply that an improvement in capacity factor in future rounds could improve the LCOE. However, it must be noted that a lifetime capacity factor analysis is a more definitive indicator of the turbine performance since it eliminates annual variables.

### 2.3.3 Reliability

The significance of reliability for the OWE sector is widely promoted (Ferguson and M. Kühn, 1998). O&M expenditure for OWTs may be up to three times higher than onshore wind turbines (Rademakers et al., 2003; Walter Musial and Ram, 2010), leading to a contribution of over 20% to the overall lifetime project cost (Blanco, 2009). The drive to reduce LCOE consequently leads to the requirement of a high reliability for turbines operating in harsh environmental conditions.

Reliability primarily depends on the wind turbine manufacturing process and is intrinsically predictable based on the expected environmental conditions the turbine is exposed to. While onshore wind turbines experience failures 1 - 3 times annually (P. Tavner et al., 2007), the expected failure rate for OWTs in early research was 0.5 failures per turbine annually (Spinato et al., 2009) subject to planned maintenance of the farm. However, data from the offshore industrial experience shows that the average failure rate for an OWT is 8.3 failures per turbine annually (Carroll et al., 2015).

A significant outcome of the ReliaWind project argued that while reliability is important for onshore wind turbines, it is a critical parameter for OWTs (Wilkinson and Garrad Hassan & Partners Ltd, 2009). Reliability nomenclature and calculation methodologies are further discussed in Chapter 3.



## **2.4 Stakeholders and technological specification**

Innovation in OWT designs continues parallel to the optimisation of designs for improved performance partly due to the involvement of a consistently larger number of manufacturers in the industry and also due to the requirements of individual deployment sites. The wind turbine industry has also shown considerable interest in the cost and performance differences arising from the deployment of various turbine concepts (Henk Polinder et al., 2006; Stefan Faulstich and Hahn, 2009).

### **2.4.1 Wind turbine manufacturers**

The weakening of the pound relative to the euro, rising labour and other commodity prices as well as the lack of competition in the offshore wind market contributed to the increasing turbine prices between 2000 and 2008 (UK Energy Research Centre, 2010). At the time, Siemens and Vestas were the two major companies involved, however, the entry of General Electric, Mitsubishi, Clipper, Acciona, Nordex placed downward pressure on the wind turbine prices. Current major developers in the the UK offshore wind industry are identified in existing publications (The Crown Estate, 2014) and their proportionate global market share can be seen in the tree diagram in Figure 2.5 based on data from the Wind Monitor established by Fraunhofer Institute for Energy Economics and Energy System Technology (2018).

It can be seen that Siemens had the largest market share, with 61% of the overall global share and 47% of the new installations in 2017, while MHI Vestas was the second biggest player in the global offshore market with 859 new turbines deployed. Numerous prototypes and functional models (DNV GL, 2016b; Marijuán, 2017; Ehrnberg, 2017; DTU Wind Energy, 2018) in their early stages of development constituted about 5% of the market share. However, they are expected to contribute to the competition of the market in the near-future to curtail the monopoly of the larger firms and drive down costs. As of 2018 the top 3 companies, namely Siemens, Vestas and Senvion, together represent 98% of all turbines installed with a marked increase in Siemens market domination (WindEurope Business Intelligence, 2019).

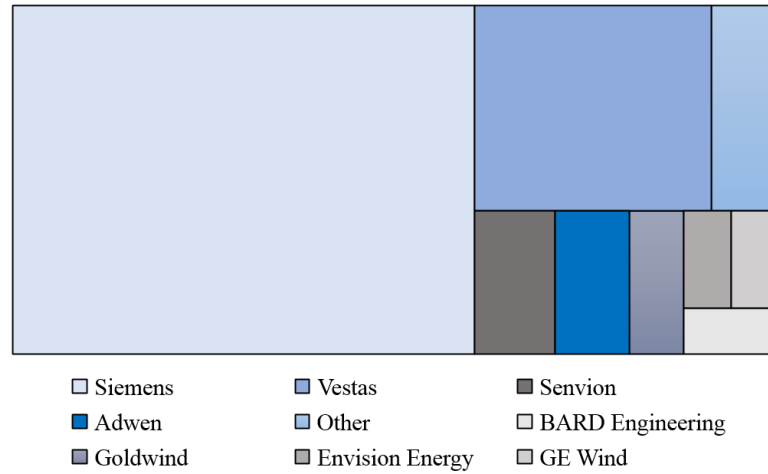


Figure 2.5: Proportion of turbine numbers in the global market share by various manufacturing companies based on data collected by the Wind Monitor in 2018 (Fraunhofer Institute for Energy Economics and Energy System Technology, 2018).

### 2.4.2 OWT taxonomy

To eliminate possible confusion regarding constituent components when discussing various OWT subassemblies, the taxonomy used in this thesis is based on British Standards Institution (2009) as shown in Figure 2.6. A horizontal axis wind turbine can broadly be divided into the rotor-nacelle assembly (RNA) and the support structure.

The RNA is composed of the rotor, hub, blades and the nacelle housing the generator and drive train (Natarajan, 2016). The supporting structure is divided into the tower, transition piece, platform, substructure and the foundation. For some structural design tools, the transition piece and the platform are not distinguished, however, Figure 2.6 shows them as individual subassemblies.

Each assembly of the OWT experiences and contributes to loading. The structural subassemblies, including the RNA structural subassemblies and support structure, of the OWT experience wind loading whereas, the latter is additionally exposed to wave and current-induced loading for submerged parts (British Standards Institution, 2009). Although the wind acts along the length of each blade, the blade root is exposed to maximum loading due to torsional forces. For nacelles with an active yaw system, wind direction sensors produce torque to rotate the nacelle against the stationary tower exerting axial yaw bearing loads. Due to the load-bearing nature of the support structure, it must be designed to withstand

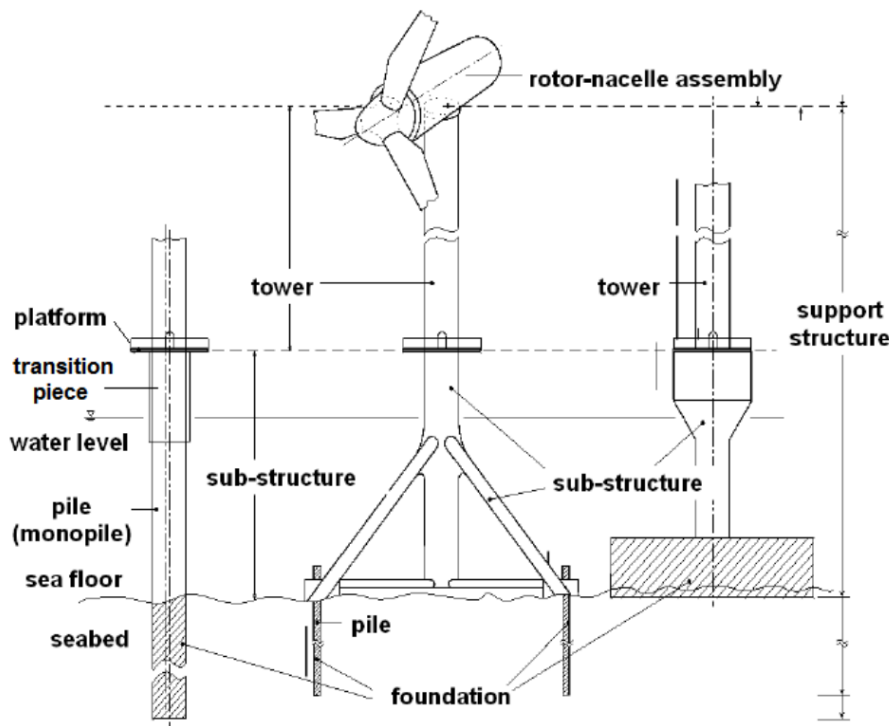


Figure 2.6: Wind turbine configuration taxonomy standard followed for the scope of this thesis (British Standards Institution, 2009).

the weight of the RNA, mechanical loads like yaw loads as well as environmental loads in addition to fatigue causing repetitive fore-aft motion and vibrational loads. Structural elements must be designed to facilitate the transfer of loads to the ground safely and durably.

### 2.4.3 Foundation Concepts

Foundation elements may be described as design components through which the support structure is connected to the seabed and they facilitate the transfer of the loads on the structure safely and durably into the ground. Figure 2.7 is a pictorial description of some available concepts in the market along with a reference onshore turbine. It is in no way an exhaustive description of the available fixed-bottom OWTs which include gravity, suction caisson, tripod and tripile concepts, however, it does display the inherent deployment limitations faced by fixed-bottom structures due to cost implications.

Figure 2.8 categorises the global distribution of wind turbine projects based on foundation concept. The size of each bubble corresponds to the capacity (MW) of the project, therefore, it can be seen that monopiles are the predominant design

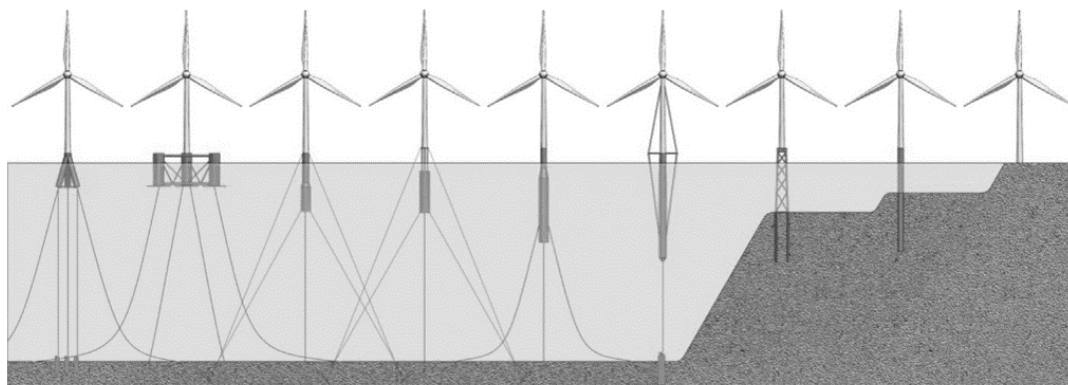


Figure 2.7: Illustration of various turbine foundation concepts, left to right: Tension leg platform, Semi-submersible, Tension leg Buoy, Spar buoy, Tension leg spar, Jacket, Monopile, Onshore reference (adapted from Myhr et al. (2014))

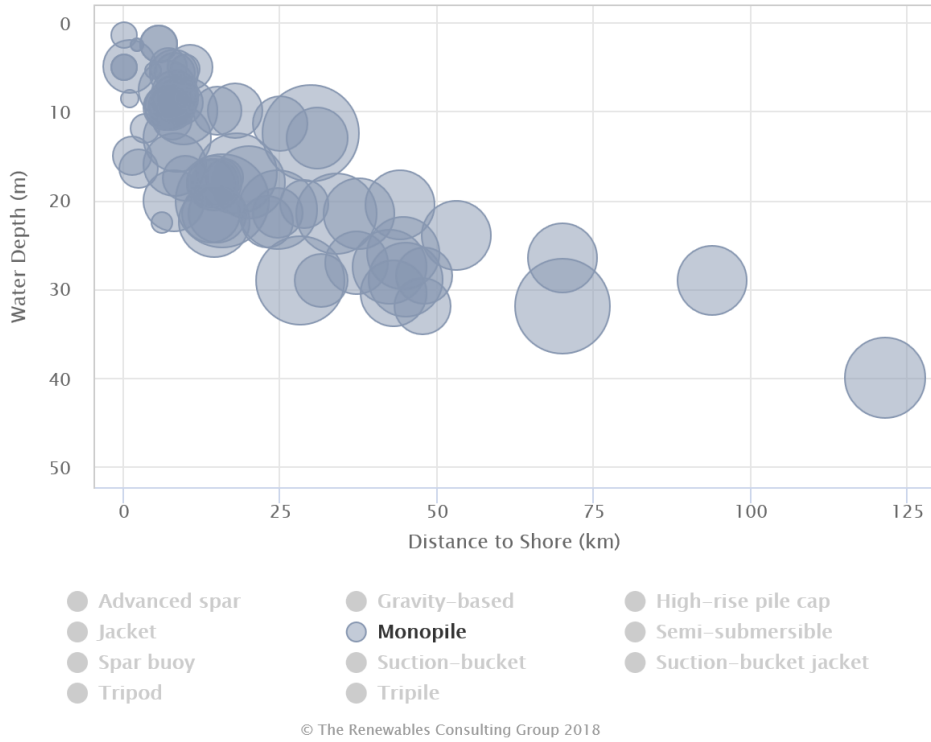
concept.

Conventionally for water depth between 30 to 50 m, the more capital intensive jacket foundation is believed to provide a suitable opportunity to harness wind energy, however, for further increase in depth, it does not provide an economically feasible option.

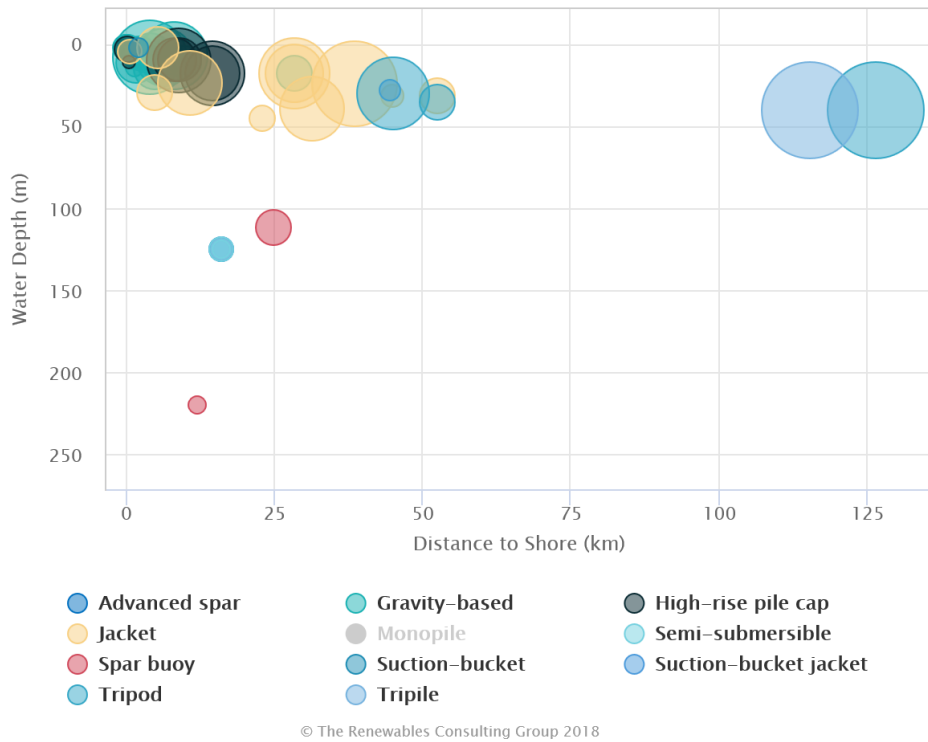
To utilise the improved wind resource further offshore in water depths  $> 50$  m, floating OWT concepts provide a viable alternative. Reduced wave loads and installation costs make floating offshore wind a lucrative avenue for the OWE industry to advance in. For floating wind the technical feasibility of most concepts has been demonstrated, therefore, the current focus of the industry is to increase the Technology Readiness Level (TRL) whilst reducing the cost of energy.

However, monopiles continue to dominate the market due to their quick and easy fabrication process with reduced complexity which allows for high serial production. Of foundations installed in 2018 in Europe, 49% were supplied by EEW Special Pipe Constructions GmbH (WindEurope Business Intelligence, 2019) of which 80% were monopiles.

The monopile reaches its engineering limit with respect to feasible geometric features like pile thickness, length and diameter at depths between 25-30 m. However, with the introduction of XL monopiles (Hermans and Peeringa, 2016), these application limitations have been shifting. To accommodate increase in turbine sizes and forge into deeper waters of the lease sites further offshore, Ramboll has



(a) Monopile



(b) Other foundation concepts

Figure 2.8: Depth, distance-to-shore and project size for various foundation concepts of OWFs based on Global Renewable Infrastructure Project database (The Renewables Consulting Group, 2018)

designed 150 monopiles for the Gemini wind farm in the Dutch waters catering to depths of up to 37 m for 6 MW turbines (Ramboll Group, 2018). Monopile diameters have been increased to achieve appropriate stiffness levels and ensure structural integrity of the turbines.

In Europe, 81.9% of all turbines are supported by a monopile. While still the dominant concept in Europe in 2018, monopiles represented 66% of the used foundation concept down from 86% in 2017 (WindEurope Business Intelligence, 2019) representing a move into deeper waters where the feasibility of jacket deployment is higher. Jackets were preferred for Beatrice 2, East Anglia 1 and Aberdeen OWF in 2018 leading to a rise in percentage of jacket deployment.

The Offshore Wind Cost Reduction Task Force Report (DECC, 2012) highlights the value of having reliable turbines requiring fewer maintenance visits towards cost-reduction and safety. In particular it identifies various avenues for cost-reduction pertaining to foundations including:

- streamlining the supply-chain of foundations to remove project bottle-necks;
- encouraging innovation to develop and adopt new foundation concepts particularly in water depths greater than 30m;
- identifying foundation concepts with potential for serial manufacturing;
- providing improved access to test sites for timely foundation testing;
- encouraging integrated cost-optimised design approach to the turbine system; and
- facilitating load data access at earlier design stages (pre-consent) to inform turbine design.

By addressing these issues, it may be ensured that the fabricated foundations provide sufficient support to withstand stochastic loading on the structure whilst achieving further cost reductions.

## 2.5 Stochastic processes

Design challenges for an OWT due to the stochastic environment have increased with the size of the turbines and discovery of more dynamic installation sites

(Veers and Butterfield, 2001) as the application of large safety margins becomes more expensive. Similarly, inaccurate estimation of loads leading to failures (Dalryn et al., 2017) mandates improved structural load modelling utilising detailed environmental data.

Environmental loads on structures and their resulting responses vary in the time domain, therefore, the data can be displayed as analog time series signals and summarised by using basic statistical parameters. Common phenomena observed in structural design process include:

- Deterministic events: The behaviour of the event can be predicted with absolute certainty;
- Random events: Time-varying event that cannot be reproduced or predicted with available knowledge of physics or existing measurements.

Wind and wave loading and consequent turbine response are random or stochastic processes (Haver, 2001). Analysis of random data is possible through stationary conditions whereby the statistical parameters of each realisation yield a constant result.

### 2.5.1 Environmental parameters

Application of offshore environmental data in the OWE industry ranges from installation and maintenance planning, farm siting, structural design to fatigue analysis (Jacobsen and Rugbjerg, 2005). Dynamic analysis of existing foundation concepts is required for the design phase to avoid resonant frequencies which increase the risk to the structural integrity. Global vibrations of the OWT structure show variable sensitivity to the wave and current loading based on the foundation concept. It is observed that stiff structures, like jacket foundations, are transparent to wave loading, therefore, their response is governed mainly by wind loads. On the other hand, response of softer structures like monopiles is affected by a combination of wind and wave loads, therefore, the interdependent responses induced by each load is significant (Seidel and Kelma, 2012).

### 2.5.1.1 Wind

The large scale global wind circulation is disturbed by localised non-uniformities at the surface of the earth. The non-linear interaction of these variations leads to chaotic wind conditions which is at the root of the geographical variation in the resource (Burton et al., 2001). The wind resource, usually determined by the wind speed, is an important decision parameter for OWT resource characterisation.

The kinetic energy of the wind applies a lift force on the blades to produce power. The wind power available to a turbine from a steady airstream at a location for assumed stationary conditions can be calculated as:

$$\text{Extractable power} = \frac{1}{2} \cdot \rho \cdot V_t^3 \cdot \frac{\pi D^2}{4} \cdot C_p \quad (2.4)$$

Whereby,  $\rho$  is the air density usually taken as  $1.225 \text{ kg/m}^3$ ,  $V_t$  is the wind speed,  $D$  is the rotor diameter to estimate the rotor swept area and  $C_p$  is the Lanchester-Betz limit. The Betz limit, estimated at 59.3% (Okulov and Kuik, 2012), is the theoretical limit on the amount of power an OWT can extract from the airstream (Andrews and Jelley, 2017). Additional factors curtailing the extracted power include structural limitations such as the generator and gearbox efficiency.

Resource availability is a highly significant factor in wind farm siting onshore and offshore. Based on Equation. 2.4, an increase in rotor blade size increases the extracted power, however, the dependence of extracted wind power on the cube of wind speed makes it highly sensitive to prevalent wind conditions. However, in addition to dictating the turbine power production, wind also induces loads on the structure which qualify as an important cause of failure. OWT failure rate shows a higher correlation with the dominant wind conditions with a slope of 1.77 (Carroll et al., 2015) relative to 0.08 for onshore wind turbines (Wilson and McMillan, 2014).

To minimise wind-induced failure and optimise OWT performance, manufacturers design turbines to operate at wind speeds in the range of cut-in,  $V_{in}$ , and cut-out  $V_{out}$ , wind speeds. Below the cut-in speed, the turbine does not produce sufficient torque to generate power. Above the cut-in speed, the power output of the turbine increases until the rated speed at which the turbine produces the optimal power (Kaidis, 2012). Increase of wind speed beyond the rated speed does not yield a further increase in power output since the turbine begins to limit its response to the wind load. Predominantly for OWT design, this is done by the



blades pitching into the wind to reduce the lift, thus, reducing the operational loads. Operating at higher wind speed increases possible risk to the OWT structural integrity, therefore at the cut-out wind speed, the braking system is employed to bring the turbine to a stand still to eliminate operational loads.

Time scales for wind, relevant to applications for an OWT, can be broadly categorised into the slow-varying and rapid-fluctuating types. Wind speed over short periods of 10 minutes to 1 hour may be regarded as stationary (Veritas, 2010) to facilitate analysis of the stochastic data. For realistic estimation of the wind profile, the overlay of the fluctuating component to the quasi-static wind component is essential. The resulting wind speed,  $V_0$ , can then be written as:

$$V_0 = V_t(t) + V_T(t) \quad (2.5)$$

The mean wind speed,  $V_t$ , falls in the former category, whereby, it may be considered constant for short time intervals of up to 3 hours (DNV GL AS, 2016b). Turbulence effects lead to a contributing wind component,  $V_T$ , with fluctuations on time scales of minutes to seconds. This turbulent component of the wind can be characterised by the turbulence intensity which is calculated as the ratio between the standard deviation of  $V_0$  and  $V_T$ , respectively.

While producing unfavourable power generation environment for the OWT and contributing to failures (P. Tavner et al., 2011), turbulence also leads to an increase in difficulty of structural modelling by contributing to the unpredictability of the wind intensity and direction. Turbulence conditions can be simulated by use of various turbulence models. Det Norske Veritas (2014) recommends the use of the Kaimal turbulence spectrum given that the wind data does not indicate the use of an alternate spectrum. The IEC Kaimal model is defined by International Electrotechnical Commission (2005) as:

$$S_G(f) = \frac{4\sigma_G^2 L_G / \bar{V}_{thub}}{(1 + 6f L_G \bar{V}_{thub})^{5/3}}$$

where,  $S_G(f)$  is the single-sided velocity component spectrum for the direction  $G$  ( $G = 1$  : longitudinal,  $G = 2$  : lateral, and  $G = 3$  : upward) expressed as a function of  $f$  that is the cyclic frequency in Hertz.  $\bar{V}_{thub}$  is the wind speed at the hub height in m/s,  $\sigma_G$  is the velocity component standard deviation,  $L_G$  is the velocity component integral scale parameter.

Long-term wind conditions may also be represented by their statistical parameters, whereby, long-term parameters are defined over a 10 year period. Wind data may be represented as a wind spectra or Power Spectral Density (PSD) function for short term stationary conditions and generic distributions or scatter diagrams of wind speed and standard deviation for long term probability distributions. The PSD for a location may be estimated by representative statistical model spectras which have general agreement in the high frequency range but display differences in the low frequency range.

Therefore, wind data at a potential site is analysed by fitting a probability function to the field data whilst identifying a suitable distribution to characterise the wind regimes. The natural stochastic fluctuation in the wind speed characterised by the mean wind velocity and standard deviation can be described by the Gaussian distribution. However, unless indicated by in-situ wind data, a Weibull distribution is associated to the available mean wind speed at the given height above Mean Sea Level (MSL) (Det Norske Veritas, 2014).

### 2.5.1.2 Wave

For the hydrodynamic processes, the stationary condition for random data analysis is called the sea state and conventionally it spans over a reference period of three hours. To simplify the random event data processing, a transformation into the frequency domain to reduce noise and allow the identification of characteristic responses in the signal may be conducted. This can be done by the Fourier transformation which assumes that a random data signal can be represented as a sum of a finite number of discrete sinusoids or wavelets with their respective amplitude, frequency and phase angle. This mathematical tool then shows the distribution of the sinusoidal components of the signal. The random wave signal may be recreated if information from the Fourier transform is preserved.

Offshore structures with considerable dynamic response require stochastic modelling of the time-domain kinematics of the sea surface. Ocean wave generation depends on multiple factors including wind speed, the length of time the wind blows over the sea surface, fetch (linear distance over which the wind blows over the sea), water depth as well as the tidal speed and direction. While wind speed and duration are location-independent, the fetch is dictated by the location. As

an example, fetch is limited in the sheltered Irish Sea since it is semi-enclosed.

Whilst wave speed is closely linked to wind speed, it can be highly localised as displayed by the reduced peak wave height in the Irish Sea due to the limited fetch. Additionally, the Southern North Sea displays a similar reduced peak wave height despite the longer potential fetch relative to the Central and Northern North Sea. This may be attributed to either the direction of the storm tracks or complex shallow water geometry. Storm tracks passing over the Southern North Sea cause the winds to blow in a west to east direction rather than the direction of the longest available fetch towards the North. Trends in the marginal distribution of wave period for the various regions in the UKCS, reinforce the fetch-limited nature of the sea states in the Irish Sea and Southern North Sea (Fugro GEOS, 2001). Highest recorded peak wave heights are generally on the west of the UKCS, where the winds have virtually unlimited fetch over the North Atlantic and the wave growth is only limited by the duration of wind.

The wave spectrum is the sum of the energies from wind-sea and swell. Wind waves are locally generated with a wide directional range leading to irregularity in sea state. On the other hand, swell is formed at a distant location and has a narrow range of directional propagation, therefore, displays a more regular behaviour than wind-waves. Since longer wavelengths have a higher speed of propagation, the wavelength and speed of the swell increase while the amplitude decreases with time and distance from the point of origin. Therefore, swells are characterised by linear, coherent, small-amplitude waves with longer periods relative to wind-waves.

While ranges of the period of wind-waves and swell can overlap considerably, it is still possible to differentiate the two types of surface gravity waves based on their period, with the former characterised by a period between 0.2 and 9.0 seconds and wavelengths of up to 130 metres and the latter by periods greater than 9.0 seconds and wavelengths in the range of hundreds of metres. While the Irish Sea and Southern North Sea are fetch-limited, the West Shetland Shelf, Hebrides and Celtic Sea have a significant contribution from the swell and within the North Sea, the wave period reduces from the north to south.

Sea surface gravity waves (including wind-waves and swell) can be recorded by a plethora of instruments, including classical moored wave buoys, platform or ship based X-band radar and Acoustic Current and Wave Profilers, and visualised by a time varying signal of sea surface elevation at a single point on the surface is

observed.

In common engineering applications, irregular sea states are characterised by statistical variables including:

- Significant Wave Height ( $H_s$ ) – Incorporating the effect of both wind-waves and swell, it is calculated as four times the square root of the integral of the wave spectrum. It closely corresponds to the mean of the highest one third of waves (Holthuijsen, 2010);
- Peak wave period ( $T_p$ ) - Peak of the power spectral density curve;
- Mean wave propagation direction ( $\theta_W$ ) – Mean direction from which the wave is propagating; and
- Site water depth ( $d$ ) - Defined as the vertical distance between the seabed and still water level; for the scope of this project MSL is taken to be equivalent to the still water level.

It must be noted, however, that the use of the old definition of  $H_s$ , which represents the mean wave height from trough to crest of the highest third of the zero-upcrossing waves, is still widespread. While it shows good correlation with visual estimates by sailors and is still applicable to sea states with a narrow-band of frequencies, for other sea states it leads to an underestimation of  $H_s$  by approximately 5% (Forristall, 1978). For all calculations conducted as part of this project,  $H_s$  is taken to be four times the standard deviation of the sea surface elevation time series (Tempel, 2006).

The surface elevation at any one point of an irregular sea surface is estimated as the superposition of many simple wavelets with various amplitudes, periods and wavelengths. Spectral analysis allows to determine the amplitude and phase of these wave trains as a function of frequency. The wave energy distribution of the wavelets as a function of the frequency is called the wave energy spectrum. Wave parameters representing sea surface waves over a discrete period may be estimated from the spectrum.

The concept of deep water is highly wave dependant and is characterised by a ratio between depth and wavelength as described in §4.2.6.1 of the DNV standard for loads and site conditions (DNV GL AS, 2016b). If the ratio is greater than 0.05, the sea is considered to be shallow, however, once it exceeds 0.5 it is said

too be deep water. Spectral representation of deep and shallow water displays considerable difference.

To encapsulate the random nature of waves numerically, numerous models have been developed over the years. The Pierson-Moskowitz spectrum 1964 is a suitable model for fully developed sea, whereby, the growth of waves is not fetch-limited and the high-frequency waves have achieved an equilibrium state. The spectrum was fitted to in-situ measurements from the Atlantic Ocean during extensive periods of constant environmental conditions and is a suitable estimate for sea states in most regions. However, further measurements in the Joint North Sea Wave Project (JONSWAP) lead to the development of the JONSWAP spectra for partially developed sea states under a particular wind condition (Hasselmann et al., 1973). The JONSWAP spectrum is an enhanced version of the Pierson-Moskowitz spectrum with the additional detail of a peak shape parameter,  $\gamma$ .

Most hydrodynamic modelling tools provide the capacity to generate regular (periodic) or irregular (stochastic) as well as long-crested (unidirectional) or short-crested (with directional spreading of energy) waves. Ocean waves are irregular and display randomness in shape, height, length and propagation speed, therefore, a realistic sea state can be simulated by a random wave model. This model may be linear or non-linear. The linear random wave model is the most common method employed to model stochastic ocean waves, however, such models underestimate the wave loads on the structure in shallow waters (Det Norske Veritas, 2014).

### 2.5.1.3 Relationship between $V_t$ and sea state

The Beaufort scale, used by the Met Office, for marine forecasts provides an empirical link between wind speed and observed sea state. The Beaufort Force is derived using the Beaufort Scale and is defined as the measure of the influence of wind forcing on the sea surface. Reproduced from the UKMO Observer's Handbook 1927, the scale is shown in Table 2.1.

The values of the Beaufort scale are expected to represent well-developed wind waves of the open sea ignoring near-shore effects. With values ranging from 1 - 12, it provides comprehensive descriptive parameters for wind speed and accompanying sea states from calm to hurricane conditions, respectively.

Table 2.1: The Beaufort Force with associated wind speed limits and sea state description (United Kingdom Met Office, 1927).

Beaufort Force	$V_t$ limits at 10 m above MSL [m/s]	Sea state description
0	0.0 - 0.2	Calm
1	0.3 - 1.5	Light air
2	1.6 - 3.3	Light Breeze
3	3.4 - 5.4	Gentle Breeze
4	5.5 - 7.9	Moderate Breeze
5	8.0 - 10.7	Fresh Breeze
6	10.8 - 13.8	Strong Breeze
7	13.9 - 17.1	Near Gale
8	17.2 - 20.7	Gale
9	20.8 - 24.4	Strong Gale
10	24.5 - 28.4	Storm
11	28.5 - 32.6	Violent Storm
12	$\geq 32.7$	Hurricane

#### 2.5.1.4 Long-term environmental parameters

Offshore structures are susceptible to cumulative fatigue damage, therefore, annual metocean characteristics for the deployment sites are required to estimate the service lifetime of the device structural components. Environmental parameters vary considerably on temporal and spatial scales, particularly in the shallower continental shelf region where most OWE deployments are concentrated currently. To determine environmental conditions at the turbine location, data from theoretical models, advanced hindcast models or documented meteorological data from in-situ measurements and met masts at adjacent locations can be used.

Numerous instruments and techniques can be used to gather metocean data by in-situ deployment or remote sensing including wave rider buoys, acoustic doppler current profilers, satellite altimeters, high frequency radars and space-borne synthetic aperture radar (SAR) systems. Each system has its advantages along with the inherent limitations as discussed in existing publications (Barstow et al., 2009;

Kasinatha Pandian et al., 2010).

While in-situ measurement instruments provide robust estimates for the environmental parameters, they are expensive to maintain and usually do not provide continuous data for extended periods to account for seasonal, annual and long term variations (such as those due to El Niño or La Niña events).

In the absence of comprehensive in-situ wind profile, available wind speed data should be adjusted for spatial and temporal variations at multiple scales accounting for inherent uncertainties to improve estimation of the random field in space and time. Available methods include measure-correlate-predict methods (Carta et al., 2013), shearing effects (Sakagami et al., 2015) and local flow modelling (Barthelmie et al., 2008).

In consideration of the limitation of long-term empirical metocean databases at the sites of interest,  $H_s - T_p$  and  $H_s - V_t$  scatter plots from available reanalysis and hindcast models allow for estimation of annual metocean characteristics. By allowing the derivation of the associated probability for the occurrence of each state in a representative year, these scatterplots inform the accumulated fatigue damage and the consequent fatigue life of the structure. Hindcast models use historical meteorological data to drive numerical water level, current and wave models to reproduce oceanographic conditions for the past. They provide the benefit of having a higher spatial coverage relative to metocean instrument measurements since most of this data originates from areas of industrial activity or hazard-prone coastal regions. With the possibility of continuous data availability, hindcast models provide a comprehensive temporal coverage as well, whilst, the performance of the environmental monitoring systems may be compromised by storm events and/or maintenance activities. Additionally, the hindcast data eliminates risks of the introduction of uncertainties in the data due to variation in instrumentation or sampling methodology.

However, caution is warranted when using hindcast data since that uncertainties in the input wind and pressure fields as well as bathymetric input driving the model along with numerical uncertainties may lead to a poor representation of the environmental parameters. Whilst a finer grid resolution of models allows for obtaining the metocean data closer to the location of interest, the model does not incorporate geographic features with dimensions less than the grid resolution. Finally, the use of hindcast data for reliability prediction assumes that histori-

cal metocean data is representative of future conditions that a structure may be exposed to.

Many meteorological centres run regional and global scale models to simulate the metocean conditions at various resolutions using a spectrum of underlying principles. Two such publicly available databases are the North European Storm Study Extension (NEXT) hindcast databases by a consortium of oil companies and the ECMWF Re-Analysis (ERA)- Interim database by the European Centre for Medium-Range Weather Forecasts (ECMWF).

During the WERATLAS project, there was agreement that the ECMWF data is the best available database (Barstow et al., 2009) due to high quality wind field input and incorporation of SAR data as well as satellite altimetric data. Additionally, a comparison of the Scatterometer data over the Adriatic Sea with available global model estimates shows that the ECMWF data shows best agreement (OGP-IPIECA, 2015).

### 2.5.2 Loads

While performance is a significant design consideration, the final design of an OWT is also informed by parameters related to structural integrity. To identify the structural requirements of an offshore wind turbine, a comprehensive loads analysis must be conducted. Loads are forces that act upon a structure which can be quantified by frequency, duration and intensity. For an OWT, they can be classified into various categories as shown in Table 2.2 (Rivkin and Silk, 2013).

Cyclic loads result from regular or irregular, low frequency magnitude changes and may involve directional changes, whereas, static or quasi-static loads result from impacts with a monotonic structure and do not undergo frequent change (Federal Maritime and Hydrographic Agency, 2007). Dynamic or transient loads in the OWT occur due to high-frequency periodic vibrations or transient effects occurring intermittently contributing to a high stress whereby, the inertial forces become considerable enough to cause structural deformations of a quasi-elastic nature.

While the steady and cyclic loads are internal to the turbine and can be accounted for with relative ease, the transient and stochastic loads are attributed to external forces which must be appropriately incorporated during the design pro-



Table 2.2: Categories of loads experienced by on an OWT shown in the order of decreasing ease of predictability.

Load types	Explanation	Example occurrence on OWT
Steady	Known load with predictable behaviour	Internal loads like weight of support structure
Cyclic	Predictable loads displaying cyclic behaviour	Blade weight for an operational turbine
Transient	Short-term loads with known or predictable intensity	Mechanical loads such as braking loads on drive shaft
Stochastic	Random loading estimated by numerical modelling	Turbulent wind loads on turbine

cess. From the design perspective, the increased difficulty in the predictability of a load introduces a source of uncertainty in the structural loads analysis. In addition to the loads listed in Table 2.2, cyclic loading at the resonant frequency introduces another important failure mode for an OWT. Vibrations at the natural frequency cause a peak in fatigue of the structure which may lead to failure, therefore, care is taken at the design phase to ensure that the natural frequencies of the structure are avoided. In addition to the inherent difficulty in modelling the load categories identified in Table 2.2, the complexity of structural modelling is compounded by the dynamic interaction between the subassemblies of the OWT. For structural analysis, possible types of loads must be considered separately and in combination to account for their interactions. Different combinations of loads create unique conditions for the structure and are referred to as load cases. Numerous load cases must be examined to ensure accurate quantification of reliability for an OWT as published by British Standards Institution (2009). This standard identifies a set of 34 design load cases, of which 7 are reported to be applicable to simplified fatigue load assessment in OWT structural analysis and are shown in Appendix B.

Introducing moving parts into a structure increases the complexity of the design problem due to the combination and variability of the steady and dynamic loads or forces. Therefore, for an OWT, stochastic external loading, load-induced and mechanical vibration, biplanar and eccentric loading further add to the complexity of the design problem and the structural assemblies (RNA and the support structure) are most affected by loading (Rivkin and Silk, 2013).

Hau (2013) observed that the fluctuating and alternating loads are critical for determining the structural integrity, therefore, a combination of the cyclic, transient and stochastic loads can provide an improved estimate of fatigue life.

### 2.5.2.1 Environmental loads

Based on the fatigue relevant design load cases tabulated in Appendix B, the associated environmental states for simulating dynamic structural response can be identified. Each environmental state may be composed of numerous environmental loads that interact with the structure. Classical examples of environmental loads for offshore structures include wind, wave and current. Additionally, ice on blades and support structure, marine growth, temperature, ship collision risk, lightning and convective weather, seismic loads, soil properties and scour may also be qualified as potential contributors. Comparison between the local sensitivities of  $T_p$ , MSL, soil properties and  $H_s$  (Ziegler et al., 2015) shows that for a 4 MW offshore monopile, the first two factors display a higher influence on the equivalent fatigue life estimates at the mudline as well as the transition piece relative to the latter factors.

As discussed, typical duration of the stationary environmental states is 10 minutes or one hour and they are characterised by environmental loads with constant intensity parameters. Intensity parameters for environmental loads relevant to the scope of this research include  $H_s$  and  $T_p$  for waves and  $V_t$  for wind speed.

### 2.5.2.2 Combination of environmental loads

In the offshore industry, a simplified lumping of load cases is adopted under the assumption of quasi-static wave response. However, the issue is more evolved for OWTs attributed to two reasons. Firstly, the importance of the wind and wave fatigue loading on their dynamic response. Secondly, incorporating the influence of operational loads is also significant. These result from the operation and control of the OWT including rotor speed and torque control by blade pitching or other aerodynamic devices, transient loads due to rotor start-up and shut-down, mechanical brake application, yaw motion and generator activity.

Quasi-static models like this linearize the system and for the short-term period, the combined load effect may be calculated by linear combination of the

concurrent wind and wave loads on the structure or direct simulation. When calculated separately and superimposed for load calculations, it must be established that there is no dynamic effect from the individual environmental loads or any combination thereof.

It is important that the wind loads appropriately account for the damping resulting from the structure, aerodynamics, hydrodynamics and the soil. This damping allows for an adequate structural analysis to determine the wave load. Operational and environmental conditions stated in Det Norske Veritas (2014) are significant to accurately determine the damping effect, therefore, the damping is best determined by an integrated model.

For the scope of this work, a global, dynamic structural analysis model is used instead with direct application of concurrent load simulations in the time domain for wind and wave loads simultaneously.

## 2.6 Design methods and system analysis

Design constraints for OWT systems can be categorised as extreme or fatigue-causing. While the former only relies on the turbine response analysis based on the single largest load expected to level against it during turbine lifetime, the latter requires load estimation for all possible input conditions which is then weighted based on occurrence frequency to be aggregated to yield device fatigue estimates (Manuel et al., 2001).

### 2.6.1 Design standards for offshore wind energy

Structural engineering is based on the principle of the prediction of the magnitude of the loads that are likely to be applied to a structure over its design life. To this purpose, appropriate design standards are implemented which identify probable load sources and their potential combinations.

Design standards for offshore wind turbine (International Electrotechnical Commission, 2005; Federal Maritime and Hydrographic Agency, 2007; British Standards Institution, 2009; Det Norske Veritas, 2014; British Standards Institution, 2009) instruct the user to calculate wind turbine loads during steady state and transient events for different combinations of environmental parameters. It is

recommended that these load cases must be defined such that they incorporate combinations of environmental parameters associated with ultimate limit state and fatigue limit state design for normal turbine operation. Additional load cases, pertaining to a turbine experiencing severe faults, must capture extreme environmental conditions for structures designed in the ultimate limit state.

Available design standards provide an inexhaustive list of requirements based on the most updated knowledge and are continuously improved as new constraints are revealed or weakness in application of existing constraints is detected. This inclusion or improvement of a code may lead to increased capital investment, therefore, codes aim to achieve a balance between risk and cost.

The available standards can be utilised to inform design decisions by outlining methods to determine material strength and structural loads.

### 2.6.2 Material strength and loading conventions

In materials engineering, the strength of a material is described as its ability to withstand applied loads without failure and a material failure is defined as the limit beyond which the material member suffers a loss of its load carrying capacity (Collins, 1993). An applied load induces internal forces per unit area on the mechanical member called stresses which produce material deformation based on its stiffness parameters. The strength of a member is its capacity to withstand loads, however, this load-carrying capacity of the member is usually defined in terms of the member stresses (Brondsted and Nijssen, 2013). The yield and ultimate strength of the material are, therefore, also referred to as the yield and ultimate stress points, respectively.

To determine the load capacity, deformation and stability of a mechanical member, the stresses and strains must be quantified using the applied loads and the geometric description. These calculated stresses and strains may then be compared to a measure of material strength based on the failure theory used to determine strength of the member.

Stress is a physical quantity which describes the effect of loading on a structure resulting in material deformation, namely strain. To determine the mechanical properties and behaviour of a material, standard specimen sizes of the material are exposed to a uni-axial loading regime in empirical studies to ensure that results

of the tests are replicable and comparable. A log of the applied load and resulting deformation of the specimen allows for the representation of material strength in a stress-strain diagram. The stress-strain diagram expands the applicability of the test results to material members of varying dimensions.

Like most materials, wind turbine construction materials display an anisotropic behaviour established by the dependence of their Young's modulus on the direction of the applied load. The fibre-reinforced composites used for turbine blade manufacturing show extreme anisotropy since their strength along the fibre is much higher than that across the fibre. To a significantly reduced extent, measured data (Gandhi, 2010) for metal alloys, like steel, used for turbine tower and transition piece construction shows anisotropic behaviour. This may be attributed to tensile test method and/or machine variability as well as grain structure orientation and is predicted to cause variation in the mechanical properties of steel. Despite this variability, metal alloys are assumed to be isotropic with an elastic modulus of 207 GPa as an input to Computer Aided Engineering (CAE) simulations of steel structures (Gandhi, 2010).

### 2.6.3 Failure theories

A failure theory enables a design engineer to estimate the set of conditions under which the material is expected to undergo failure. The characteristics of anisotropic materials allows for the use of different failure theories including the maximum principal stress theory (Rankine), maximum shear stress theory (Guest - Tresca), maximum normal strain theory (Saint - venant), total strain energy theory (Beltrami - Haigh) and the widely adopted shear strain energy per unit volume theory (Von Mises-Hencky). These are discussed in detail by Collins (1993).

### 2.6.4 Design methodology and constituent design criteria

Reliability improvement analysis is suitable for OWT and subassembly manufacturers to define where design and test efforts should be focused. Application of the design review procedures in the development phase of OWT deployment is illustrated in §5.3.3 of the publication by P. Tavner (2012). This process of certified design aims to improve the survivability of the OWT structure. The complexity of such analysis increases due to the aleatory uncertainty associated with stochastic

wind and wave loads as well as corrosion.

Failure in structural assemblies of the OWT is characterised by the possibility of formulating limit state equations outlining the failure behaviour. Numerous possible limit states can be adopted. Introduced in the 19th century, the conservative Working Stress Method was the traditionally employed design methodology, whereby, the basic presumption is that the structural behaviour of the material used is restricted within the elastic region. The allowable range for the working stresses is, therefore, in the linear region of the stress-strain curve and does not account for influences of secondary effects including creep, shrinkage and stress concentrations. This leads to a conservative design with reduced design economy.

The Working Stress Design Method is now superseded by the Limit State Method to provide more economical design solutions (Becker, 1996).

Limit states are design constraints or conditions beyond which potential failure in design is imminent. This design method is based on the theory that uncertainties existing in design can be defined in the mathematical framework of probability theory. Categories of design criteria or limit states in engineering design using the limit state method are described by Ambühl et al. (2015) and summarised below:

- Serviceability Limit State: Deals with service requirements for adequate performance of structure subjected to working loads. If fulfilled, allows the structure to remain functional for its intended purpose, however, it may not be strength or structure based;
- Ultimate Limit State: To quantify the non-linear stress-strain behaviour, the Ultimate Load Method is based on the ultimate strength of materials at ultimate loads. Deals with the maximum loading capacity of the structure. If fulfilled, the structure will behave similarly under competitive loading so safety and reliability are ensured. It may lead to underdesigning since the serviceability criteria may not be fulfilled at the ultimate loads;
- Fatigue Limit State: Fatigue rises as a significant failure mode due to the complex loading regimes acting on marine structures. Almar-Naess (Almar-naess, 1985) define fatigue as a process of cycle by cycle accumulation of damage in a structure subjected to fluctuating stresses and strains. It must be noted that the magnitude of loads causing fatigue damage is not large enough to cause immediate failure. However, exposure to the stochastic

load fluctuations leads to a progressive, irreversible accumulation of damage and the structural integrity is compromised when the accumulated damage reaches a critical level;

- **Accidental Limit State:** As indicated by the name, it is the damage incurred by a system due to an accidental event or an operational failure.

For a successful support structure design, the allowable stresses for all limit states should not be exceeded during its lifetime, and the ambient soil or rock should maintain elasticity at the monopile for the above-mentioned limit states.

For most components, fatigue loading is the design driver when generating electricity (BVG Associates, 2019; Hau, 2013) since the number of load cycles experienced by a turbine during its design lifetime is very high. As an illustrative example, for a small turbine with a rotor diameter of 80 m and tip speed ratio of 8 and 80% availability exposed to continuous wind speed of 10 m/s, there will be  $2.4 \times 10^8$  rotations over a 30 year lifetime. The maximum stresses in a wind turbine must, therefore, be lower than other structures such as aircrafts, bridges and helicopters (Andrews and Jelley, 2017) to avoid fatigue failure during design lifetime.

The methodology employed to determine fatigue lifetime for an OWT is described in Chapter 4.2 and illustrated in Figure 4.10.

### 2.6.5 Lifetime extension

Lifetime extension decisions are expected to play a larger role in the wind energy market of the UK (Rubert et al., 2018). As OWTs near the end of their design lifetime, lifetime extension decisions must be made to extend the operating lifetime of an installation. Although designed for a finite lifetime, an analytical and practical investigation into the structural integrity of the turbine can provide information about the structural reserves to inform potential lifetime extension.

A number of analytical methods discussed in DNV GL (2016a) define environmental conditions and the consequent structural loads at the deployment site as the basis for lifetime extension decisions. The deterministic *detailed approach* recommends the use of measured turbine response and local- site condition data for the assessment of the fatigue limit state. This methodology is employed in

existing publications by Ziegler (2016) and Ziegler et al. (2017) to allow turbine structural integrity to inform lifetime extension decisions.

A comparison between the structural fatigue lifetime during the design process and reassessment for a considered monopile in the Walney OWF (Kallehave et al., 2015) shows that potential for lifetime extension is in the order of 80%. This increase has been attributed to the uncertainties associated to the soil-structure interaction as well as the quantification of wave loads.

## 2.7 Structural reliability data

Structural reliability can be mathematically defined as the probability that a specimen will not achieve a specified limit state during a stated period of time. Reliability models require failure rate data from individual devices with particular operating conditions to estimate point values for reliability, therefore, a statistically robust database is vital for precision. As discussed, structural elements of an OWT experience loading by metocean parameters including wind and wave. The quantification of the lifetime loading due to these parameters and duty cycles due to operational states can allow for a more informed decision regarding the failure rate of structural subassemblies.

The usefulness of the failure rate estimates depends on the accuracy and completeness of the input parameters as well as the quality of the employed model. However, as shown in Fig.2.9 in the absence of a large industrial database, extrapolations for device and operational environment may be made using expert knowledge. As a result, high degrees of uncertainties are introduced in reliability assessment results since failure rate adjustment is subject to experts' interpretation and judgement.

When using the bottom-up statistical method to predict the reliability of a system based on sub-system failure data, it is important to accurately quantify the failure rate of devices and apply appropriate adjustment factors when required. This section describes the available resources and methods involved in the determination of failure rates for system reliability calculations:

- Adjusted empirical failure data
- Field failure data



- Simulated failure data

In the absence of industry-specific data, reliability assessment methodology allows for the use of adjusted surrogate data as shown in Figure 2.9, vetted by experts, from closely linked industries.

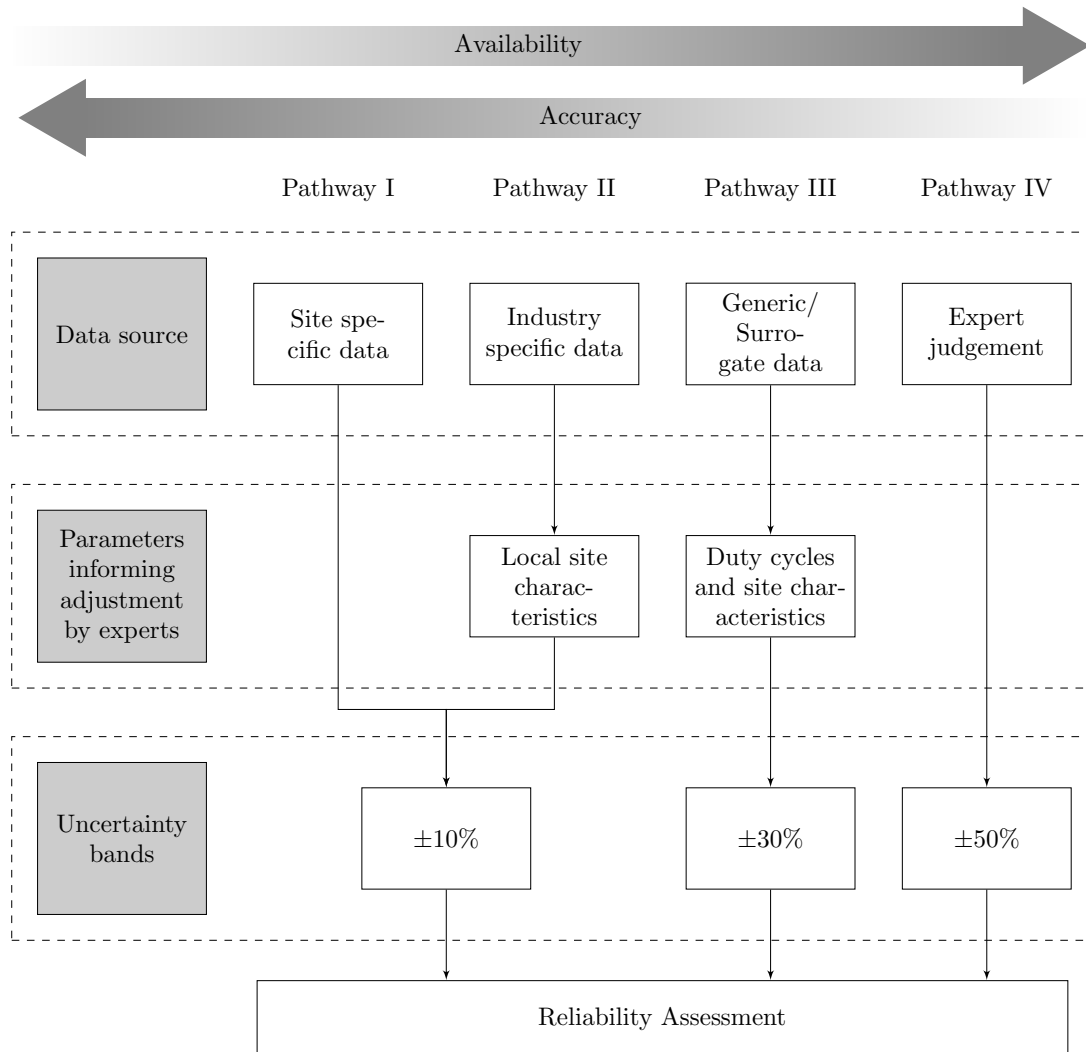


Figure 2.9: Sources, adjustment and associated uncertainty bands for failure rate databases for use in reliability assessment of OWTs based on P. Thies (2012)

### 2.7.1 Adjustment of empirical failure data

Failure rate adjustment is subject to experts' interpretation and judgement (P. R. Thies et al., 2009; Khalid et al., 2015; Delorm et al., 2012). As a result of the adoption of surrogate failure rates, high degrees of uncertainties are introduced in reliability assessment results so they can not be taken as point estimates of reliability.

A comprehensive list of databases for failure rate data from the military, electronic, mechanical, nuclear and offshore O&G sectors pertinent to offshore wind applications can be found in a pre-study for a Reliability, Availability, Maintainability, and Safety (RAMS) database for wind turbines (Pettersson et al., 2010) and academic projects pertaining to wave energy converters (P. Thies, 2012). Of particular importance to OWE are the multiple sources (M. Lange et al., 2011) for the existing onshore wind reliability data. Despite the existence of large wind industries outside of Europe, most of the documented resources are limited to Europe and there is little publicly available data regarding wind turbine reliability from other continents.

Existing OWE research readily adopts surrogate data from sources established for the O&G (Hameed et al., 2011; Delorm et al., 2012) and onshore wind industries for reliability analysis.

However, it must be noted that failure rate adjustment is subject to experts' interpretation and judgement. Generally, adjustment decisions are based on a qualitative comparison of the components' application between the system where the data was collected and the new application, thereby, introducing a higher uncertainty in reliability assessments based on adjusted data as seen in Figure 2.9.

The Military Handbook (Department of Defence, 1991) advises its users to determine whether "... environmental conditions and part quality (sic) representative of the requirements?". Therefore, environmental conditions are a significant factor contributing to failure rate, therefore, existing data should be adjusted based on environmental conditions. To account for the influence of environmental parameters, either available industrial data (Carroll et al., 2015) or surrogate data from other industries may be adjusted.

### 2.7.1.1 Wind industry

Numerous reliability studies (Niclas et al., 2017; Martin et al., 2016; Lazakis and Kougioumtzoglou, 2017; Kougioumtzoglou and Lazakis, 2015) utilise onshore wind failure databases to produce estimates for OWT failure rates.

Investigating the WMEP database for onshore wind turbines, §7.1 of the publication by Stefan Faulstich and Hahn (2009) shows that environmental parameters have a noticeable impact on assembly reliability. Existing onshore databases are

tabulated by Artigao et al. (2018) and the comparison of percentage contribution of assembly failure rates between onshore and offshore databases is shown in Figure 2.10.

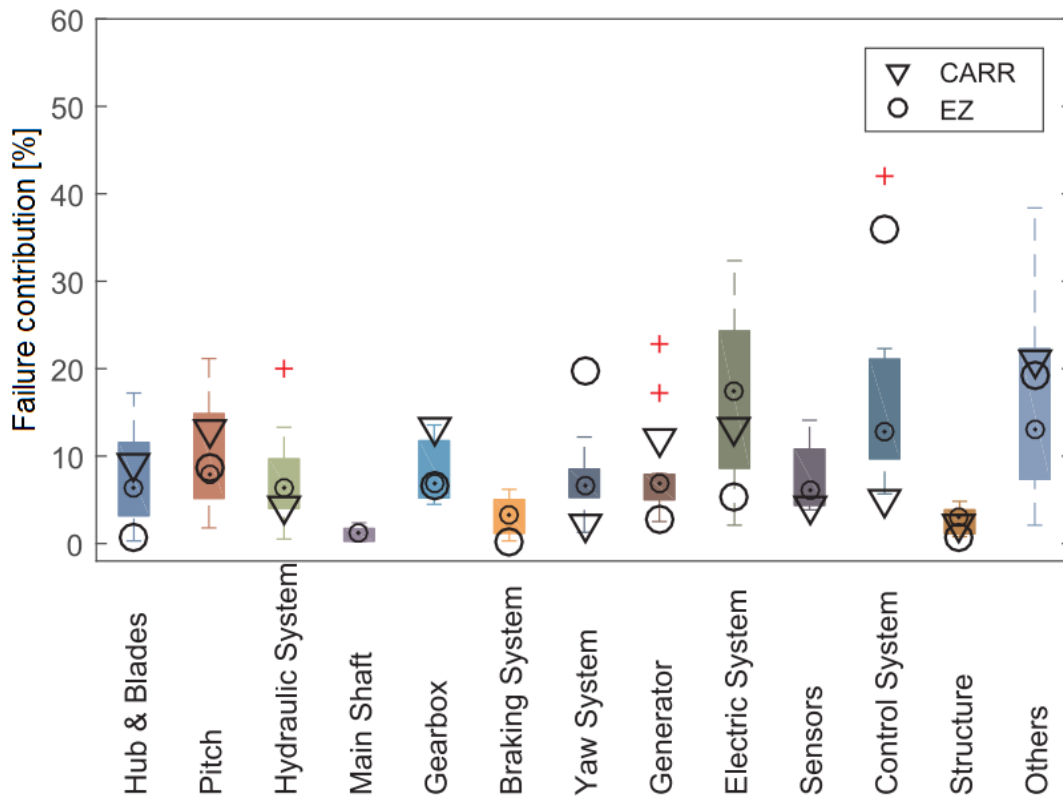


Figure 2.10: Comparison of assembly failure rates between databases for onshore and OWT deployments (Artigao et al., 2018). CARR and EZ are the available offshore failure rates, where, CARR represents data published by Carroll et al. (2015) and EZ represents data used in the study by Dinwoodie et al. (2012).

The percentage contribution of individual assemblies to system failure for onshore and offshore installations can be seen to exhibit maximum difference for the yaw and control system. The EZ study (Dinwoodie et al., 2012) proposes a larger contribution of these assemblies offshore than onshore which is in stark contrast to the CARR study. However, the EZ study only presents data collected at a single farm, therefore, the failure rate is only representative of a single turbine type and location. The CARR data is extracted from between 5 - 10 farms, therefore, represents failure rates for a more diverse offshore fleet deployed in a relatively larger region.

While the failure rate for OWTs is eight times that of onshore wind turbines (Carroll et al., 2015), extrapolation of the onshore learnings to offshore installa-

tions (Faulstich et al., 2009; P. J. Tavner et al., 2010; S. Faulstich, B. Hahn, 2010; Faulstich et al., 2011) implies that environmental factors play a role in device output prediction as well as failure rate calculations in OWTs. However, the localised variations in the reliability failures cannot be assumed to exhibit the same trend since equipment proven in the onshore conditions placed in the dynamic marine environment, with significantly altered load conditions and duty cycles, implies large changes in failure modes and mechanisms.

### 2.7.1.2 Other industries

The widely used OREDA database is a structured RAMS database which provided a sound basis for boosting the reliability of the O&G technology by collecting and exchanging data based on a standard set of guidelines and procedures. With over 35 years of experience in collaborative industrial experience, the project has published updated comprehensive reliability data handbooks (1984, 1992, 1997, 2002) and developed a standard with the International Standardisation Organisation. Reliability data for offshore (topside and subsea) and onshore equipment is included in the published handbooks and has applications for availability studies, risk analysis, Lifecycle Cost (LCC), benchmarking metric development, maintenance planning and optimisation.

The Military Handbook (Department of Defence, 1991), primarily used for military electrical equipment, provides a parts stress reliability prediction technique of multiplication of base failure rates with empirical factors to effectively translate failure rates from the data collection environment to application environment. This method is employed by existing research (Khalid et al., 2015; P. Thies, 2012). This modifies failure rate for a given component/subassembly according to its salient features (age, technical concept, environmental conditions) to account for the differences between collected failure rate data and the device-specific failure rate.

### 2.7.2 Field failure data

Populated by field or empirical test data, reliability databases are considered as a useful source to analyse system performance. It can be argued that data from reliability databases may not be representative of the sample at hand since there are numerous design variables for each component in a system, therefore, the

associated component strength can be expected to have higher or lower values than the available data from a reliability database. A comprehensive industry-specific field failure rate database for OWE is not yet available in the public domain since developers and operators may lose competitive advantage by sharing this data of commercial relevance. The now advanced offshore O&G industry was at a similar stage in the past: data confidentiality was crucial. However, soon the industry realised the significance of knowledge sharing for all involved parties and initiated the Offshore and Onshore Reliability Data (OREDA) project to deliver performance improvement across the industry. Two participating oil companies in the OREDA project claimed to reduce the cost of alternative designs by USD 70 million.

Similar gains may be achieved by the OWE industry through the SPARTA-WMEP collaborative to allow the OWE industry to proceed apace. The argument to end the restrictive practice of data confidentiality to encourage collaborative advancement of the industry gained momentum in recent years. It has resulted in the formation of the offshore wind SPARTA project administered by the ORE Catapult (The Crown Estate, 2015) in the UK and the Offshore-WMEP by Fraunhofer IWES (2013b). These cross-industrial knowledge databases aim to collate detailed data from operation and maintenance events on individual OWT basis. Collected data includes performance metrics related to power production, downtimes and subassembly failure rates. A harmonised standard set of data collection practices and evaluation methods are employed at both projects enabling comparative analysis across the platforms.

Offshore Wind SPARTA provides an anonymous database to boost reliability, availability and performance of OWE. Initialised by TCE and ORE Catapult in 2014 for the UK, the project was developed as an instrument to deliver industrial improvements through compilation of a database that may allow OWF operators to compare the performance of their wind farm against the industrial average. With TCE seed funding, the project has established and tested the data collection system and allowed the involved offshore windfarm operators to become familiar with it within the first year of the pilot operation.

Entering full operation mode, the project then commenced data collection and produced benchmarking metrics for each windfarm against the sector performance. System-level operational data from 22 participating wind farms with total energy

production of 15,057,978 MWh over the 2017/18 period is presented in the Portfolio Review SPARTA (2018) for trends analysis.

The availability of this database is currently restricted to the involved operators; they are expected to experience a number of seasonal cycles of benchmarking outputs to be able to analyse performance trends for improved operation before they are expected to be comfortable with agreeing to expanding the availability of the sector data to the wider community.

### 2.7.3 Failure data based on design methodology

In consideration of the inadequate public field failure rate database for OWE, accurate estimation of assembly failures is a key research objective. The flowchart in §6.7 of the publication by Hau (2013) shows the overall methodology followed to determine failure rate through fatigue life.

Simulation tools or design codes are useful in predicting the coupled dynamic loads and responses of OWT assemblies which may then be post-processed to determine the failure rate of the considered system. The computed rainflow matrix from the load profiles and the material's fatigue strength properties from the S-N curve allow for the determination of fatigue damage for individual components/sub-assemblies. This methodology is explained in detail in Chapter 4.

## 2.8 Research question

Based on Turner (2012), an OWF project can be described as an endeavor which utilises "human, material and financial resources" to deliver energy "...within constraints of cost...". The financial constraints and delivery of cost-effective power production are of high importance to ensure profitability in the OWE sector, therefore, it is imperative that uncertainty in projects is identified through risk management processes. Possible roots of uncertainty may be traced back to the identification of the deployment sites and their associated environmental parameters (Carbon Trust, 2008) effecting the risk and return at individual sites.

While the conventional base plan for site identification by The Crown Estate (2018b) relies on the technical resource and restrictions, an improved geospatial risk-return metric for structures may allow for a more informed site characterisa-

tion metric. The higher CAPEX and OPEX of OWFs located in deeper waters further offshore is expected to be partially offset by the increased power output (RenewableUK and BVG Associates, 2011). However, simultaneously identifying the risk at a deployment location will allow stakeholders to make informed decisions about the structural integrity requirements to tailor turbine design and structural reserve potential for lifetime extension considerations. Therefore, it is imperative to characterise the potential OWE sites based on metrics incorporating the influence of both power production and consequent structural damage to gauge the cost effectiveness of integral design decisions.

In the above context, this project aims to address the following research question:

Can an improved quantification and visualisation of site-specific OWT performance inform location-intelligent decisions for farm siting?

To address this research question, the contribution of metocean parameters of wind and wave to device reliability and energy production will be identified that will facilitate decisions by various OWE stakeholders. By contributing to effective risk management, the influence of this research may extend from the design process to the O&M regime through proactive planning to increase performance. While this does not eliminate the need for reactive planning, a comprehensive reliability mapping will reduce crisis management to an acceptable level.

### 2.8.1 Overarching reliability methodology

A review of the literature has allowed two possible methodology streams to be identified to address the above research question, as shown in Figure 2.11.

It can be seen that the choice of the adopted methodology is subject to data availability. Stream 1 is to be employed if industry - specific or surrogate failure rate data displaying effects of spatial distribution is available, whereas, Stream 2 must be employed if such a database is not available.

Using Stream 1, available failure rate data can be extrapolated to locations with similar environmental conditions using a geospatial tool to develop failure contours. Furthermore, the contour intervals of failure rate may be adjusted using expert knowledge based on environmental adjustment parameters.

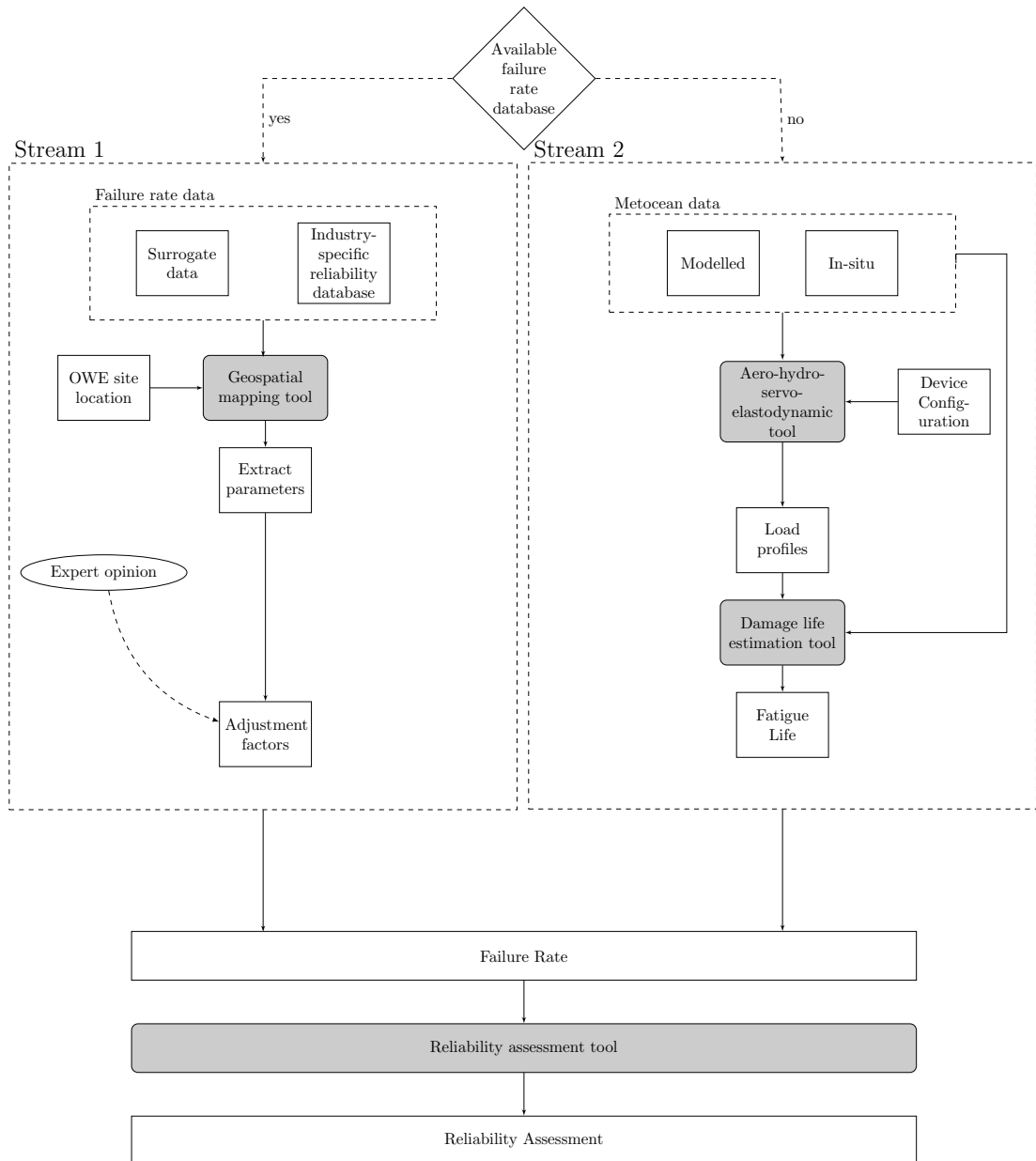


Figure 2.11: Systematic procedure flowchart that can be implemented for determination of device reliability based on availability and type of data.



In the absence of a spatially comprehensive failure rate database, Stream 2 can be employed for individual subassemblies to utilise available metocean data from various sites and translate it into fatigue life in a two step process. In step one, metocean data should be fed into an aero-hydro-servo-elastodynamic tool to generate structural response. In step two, the resulting response should be used in conjunction with the long term environmental parameters at the site and material characteristics of the subassembly to calculate fatigue life.

Since Stream 1 is computationally inexpensive relative to Stream 2, therefore, when a robust database is available, it is recommended to adopt Stream 1 for system reliability assessment.

### 2.8.2 Scope of work

This research project aims to address the research question by developing a combined risk and return metric to support location - intelligent decisions at various stages of the farm planning and operation. Reliability is taken as the indicator for risk, whereas, annual energy output is taken as the sole indicator for return on investment.

The annual energy production is determined using the site wind conditions and reliability is calculated using the methodology identified in 2.11. As displayed in Figure 2.9, although reliability estimates from Stream 1 (corresponding to Pathway I) are expected to display improved site characterisation with reduced uncertainty, limited data availability may reduce the applicability of this methodology stream. Chapter 3 attempts to apply Stream 1 to visualise the spatial distribution of turbine performance indicators, however, the lack of spatially distributed failure rate database leads to the adoption of Stream 2 in subsequent chapters.

To address the issues arising due to the large computational effort required to apply Stream 2, the scope of this research is limited to fewer variables. Firstly, a single turbine concept is used and the methodology is applied to a single illustrative assembly, namely the support structure due to its significantly large contribution to turbine CAPEX. Secondly, it is suggested that the methodology should only be applied to reliability - critical elements of individual subsystems. Thirdly, the influence of metocean parameters is isolated by using uniform depth and distance to shore.

While these limitations enable computational efficiency to allow for the successful demonstration of the suitability of Stream 2 for quantification and visualisation of the risk-return metric, they limit the universal application of the results.

## **2.9 Chapter summary**

This chapter begins by highlighting the progress of the OWE industry in the UK to-date with a policy back-drop. It then discusses expected industrial trends in the future and identifies that the ambitious plans for OWE deployment in the UK requires improved location-intelligent decision making. Characterisation of the offshore regions, existing and planned lease rounds shows that the turbines are increasingly being deployed at locations further offshore seeking to harvest the improved wind resource. However, the resource improvement is accompanied by a possible increase in associated project risk due to more dynamic metocean conditions. A review of existing key performance indicators and site decision parameters shows that there is a need for the development of a risk - return metric to quantify and visualise expected system performance.

Major stakeholders in the industry and a variety of technological concepts are presented. Two metocean parameters, namely, wind and wave, with large contribution to turbine risk and return are discussed followed by a discussion of aero- and hydro-dynamic forcings. This, in combination with structural design criteria, leads to the identification of reliability as a significant project risk. A summary of available reliability databases, possible methodologies to determine system reliability and formulation of the research question provide a roadmap for subsequent chapters.



## Part II

System and Subassembly

Reliability Methods



# Chapter 3

## System Reliability for an OWT

While exploratory data analysis has been widely adopted for investigating onshore wind turbine failure rate databases, the adoption of onshore estimates for leads to larger uncertainty bands in the reliability assessment of OWTs. This chapter provides insight into the underlying structure of industry-specific data through system reliability assessment to determine RAMS parameters for an OWT. As discussed in Chapter 2, reliability estimates from Stream 1 are expected to display improved site characterisation with reduced uncertainty, therefore, an attempt is made in this chapter to apply Stream 1 (shown in Figure 3.1) to determine the spatial distribution of risk associated to OWE deployment.

As it can be seen, industry specific field failure rate data (Carroll et al., 2015) is processed in this chapter using the reliability assessment tool, BlockSim, to follow the methodology proposed in Stream 1. To study the spatial distribution of reliability estimates, the deployment location of individual turbines is required in addition to a comprehensive failure rate database to make an informed decision about adjustment factors.

### 3.1 Reliability growth

Being the main driver for operation and maintenance expenses, system reliability assessment is imperative for OWE industrial development. An objective for the design process is to deliver continuous reliability growth (Ferguson and M. Kühn, 1998) to achieve target reliability levels and lower the life cycle costs of the system.

Reliability growth management provides an objectively designed growth standard for benchmarking existing reliability assessments to inform strategies for im-

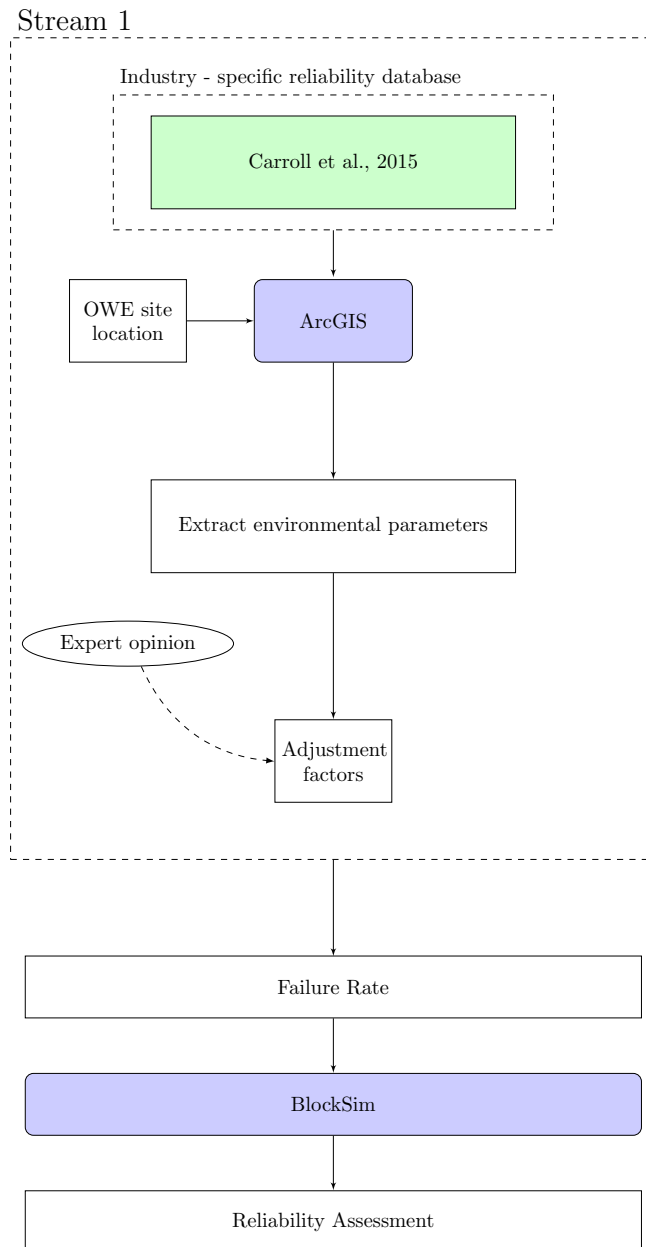


Figure 3.1: Methodology used to conduct a system reliability assessment using available field failure rate data (Carroll et al., 2015) from the OWE industry and available geospatial and reliability assessment tools, namely ArcGIS and BlockSim.

provement of the system. Reliability growth is evaluated by two processes - reliability assessment and reliability monitoring. The former provides a quantitative assessment of current reliability informed by the detection failure sources, whereas, the latter ensures timely delivery of the program plan whilst maintaining quality. Therefore, reliability assessment is results oriented, whereas, reliability monitoring is activities oriented and both methods are complimentary for controlled reliability growth.

Figure 3.2 displays a skeletal illustration of the assessment approach to the reliability growth management developed by the US Department of Defence (2011).

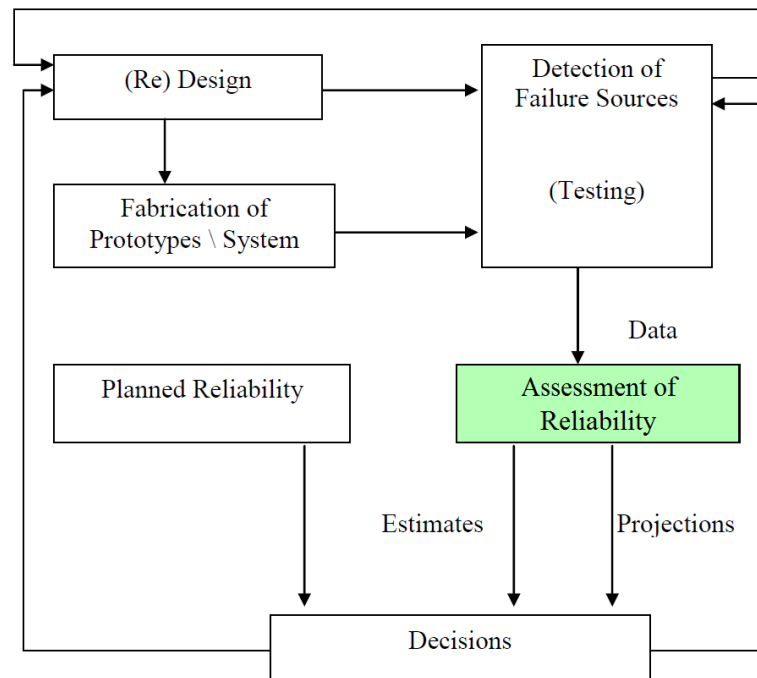


Figure 3.2: Assessment approach for reliability growth management model (Department of Defence, 2011) with the contribution of this study highlighted in green.

This recommended reliability assessment approach can be used to provide accurate evaluations of the reliability for the current system configuration. It allows comparison to an objectively developed growth standard to ensure that the program is in compliance with planned activities. If the progress is not delivering the desired results, new strategies such as reassignment of resources, schedule adjustment or re-examination of the system target reliability levels must be developed. A system reliability assessment for an OWT is conducted in this study due to its significance to reliability growth management.



While, surrogate failure rate data from onshore installations is commonly used in literature for OWT reliability assessment (Niclas et al., 2017; Martin et al., 2016; Lazakis and Kougioumtzoglou, 2017; Kougioumtzoglou and Lazakis, 2015), the unique contribution of this study is the assessment of reliability using publicly available field failure rate data by Carroll et al. (2015) for OWTs to apply the Stream 1 methodology summarised in Figure 3.1. Therefore, this work falls in the highlighted region in Figure 3.2 and can be informed by field or modelled failure rates. The resulting estimates of system reliability can be used in combination with target reliability levels to inform decisions to manage reliability growth.

Since an OWT system is composed of mechanical and structural components, two main approaches exist for reliability assessment (Ambühl et al., 2015):

- Mechanical and electrical component reliability - Based on the classical reliability theory conducted by reproducing the system configuration through components connected in parallel and/or series. Component failure rates are estimated using available data from within or similar industries. This failure rate is assumed to be constant over time and is at the bottom of the bath-tub curve of the component lifetime. Such reliability calculations are prone to uncertainties due to the possibility of inherent errors in adjusting failure rate.
- Structural reliability of the device - Probabilistic approach based on the limit state design accounts for environmental parameters and compensates for the limited amount of measurement data through use of appropriate models.

The classical reliability theory is employed for the system reliability assessment conducted in this study.

### 3.1.1 Reliability nomenclature

Systems may be broadly categorised into repairable and non-repairable systems based on the failure consequence; the former can be restored into operational condition after a repair activity whilst the latter is discarded after the first failure. Based on this premise, OWTs may be regarded as repairable systems whereby, a repair activity may refer to replacement of components, addition of new part, adjustment to settings, lubrication or cleaning.

Failure is defined as the inability of a system to perform its allocated function under specified conditions (Spinato et al., 2009). For individual system components, probability distribution function of failure  $F(t)$  is modelled as:

$$F(t) = Pr(T \leq t) \quad (3.1)$$

Where,  $F(t)$  is the probability that the item will fail within the interval  $(0; t]$ ,  $t$  is the time and  $T$  is the time to failure. Therefore, the probability of success, or the reliability of the system  $R(t)$  can be described as:

$$R(t) = Pr(T \geq t) = 1 - F(t) \quad (3.2)$$

System or component failure is commonly characterised by the Mean Time To Failure (MTTF) or Mean Time Between Failures (MTBF) for non-repairable and repairable systems, respectively. Additionally, the time taken for the system repair and restoration activities is referred to by the Mean Time To Repair (MTTR). For an OWT, classified as a repairable system, the time between two failure events is characterised by the Mean Time between Downing Events (MTBDE) which is described by the following formulation:

$$MTBDE = MTBF + MTTR \quad (3.3)$$

### 3.1.2 Lifetime failure distribution

For many systems, failure rate is not constant over time (Levin et al., 2003; Finkelstein, 2008). This characteristic is observed for onshore wind turbines, therefore, can be extended to their offshore equivalent. Using the volume of transfers as an indicator for turbine performance, it can be seen that a 50% reduction has been achieved since 2014 (SPARTA, 2018). This may be attributed to the maturation of the industry and improved methods to forecast failures and inform O&M activities.

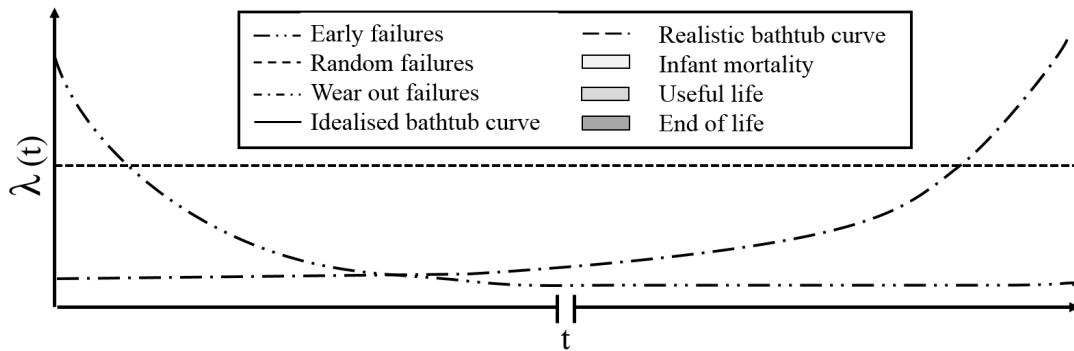
The technical properties of the component and loading profile dictate the time-dependent behaviour of the failures such as wear-out of OWT gear teeth. On the contrary, frequent control system failure at random intervals for an OWT is a characteristic pattern observed for new, unproven technology where failure mechanisms and causes are not fully understood for mitigation purposes.

Figure 3.3a presents the failure intensity function or failure rate,  $\lambda(t)$ , of the three failure phases during a product lifetime, namely early, intrinsic and detrio-

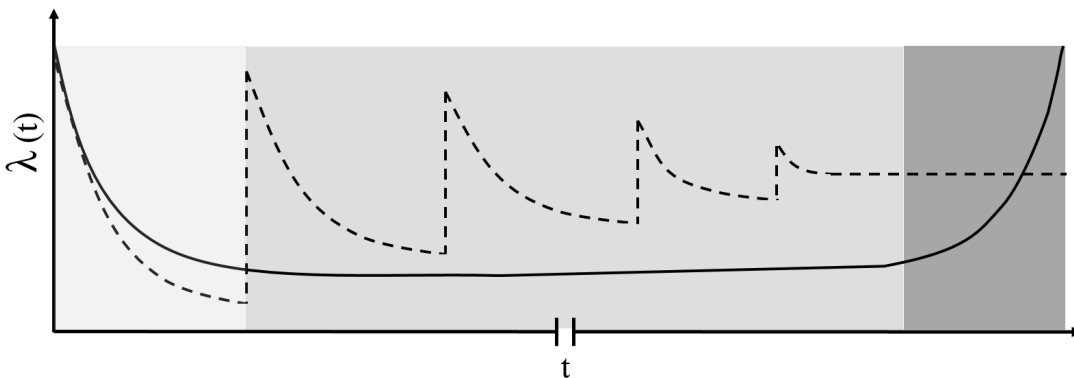
rating phases. Each phase and its characteristic failure distribution is described as follows:

- Early failure phase - Characterised by a decreasing failure intensity due to the systems teething issues
- Intrinsic failure phase - System experiences a constant low failure intensity due to its acclimatisation to the operational conditions over its useful life period
- Deteriorating phase - Marked by an increasing intensity function for the end of life of the system

Moubray (1997) provides further details regarding aforementioned lifecycle failure patterns.



(a) Failure intensity functions for the early, intrinsic failure and deteriorating phases of a device.



(b) Representation of the idealised and realistic bathtub curves describing failure rate distributions for lifetime analysis

Figure 3.3: Constituent failure rate distributions for lifetime analysis and the resulting idealised and realistic bathtub curves.

The device lifetime bathtub curve is produced by the combination of the three phases shown in Figure 3.3a. This combination may result in an idealised or realistic bathtub curve as seen in Figure 3.3b. Each peak in  $\lambda(t)$  of the realistic curve occurs due to a maintenance activity. The difference between the idealised and realistic bathtub curve shows that the observation of the entire (idealised) curve is a rare event during asset lifetime since most repairable systems have an associated maintenance regime.

Numerous statistical distributions can be used to fit the failure patterns, with the normal and lognormal distribution providing characterisation for the early failure phase and the exponential distribution providing a good fit for the intrinsic failure phase. However, the versatility of the Weibull distribution, formulated and popularised for use in reliability analysis, allows it to model failures at all three stages of the system lifetime by adjustment of the shape parameter  $\beta$ . As a general rule,  $(\beta < 1)$ ,  $(\beta = 1)$  and  $(\beta > 1)$  are chosen for early, constant and deterioration phases of a system, respectively.

For the useful life phase ( $\beta = 1$ ), where the system only experiences failure due to its intrinsic properties, Equation. 3.4 reduces to a special case of the Poisson process called the homogeneous Poisson process characterised by a constant intensity function. This allows the MTBF to be independent and exponentially distributed, thus, allowing the failure rate to be determined as the inverse of the intensity function. For the scope of this analysis, the wind turbine and all its constituent assemblies are considered to be in the useful phase, thereby, characterised by low and constant failures independent of equipment age and marked by an invariable occurrence likelihood throughout the product lifetime.

Therefore, the reliability of a complex repairable system such as an OWT can be modelled by the Power Law Process with the intensity function described in terms of the shape and scale parameter.

$$\lambda(t) = \frac{\beta t^{\beta-1}}{\eta \eta} \tag{3.4}$$

Where, the failure rate and its associated shape and scale parameters are  $\lambda$ ,  $\beta$  and  $\eta$ , respectively.

### 3.1.3 Reliability and availability

The annual energy production, availability and the capacity factor not only depend on reliability but also on the predominant wind conditions on site and the consequence of a fault (Spinato et al., 2009). The consequence of a fault is dictated by the maintenance strategy employed by the operator, weather window availability for repair and logistic delays. As is typical of any OWF, SCADA data from the Dutch offshore wind project Egmond aan Zee (NoordzeeWind, 2010) allows for the monitoring of the availability, downtime and failures of the wind farm.

Comparison of the least squared regression line between percentage stops and loss of power in Figure 3.4 shows that there is no direct correlation between the two parameters for a assembly analysis; a high number of unscheduled stops does not automatically indicate a high impact on availability. This is particularly evident in the case of the gearbox, whereby, the contribution to the number of failures is modest  $\approx 7.4\%$ , however, the loss of power is  $\approx 55.6\%$  of the total downtime.

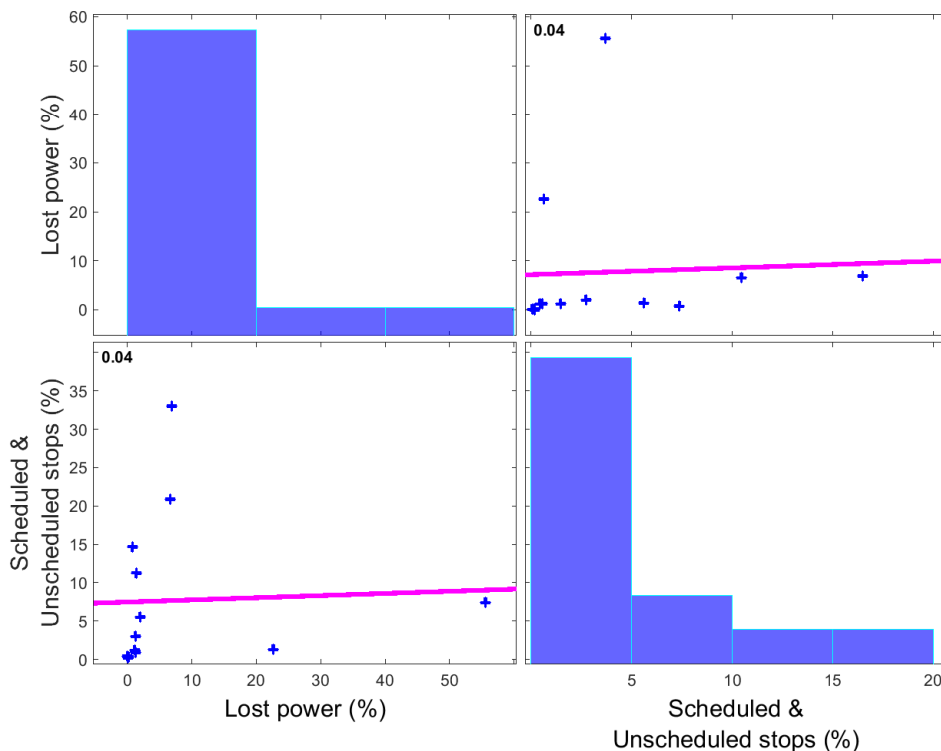


Figure 3.4: Correlation plot based on annual OWF data from Egmond aan Zee (NoordzeeWind, 2010) showing the lack of correlation between failure rate and availability.

## 3.2 Modelling parameters and methodology

Systems failure modelling facilitates the investigation of operation and failure patterns of a device by accounting for the failure distribution, repair and restoration activities, spare part availability and logistic delays to inform improved design and maintenance practices (Davidson and Hunsley, 1994). To achieve this objective, the following sequential process should be followed (Andrawus, 2008):

- Identification of suitable statistical distribution that best fits the assessed failure characteristics of the device
- Collecting and collating a parameter database from literature or estimation through modelling techniques
- Design a Reliability Block Diagram (RBD) to model asset failures
- Perform Monte Carlo simulations on the RBD for determination of key performance variables such as reliability and availability

### 3.2.1 Reliability modelling software

Existing research in the wind industry (Andrawus, 2008; Zhu et al., 2011; Hill et al., 2008; Kaidis, 2012) has shown confidence in the use of the software developed by ReliaSoft, particularly BlockSim, for system reliability analysis. Therefore, for this case study, a system reliability model is simulated using MonteCarlo simulation in ReliaSoft BlockSim 7 to assess and optimise the RAMS of the OWT taking into account the material costs and assembly failure rate.

BlockSim provides the user with freedom to choose between two computational modes, namely, analytical and simulation. The time-dependent analytical solution is suitable to fulfill the objective of having a system level failure distribution as an aggregate of the assembly level distributions.

Since an OWT is a repairable system best modelled with associated details of repair and restoration, the analytical analysis is not considered suitable to provide comprehensive turbine performance estimates. Instead, random failure events from the failure distribution of each assembly are simulated. Simulations provide the ease of solving complex scenarios by handling multiple probabilistic events such as failure rate, corrective maintenance, crew response time, spare part availability

etc, however, lead to higher computational times, dependence on the seed choice and lack of reproducibility due to the random nature of data generation.

### 3.2.2 Failure data mining for a representative OWT

System reliability calculations are largely based on the failure rate statistics which can be extracted from primary or secondary sources. Robust assessments require data from individual devices with particular operating conditions, therefore, a statistically robust database is vital for precision as discussed in Chapter 2. While failure rate data for OWTs is scarce in the public domain, industrial stakeholders are gradually accumulating a preliminary understanding of the failure events with increasing deployment experience and broadening cooperation within the industry. One such available assembly failure rate database from OWT deployment experience (Carroll et al., 2015) is used as input for the RBD, thereby, applying Stream 1 shown in Figure 2.11. The failure rates provided in the database are for an OWT with nominal power between 2 - 4 MW.

Table 3.1 tabulates the failure rate of the various assemblies of an OWT categorised into the various subsystems. Additionally, Carroll et al. (2015) divides the failures based upon the material costs for the restoration activity with the cost of minor repairs at less than €1000, major repairs between €1000 and €10,000 and major replacements with associated cost of over €10,000 as shown in Appendix C.

While Table 3.1 provides the failure rate of the individual assemblies, the failure statistic required for reliability calculations in BlockSim is the MTBF which may be calculated using the following formula:

$$\text{MTBF} = \frac{8760}{\lambda} \quad (3.5)$$

Where,  $\lambda$  is the annual failure rate. The time taken for the corrective maintenance of each assembly (Carroll et al., 2015) is detailed in Appendix C along with associated material cost.

### 3.2.3 System reliability model

A reliability block diagram is produced using failure rate data from existing offshore installations to assess system reliability and the influence of major and minor assembly failures as well as replacements on overall system performance.

### 3.2. Modelling parameters and methodology

Table 3.1: OWT assembly failure rate categorised into subsystems with corresponding repair strategy (Carroll et al., 2015).

Assembly	$\lambda_B$ [1/annum]				
	Replacement	Major repair	Minor repair	No cost data*	Total
Rotor module					
Blades	0.001	0.01	0.456	0.053	0.52
Pitch/Hydraulics	0.001	0.179	0.824	0.072	1.076
Hub	0.001	0.038	0.182	0.014	0.235
Nacelle					
Yaw system	0.001	0.006	0.162	0.02	0.189
Control module					
Controls	0.001	0.054	0.326	0.018	0.399
Sensors	0	0.07	0.247	0.029	0.346
Drivetrain Module					
Gearbox	0.154	0.038	0.395	0.046	0.633
Generator	0.095	0.321	0.485	0.098	0.999
Power Module					
Electrical components	0.002	0.016	0.358	0.059	0.435
Contactors/ Relay/Circuit breaker	0.002	0.054	0.326	0.048	0.43
Power supply/ Converter	0.005	0.081	0.076	0.018	0.18
Transformer	0.001	0.003	0.052	0.009	0.065
Auxiliary System					
Grease/Oil/Cooling liquid	0	0.006	0.407	0.058	0.471
Pumps/Motors	0	0.043	0.278	0.025	0.346
Safety	0	0.004	0.373	0.015	0.392
Heaters/Coolers	0	0.007	0.19	0.016	0.213
Service items	0	0.001	0.108	0.016	0.125
Other components	0.001	0.042	0.812	0.15	1.005
Structure					
Tower/Foundation	0	0.089	0.092	0.004	0.185

No cost data available for failures included in this category.



### 3.2.3.1 System configuration

OWE is a very dynamic industry at the moment: new devices and new processes are continually developed and demonstrated, making it difficult to conduct reliability assessments. This is due to the lack of universal processes and system configurations which leads to use of variable subsystems with individual failure rates. Therefore, to fully understand the OWT reliability, it is imperative to differentiate between the system, subsystems, assemblies and their constituent subassemblies.

Through the course of this thesis, a consistent hierarchical nomenclature is used. For the system categorisation developed to categorise the failures calculated in Carroll et al. (2015) and displayed in Figure 3.5, the following terminology is used based on the onshore ReliaWind project (Wilkinson et al., 2010):

- System - An integrated set of elements accomplishing a defined object; the complete OWT is the system under consideration in this thesis.
- Subsystem - A system in its own right but does not serve a useful function such as the Rotor Module.
- Assembly - Refer to all elements at a lower level of hierarchy than the subsystem such as the Blades in the Rotor subsystem.
- Subassembly - Collection of parts put together as a unit, to be used in the making of a larger assembly.
- Component - Individual elements in the subassembly.

### 3.2.3.2 Reliability Block Diagram

An RBD is a top-down, sequence-independent method which provides a diagrammatic representation of the system reliability and is employed to model time-dependent failure distributions and other properties, such as repair/restoration time distributions. It is a success oriented method; for an OWT this is the ability to produce power. The OWT systems are divided into subsystems represented by statistically independent blocks which reflect the logical behaviour of the system. After connecting the blocks in the system configuration, associated failure rates are used to compute system reliability (Rausand and Høyland, 2003).

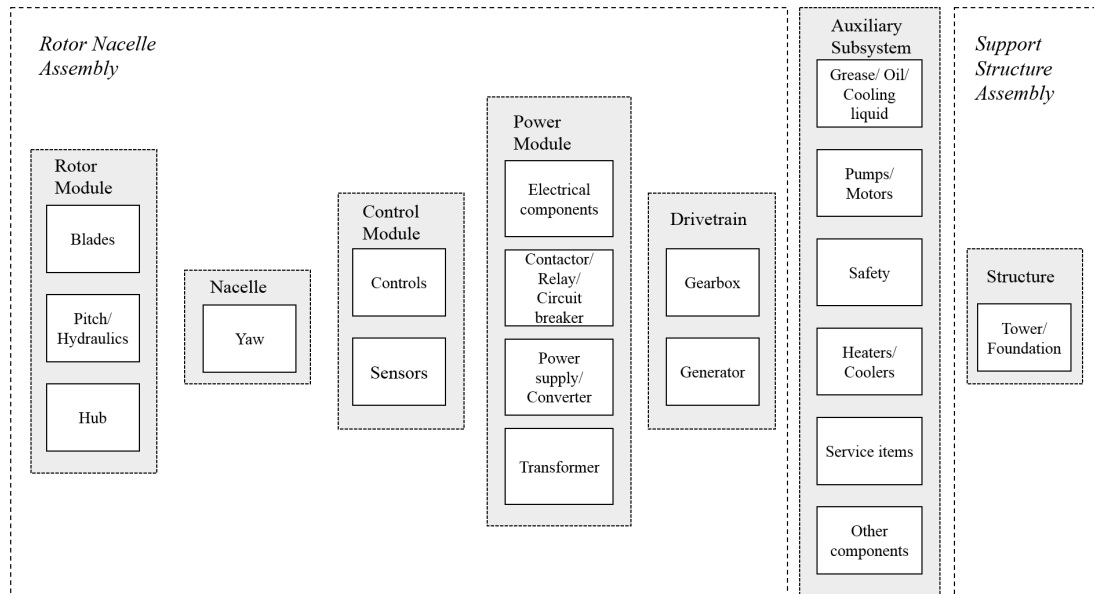


Figure 3.5: Subsystems and constituent assemblies of a standard OWT categorised into subsystems based on Wilkinson et al. (2011).

The subsystems are assigned a probabilistic distribution describing their time dependent failure rate statistics, and another distribution for the time to repair. When allocating lifetime failure characteristics to the constituent assemblies, the 2 parameter Weibull distribution was used but due to limited data regarding the influence of aging on the device,  $\beta = 1$  was used for all assemblies.

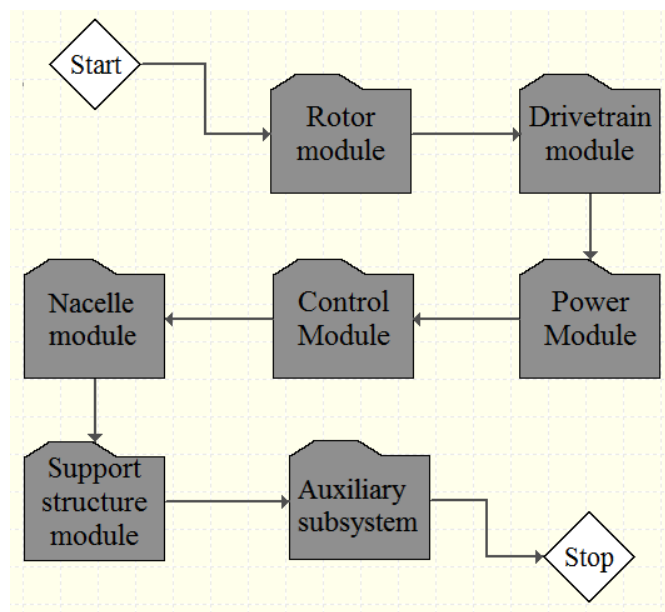


Figure 3.6: Reliability block diagram for an OWT system.

These failure rates are then combined in accordance with the associated assem-

bly configuration to yield the subsystem failure rates based on the categorisation displayed in Figure 3.5.

Figure 3.6 shows the OWT RBD produced using the constituent subsystems recommended by Wilkinson et al. (2011) in ReliaSoft BlockSim 7 software. Assuming that failure of any subsystem leads to the failure of the complete OWT system, all subsystems are connected in series (Peters et al., 2012). Furthermore, the constituent assemblies in each subsystem are also connected in series. This allows the analyst to treat the event frequency of OWT failure frequency as multiplicative with associated analytical system reliability calculated as shown in Equation 3.6.

$$R_{\text{System}} = \prod R_{\text{Assembly}} \quad (3.6)$$

This provides a conservative estimate of the reliability,  $R$ , of a system as a product of the assembly reliability since the failure of any assembly will lead to the failure of the entire OWT system.

### 3.2.4 OWT Maintenance characteristics

The maintainability of a system is defined by the probability of performing a successful repair action within an allocated period of time (ReliaSoft, 2007), namely MTTR, which may include the time taken for the following activities:

- Fault diagnosis
- Procurement and delivery of parts to perform repair
- Time taken to recover faulty parts
- Time taken to replace/repair and install the fixed/new parts
- Time taken to ensure operation of system within a safe mode and then return to normal operation

MTTR characterises the maintainability of a system based on a deterministic or probabilistic distribution. Investigation of the uncertainties in the MTTR estimates due to the use of deterministic values as well as exponential and lognormal distributions (Seyr and Muskulus, 2016) for OWTs shows discernible differences. At the average assembly MTTR of 21 hours, the exponential distribution is seen to

suitably represent the repair time density function, therefore, the MTTR for this RBD is modelled using the single parameter exponential distribution, whereby, maintainability is expressed by Equation. 3.7.

$$M(t) = 1 - e^{-\frac{1}{MTTR} \cdot t} \quad (3.7)$$

Where,  $M$  is the maintainability expressed as a function of time,  $t$ , and mean time to repair,  $MTTR$ . BlockSim provides the opportunity to define and use three different maintenance policies for each assembly in the system, namely, corrective maintenance, preventative maintenance and scheduled inspection. While an ideal preventative maintenance regime would prevent all assembly failures, thus, ensuring 100% reliability, it is only considered when its overall cost is lower than the expense of a corrective action. Additionally, there is an associated fallacy with the usefulness of employing a preventative maintenance policy for an assembly in its useful life phase where it is characterised by constant failure rate (ReliaSoft, 2007), therefore, no preventative policy is used for the OWT system. Similarly, no regular inspection policy is associated for turbine maintenance and maintenance activities are only undertaken correctively when a block fails and causes the system to come down.

Based on existing research (Seyr and Muskulus, 2016), an exponential distribution is considered appropriate for modelling the repair times. For all assemblies, it is assumed that the corrective maintenance brings the system down during the period of the activity and the assembly is returned to as-good-as-new condition through the action. Also, it must be noted that an unlimited supply of spare parts is assumed for the maintenance activity thus neglecting the effect of insufficient inventory management.

### 3.3 System reliability simulation results

As a rule of thumb, the simulation end time should be at least three times larger than the system MTTF, in this case it is taken to be equal to the OWT lifetime of 20 years (175200 hours).

Results of assembly as well as the overall system states categorised based on major replacement, major and minor repairs are presented to determine the critical subsystems for each type of repair and restoration activity.

### 3.3.1 Reliability statistics and failure rate distribution

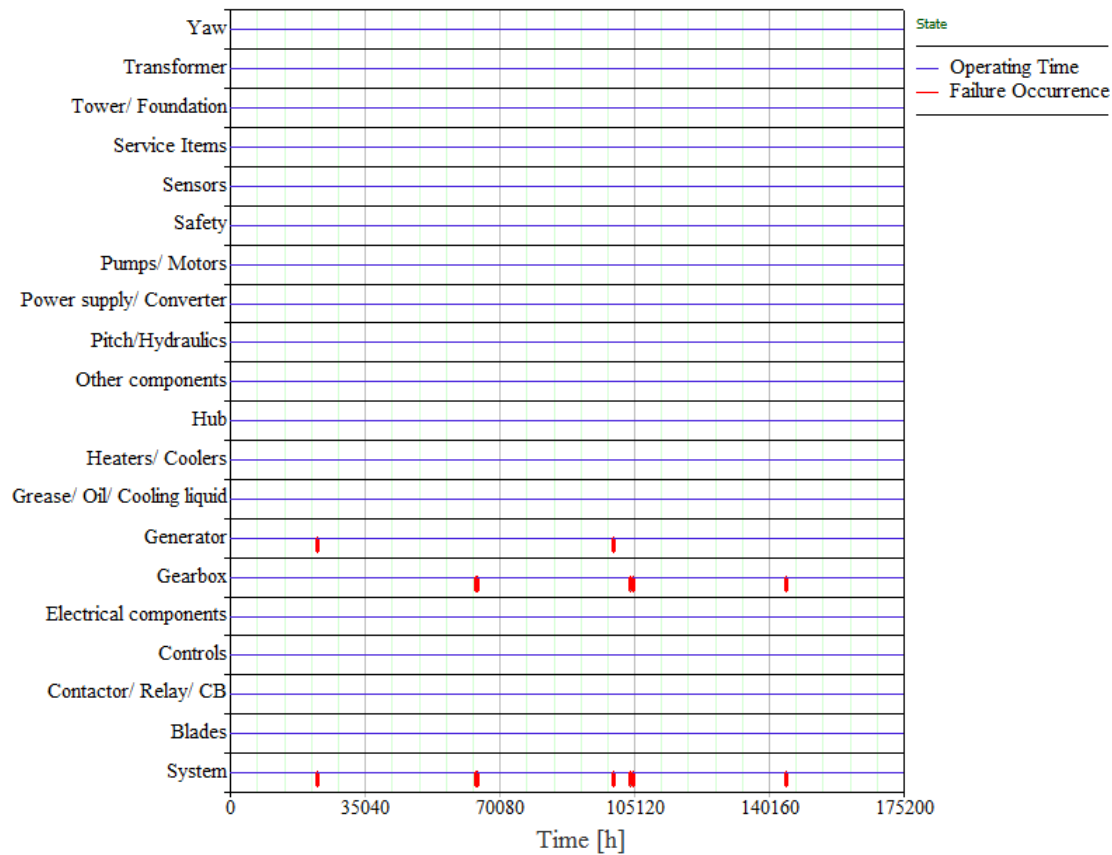
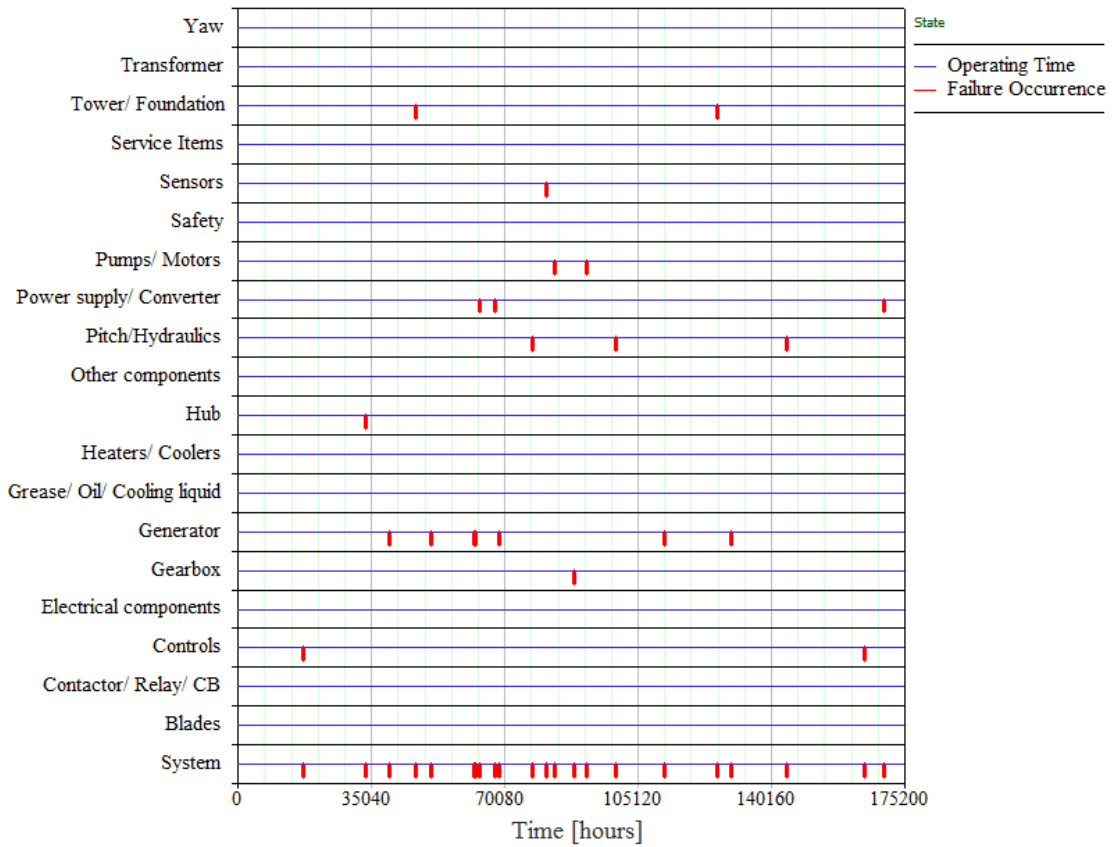


Figure 3.7: Block states for major replacement simulations

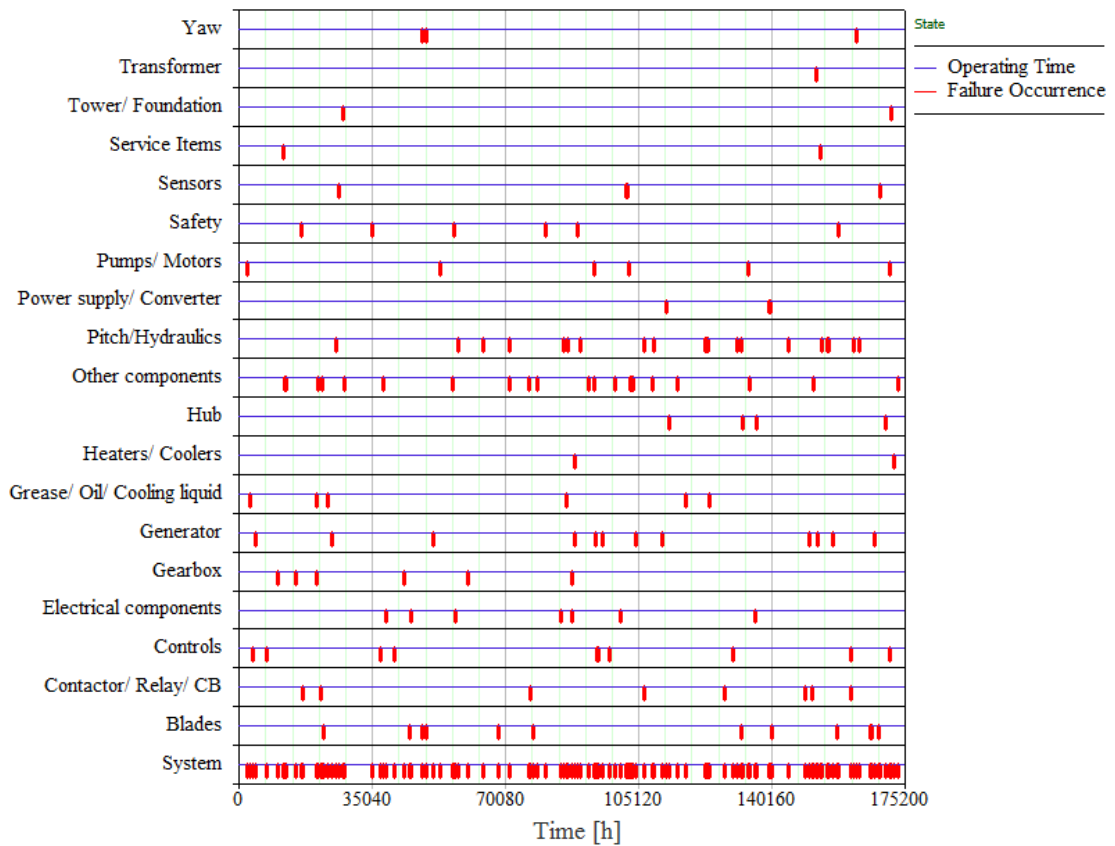
As shown in Figure 3.7, the system is brought down for major replacements during its lifetime solely due to the failures associated to the drive train module, particularly the gearbox. However, other assemblies actively contribute to the system downtime for the major (Figure 3.8a) and minor (Figure 3.8b) repairs with the maximum downtime attributed to the generator and pitch/hydraulics, respectively.

During the turbine lifetime, each assembly experiences at least one minor failure, whereas, major failures are mainly attributed to the drivetrain, rotor and controls module with possible events for the structural subsystem of the hub and support structure. The rotor module has the highest contribution to system downtime resulting in minor repairs particularly due to the increased pitch/hydraulic failures.

When the individual downtime per failure is compared in Table 3.2, it can be seen that the average downtimes range from 160 hours/failure to 6.3 hours/failure for major replacements, major repair and minor repair restoration activities. There-



(a) Block states for major repair simulations.



(b) Block states for minor repair simulations

Figure 3.8: Block states for the major and minor repairs.

fore, results indicate similar trends to the NoordzeeWind (2010) data, whereby, the larger number of failures may not directly translate to a large consequence for the turbine power output.

### 3.3.2 Failures and associated cost

Realising that the purpose behind device optimisation is a decrease in LCOE leads to the conclusion that assembly maintenance costs must be factored into the equation for a more pragmatic assessment of target reliability levels. These targets can be realised by technological improvement of the individual assemblies or introduction of redundancy in the system where possible.

To encapsulate the influence of failures on the OPEX of the OWT, the expected failures and their associated restoration costs for individual assemblies is presented for major replacements, major and minor failures. Figure 3.9, displays the cost of system restoration based on material expense due to the failures leading to major replacement of assemblies.

The restoration activities requiring major replacements within the cost bracket of €10,000 and above are majorly dominated by failures in the drivetrain. The main assembly contributing to these failures is the gearbox followed by the generator repairs at about a seventh of the cost as seen in Table 3.2.

Similarly, as seen in Figure 3.10, the drive train has the highest contribution to the major repairs as well. The cost of major repairs to the drivetrain is dominated by the failures in the generator. Failures in the rotor module due to pitch or hydraulics are the second largest contributor to failure rate, however, due to their associated lower cost, their contribution to the overall lifetime repair costs is lower than the power module which has high economic consequence due to the failures occurring in the power supply or converter as seen in Figure 3.10.

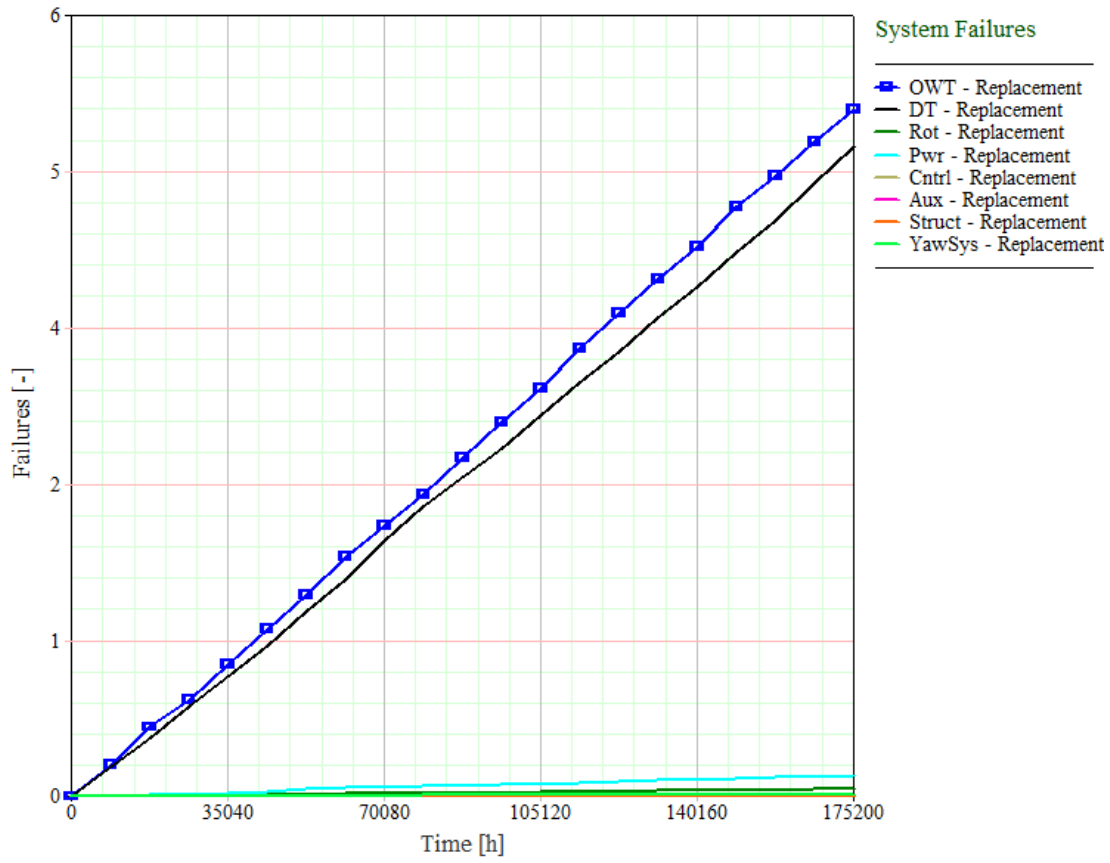
Finally, minor failures and the associated repair costs are dominated by failures in the auxiliary subsystem, however, assembly-level analysis shows that the maximum contribution towards the failure rate and restoration costs can be attributed to the pitch and hydraulics from the rotor module. This is recorded in Figure 3.11. Tabulated results in Table 3.2 show that the economic consequence of the failure due to replacement activities is much higher than due to minor replacements based on downtime as well as material costs. With replacement costs at over 800 times

### 3.3. System reliability simulation results

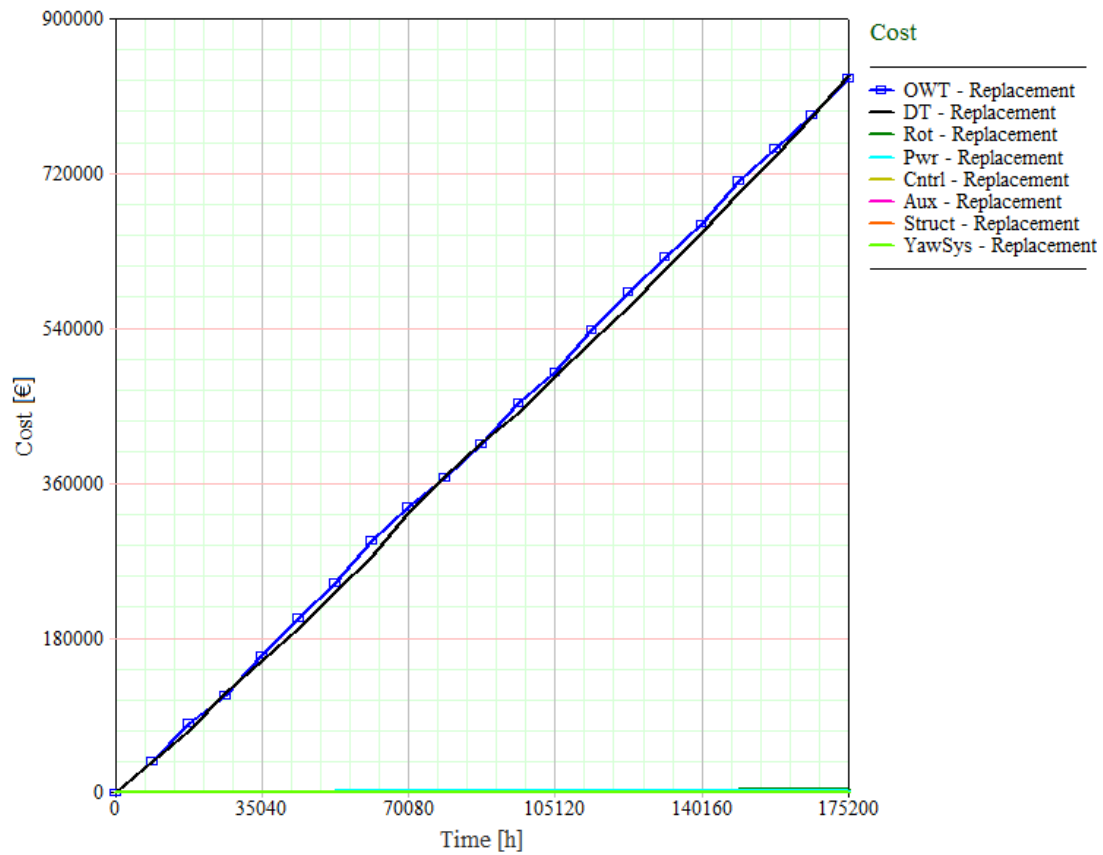
Table 3.2: Summary results for the system reliability assessment for an offshore wind turbine providing estimates for the lifetime failures, downtime and associated costs. The assemblies with the highest failure consequence are listed based on contribution to downtime and restoration costs.

Parameter	Units	Ranking	Replacement	Major repair	Minor Repair
Lifetime failures			5.3	21.2	123.6
System Downtime	hours		851.5	379.4	777.1
Downtime per failure	hours		160.7	17.9	6.3
Material costs	euros		830419	54399	21775
Cost per failure	euros		156682.8	2566	176.2
Downtime ranking					
Assembly name		1	Gearbox	Generator	Pitch/ Hy- draulics
Associated downtime	hours		675.5	148.2	147.8
Assembly name		2	Generator	Pitch/ Hy- draulics	Other compo- nents
Associated downtime	hours		154.6	68.9	81
Assembly name		3	Blades	Hub	Blades
Associated downtime	hours		6.7	32.9	79.3
Restoration cost ranking					
Assembly name		1	Gearbox	Generator	Pitch/ Hy- draulics
Associated cost	euros		709780	22470	3470
Assembly name		2	Generator	Power supply/ Converter	Pumps/ Mo- tors
Associated cost	euros		112320	9098	1890
Assembly name		3	Transformer	Pitch/ Hy- draulics	Heaters/ Coolers
Associated cost	euros		1960	7112	1810



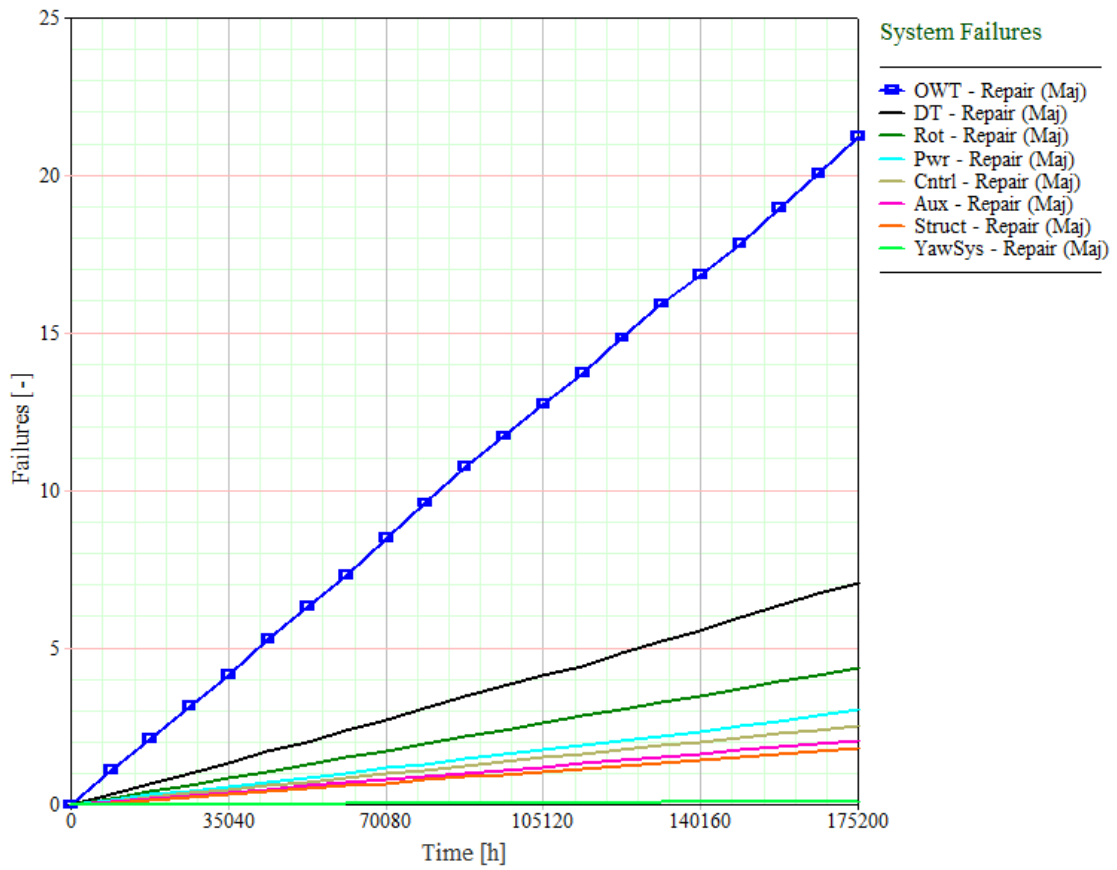


(a) Replacement failures

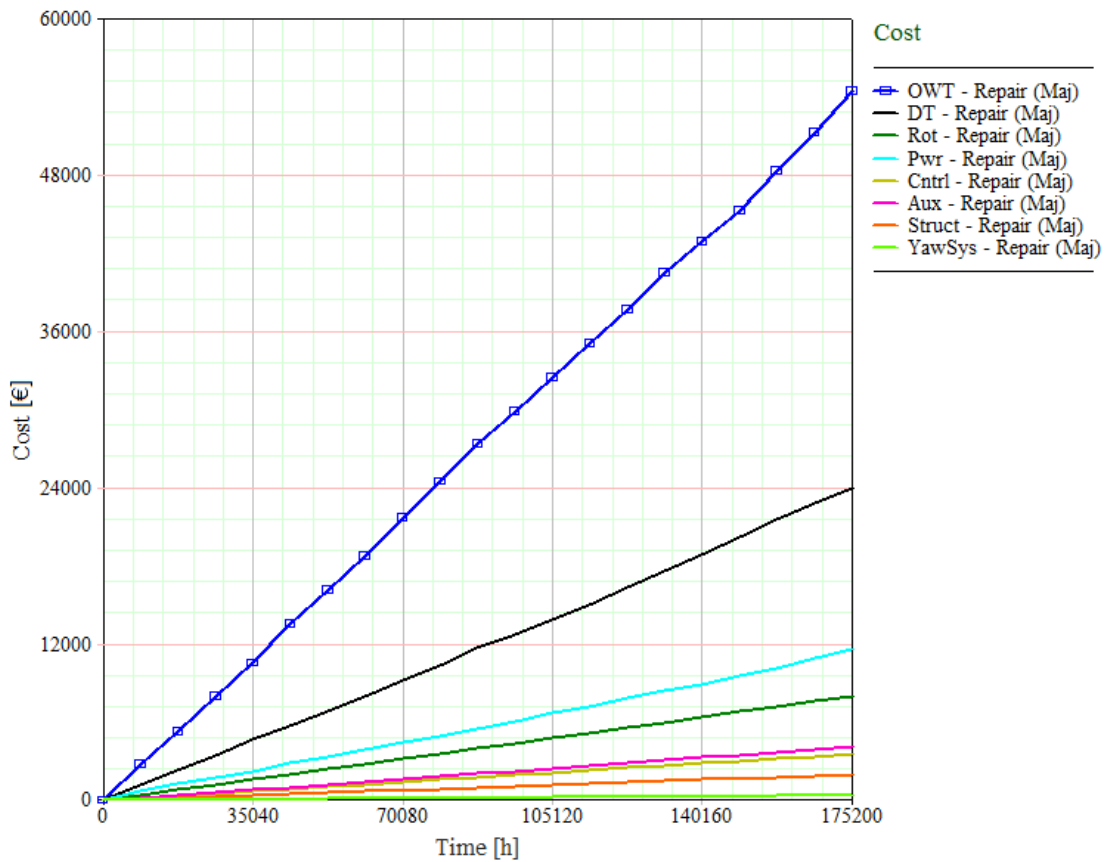


(b) Replacement costs

Figure 3.9: Failures and cost for major replacements.

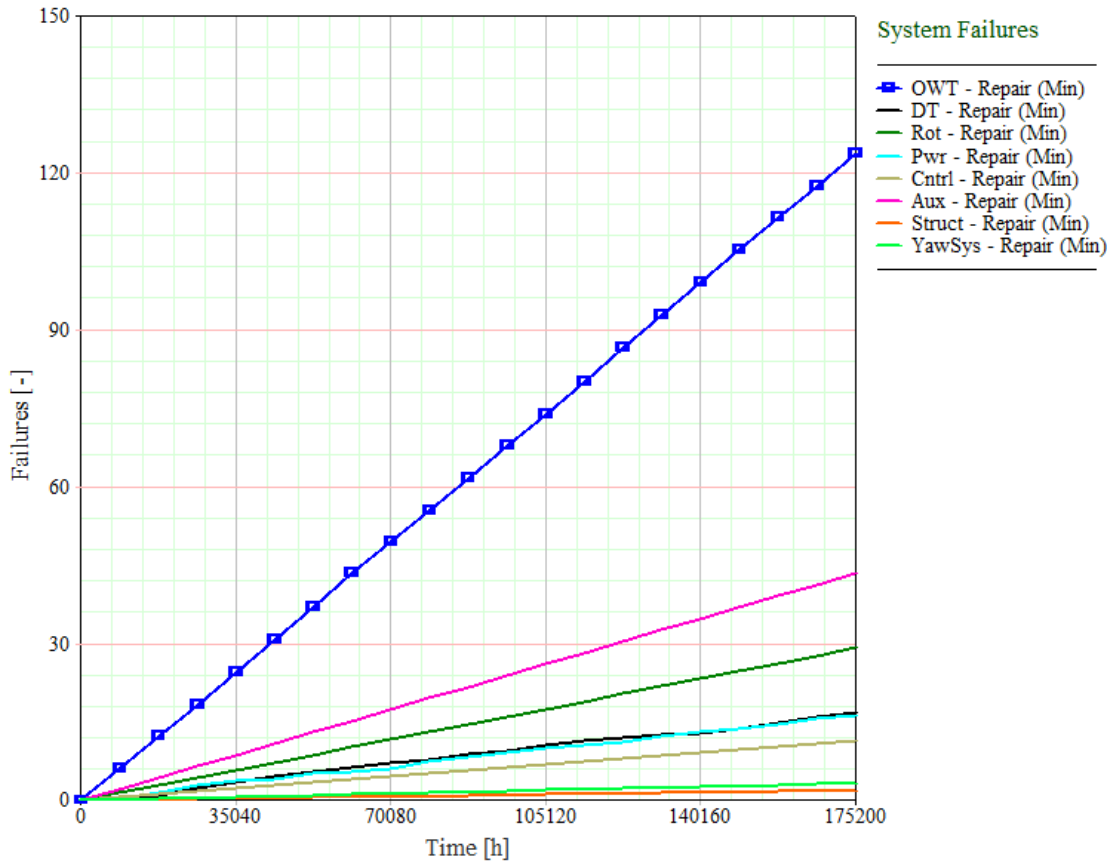


(a) Major failures

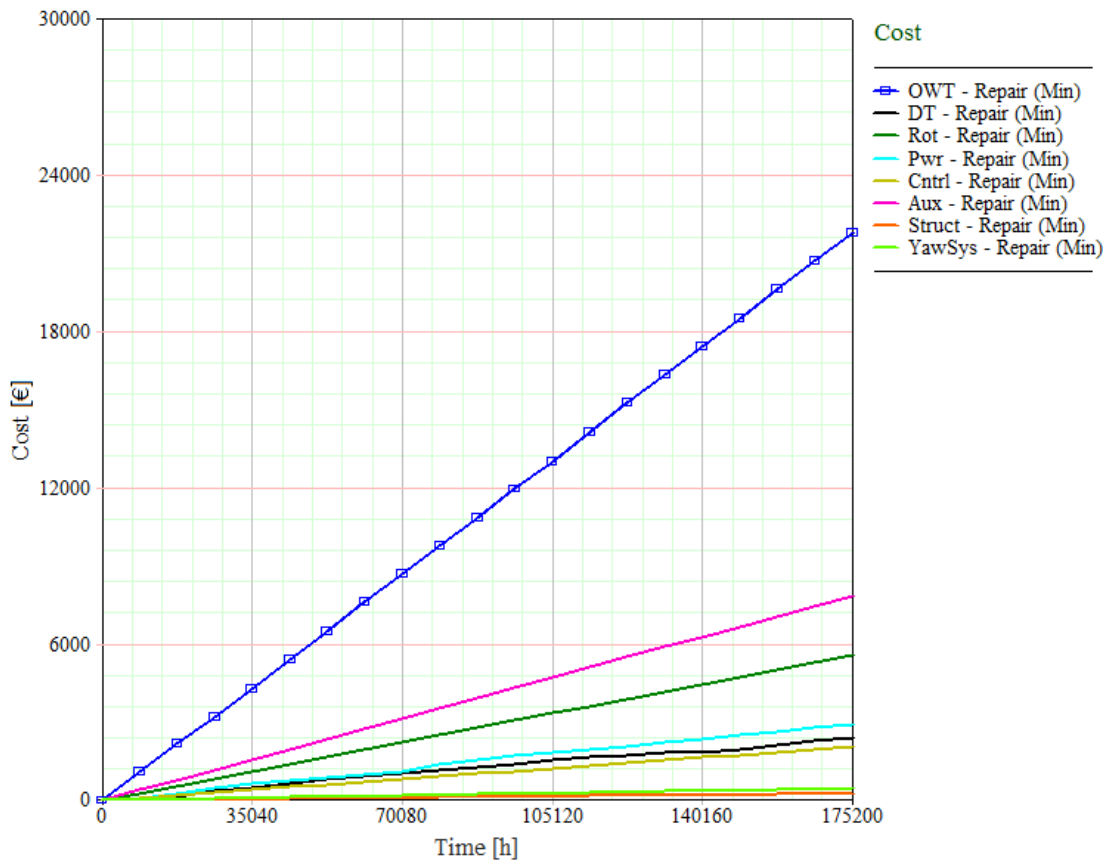


(b) Major costs

Figure 3.10: Failures and cost for major repairs.



(a) Minor failure



(b) Minor costs

Figure 3.11: Failures and cost for minor repairs.

the cost of a minor repair and 25 times as much repair time, the replacement activities are highly cost intensive and must be mitigated to reduce OPEX and improve the LCOE for electricity generated from offshore wind.

### 3.4 Discussion of results

The categorisation of failure rate data based on the associated repair costs provides a suitable indication of the consequence of the failure for each assembly. The OWT failure occurrences can be attributed to a range of assemblies with diverse failure modes; while the pitch and hydraulics are expected to fail annually, the transformer is expected to develop a fault every 15 years. The associated consequence of failure displays trends directly translated from onshore deployments to offshore deployments (Faulstich et al., 2009; S. Faulstich, B. Hahn, 2010), whereby the largest contribution to failures is due to pitch/hydraulics, whereas, the gearbox has the largest contribution to system downtime. Therefore, for the minor failures with material cost of  $\leq 1000$  euros, the rotor and auxiliary modules provide the highest contribution to failure rate. While the failure rate is magnified for the auxiliary module as it is composed of an array of assemblies, the pitch and hydraulics are the main drivers for the higher failure rate of the rotor module. As the associated cost of the failure events increases, the failure events can be seen to transition towards the drivetrain module composed of the gearbox and generator.

Since the used cost data only provides information about the material costs, therefore, for major repairs and replacements, the overall contribution of each failure to OPEX is higher than that displayed by Figure 3.9 if the ancillary tangible or intangible costs such as loss of production and technician wages are considered. The combination of logistic delay, weather window availability and the high associated repair times for the generator ( $\approx 70$  hours) and gearbox ( $\approx 230$  hours) relative to the pitch and hydraulics ( $\approx 25$  hours) (Carroll et al., 2015) leads to a large variation in the consequent downtimes.

Investigations into the implications of the statistical uncertainty due to the choice of distribution describing the failure rate show that the choice of a different distribution may cause variation in estimates of wind farm availability of up to 20% (Niclas et al., 2017). The simplistic assumption of constant failure rate may introduce a significant positive or negative bias in the system reliability. In order to

conduct a robust reliability assessment, the influence of early and wearout failures on structural reliability of an OWT must be accurately quantified (Lantz, 2013).

Additional uncertainty may be introduced due to the probabilistic characterisation of repair times (Seyr and Muskulus, 2016) for corrective maintenance. While an annual preventative maintenance regime is an industrial standard (Verbruggen, 2003), the conducted reliability study did not explore the impact of preventative maintenance on OWT. Furthermore, the study does not account for logistic delays due to weather window, spare part and/or crew availability when characterising downtimes for the system, therefore, these additional variables may be incorporated for improved understanding of production losses from the system.

The economic consequence of the failure is highlighted by the cost of the material used for the restoration only, therefore, further analysis incorporating the cost of the crew and vessel hire should be conducted.

Utilisation of the weighted allocation analysis in BlockSim 8 to derive improved failure rates based on weighting factors may allow for improved application and utilisation of this study. With sufficient industrial data, these factors must be determined by analysing the complexity, technological limitations and maturity of the assembly design.

Although the configuration and rating of the turbine for which the failure data was retrieved is not known, this system reliability study has provided an understanding of the dependence of reliability on the individual assemblies of the OWT. However, the application of these generic OWE industrial failure rates to the various deployment sites in the UKCS may not provide comprehensive system reliability predictions. Therefore, for robust reliability estimates, site-specific failure rates based on environmental conditions is imperative.

### 3.5 Chapter summary

This chapter aims to apply Stream 1 of the methodology shown in Figure 2.11 to quantify site-specific OWT performance to inform location-intelligent decisions for farm siting. At the outset, it presents reliability nomenclature and describes lifetime failure distribution. Due to its significance to reliability growth management, system reliability assessment for an OWT is conducted using a field reliability database published by Carroll et al. (2015) in the ReliaSoft BlockSim software.

The failure rate data is categorised by Carroll et al. (2015) into major and minor failures and replacement failures based on the cost of repair. For each repair cost category, a top-down statistical approach, namely the reliability block diagram is produced by connecting the subsystem and assembly modules in series. System reliability is simulated over a 20 year OWT design lifetime assuming the turbine is in the useful life stage with constant failures characterised by a 2 parameter Weibull distribution. Only a corrective maintenance strategy is applied with system being restored to an as-good-as-new condition and repair times are exponentially distributed. The associated assembly repair costs listed by Carroll et al. (2015) with assumed fixed values across the lifetime of the OWT are used to provide estimates for the increase in OPEX due to the failure events.

Outputs of this chapter allow for the identification of the reliability - critical and availability - critical subsystems. However, the attempt to use field failure rate data to quantify spatial distribution of system reliability using Stream 1 was unsuccessful since the used failure rate database does not provide information about the deployment locations of the turbines. The lack of this information eliminates the possibility of an informed adjustment of failure rates, therefore, Stream 2 is identified as a more feasible option for quantification of a spatially distributed risk-return metric.



# Chapter 4

## Methodology

Current practices in the OWE industry regard annual resource potential as a simplistic but viable estimate of the revenue of the energy produced at an offshore location. However, after the assessment of the end-user requirement of site characterisation parameters, a metocean-centric performance metric encompassing the influence of power production and reliability is proposed in Chapter 2.

Figure 2.11 provides a schematic representation of the multiple possible pathways to conduct reliability assessment. As it can be seen, the availability of the failure rate database is a decision parameter right at the outset of the project which affects the possible pathways that can be chosen. As identified in Chapter 3, industry-specific data for site-specific OWE reliability analysis is not readily available at this embryonic stage of the industry. Therefore, to achieve the aim of this thesis, Stream 2 from Figure 2.11 is employed to produce site-specific fatigue lifetime estimates. Reproduced in Figure 4.1, the Stream 2 methodology is a dual-phase process which allows the translation of spatial metocean parameters into spatial reliability indicators.

Data from existing archives for metocean parameters in the UKCS is retrieved and processed using an aero-elastic-hydro-servodynamic tool for device response characterisation. Additional data analysis methodologies are employed for data analysis to calculate enhanced parameters for improved site identification of OWE through reliability indicators.

The estimation of the fatigue lifetime of an offshore wind turbine requires the identification of critical assemblies. These critical assemblies may then be exposed to a large number of time-domain simulations to account for the range of load



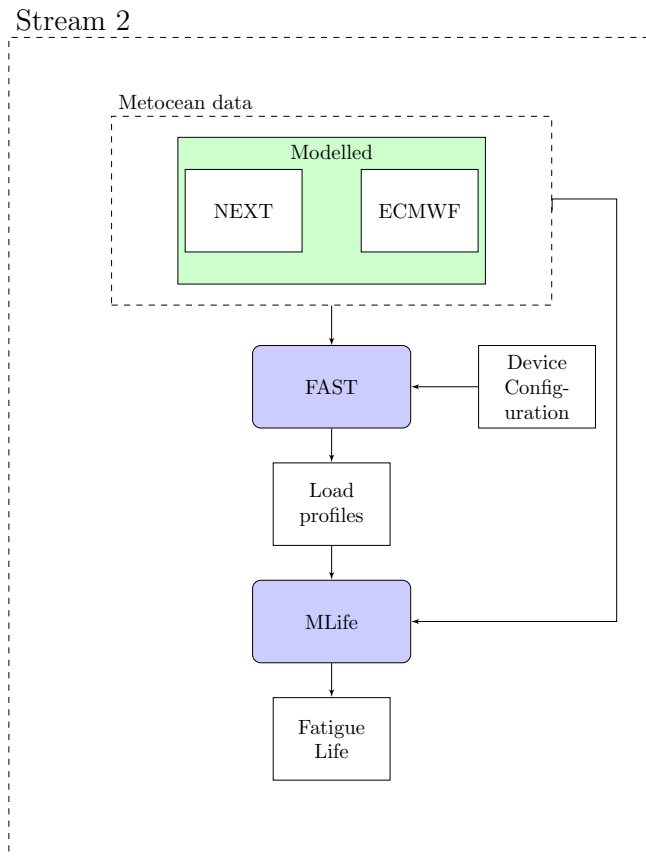


Figure 4.1: Dual-phase methodology using an aero-elasto-servo-dynamic tool in conjunction with a damage life estimation tool to conduct a spatial system performance analysis using modelled metocean data.

conditions that a turbine may experience when deployed at a particular site.

Widely used in offshore engineering for the characterisation of the resource potential, scatterplots of meteorological parameters can also be used for the fatigue life prediction. Using representative metocean scatter plots, combined assessment of the two parameters, namely, power production and fatigue life can be used to inform location-intelligent siting decisions. Produced failure estimates for individual assemblies may be used to conduct a system reliability assessment for the proposed sites at an early stage of the project.

Drawing on the extrapolation of environmental conditions and loads from modelled and simulated data for allocation of assembly failure rates, a Geographical Information System is used to characterise the existing and planned OWE deployment sites on the basis of a production-reliability metric.

This chapter provides a description of the various tools and overarching methodologies involved in acquiring the site-specific power production and reliability metrics. Additional details about the structural, environmental and numeric parameters can also be found in the subsequent chapters.

### 4.1 Structural Response

Analytical models of the decomposition of the spatial domain by using an iterative process to solve for continuous coupled sub-systems do not produce tractable closed-form solutions. Therefore, approximation by discretisation is popularly done using the Raleigh Ritz (Angelov, 2018), boundary element (Alesbe et al., 2017) or finite element method (Hearn and Edgers, 2010). To solve larger and more complex systems, further optimisation of the approximation process can be introduced by dividing the structure into sub-domain and iteratively solving the interface coupling by using the engineering tool of dynamic substructuring.

Further streamlining of the process is obtained by reducing the complexity of the sub-systems by representing the sub-system response by general response instead of detailed discretised response.

For an uncoupled analysis of offshore wind turbines, the interface usually lies at the transition piece since this is commonly where the design responsibility is divided between the turbine designer and the substructure designer. The output of an aero- and hydro-dynamic code can be used as an input for the structural

response software at the interface. However, over the past two decades, numerous sophisticated fully coupled multi-physics software tools have been introduced for reliable representation of onshore wind turbine structures and have evolved for use in the OWE industry. For the scope of this study, the functionality of two such softwares is explored.

### 4.1.1 CAE design tools for OWF structural analysis

Software tools used for reliable representation of onshore wind turbine structures have now evolved for use in the OWE industry. Garrad Hassan Bladed (Hassan, 2003) is one such commercially-available, modular, time-domain design and modelling tool which allows the calculation of structural loads of fixed and floating OWTs to assess turbine performance. Wind turbine structural components and environmental parameters are defined using the graphical user interface to execute wind turbine dynamic response assessments and the results can be post-processed and drafted as reports. However, only the Educational version of Bladed was available for this project which has reduced functionality for analysis of the variable responses of OWT subassemblies. Restrictions include: limit on simulation period to 60 s, inability of batch process calculations, reduced structural element discretisation, singular turbulence component, fixed random seed, fixed tower geometry to a tubular axisymmetric tower and possibility of post-processing using only a single output channel. Additionally, the temporal limitation imposed by Bladed at 60 s simulation length produces weakly stationary metocean parameters, and consequently stationary forces on the OWT structure.

Owing to the above limitations, FAST (Fatigue, Aerodynamics, Structures and Turbulence) is used to predict coupled dynamic response of an OWT. FAST is a CAE design code, developed by the National Renewable Energy Laboratory (NREL) in 2002, suitable for the determination of extreme and fatigue loads. Despite the similarity in the design philosophy of FAST and Bladed, they display differences in the aero-elastic theories which gives rise to differences between the codes' outputs (Passon et al., 2007).

With an evolved flexibility allowing the simulation of a range of offshore environmental and turbine structural characteristics, FAST is chosen as the aero-hydro-servo-elastodynamic response simulator for this project. 10-minute long

simulations are run for each DLC to quantify the environmental parameter profiles by interfacing with the aerodynamic (AeroDyn) and hydrodynamic (HydroDyn) modules of FAST.

Dynamic substructuring, a domain-independent toolset, allows for the modelling and analysis of the mechanical system by analysing the dynamic behaviour of the components or sub-systems separately. It allows for the system to be optimised at the assembly level and facilitates test combinations of various subassemblies. Additionally, it reduces the numerical computational effort required by simulating the sub-systems separately rather than the complete system. The resulting dynamics are then coupled for calculation of fatigue for the complete system. FAST provides the capability to conduct time-domain analysis, therefore, the analysis conducted is limited to the time-domain. Integrated time-domain analysis, involving fully coupled analysis of the complete OWT system, is pivotal for informing design decisions in OWE.

The publically available FAST glue code loosely couples well-defined data exchange interfaces or modules under a modularisation framework to model a coupled non-linear aero-hydro-servo-elastic system. For the scope of this project, the FAST v8.16.00a-bjj glue code is compiled in double precision with the following modules:

- ElastoDyn v1.04.00a-bjj
- InflowWind v3.03.00
- AeroDyn v14.04.00
- ServoDyn v1.06.00a-bjj
- HydroDyn v2.05.01
- SubDyn v1.03.00

These modules correspond to various physical domains of the fully coupled solution for the wind turbine and are further explained in Chapter 4.1.6.

### 4.1.2 Turbine specification

Analytical formulations derive load time series from the input set of inflow conditions and turbine operational parameters to describe the dynamic behaviour of an OWT. Since existing research (Sutherland, 1999) indicates that the correlation between damage estimates and inflow parameters is highly site and turbine specific, therefore, this research project restricts the type of considered turbine whilst highlighting the site dependence of the structures.

An investigation into the metocean parameter influence on OWE devices requires detailed information regarding a model turbine with realistic parameters. Although turbines with ever-increasing power rating are being deployed offshore, during the conception phase of this research the annual average rating of OWTs was 5 MW as seen in Figure 4.2. Therefore, the wind turbine used for the scope of this study is the offshore 5-MW reference turbine by NREL (Jonkman et al., 2009) which is a three-bladed, geared upwind turbine with yaw capability. It is a variable speed device which is controlled by variable blade-pitch-to-feather.

It is a theoretical turbine that has been defined specifically for research purposes and does not represent a real device, but is designed to be representative of the large 5-10 MW class turbines. It is largely based on the REpower (now Senvion) 5 MW turbine (Jonkman et al., 2009) and has been widely used in research as the baseline for offshore turbines to provide robust results for loading regimes. Figure 4.3 shows a diagrammatic representation of the baseline turbine along with tabulated generic properties of the modelled device in Table 4.1.

The hub of the baseline turbine is located 5m upwind of the tower top and 90m above the mean sea level (MSL). The vertical offset of the hub is set at 2.4 m, therefore, the yaw bearing is located at a height of 87.6 m above MSL.

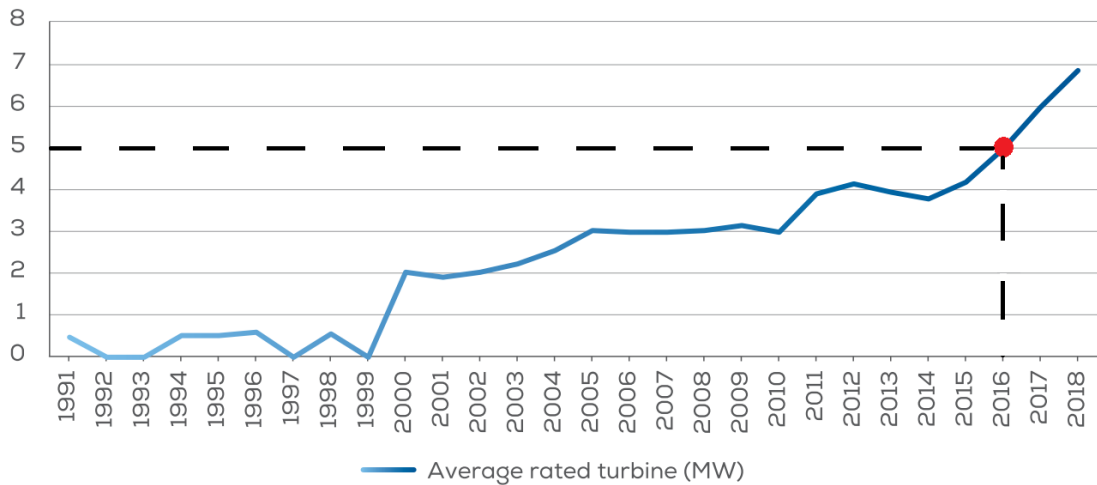


Figure 4.2: Average annual OWT rated capacity (MW) for newly installed devices (WindEurope Business Intelligence, 2019) in Europe between 1991-2018. At the conception of this project in 2016, the average rating of a turbine was 5 MW.

Both control systems, generator torque controller and full-span rotor-collective blade-pitch controller of the baseline turbine, work independently of each other. Below rated speed, the turbine is mainly controlled by the torque controller to

maximise power capture, whereas, above rated speed, pitch feathering allows the regulation of generator speed. The drivetrain of the turbine is modelled as a system of a generator with a rated speed of 1173.7 rpm and gearbox with 97:1 ratio.

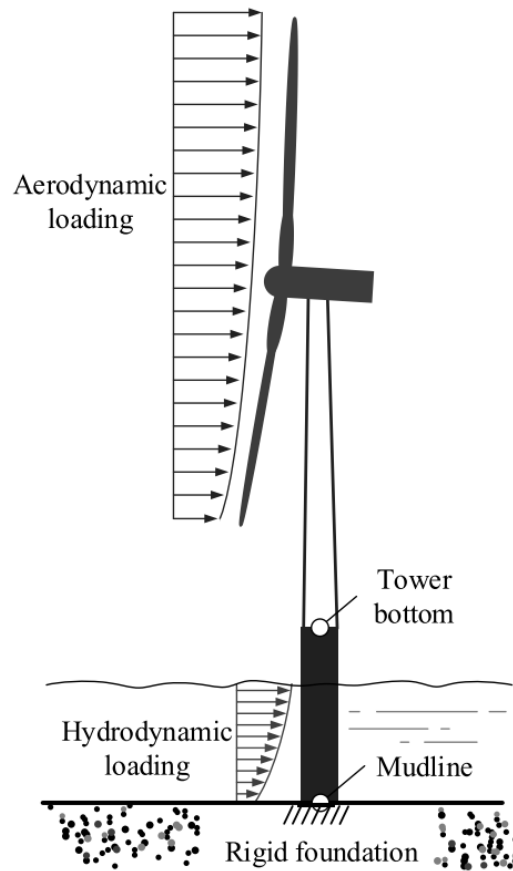


Figure 4.3: Diagrammatic representation of the modelled NREL 5-MW baseline monopile wind turbine (Ziegler, 2016). The tower bottom corresponds to the location of the TP for this research.

### 4.1.2.1 Subassembly properties

As described in Chapter.2, the RNA and the support structure are the two main assemblies of the turbine with structural components. Due to the restriction of the focus of this project to structural components, a brief description of the geometric and material properties of the structural subassemblies is provided here.

#### 4.1.2.1.1 Blade design and aerofoil properties

The baseline turbine of choice is a conventional-three bladed device with blade structural properties based on the 62.6 m LM Glasfiber blade analysed in the

Table 4.1: Summary of specifications for the modelled NREL 5-MW baseline monopile wind turbine (Jonkman et al., 2009).

Parameter	Specification
Rotor diameter	123 m
Number of blades	3
Hub height	90 m
Offset of hub to side of tower centre	0 m
Tower height ( $T_{Ht}$ )	87.6 m
Rotational sense of rotor, viewed from upwind	Clockwise
Position of rotor relative to tower	Upwind
Transmission	Gearbox
Aerodynamic control surfaces	Pitch
Fixed / Variable speed	Variable
Cut in windspeed	3 m/s
Cut out windspeed	25 m/s

Dutch Offshore Wind Energy Converter (DOWEC) study (Jonkman et al., 2009). All three blades are identical and divided into ten identical sections or aerofoils.

Eight different aerofoil datasets, namely Cylinder 1, Cylinder 2, DU40\_A17, DU35\_A17, DU30\_A17, DU25\_A17, DU21\_A17, NACA64\_A17 recreate the aerodynamic properties of the blade. In the aerofoil names, ‘DU’ is an acronym for Delft University and ‘NACA’ for National Advisory Committee for Aeronautics. The two aerofoils closest to the blade root are cylindrical, whereas, the remaining aerofoils are modelled (Jonkman et al., 2009) by making corrections to the six aerofoils in the DOWEC study. Additional details regarding the angle of attack, pitch moment coefficient, lift and drag coefficients may be found in the Appendix B of the technical report defining the turbine (Jonkman et al., 2009).

#### 4.1.2.1.2 Tower and Support structure properties

Support structure integrity is a key determinant in lifetime extension decision of offshore wind installations as more turbines reach their design lifetime (Ziegler, 2018). As discussed in Chapter 2, the selection of the support structure depends on

Table 4.2: Tower properties for the 5MW NREL baseline turbine extracted from §6 of (Jonkman et al., 2009) appended with substructure properties from the OC3 monopile (B. J. Jonkman and Jason Jonkman, 2016).

Station Number	Height [m]	Diameter [m]	Wall thickness [mm]	Mass/unit length [kg/m]	Stiffness [Nm <sup>2</sup> ]	Shear stiffness [N]
1	-20	6	0.027	5590.87	6.143E+11	1.381E+11
2	0	6	0.027	5590.87	6.143E+11	1.381E+11
3	8.76	5.469	0.025	5232.43	5.348E+11	1.293E+11
4	35.04	4.936	0.023	4227.75	3.419E+11	1.045E+11
5	61.32	4.403	0.021	3329.03	2.065E+11	8.225E+10
6	87.6	3.87	0.019	2536.27	1.158E+11	6.266E+10

the geographical properties of the installation site, including water depth, seabed features, ocean conditions and the type of turbine used. Suitable to water depths of up to 30 m (now 37 m), monopiles are the default choice for wind turbine foundation design at present due to the associated ease of fabrication and installation. Effectively, a monopile is a direct extension of the turbine superstructure through the transition piece which serves as a flange sealed by grouting. Structurally, it consists of a cylindrical steel pile driven into the subsoil by heavy duty hydraulic hammers. Due to its favourable properties of withstanding high tension and compression forces, steel is a common construction material for OWT sub-structures. The DOWEC study, which forms the basis of the 5-MW NREL turbine, recommends an elastic modulus of 210 GPa (Jonkman et al., 2009) for steel.

The 30m rigidly fixed-bottom substructure investigated in the OC3 project (Passon et al., 2007) is used in conjunction with the baseline turbine to support the RNA on a 77.6 m tower. Details of the support structure of the reference wind turbine includes model parameters for a tower which is mounted on a uniform substructure rigidly fixed at the mudline. These are tabulated in Table 4.2.

The height of the stations is the elevation along the centerline from the MSL, therefore, the submerged points below station 2 have negative values. The substructure is seen to be an ideal uniform beam with isotropic material properties and uniform geometry, whereas, the tower is a linearly tapered structure.



Along with the loads induced due to the wind and wave dynamics, the support structure is also designed to withstand loads induced in any other subassembly of the OWT transferred to the support structure. The environmental parameters acting on the OWT tower cause a bending stress along the entire length of the structural member. The support structure is modelled as a cantilever member; fixed at the foundation and free to move at the tower top. Therefore, the environmental actors aim to rotate the structure at the mudline producing moment around all three axes.

### 4.1.3 Site environmental characteristics for illustrative location

To illustrate the suitability of various inputs and sample outputs, the environmental parameters for the Hornsea Offshore Wind Farm Project One owned by DONG Energy (now Ørsted) are used in this chapter. About 120 km off the coast of Yorkshire at  $53.883^\circ$  N and  $1.922^\circ$  E, it is a 1.2 GW project which was granted consent in 2014 under Round Three of the OWF development zones. The 174 Siemens turbines in the project utilise foundations by EEW Special Pipe Constructions GmbH and transition pieces by Bladt Industries with Offshore Structures Britain, and Steelwind with Wilton Engineering. Second generation wave model United Kingdom Met Office (UKMO) data from a representative point near the leased project site in the Southern North Sea is used to characterise the site (SMart Wind Limited, 2013) for the project environmental statement. With a median wind speed of 7.2m/s (10m above MSL) and significant wave height of 1.1 m, the site is dominated by the influence of waves from the first quadrant of the direction spectrum.

Table 4.3 shows the input parameters used to calculate fatigue for a hypothetical 5MW fixed bottom, piled wind turbine at the Hornsea project site. Where,  $V_t$  is recorded 10 m above MSL,  $T_p$  is calculated as 1.408 times the zero-crossing period,  $T_z$ , and  $\theta_W$  is the direction of the incident waves which is aligned with the wind direction. Throughout the course of this thesis, the HornSea site is used as a representative site to illustrate the development of the methodology and interim results.

The following subsections discuss additional generic details regarding the meto-

Table 4.3: Input metocean parameters for a 5MW monopile OWT deployed at the Hornsea Project One site.

Parameter	Variable	Value	Units
Wind	$V_t$	7.2	m/s
	$H_s$	1.1	m
Wave	$T_z$	3.8	s
	$T_p$	5.35	s
	$\theta_W$	0	degree

cean parameters used throughout this thesis.

#### 4.1.3.1 Wind

A potential offshore site can be characterised by its wind parameters of mean speed, directionality, shear and turbulence intensity. As described in Section 4.1.2, the modelled turbine has a cut in speed of 3 m/s and a cut-out speed of 25 m/s, therefore, it will be operational between Beaufort scale 3-10 from Table 2.1.

Friction due to planetary contact in the atmospheric boundary layer effects the vertical wind profile called the shear profile. Since the mean wind speed is defined at 10 m above MSL for the UKMO model, shear affects must be encompassed for defining the wind profile at hub height. An isolated offshore wind turbine will be exposed to low turbulence intensity since turbulence intensity depends on the altitude and roughness of terrain. This can be modelled using the logarithmic or power law. A logarithmic shear profile with the default FAST ground roughness length is used.

It is industrial standard to model wind data at 10 m above MSL, therefore, the wind speed data from most databases must be sheared using the following equation (Emeis and Matthias, 2007):

$$V(z) = V(z_{ref}) \frac{\ln\left(\frac{z}{z_0}\right)}{\ln\left(\frac{z_{ref}}{z_0}\right)} \quad (4.1)$$

Where,  $z$  is the elevation,  $V(z)$  is the  $V_t$  at elevation  $z$ ,  $z_{ref}$  is the reference elevation,  $V(z_{ref})$  is  $V_t$  at the reference height and  $z_0$  is the roughness length.

Roughness length, the measure of the roughness of surface terrain, is considerably reduced for offshore conditions and is allocated a default value for these simulations assuming a logarithmic vertical wind profile.

While the logarithmic shear profile is known to not be suitable for all atmospheric stability conditions, this idealised shear profile is commonly used (Det Norske Veritas, 2010) since data for the shear profile at individual sites at different atmospheric stability conditions is not readily available.

#### 4.1.3.2 Wave

In addition to production of aerodynamic loads, local wind conditions also influence wave loads on the OWTs since wind is the main driver behind sea waves. The response of the substructure is highly dependent on the hydrodynamic loading due to wave particle velocity and acceleration. Hydrodynamic loads on the slender substructure can be calculated as the sum of the drag and inertia loads.

As discussed in Chapter 2 various spectra aim to emulate site-specific measured wave spectra with a distinct set of conditions including the frequently fitted Pierson-Moskowitz or JONSWAP wave spectra. The former describes sea surface elevation based on a single input parameter (wind) for a fully developed sea at finite fetch while the latter is representative of a sea state that is not fully developed.

The UKMO model provides the mean period, whereas, the peak period is an important input to the fatigue model. Therefore, the mean period was transformed into peak period by fitting a JONSWAP wave spectrum with a gamma factor ( $\gamma$ ) of 3.3.  $T_p$  is the inverse of the frequency at which the peak of the power spectral density curve occurs which allows the enhancement of the Pierson-Moskowitz spectrum by informing the peakedness parameter. Inputs to the JONSWAP spectra include  $H_s$ ,  $T_p$  and  $\gamma$ . However, it is common practise in atmospheric modelling to provide the mean zero-crossing period as a wave parameter. When approximating the peak period for the JONSWAP spectrum from the mean zero-crossing period, the following relationship based on the two-peak spectral model (Torsethaugen et al., 1985) is used:

$$\frac{T_p}{T_z} \approx 1.30301 - 0.01698 * \gamma + \frac{0.12102}{\gamma} \quad (4.2)$$

Where  $T_z$  is the zero-crossing period.

With  $\gamma = 1$ , the peak period is calculated as  $T_p = 1.408 * T_z$  (British Standards Institution, 2009) for the fully developed seas represented by the Pierson Moskowitz spectrum. On the contrary,  $\gamma$  may vary between 1 - 7 for the JONSWAP spectrum and is best estimated by the statistical analysis of the recorded wave spectrum at any site. However, a typical value of the peak shape parameter for a standard JONSWAP spectrum is 3.3. This, in conjunction with Equation. 4.2 (WAFO Group, 2000), is used for all conversions from  $T_z$  to  $T_p$  for the scope of this project.

### 4.1.3.3 Tidal currents

The analysed case considers a still water level of 0 m since this is representative of an average tidal state and no modulation of wave conditions has been observed in local measurements due to the tidal signal. The influence of tidal turbulence is discounted since tidal current velocity variation is considered to be of generally a larger time-scale than OWT design load variations.

### 4.1.4 Model set-up guidance

The time-marching fatigue analysis for a standard NREL 5 MW turbine is conducted using the multi-physics aero-servo-hydro-elastodynamic FAST software in conjunction with its various modules. Standard recommendation (Det Norske Veritas, 2014; British Standards Institution, 2009) follows that the first “5 s of data (or longer if necessary)” may be discarded from the analysis interval to eliminate the influence of initial conditions on the dynamic solution. Start-up transient behaviour due to the influence of gravity and rotor-rotation on structural displacements during computational analysis may lead to numerical instability. The transients die out due to structural damping after 30 seconds or more based on the choice of initial conditions, natural frequencies of the system and controller settings. Therefore, the use of proper initial conditions is recommended based on Figure 9-1 of the publication by Sandia National Laboratories (2013) and modelling tips by B. J. Jonkman and Jason Jonkman (2016) provide recommendations to address any additional possible instabilities. As a general practice in the use of the aero-elastic codes for offshore wind turbine (Passon et al., 2007), the first 30 seconds of the simulation are discounted as transient. However, based on sim-

ulations and recommendations through literature (Haid et al., 2013) for floating OC3-Hywind spar buoy using FAST this discounted time is increased to 60 seconds.

Frequencies and mode shapes of a specified number of modes for the model set-up should be analysed. Modal analysis needs to be run after a model has been completed, and before any dynamic simulations are run. If some of the modes are observed to have high frequencies, it may be preferable to specify fewer modes, since high frequency modes cause the simulations to run more slowly, and tend to have less influence on loads than the modes of lower frequency. Typically, 4 blade modes and 7 tower modes are sufficient for accurate results from FAST simulations.

Wind inflow for the turbine is calculated using InflowWind (Platt et al., 2016) and full field turbulence is simulated using logarithmic shear wind profile and the Kaimal spectrum in TurbSim. Ten minute long simulations of hydrodynamic and aerodynamic loads are run by interfacing the modules HydroDyn and InflowWind, respectively, and turbine reaction forces are simulated using ElastoDyn, AeroDyn and SubDyn.

### 4.1.5 Choice of variables

Tables 16 - 44 (Jason Jonkman and Marshall L Buhl, 2005) show the possible outputs generated by the 10 minute FAST simulation for loads at and reactions of various structural subsystems. Using the modal formulation for the tower and substructure, nodal outputs are produced for 5 and 3 members, respectively with node 1 being closest to the mudline. A list of the important outputs extracted from FAST is attached in Appendix D. A subset of these outputs is post-processed to calculate basic statistics as well as fatigue life for the selected structural components.

#### 4.1.5.1 Coordinate system definition

It can be seen in Appendix D that there is a range of possible output variables based on the coordinate system selection, nodal reduction and physical formulation that can be post-processed for fatigue life determination. Also, there is an overlap of nodes observed at the interface between the dynamic substructures. As an example, the node at the tower base (TwrBsFxt) coincides with that at the topmost

Table 4.4: Relevant coordinate system extensions for the NREL 5 MW turbine (B. J. Jonkman and Jason Jonkman, 2016; Damiani et al., 2015).

Subassembly name	Extension	Description
Substructure	ss	Global and substructure coordinate system
	e	Element coordinate system
Tower	t	Coordinate system fixed in the tower base
	p	Coordinate system fixed in tower-top or base plate with no translation with nacelle yaw
	n	Coordinate system translating and rotating with the tower top and yaws with the nacelle

member of the substructure (M3N2FKxe) and the transition piece (IntfFXss).

Additionally, multiple coordinate systems introduced in the FAST modules may also lead to a variation of results. The extensions of the variable names provide information as to what coordinate system is used and are described in Table 4.4. To ensure the similitude between the available variables to facilitate the accurate choice of variables for analysing FAST outputs, the shear force and bending moments for each of the points of interest are tabulated in Table 4.5 are plotted in Figure 4.4. It can be seen that for the extracted section of the load time series, a high variation is not observed between the overlapping nodes or variable coordinate systems at the mudline, transition piece or tower top.

For the substructure, only the element coordinate system provides the possibility of load evaluation at the nodes, whereas, the global coordinate system provides forces and moments at the interfaces, namely the transition piece and mudline, only. The nacelle/yaw rotating coordinate system for the tower provides a good estimate since it accomodates the influence of all the degrees of freedom in the OWT.

Table 4.5: FAST output variables at the mudline, transition piece and tower top based on coordinate system selection, nodal reduction and physical formulation.

Subassembly name	Variable name	Description
Mudline	React $\zeta$ Xss	Reaction loads in the global and substructure coordinate system
	M1N1 $\zeta$ KXe	Reaction loads in the element coordinate system
Transition piece	IntfFXss	Reaction loads in the global and substructure coordinate system
	TwrBs $\zeta$ xt	Reaction loads in the coordinate system fixed in the tower base
Tower Top	M1N1 $\zeta$ KXe	Reaction loads in the element coordinate system
	YawBr $\zeta$ xp	Reaction loads in the coordinate system fixed in tower-top or base plate with no translation with nacelle yaw
	YawBr $\zeta$ xn	Reaction loads in the coordinate system translating and rotating with the tower top and yaws with the nacelle
	TwHt5 $\zeta$ Lxt	Reaction loads in the coordinate system fixed in the tower base

$\zeta = F$  for shear force and  $\zeta = M$  for bending moment

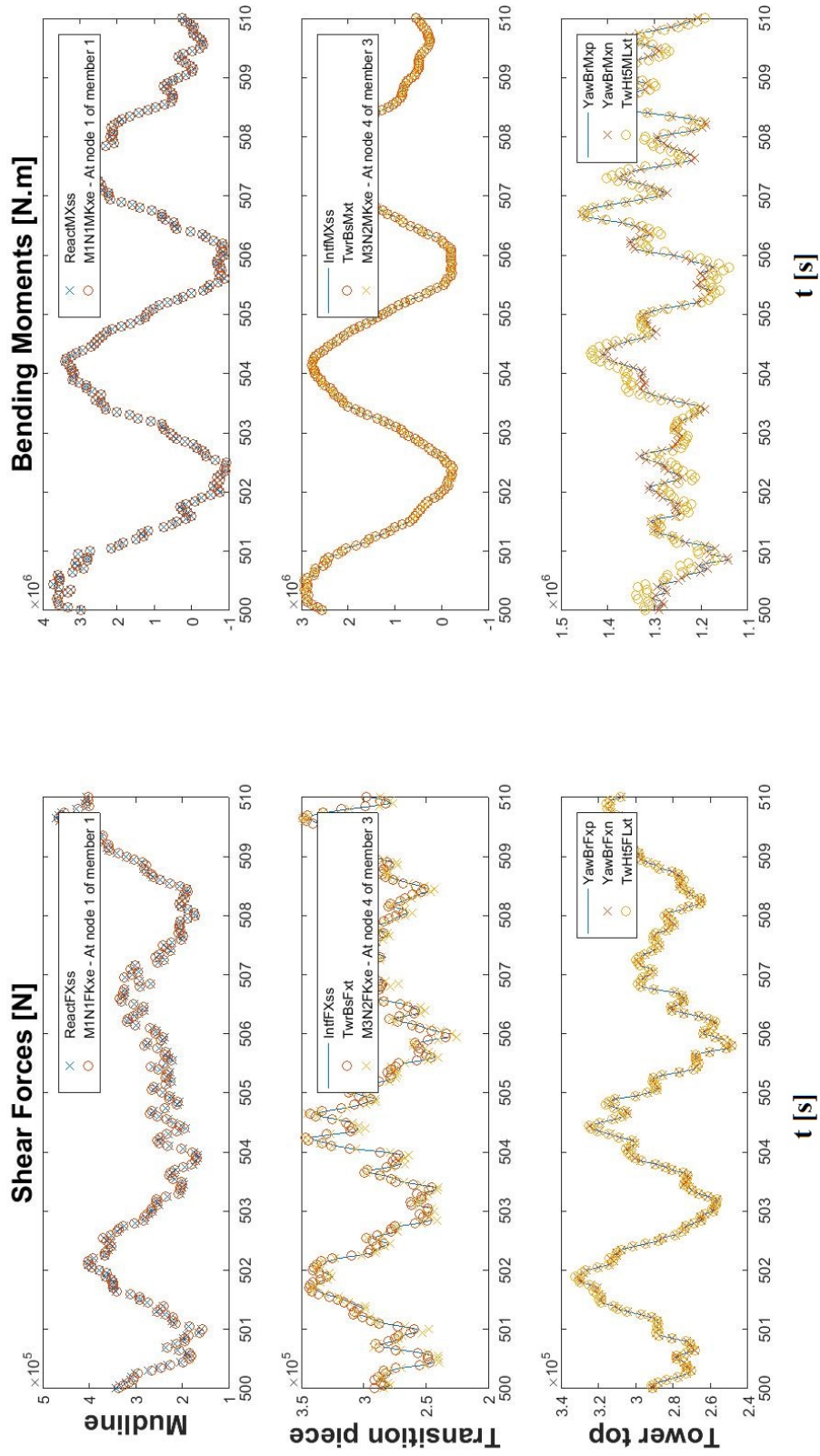


Figure 4.4: Comparison of load time series for possible variables to inform choice of variable for analysis of OWT dynamic response.



#### 4.1.5.2 Motion degrees of freedom

Transverse loads on the wind turbine cause bending moments and shear forces, which induce a normal stress and a shear stress, respectively. Transverse loading refers to incident forces which are perpendicular to the neutral axis of the structure. The bending moment and shear forces vary along the length of the beam and can be visualised by sketching a qualitative shear and moment diagram based on the knowledge of load distribution and the type of support. The support structure for the NREL 5 MW turbine is a tapered, cantilever beam with a circular tubular cross-section.

Proposed by Von Mises, stress is widely used to describe material failure when the yield criterion is reached. The theory behind Von Mises stress stems from the distortion energy failure theory or the energy associated with change in shape of the material. The distortion element ( $U_d$ ) of strain energy may be calculated as the difference between the strain energy density ( $U_0$ ) and the dilatational energy ( $U_h$ ).

$$U_d = U_0 - U_h \quad (4.3)$$

Based on this theory, ductile material yielding is expected when the distortion energy per unit volume in an actual case exceeds that obtained from a uniaxial tensile test. When using the fatigue limit state method described in Chapter 2 for design of offshore structures (Det Norske Veritas AS, 2014), yielding of members is investigated when excessive yielding is identified as a possible failure mode. Individual design stress components and the Von Mises resultant stress must all be limited under the structural resistance for a successful design. However, for a multiaxial case, it is customary to express distortion energy of a member in terms of principal stress values and an equivalent simple tension case at the time of failure as shown in Equation 4.4.

$$U_d = \frac{1 + \nu}{3Y} \sigma_y^2 \quad (4.4)$$

Where,  $\nu$  is the Poisson's ratio,  $Y$  is the Young's modulus and  $\sigma_y$  is the tensile yield strength.

For an isotropic, symmetric sample subjected to loading, the neutral axis is the geometric centroid where the stress and strain are zero. Conversely, the maximum tension and compression bending stresses for a given cross section occur at the

points furthest away from the neutral axis. It is therefore assumed that bending or flexure stress developed in a member due to perpendicular loading varies linearly with distance from the neutral axis and can be expressed as:

$$\sigma_b = \frac{My}{I} \quad (4.5)$$

Where  $M$  is the bending moment induced in the member,  $y$  is the distance from the neutral axis and  $I$  is the centroidal moment of inertia around the neutral axis. To determine the integrity of beam structures, it is equally important to calculate the shear stresses developed due to the parallel loads as follows:

$$\tau = \frac{QV}{Ib} \quad (4.6)$$

Where,  $Q$  is the calculated statical moment,  $V$  is the calculated shear force and  $b$  is the width of the beam structure.

### 4.1.5.3 Directionality

Applied loads on a mechanical member may be moment- or force-based. Despite the capability of FAST to simulate the natural metocean environment characterised by multidirectional flows (as displayed in Figure 4.5), this research limits the modelling process to an aligned codirectional wind and wave condition to generate the structural loads. Although this provides a simplistic estimate of the overall loads for establishing the metocean-centric metric, it does not provide the best estimate of the fatigue life.

For codirectional wind and wave, wind loads are compounded by the wave loads leading to larger structural damage. However, substantial misalignment between wind and wave in the operational state could result in a high resonant response by the turbine due to the reduction in the lateral aeroelastic damping. The convention for defining the direction for the environmental loads in FAST is described in Figure 4.5.

It can be observed that the wind and wave directional framework has different attributes as defined in InflowWind and HydroDyn; incident waves are produced in an anticlockwise direction, whereas, wind is propagated in the clockwise direction from the positive x-axis. For the scope of this thesis, to produce aligned wind and wave loads in the direction of the principal stress, the direction of both is set to zero.

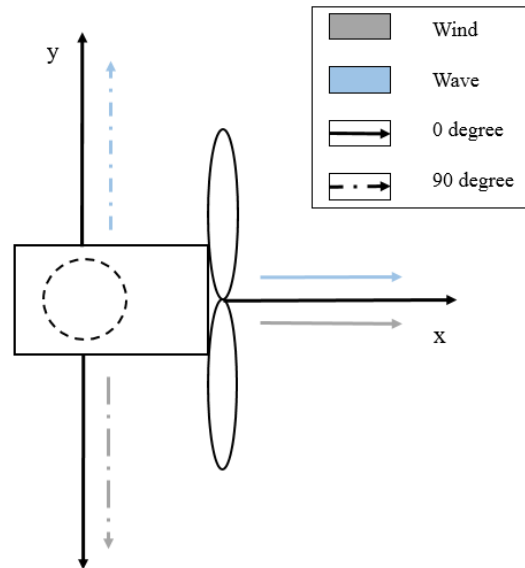


Figure 4.5: Downwind rotor wind and wave direction convention

FAST provides the capability of generating load profiles in six degrees of freedom for the structure, therefore, the multiaxial loads must be appropriately accommodated in the fatigue calculations. A comparison of the loads induced at the mudline, TP and tower top can be seen in Figure 4.6 for shear forces and bending moments.

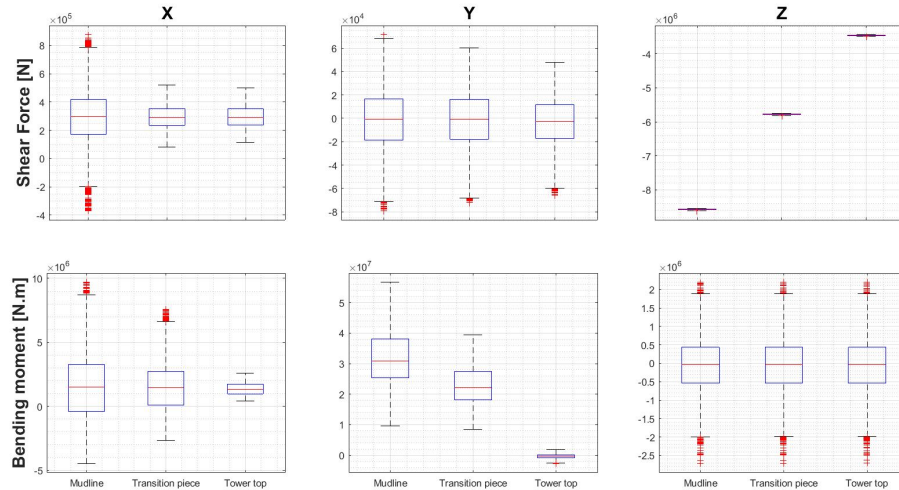


Figure 4.6: Comparison of the directionality of the subassembly loads.

It can be seen that the dominant direction of loading coincides with the main direction of wind and wave impact shown in Figure 4.5 at least in the order of a magnitude. Therefore, for the scope of this research, a vector sum of the bidirectional loads, surge and sway for shear forces and pitch and roll for bending

moments are used for fatigue life calculation. This is in compliance with the recommendation of the (British Standards Institution, 2009), whereby, it is suggested that the orthogonal load time-series at critical locations should be combined as a single signal for fatigue calculations to preserve phase and magnitude.

### 4.1.6 FAST modules

Finite element modelling is commonly used in the offshore wind energy industry to model support structures with dynamic analysis allowing for the determination of time-dependent structural response as a transfer function. However, considering the increasingly large number of design load case simulations recommended by design standards and large number of degrees of freedom (in the order of  $10^3$ ) in the structure, this modelling technique becomes computationally intensive. To address this issue, state-of-the-art design software uses schematisations involving model reduction methods for dynamic aero-hydro-elastic wind turbine analysis.

For fixed-bottom offshore structures, there is little coupling between the wind and wave loads, therefore, Kühn (2001) recommends separate computation of aero- and hydro-dynamic loads and consequent fatigue and weighted quadratic superposition of the results. The FAST glue-code allows for this superposition using outputs from its various modules.

Coupling between ElastoDyn, SubDyn and HydroDyn allows FAST to model ground-fixed offshore turbines. The tower and monopile are modelled in the ElastoDyn and SubDyn modules, respectively in FAST v8. The OWT platform is located at the transition between the tower and the monopile at the tower base. Therefore, to model a rigid foundation, all platform degrees of freedom must be enabled to allow complete coupling between ElastoDyn and SubDyn and constrain a node at the seabed within SubDyn. For appropriate coupling of SubDyn to FAST for structural dynamics modelling of the substructure, the six degrees of freedom related to translational (surge, sway, heave) and rotational (roll, pitch, yaw) motion of the platform must be enabled in ElastoDyn.

The FAST simulation outputs are time-marching load cycles for the baseline turbine at locations of maximum stress e.g. root for the blade subsystem at the specified metocean conditions. After determining the total run time for the glue code simulation, it is essential that a small enough module time step is used to pro-

vide a high enough sampling rate to characterise all key frequencies of the system whilst maintaining computational efficiency. The glue-code time step allows to ensure numerical stability of the selected time- integrators and the FAST module coupling. A rule of thumb is to set the glue-code timestep to 0.1 times the highest natural frequency (in Hz) of coupling between modules.

This section provides an insight into the methodologies used by the FAST modules to compute time histories of load data. On the outset, Figure 4.7 provides an overview of the various modules, their mutual interaction and their associated environmental parameters and/or structural components .

### 4.1.6.1 ServoDyn

Realistic modelling of the power train is essential in determining the electrical power that can be generated. A good controller ensures that the turbine operates at maximum efficiency, and also reduces structural loading by monitoring operation and responding dynamically to avoid resonances. The controller also protects the turbine by triggering shutdowns in the event of faults, grid failures or extreme climatic conditions. The control and electrical systems dynamics module uses the generator-torque and blade-pitch control system properties of the NREL 5 MW baseline wind turbine written for use in the OC3 project (Jason Jonkman et al., 2008).

### 4.1.6.2 TurbSim and InflowWind

A turbulent wind file, the time history of the variation and distribution of the wind within a volume into which the turbine is placed, almost like a virtual wind tunnel is significant for the assessment of wind. The velocity spectra and its standard deviations of the Kaimal mode are assumed to display no variation except the variation introduced in the longitudinal component due to the spatial coherence model.

Non-linear, turbulent, full-field wind flows are synthesised by TurbSim and corresponding time series' generated based on the spectral representation of turbulence. Unless stated otherwise, the Kaimal model is used based on the turbulence intensity distribution defined in the IEC 61400-3 standard for offshore wind turbines (British Standards Institution, 2009) with a medium turbulence intensity of

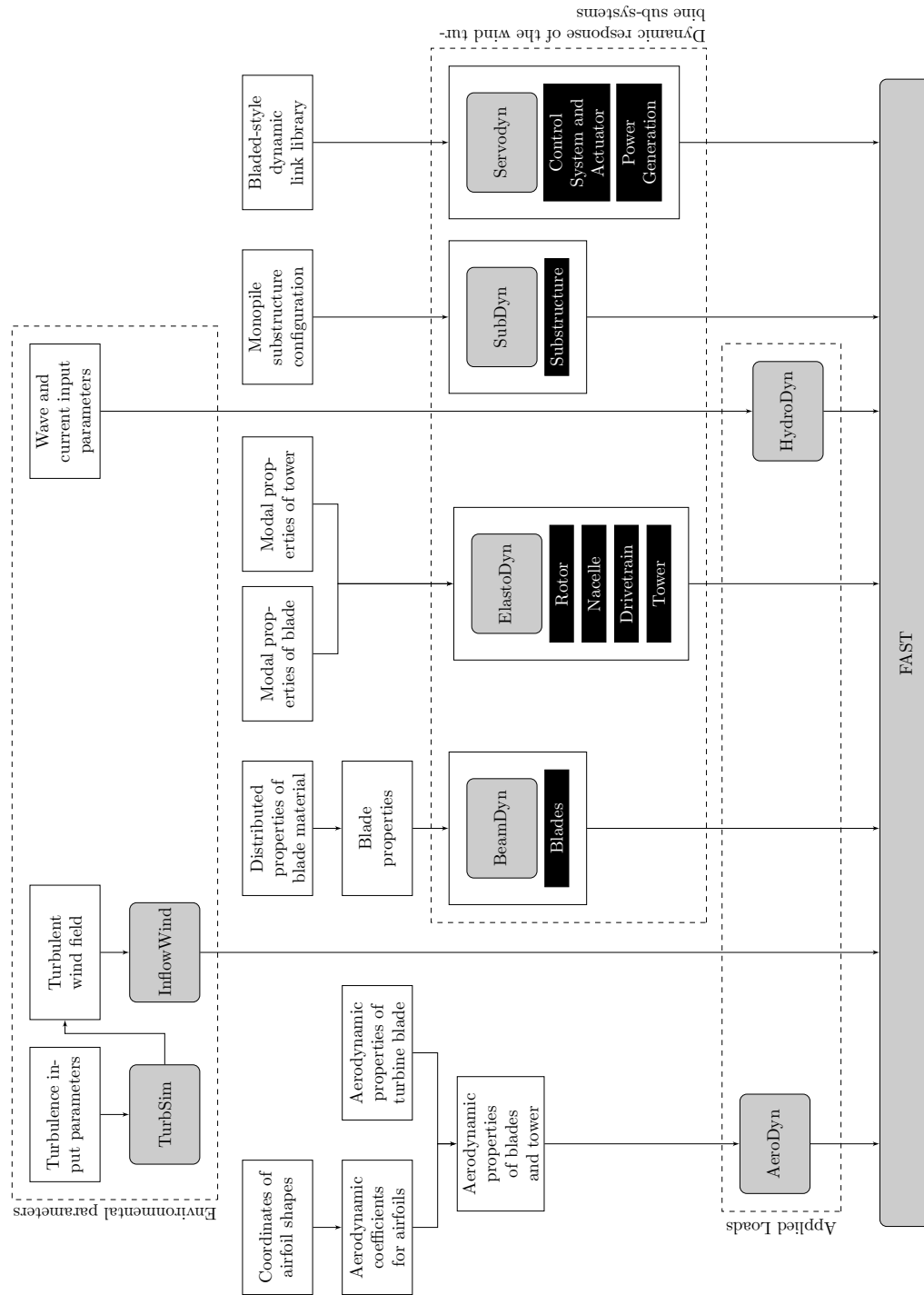
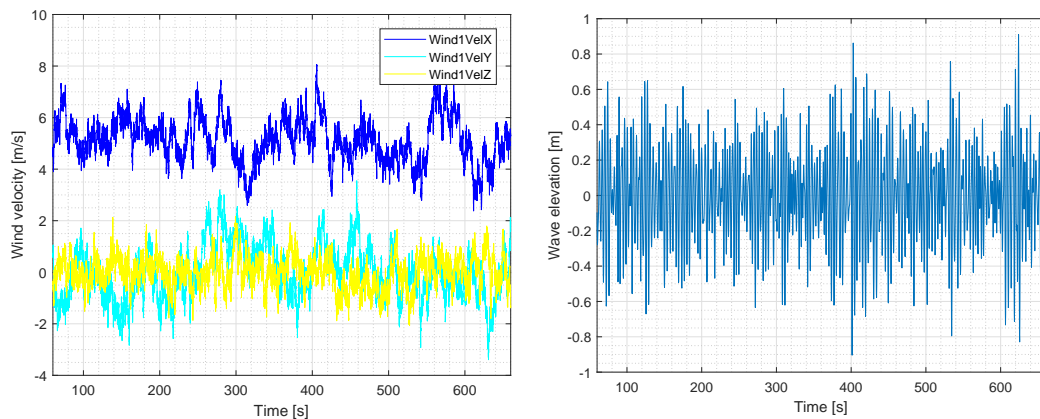


Figure 4.7: Dynamic interaction between the offshore environmental conditions, applied loads and wind turbine sub-systems based on the FASTv8 modularisation framework

14% from category B (Madsen, 2008) using a normal turbulence model.

InflowWind has broad input options for wind files, including full-field wind data which may be generated using TurbSim. The wind data includes two-dimensional grids of three-component time-marching winds generated using a mean speed. Binary full field 3-dimensional wind data from TurbSim generates the turbulent and stochastic three component wind inflow velocity vectors in the streamwise  $u$ , transverse  $v$  and vertical  $w$  direction based on a two dimensional, rectangular, evenly spaced grid. InflowWind translates this data using Taylor’s frozen turbulence hypothesis and interpolates the grids using a tri-linear interpolation scheme to generate a mean wind profile. Regardless of the discretisation in the vertical direction, TurbSim always generates a point at the hub. Similarly, an odd number of grid points in the horizontal direction allow points to fall along the undeflected tower centerline.

Figure 4.8a shows the simulated wind speed for the sample 5-MW NREL when exposed to a characteristic wind speed of 5.1 m/s extracted from the 13 x 13 grid generated by TurbSim. The grid resolution is chosen since it provides detailed outputs whilst maintaining computational efficiency.



(a) 3-D wind field generated by Turb- (b) Wave elevation above the WAMIT refer-  
Sim  
ence point generated by HydroDyn.

Figure 4.8: Output time series data for metocean parameters generated by FAST

### 4.1.6.3 AeroDyn

AeroDyn’s airfoil tables have normalised cartesian coordinates for each airfoil and FAST applies aerodynamic forces orthogonal to the deflected blade. Unlike Aero-

Dyn v14, AeroDyn v15 takes the tower displacement in the tower drag model into account, therefore with the introduction of AeroDyn15, the application of the model is extended from fixed turbines to floating structures as well. However, since this research only deals with fixed-bottom structures, AeroDyn v14 is considered to produce sufficiently representative results.

Blade and tower structural discretisation in the AeroDyn module are independent of those in ElastoDyn or BeamDyn. It can be argued that FAST outputs from ElastoDyn are more suited for finite element or analytical model analysis than AeroDyn outputs since the former incorporates body forces arising from the sub-system mass and inertia.

### 4.1.6.4 ElastoDyn

ElastoDyn is the structural dynamics module that includes structural models of the rotor, drivetrain, nacelle, tower and platform split out as a callable module in the framework of FAST v8. Aerodynamic and hydrodynamic loads along with controller commands and substructure reactions at the transition piece are used as inputs from other modules, namely, InflowWind, HydroDyn, ServoDyn and SubDyn. Turbine geometric configuration, degrees of freedom, initial conditions, mass/inertia, stiffness and dampness coefficients are dictated by inputs into the ElastoDyn module file. These in conjunction with the inputs from other modules stated earlier produces displacement, velocity, acceleration and reaction loads as outputs for the tower and blades.

ElastoDyn is applicable to straight blades of isotropic orientation whereas finite element blade structural dynamics for geometric non-linearities in blades may be modelled by BeamDyn. BeamDyn implements the geometrically exact beam theory with the Legendre spectral finite elements using full finite element mass and stiffness matrices (B. J. Jonkman and Jason Jonkman, 2016). Since these additional features are applicable to the structural dynamics of the rotor, therefore, the blades are also modelled by ElastoDyn in addition to the drivetrain, nacelle, tower, and platform. The tower subassembly of the support structure is modelled as a truncated conical surface.



#### 4.1.6.5 HydroDyn

HydroDyn provides the capacity to analytically generate regular periodic waves with or without user-specified phase, irregular waves based off the JONSWAP, Pierson-Moskowitz or white-noise spectrum as well as externally generated wave-elevation or kinematics time series. It allows simulation of first-order (linear Airy (Craik, 2004)) or hybrid first- plus second-order waves (Sharma, Dean, et al., 1981) for a finite depth. There is possibility of introducing directional spreading, however, there is yet no functionality of introducing wave stretching or higher order wave theories. This limits the generation of the wave kinematics to the spatial domain between the MSL and the flat sea bed.

The HydroDyn module of FAST provides the capability of generating hydrodynamic loads based on the potential flow theory using the Morison's equation as well as the strip theory using a variant of the Morison's Equation. Currently, HydroDyn provides the functionality of outputting lumped loads at the Wave Analysis At Massachusetts Institute of Technology (WAMIT) reference point (J. M. Jonkman et al., 2015) as well as individual loads on the nodes of a multi-member element. Using the potential-flow solution of HydroDyn, only lumped loads at the WAMIT reference point may be calculated. To apply distributed pressure along the members, the strip-theory solution based on the Morison submodule is used.

Input to the strip-theory includes member-based hydrodynamic coefficients and outputs include viscous-drag, fluid-inertia, buoyancy, marine growth, added-mass and flooding mass inertia force contributions at various nodes of the identified members. Exponential decay of hydrodynamic loads with increased depth requires discretisation with higher resolution near the free surface to appropriately capture wave loads. For loads per unit length between two nodes, a linear interpolation can be assumed between the two nodes.

Second order wave kinematics and second order diffraction loading may be generated using the HydroDyn module. Encompassing the influence of second-order waves enables improved reproduction of nonlinearities in the sea state, and consequent wave load, simulations albeit at the expense of computational efficiency of the hydrodynamic model. It is possible that the magnitude and frequency of the nonlinear hydrodynamic loads may excite the natural frequencies of the structure, therefore, incorporating their influence provides a better estimate of fatigue life

(J. M. Jonkman et al., 2015).

The second-order hydrodynamic implementations may be performed based on sum- or difference-frequency. While the former is significant for fixed bottom structures and Tension Leg Platform (TLP), the latter contributes to analysis of compliant structures like spar-buoys and semi-submersibles.

The HydroDyn user's guide (J. M. Jonkman et al., 2015) recommends the use of a strip-theory only model for a fixed-bottom system like the monopile. To ensure that the module does not apply static and dynamic pressure loads on the bottom of the structure, the joint for the lowest member must be embedded into the seabed. Therefore, for water depth of 20m in this case, considering only one member for the substructure, the joints are located at 10m above and 20.0001 m below MSL.

Consequently, a second-order hydrodynamic implementation with the sum-frequency is used to generate hydrodynamic loads. The JONSWAP spectrum using a default peak parameter based on the methodology in Annex B of IEC 61400-3 is used to simulate the incident wave elevation profile based on  $H_s$  and  $T_p$ . While it is known to provide good representation for waves in shallow waters, the Pierson Moskowitz Spectrum must be used for deep water locations which are not fetch-restricted.

Figure 4.8b shows the wave-elevation time series generated by HydroDyn using a JONSWAP spectrum with a significant wave height of 1.1 m and peak period of 3.8 s in water depth of 20 m. The codirectional waves are in the fore-aft direction with no directional spreading. It is assumed that the currents have no influence on the hydrodynamic loads, therefore, no current profile is included in the simulation.

### 4.1.6.6 SubDyn

Substructure models of offshore wind turbines are susceptible to nonlinearities including large displacements, axial shortening due to bending of the structure inherent material non-linearities and transverse shear effects, however, a linear finite element method is found to be suitable for dynamic analysis (Damiani et al., 2013). SubDyn employs two different engineering theories including linear finite element beam model and system reduction using Craig-Bampton in conjunction with static improvement to efficiently simulate the substructure load response.

Therefore, the SubDyn module allows to model non-floating substructural dynamics of turbines in shallow and transitional waters with the substructure clamped at the seabed and with a rigid connection to the reference point of the transition piece at the interface nodes. Although tailored for substructures, it is possible to model the complete tower in SubDyn instead of ElastoDyn. This provides the freedom of including more than the first two bending modes in the fore-aft and side-to-side directions providing more flexibility in the tower and its components. However, ElastoDyn is more suited for modelling of tubular towers since it considers geometric non-linearities.

The hydrodynamic loads including the buoyancy are computed at the submerged nodes by HydroDyn and transferred by the FAST glue code to SubDyn. Additionally, the distributed self-weight load from gravity is calculated by SubDyn and applied at these nodes.

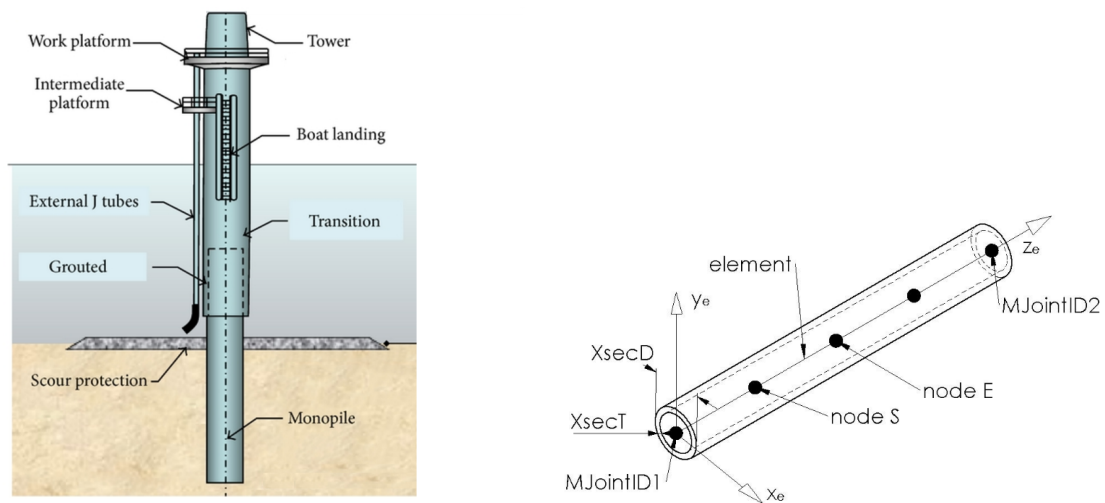
The finite element model for the substructure builds on the linear beam theory and consists of an arbitrary number of user-specified joints connected by straight, possibly tapered and hollow cylindrical members which may be further divided into nodes to increase the model resolution. Inputs to SubDyn include substructure geometry including outer diameter and wall thickness and material properties defined at the joints by the Young's modulus, shear modulus and mass density. The member geometry is defined by the joint coordinates of the structure in the global reference system with the origin at the intersection of the mean sea level and tower axis. material properties cannot change within the same member unlike geometric properties. Other inputs include integration and simulation options like restraints, finite-element resolution, number of retained modes and modal damping coefficients (Damiani et al., 2015).

SubDyn provides the option of using a Craig-Bampton reduction to reduce the modal space to improve computational efficiency. The Craig-Bampton reduction recharacterises the finite element model reducing processing time while retaining the fidelity of the structural response by reducing the degrees of freedom. This introduces the problem of excluding high frequency axial modes which capture static load effects. To mitigate this problem, the static improvement method is employed which computes two static solutions at each time step using the stiffness matrices with and without Craig-Bampton reduction. The two static solutions are then superimposed by the Craig-Bampton dynamic solution to provide a quasi-

static contribution of the modes not included in the dynamic solution.

Due to the mesh-mapping utility of FAST which provides transferability to loads and motions across joints and members, it is not necessary to have consistency between joints and members in SubDyn and HydroDyn but it is advised. SubDyn is currently limited to a rigid connection between the bottom of the substructure since soil-structure interaction is not modelled. Also, the substructure top nodes (interface nodes) and the transition piece (TP) are rigidly connected. However, a realistic modelling of a flexible foundation can be done by using the ‘apparent fixity’ model (Løken, 2009). The premise of the apparent fixity model is to mimic the stiffness of the soil-pile system with a fictive cantilevered beam, fixed at its lower end at a certain point below the mudline.

Unlike HydroDyn, the bottom joint for the member embedded in the seabed is considered rigidly clamped, therefore, can be set at the water depth unless using the apparent fixity method. Figure 4.9a illustrates the configuration of the substructure including its various auxiliary components. The geometric parameters for a member defined in SubDyn using the element coordinate system can be found in 4.9b. Due to the fixed boundary of the support structure at the mudline, neither lateral nor rotational movements are allowed at the seabed connection. Therefore, the substructure is modelled as a rigid fixed base with no flexibility.



(a) Substructural components

(b) Geometric input parameters for SubDyn

Figure 4.9: Structural components of the substructure (Lombardi, 2010) and analysis nodes of a member in the element and substructure coordinate systems (Damiyani et al., 2015)

### 4.1.7 Validation

Immense research is dedicated to the calibration of offshore wind energy modelling tools. Three research projects were initiated under the International Energy Agency:

- OC3 - Offshore Code Comparison Collaboration (2005-2009) (Jason Jonkman and Musial, 2010)
- OC4 - Offshore Code Comparison Collaboration, Continuation (2010-2013) (Fraunhofer IWES, 2013a)
- OC5 - Offshore Code Comparison Collaboration, Continuation, with Correlation (2014-2017) (Robertson et al., 2015)

While, the former two projects aimed to verify the CAE tools by conducting an intensive intra-tool analysis, the latter focused on the validation of simulations results of ultimate and fatigue loads at the support structure by conducting a comparison to tank and open ocean deployment test data. The OC5 validation study (Robertson et al., 2015) compared fatigue and ultimate loads by assessing the shear forces at the tower top and tower base for the fixed structure and the loads on the upwind mooring line. The results highlighted the inherent underestimation of loads by the code outputs relative to test data for all wind/wave conditions.

The underestimation was more pronounced for fatigue loads than ultimate loads and at the tower base than at the tower top for all considered load cases. Additionally, discrepancies were found in the loads analysis using Potential Flow and Morison Equation based strip theory. The OC6 project, Offshore Code Comparison Collaboration, Continuation, with Correlation, unCertainty, is now in the conception phase (Department of Energy, 2018) and is due to be launched in 2019.

As recommended by the HydroDyn user's guide (J. M. Jonkman et al., 2015), fixed-bottom structures should be modelled using the strip theory, whereas, floating systems may be modelled using potential flow theory, strip theory or a hybrid of both. A comparison of first- and second-order wave excitation shows that at low frequencies and low diameter-to-wavelength ratios, strip theory and potential flow show agreement if two conditions are satisfied. Firstly, the quadratic sum-frequency value is relatively smaller compared to the total sum-frequency

second-order force, secondly when the difference-frequency force has insignificant contribution to the overall second-order force.

### 4.2 Accumulated lifetime damage

Fatigue-induced material failure occurs when the structure fractures after being subjected to cyclic loads well below its static strength. These repeated stress level changes cause the initiation and propagation of cracks in the material particularly at discontinuities such as sharp corners or deformations.

Lifetime damage of the OWT is estimated by extrapolation of the collected representative short-term load time series data over the turbine lifetime. It is common practice in OWT design engineering to scale the sampled loads directly with normal operational loads based on the annual wind speed distribution. This is done on the assumption that the available samples are representative of the deployment site (C. H. Lange and Winterstein, 1996) and accurately capture all necessary load cases to provide an estimate for fatigue life.

Life prediction methodology used for the scope of this thesis is shown in Figure 4.10, whereby, the material, structural geometric properties and environmental parameters inform the S-N curve. This, in combination with the rainflow counted loading history produces the cumulative damage model to provide an estimate of component lifetime estimation.

However, while performing such analysis it must be noted that the low frequency, high stress-inducing events contained in the tail of the load distribution are highly sensitive to the length of the data record with more data populating the extreme load cases as the data record increases in length. Extrapolating data from smaller representative samples risks the exclusion of fatigue effects induced in the structure due to these infrequent load cases. Therefore, statistical data measures can provide useful information for deducing the magnitude and occurrence probability of the high-stress events. It can, however, be argued that whilst such large loads are possible under a probabilistic framework, their occurrence is often difficult to estimate from data. Additionally, due to their low occurrence probability, extrapolation of the short time-series data to the design lifetime of the turbine involves a high degree of approximation. It can, however, be concluded that the discussion regarding incorporation of high stress tail loads is significant

for fatigue load calculation while the exact extent of their influence may be hard to determine.

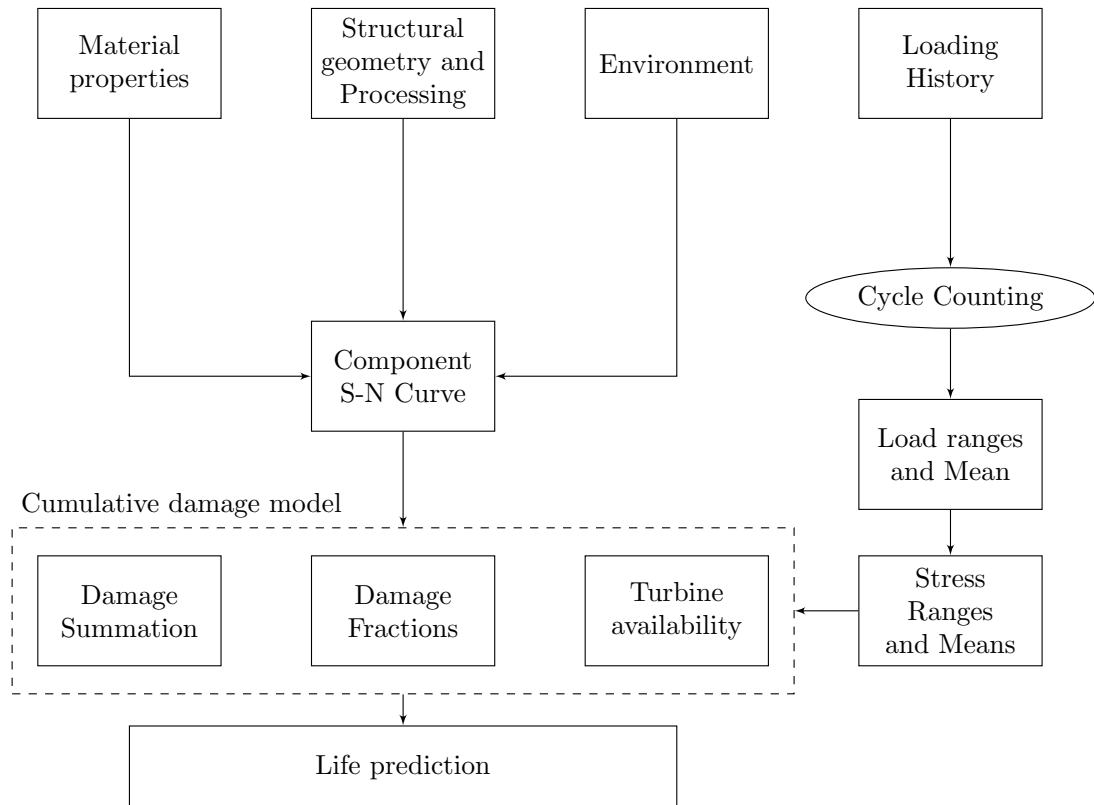


Figure 4.10: Sequential analysis to predict fatigue life using the S-N approach

### 4.2.1 Fatigue Nomenclature

With fatigue damage being a critical design driver, multiple approaches for fatigue estimation exist. The fatigue cycle is a closed hysteresis loop in the load timeseries of a structure. For each fatigue cycle, the maximum ( $L_i^{max}$ ) and minimum load ( $L_i^{min}$ ) are the algebraic maximum and minimum of the individual cycle  $i$ , respectively. Further fatigue parameters can be seen in Table 4.6 along with an illustrative example of an ideal sinusoidal load cycle in Figure 4.11.

Load ratios or R values are a direct indicator of the tensile and/or compressive nature of the stresses, for  $0 < R < 1.0$  corresponds to tension loading,  $-\infty < R < 0.0$  corresponds to tension-compression loading, whereas, loading with  $1.0 < R < \infty$  causes compression stresses in the structure.

Table 4.6: Fatigue nomenclature for cycle  $i$  and their corresponding calculation method.

Mean load	$L_i^{MF} = \frac{L_i^{max} + L_i^{min}}{2}$
Load range	$L_i^{RF} =  L_i^{max} - L_i^{min} $
Load amplitude	$L_i^A = \left  \frac{L_i^{max} - L_i^{min}}{2} \right $
R ratio	$R = \frac{L_i^{min}}{L_i^{max}}$

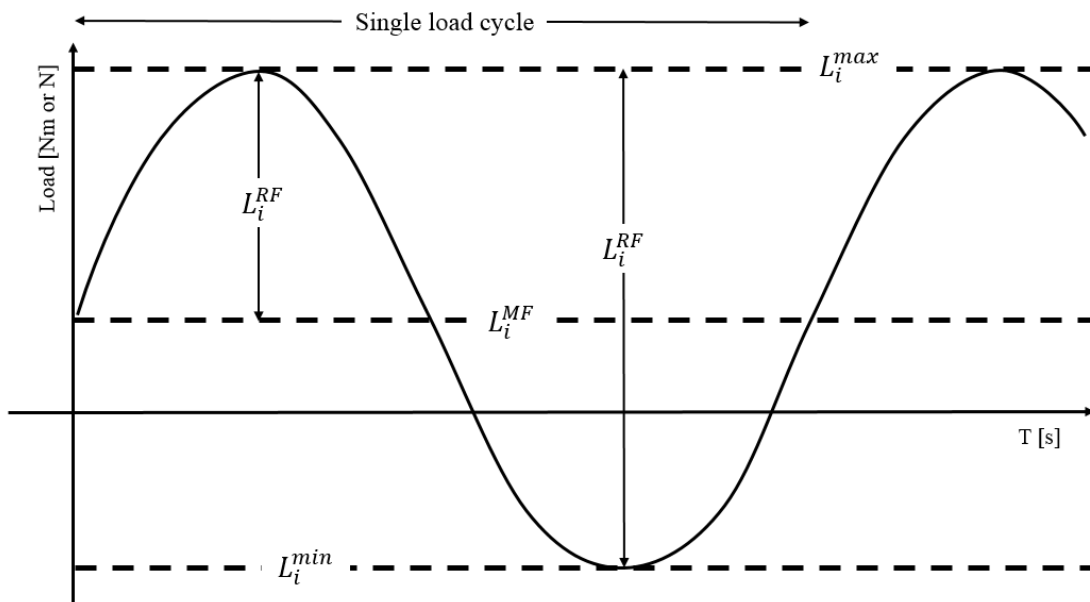


Figure 4.11: A representative sinusoidal fatigue cycle with associated nomenclature.



### 4.2.1.1 Fatigue life prediction methods

Alternating loads and stresses create fatigue in the OWT structure and produce heat as a by-product which could possibly change the material behaviour. The structural integrity of column structures is commonly compromised by buckling, therefore, this is a significant failure mode for fixed OWT structures. Whilst it is financially attractive to have tall and thin towers to harness the power of stronger winds and reduce material costs, however, this increases the risk of buckling in the tower due to aero- and hydro-dynamic loads.

Loading a structural member causes deflection as a response of the structure to accommodate the load. Excessive deflection can cause stress beyond the ultimate strength of the structure, therefore, the design should aim to minimise deflection to eliminate this failure mode. Whilst the aforementioned fatigue loads can be reduced significantly by the use of light, yet strong material, however, cost is a limiting factor in design considerations.

In common industrial practice for fatigue life prediction, three major approaches exist:

- S-N curve approach - The linear stress-based approach is the earliest yet most frequented method for fatigue life prediction, whereby, structural failure occurs after the structure is exposed to a number of loading cycles (Moriarty et al., 2004);
- Dirlik's method - An empirical method designed to approximate the rain-flow count values. Spectral technique to estimate stress range probability distribution based on spectral moment of the load for fatigue life calculation (Yeter et al., 2014); and
- Fracture mechanics model - A computation-intensive method based on crack propagation of dominant cracks under cyclic loading (Johnston, 1982). Experimental procedures provide validation to the method by tracking the number of cycles required to extend the crack by a unit length.

The fracture mechanics approach is suited to the estimation of the reliability of high integrity welded structures, however, the computational and experimental effort required introduces a complexity in adopting this methodology at a systems level with insufficient improvement in the accuracy of the resulting fatigue life

prediction. Using spectral information, Dirlik's method allows computationally expensive simulation and rainflow counting to be bypassed for prediction of fatigue loads. However, its performance capability is limited to some, not all wind turbine components, as well as rather benign environmental conditions (Ragan and Manuel, 2007). Dirlik's method provides a conservative estimation of fatigue life compared to the S-N approach. This is because there is a systematic bias in the Dirlik's method since it is not equipped to handle large periodic components in the load time series. However, it is also possible that the conventional S-N method overestimates fatigue life since the industrial standard of ten minute simulations is not sufficient to capture the uppermost tail of the stress histogram. Further details regarding the comparison between time and frequency domain fatigue analysis can be found in Ragan and Manuel (2007).

Based on common industrial practice, recommendations by existing standards (Det Norske Veritas, 2014) and the computational ability of the NREL tool MLife (G. J. Hayman, 2012), this project utilises the S-N approach for fatigue life prediction of ORE structural sub-systems.

### 4.2.1.1.1 S-N approach

Empirical design methodology is commonly applied to account for fatigue damage in structural design by subjecting numerous specimens to a range of sinusoidal stress variations. Based on Wöhler's laws, cycles to failure,  $N$ , for the various magnitudes of alternating stress regimes,  $S$ , are recorded and plotted as a scatter diagram. To achieve a plausible design  $S - N$  (or Wöhler) curve from the scatter plot, a linear regression analysis of the empirical data is performed to yield a family of curves describing material fatigue properties. Basquin (1910) argued that for engineering purposes, it is sufficient to model the  $S - N$  curve using a straight line logarithmic distribution for fatigue life approximation. It is, therefore, an industry standard to describe high cycle empirical fatigue data using the Basquin equation:

$$N_f = K \cdot S^{-m} \quad (4.7)$$

$$\log N_f = \log(K) - m \cdot \log(S) \quad (4.8)$$

Where,  $N_f$  is the number of cycles to failure sustained by a specimen,  $K$  is the y-intercept parameter,  $m$  is the empirical Wöhler exponent and  $S$  is the applied

alternating constant-amplitude stress range. Graphically, the Wöhler exponent may be calculated as the slope of the log-log  $S - N$  curve.

Most S-N curves have a negative slope, depicting that a material exposed to higher amplitude cyclic stress has fewer cycles to failure. While the S-N description for fatigue characteristics of a material depends on the mean and an additional parameter (range, amplitude, tension maximum or compression minimum) of each stress cycle, generic  $S - N$  curves do not account for the influence of cyclic frequency on failure. This must be accounted for since increased frequency of nominal stress lowers the  $S - N$  curve, thereby, decreasing the fatigue life. Additionally, the consequence of the alignment of loading frequency with the natural frequency of the material will amplify the structural response. Furthermore, environmental stressors like temperature, humidity and corrosion will effect the material strength and the  $S - N$  curve must account for these influences.

It must be noted that the above probabilistic model assumes that annual variation in stress ranges is negligible. Consequently, it is important that the loading data where the S-N approach is applied is representative of the sea state where the respective device will be installed. Application of this approach to annual data from an El Niño or La Niña year may lead to under or over estimation of fatigue life, respectively.

### 4.2.1.2 Cycle counting methods

The simulated or measured time series data for subassembly response to environmental and operational stressors must be post-processed in terms of time to crack initiation for fatigue life analysis. Numerous methods, including the level crossing, peak, range, reservoir and rainflow counting, exist for the determination of the number of stress cycles. The most widely used of these is the Rainflow Counting method (Marsh et al., 2016).

The time-varying simulations are transformed into a series of local maxima and minima for use in the classical formulation of a rainflow counting algorithm which may be used to calculate damage equivalent loads (DELs). A preprocessor characterises the crests and troughs forming a hysteresis loop by a change in slope as the algorithm runs through the time series. Introduced by **endorainflow** and defined by Rychlik (1987), the rainflow counting algorithm is a cycle counting

technique encapsulating slow and rapid load variations recommended for wide-banded stress time histories.

To demarcate a single stress cycle Rychlik (1987) recommends a five step process as described in §4.1.3 of the publication by the WAFO Group (2000):

- Identify a local maxima,  $Max_k$ , in the load signal
- Mark crests above the level of  $Max_k$  in the time series to the left and right of  $Max_k$
- The minima between  $Max_k$  and the marked crest to the left and right are identified as  $Min_k-$  and  $Min_k+$ , respectively
- The minima with the smaller deviation from  $Max_k$  is regarded as the rainflow minimum,  $Min_k^{RFC}$
- The  $k$  :  $th$  rainflow cycle is defined as as  $Min_k^{RFC}$  and  $Max_k$ , respectively

It must be noted that the rainflow counting is based on the simulated load time series, therefore, the time step for the load time series must be small enough to be able to capture the local extrema effectively. A parabolic curve-fitting algorithm may be applied to data points surrounding each extrema to extrapolate the data for robust identification of the actual local extrema. A range filter may be applied to the load time series to reduce noise in the signal as well as eliminate small cyclic stress events which do not have a significant contribution to the sub-system damage.

The counted peak-valley are stored in a two-dimensional histogram of cycle range and mean stress levels. Additional details of the hysteresis loop including loading sequence may also be preserved for use in further statistical analysis involving Markov matrices.

As the rainflow counting algorithm runs through the random stress amplitude time series to pair minima and maxima to form closed hysteresis loops, a series of unmatched extrema referred to as 'residual cycles' are also collected as the remainder. In addition to the largest maxima and minima of the time series, the series of residual cycles constitutes other large range stresses, therefore, the most damaging events in the loading record. To prevent over-estimation of fatigue life, these extrema must be incorporated into the analysis. Numerous techniques

(Marsh et al., 2016) have been proposed by researchers for handling residue cycles in wind turbine application including:

- Half-cycle counting
- Simple Rainflow counting
- Residue concatenation counting

An understanding of the use of the above methods for wind turbine fatigue life determination may be found in literature (Marsh et al., 2016; Sutherland, 1999).

### 4.2.1.3 Miner's Rule

The widely used Palmgren Miner cumulative damage hypothesis (Palmgren, 1924; Miner, 1945) is a strain energy-based, linear damage accumulation model for structures exposed to loads of varying amplitude. Failure is expected when the sum of the strain energy due to cycles of variable amplitude load history equals the sum of strain energy from constant amplitude stress cycles. The Palmgren Miner cumulative damage hypothesis may be defined as:

$$D = \sum_i^M \frac{n_i}{N_i(L_i^{RF})} \quad (4.9)$$

where,  $M$  is the total number of load ranges,  $n_i$  is the number of cycles,  $N_i(\cdot)$  are the cycles to failure at the respective load range block  $i$  and  $L_i^{RF}$  is the cycle's load range about a fixed mean load value.

The number of cycles,  $n_i$  may be taken as close hysteresis loops, number of reversals or number of zero-crossings whereas the stress blocks may be stress amplitude or range at a defined  $R$  value or mean stress. The cycles to failure based on the S-N curve can be expressed in terms of load ranges, mean load ( $L^{MF}$ ) and ultimate load ( $L^{Ult}$ ) as shown in Equation. 4.10.

$$N_i = \left( \frac{L^{Ult} - |L^{MF}|}{0.5L_i^{RF}} \right)^m \quad (4.10)$$

Equation. 4.10 assumes that fatigue cycles occur over a fixed  $L^{MF}$ .

Theoretical requirements dictate the simplistic assumption that structural failure occurs when the fatigue damage ratio is 1, however, load uncertainties, material properties and modelling errors may lead to ratios between 0.79 and 1.53 (Veers, 1988). Therefore, accumulated damage life prediction and measured failure rates

may differ for up to a factor of two. Another limitation of the Miner hypothesis frequently criticised is its inability to account for the influence of the sequence of load-time history.

### 4.2.2 Post-processing tools

The time-marching FAST output simulations must be post-processed to yield useful information to inform OWT fatigue life. Multiple softwares exist to facilitate the process and this section provides details regarding the considered softwares.

#### 4.2.2.1 Extreme value generation

Extreme value generation for an output channel of the FAST simulation can be used to determine important failure modes as well as provide an indicator of the ultimate loads which the structure may be exposed to assist in fatigue life calculations.

NREL MCrunch (M. L. Buhl, 2009) can be used for generating extreme-event tables for a single or multiple FAST simulation outputs, however, a more computationally efficient alternative is the MExtremes (G. Hayman, 2015) set of MATLAB scripts by NREL. Whilst both sets of codes generate the same output, the algorithms differ in that only one time series resides in memory when using MExtremes, therefore, reducing the computational time required to produce the results (G. Hayman, 2015). Therefore, using a text-based settings file and the required FAST simulation output files, MExtremes v1.00 is used for extracting extreme value events from FAST simulation outputs.

#### 4.2.2.2 Fatigue life calculation software

Offshore wind turbine fatigue analysis is a dual phase procedure whereby CAE tools like FAST perform a time-varying dynamic excitation analysis to predict system response for the turbine including the influence of aero-, hydro-, structural- and controller- dynamics. Generated outputs from FAST include component level loads like lumped shear forces and bending moments at a cross section in multiple coordinate systems. A two-pronged approach may then be used to further process the data, either a static finite element model or simple analytical model of individual components to calculate physical quantities like induced stress, strain

and buckling. Since responses computed by FAST intrinsically account for inertial and dynamic loads, a static finite element stress analysis model captures dynamic influences sufficiently. It is, however, commonplace to use loads like damage-equivalent-loads to perform fatigue analysis. MLife and MCrunch use the latter approach for fatigue life prediction.

Numerous sophisticated softwares are available to post process load simulations for fatigue life prediction. Due to their diverse functionality as shown in Table 4.7, this thesis investigates the three open-source softwares tailored for use in random loading regimes, namely, MLife (G. J. Hayman, 2012), MCrunch (M. L. Buhl, 2009) and WAFO (WAFO Group, 2000). For the scope of this thesis, Wafo version 2017, MCrunch v7.16 and MLife v7.16.

MCrunch and MLife, post-processors developed by the NWTC at NREL, are sets of Matlab routines that are tailored to process test and simulation data for wind turbines. MCrunch includes a wide variety of features with enhanced visualisation, however, it stores the entire dataset concurrently while performing the computation. Since fatigue life prediction draws from hundreds of simulations, this might prove to be computationally inefficient. Therefore, a specialised tool for sequential file processing, MLife, was developed by NREL for general statistical and fatigue estimates.

Similarly, the Wave Analysis for Fatigue and Oceanography (WAFO) is a Matlab toolbox with scripts for simulation and statistical analysis of random waves and loads in offshore conditions. Fatigue analysis with WAFO is a dual-stage process as well with the production of the rainflow cycle count matrix which is then used in conjunction with the substructure material properties to assess the accumulated damage at the location of investigation.

For the scope of this thesis, the computationally efficient MLife tool is chosen since it is tailored to handle FAST outputs effectively.

### 4.2.2.3 Post-processing with MLife

The postprocessing tool for fatigue analysis, namely, MLife uses the load extrapolation techniques recommended in OWT standards (International Electrotechnical Commission, 2005) for lifetime damage calculation. Fatigue failure occurs due to the accumulated damage from each hysteresis cycle of the fluctuating loads in the

Table 4.7: Features of considered fatigue life post-processors.

Features	MCrunch	MLife	WAFO
Basic Statistics	×	×	×
Linear S-N curve	×	×	×
Log S-N curve			×
Load Roses		×	
Goodman correction		×	
DEL amplitude		×	×
DEL range	×	×	×
Application of partial safety factors		×	
Visualisation of results	×		×

load time history. A rainflow counting algorithm is used to analyse the simulated load time series by discretising the time series into individual cycles with local maxima and minima to calculate the number of load cycles for a given stress range. Characterised by the load mean ( $L^{MF}$ ) and range ( $L_i^{RF}$ ), these cycles are then stored in a rainflow matrix for further analysis.

The S-N or Wöhler curve, defined by the parameters  $L^{Ult}$  and type of  $L^{MF}$ , is used by MLife for the fatigue analysis. MLife also adheres to the recommendation of the IEC 61400-1 standard 2005 by using the unclosed cycle counting method to handle residual cycles for fatigue analysis. Additionally, it provides the functionality to use a racetrack filter to eliminate small cycles when performing the rainflow analysis.

#### 4.2.2.3.1 Damage equivalent loads

Metocean loads on offshore structures are stochastic processes which are cyclic in nature and may be approximated as dynamic ergodic processes. In addition to lifetime damage and time until failure, DELs are a useful parameter to characterise structural fatigue. DELs are fluctuating loads generated based on constant frequency and amplitude causing damage equivalent to the stochastic loads of the input time series. The amplitude and frequency are provided as user specified input in MLife.

MLife provides the capability to calculate short-time DELs based on the provided load time-series as well as lifetime damage DELs weighted by the occurrence



probability of the metocean parameters to inform wind turbine design.

Using the provided short-term load time-series, MLife extrapolates the damage-cycle counts over the whole lifetime of the structure based on its availability. Based on the Miner's rule, described in Section 4.2.1.3, short-term damage and long-term accumulated damage may be expressed as:

$$\begin{aligned} D_j^{ST} &= \sum_i \frac{n_{ji}}{N_{ji}} \\ D_j^{life} &= \sum_i \frac{n_{ji}^{life}}{N_{ji}} \end{aligned} \tag{4.11}$$

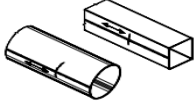
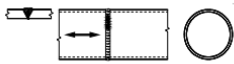
where,  $D_j^{ST}$  is the accumulated short term damage from the time series  $j$ ,  $D_j^{life}$  is the extrapolated fatigue damage over the design life due to the  $j^{th}$  time series,  $n_{ji}$  is the cycle counts and  $N_{ji}$  are the total cycles to failure.

### 4.2.2.3.2 Wöhler exponent

Relative to 15% for an onshore wind turbine, the cost breakdown of an offshore wind turbine shows that 25% of its overall cost can be attributed to the tower and support structure (Fraunhofer IWES, 2015). Det Norske Veritas (2005) proposes a series of S-N curves for use for steel structures in air and seawater environment with cathodic protection with the slope of the curves ranging between three and five. For offshore structures subjected to characteristic wind and wave loading, the main fatigue damage can be attributed to cycles  $> 10^7$  so it is recommended to use a bi-linear S-N curve with a region boundary at  $10^7$  cycles. An  $m_2$  value of 5 in the high cycle region is unanimous beyond the regional boundary, whereas, values of  $m_1 = 3$  and  $m_1 = 4$  are used below this regional boundary.

The wind turbine tower and substructure are composed of conical and cylindrical tubular segments, respectively. These are fabricated by conventional manufacturing methods involving production of 20-30m plates that rolled into a 'can' through longitudinal or seam welds. Multiple cans are then joined through multipass butt welds circumferentially. After the assembly of the support structure sections, ancillary equipment, such as ladder, is added and the resulting tower and pile along with the RNA assembly are transported to the installation site. Welding requirements are dictated by tower size as well as the plate thickness. While increasing tower height provides access to higher wind speeds to improve power production and increased tower thickness improves fatigue life estimates (Løken,

Table 4.8: Welds in the OWT support structure with associated S-N curve (Det Norske Veritas, 2005).

Type of weld	Description of weld	S-N curve
	Longitudinal seam weld	B2
	Circumferential butt weld made from both sides dressed flush	C1
	Circumferential butt weld made from both sides	D
	Circumferential butt weld made from both sides made at site	E
	Circumferential butt weld made from one side on a backing bar	F
	Circular hollow section butt welded end to end with an in-termediate plate	G

2009), welding a higher number of thicker steel sections requires larger weld joints which consequently increases the time and cost of the welding process. Additionally, it increases the risk of plate buckling during pile driving (LEANWIND, 2017).

As Table 4.8 shows, curve B2 (Det Norske Veritas, 2005) for structures in sea-water with cathodic protection represents the longitudinal seam welds and multiple possible curves exist for describing butt welds. A possible failure mode is the cracking of welded joints. The Wöhler exponent for the longitudinal welds is taken as 4 and that for the circumferential welds is taken as 3 up to the regional boundary, therefore, it can be assumed that the butt welds are more fatigue-critical. MLife does not provide the option of using a bilinear S-N curve, therefore approximations have to be made by the use of a combination of linear S-N curves. In addition to the Wöhler exponent, the shape of the S-N curve is also dictated by the ultimate design load and the mean load.

### 4.2.2.3.3 Ultimate design load

MLife requires  $L^{Ult}$ , the ultimate design load, input to determine fatigue life of the structural component. This is the highest load the component cross-section can withstand based on its ultimate strength and is dependant on the analysis channel; for a force channel,  $L^{Ult}$  is the ultimate force, for a moment channel, it is the ultimate moment. It is ideally determined by a finite element analysis (FEA) of the component, however, in the absence of a detailed FEA model of the structure, analytical approaches are recommended (National Renewable Energy Laboratory, 2018). This guidance shows that  $L^{Ult}$  may be obtained as a product of the extreme loads calculated using MExtremes and Ultimate Load Factors (ULF) in the range of 1.25 - 20.

Parametric study of  $L^{Ult}$  (Matha et al., 2010) for various floating offshore wind turbines assumes that the extreme load may be extracted from analysis of a typical land based turbine. Analysis of extreme events for 2500 load cases in Table 6-3 (Jason Jonkman, 2007) for a land based turbine show that this maximum load is 153 MNm for tower base bending moment. Comparison of the variability of fatigue loads over a range of arbitrarily determined  $L^{Ult}$  values shows that the ultimate load factor has a minor effect on damage equivalent loads for low ULF and asymptotically approaches a fixed value for ULF greater than 10 (Matha et al., 2010).

Fatigue life results are heavily dependent on the choice of ULF, therefore, a different analytical approach based on the flexure formula defined in Equation. 4.5 is also recommended (Løken, 2009; National Renewable Energy Laboratory, 2018) for loads inducing normal stresses.

$$\text{Ultimate bending moment} = \frac{\sigma_y * I}{y^{max}} \quad (4.12)$$

Where,  $\sigma_y$  is the material yield strength preferably reduced by a safety factor,  $I$  is the centroidal moment of inertia and  $y^{max}$  is the perpendicular distance of the point of maximum stress from the neutral axis, therefore, the outer radius at the respective location in the support. This formulation has the inherent assumption of a simple beam in pure bending fabricated from isotropic material discounting the effect of shear forces on the structure.

The material yield strength depends on the steel grade used: as of 2015, the offshore practice is based on the use of mild steel rather than higher grade steel.

Additionally, the standards are based on rigid and simplified classification of structural detail. As argued by ArcelorMittal (2012), the threshold for the economic viability for OWE is to use steel with yield strength of 460 MPa, however, it is more common practice to use S235 and S355 (slightly lower grade steel with yield strength of 235 and 355 MPa, respectively).  $I$  for a hollow cylindrical beam structural component can be calculated as:

$$I = \frac{\pi}{64}(D_{out}^4 - D_{in}^4) \quad (4.13)$$

Where,  $D_{out}$  is the external diameter of the structure and  $D_{in}$  is the internal diameter. To assess the failure due to the axial shear forces, the maximum shear stress inducing load can be calculated based on the formulation described in Equation. 4.6 and simplified to Equation. 4.14.

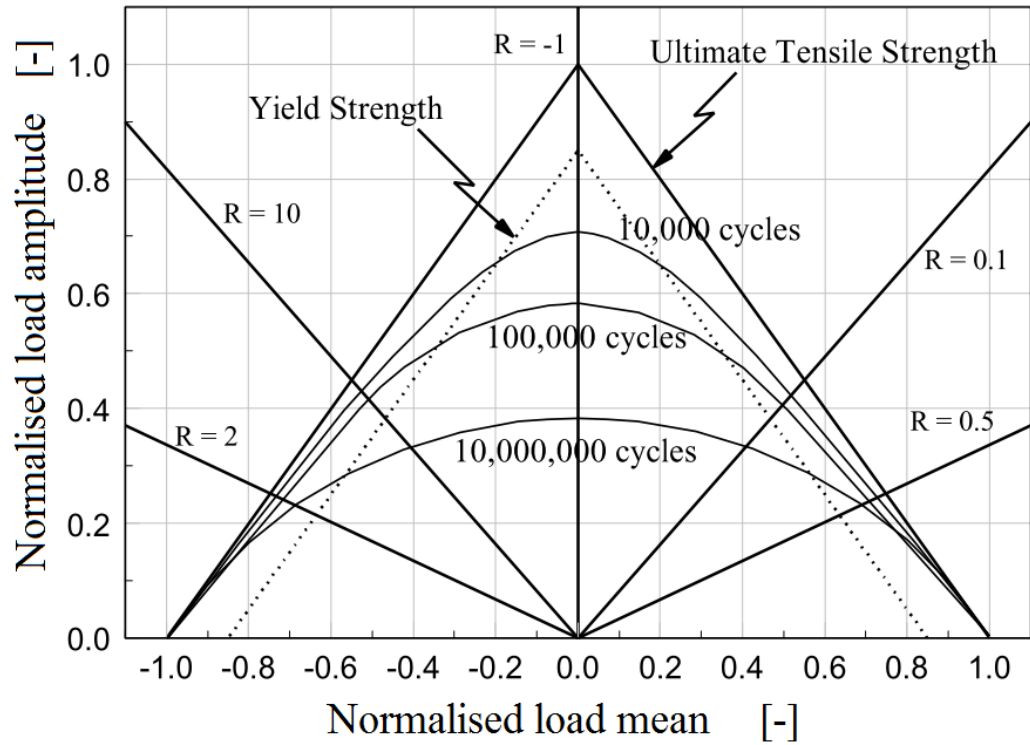
$$\text{Ultimate shear force} = \frac{4S_f}{3a} \cdot \left( \frac{r_{out}^2 - r_{out} \cdot r_{in} + r_{in}^2}{r_{out}^2 + r_{in}^2} \right) \quad (4.14)$$

Where,  $r_{out}$  is the external radius,  $r_{in}$  is the internal radius and  $A$  is the area of the tubular cross-section.  $S_f$  is the shear force acting on the location of interest.

#### 4.2.2.3.4 Goodman correction

Empirical evidence shows that in addition to alternating loads, mean loads have a marked effect on the fatigue life of a member. However, establishing this relationship for a specific material under specific loading conditions would require a large amount of empirical data. Therefore, for simplification a total life approach may be adopted which does not differentiate between different stages of fatigue.

The interaction of mean load with alternating load when determining the fatigue life of a structural component is expressed by a mean stress correction model. A graphical representation of the loci of all stress states which result in a particular fatigue life can be illustrated by a conservative approximation of the Gerber line called the Goodman Line. Structural design engineers utilise the Goodman diagram, as seen in Figure 4.12, for estimating the consequence of stress or strain adjustments on the lifetime of a member. With equal ultimate tensile and compressive strength, metals are described as symmetric materials characterised by the absolute value of the mean load, thereby, usually only the right side of the Goodman diagram is plotted for metals.



[htbp]

Figure 4.12: Simplified symmetric Goodman diagram adjusted from Sutherland (1999).

The relationship between the  $L^{MF}$  and  $L^A$  normalised by  $L^{Ult}$  of the material is illustrated by the symmetric Goodman diagram for equivalent compressive and tensile loading (left and right of  $L^{MF} = 0Nm$ ). The constant R ratios are represented as straight lines with a fully reversed bending ( $R = -1$ ) with a mean stress of zero for all amplitudes. Each of the constant life curves at 10,000, 100,000 and 10,000,000 cycles are constructed from a family of S-N curves.

To account for the variability in load means across the time series, MLife can be used to apply a Goodman correction to the fatigue calculation. The Goodman correction fit postulates that the fatigue life at alternating load and mean stress is equal to fatigue life at an equivalent zero mean stress using the ultimate material strength. With a Goodman exponent of 1, this relationship can be expressed as:

$$L_i^{RF} = L_i^R \left( \frac{L^{Ult} - |L^{MF}|}{L^{Ult} - |L_i^M|} \right) \quad (4.15)$$

where,  $L_i^R$  is the range of the  $i^{th}$  cycle about the corresponding mean load,  $L^{Ult}$  is the ultimate load,  $L^{MF}$  is the fixed mean load and  $L_i^M$  is the mean load of cycle  $i$ . Throughout this research, the Goodman correction to the load ranges from each cycle from the rainflow count to a mean load is applied. This mean load may be

specified as zero or may be input as:

- Weighted channel mean calculated by MLife on a per file basis using the specified Weibull distribution;
- Aggregated channel mean across all load input time series; or
- Explicitly entered value by the user.

It is possible to use MLife to bin fatigue cycles based on load ranges. The type of requested result influences the choice of load range type used to compute the maximum load range present in the rainflow cycles across all input time series. Possible values include uncorrected fatigue cycles, Goodman-corrected cycles about a fixed-mean, Goodman-corrected cycles about a zero-mean.

### 4.3 Chapter summary

This chapter outlines the Stream 2 methodology that can be used in the absence of the location-dependant failure rate data in the OWE industry to address the research question. The flowchart in Figure 4.13 summarises the dual-phase Stream 2 methodology.

Phase 1 uses FAST to generate structural response by the combined affects of the operational, aero- and hydro-dynamic forcings and Phase 2 uses MLife to translate this response into lifetime accumulated damage by utilising the material properties of the structure and the prevalent environmental conditions at the site. A description of FAST modules, their interactions, software validation and comparison studies is provided in this chapter followed by the description of methods used to implement the fatigue limit state. The latter involves a maximum load analysis by MExtremes and lifetime accumulated damage assessment by MLife. These include the rainflow counting of the load cycles, the S-N curve approach for damage estimates and the linear Miners rule for lifetime accumulated damage.

To reduce the computational effort required to apply Stream 2 and isolate metocean-centric effects, the number of variables in the lifetime damage analysis are reduced by introducing assumptions regarding the uniformity of certain parameters. The spatial lifetime damage analysis in subsequent chapters delivers the results assuming uniform water depth and soil conditions at all considered locations. The same bottom-fixed NREL 5 MW turbine with a rigid connection and

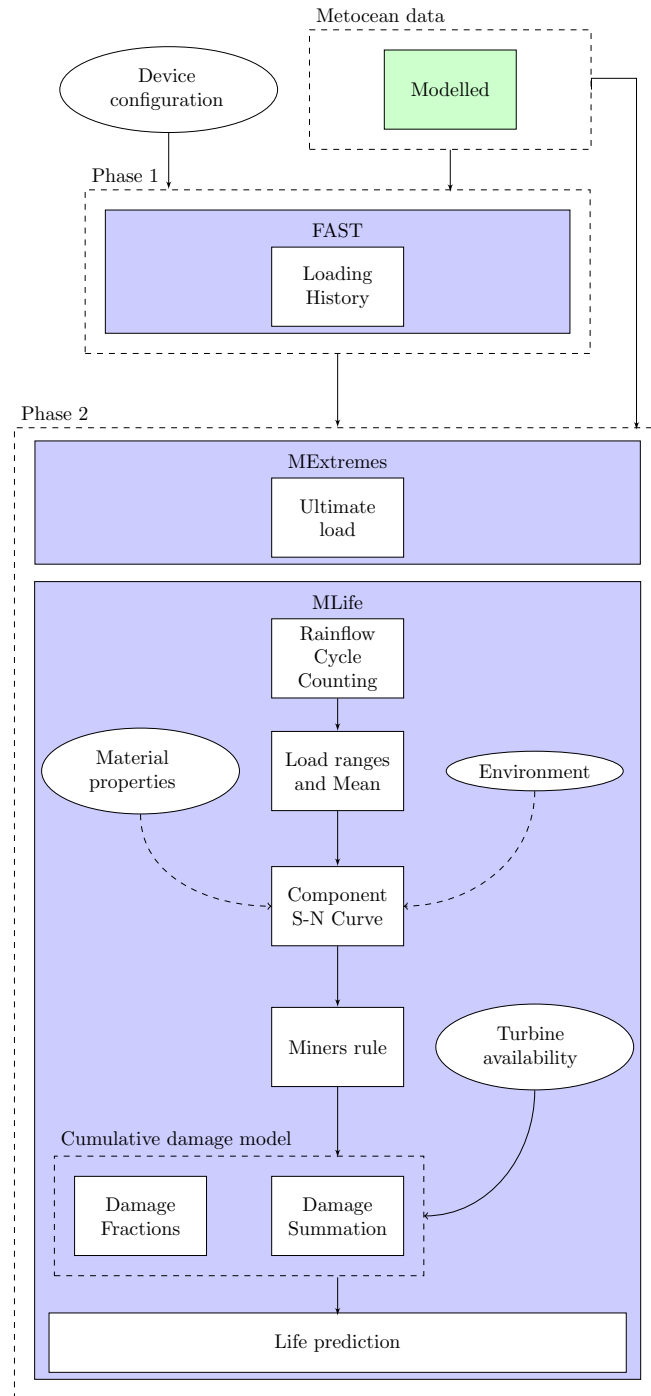


Figure 4.13: The dual-phase Stream 2 methodology developed to provide location-specific performance indicators to facilitate informed site selection for OWT deployment.

uniform control system is assumed to have been deployed at all locations. The simulated turbulent wind field is always generated using the Kaimal spectrum and the site wave characteristics are produced based on the JONSWAP spectrum. Furthermore, the directionality of wind and wave forces is ignored and they are assumed to be aligned at all times.





# Chapter 5

## Reliability-critical Subassembly Identification

Acceptable structural engineering design philosophies aim to meet the criteria of safety, structural integrity, serviceability, functionality and economic viability for a structure. There are numerous design criteria that must be examined to account for all possible failure modes and determine the robustness of the design of an OWT design including ultimate strength, fatigue, stability and deflection. The LCOE from offshore wind shows high sensitivity to steel price fluctuations and existing support structure fabrication processes rely heavily on structural steel. Therefore, this chapter takes a fatigue analysis approach to identify the reliability-critical subassembly in the support structure. This is done to assess areas of safety margins to identify whether a structure is over-, under- or optimally designed for a site under consideration. This subassembly is then used as an illustrative example in subsequent chapters to develop the methodology for geospatial mapping of a risk-return metric for OWE deployment in the UKCS.

In current OWT engineering practices, while fatigue loads for preliminary design processes are estimated by frequency domain models, the certification process (International Electrotechnical Commission, 2014) requires fatigue assessment by computationally intensive, dynamically coupled time-domain simulations of a range of load cases (Seebregts et al., 1995). To determine the viability of the developed methodology for the variability of fatigue in OWT structures based on site-specific metocean conditions, a robust dynamic time-domain analysis is conducted.

## 5.1 Industrial cost drivers

Commodity price fluctuations have a significant impact on the overall CAPEX of the offshore wind turbine structure since the wind turbine structure contributes to 50% of the overall CAPEX. Based on reports by the British Wind Energy Association, now RenewableUK, steel contributes to 12% of the overall project cost (BWEA, 2009) since it contributes to much of the structural components within the nacelle, transition piece as well as the turbine foundation. Sensitivity to steel prices was a significant contributory factor to rising turbine costs by 67% from £0.9m/MW to £1.5m/MW between 2000 and 2008 (UK Energy Research Centre, 2010).

A summary of the LCOE breakdown of OWE by multiple resources (RenewableUK and BVG Associates, 2011; BVG Associates, 2012; Crabtree et al., 2015) shows agreement between analysis of the multiple institutes that the foundation or support structure contributes significantly to the CAPEX. A major design challenge for cost-effective deployment of OWTs is the use of site-specific support structures. Despite the economic benefits associated to design standardisation and mass production (BVG Associates, 2012), currently there is limited possibility for design convergence due to the variable OWT site characteristics including water depth, soil type and metocean parameters.

For the OWT foundation, costs increased from £250,000 to £700,000/MW between 2004 and 2009 (UK Energy Research Centre, 2010). Comparison with trends in steel price display that this can be directly attributed to the hike in structural steel prices since around 75% of the foundation costs relate to material costs. It is suggested by the UK Energy Research Centre that material costs are major drivers for escalation in wind turbine costs closely followed by adverse exchange rate movements (UK Energy Research Centre, 2010). An additional intrinsic cost driver was the increasing depth and distance of the more ambitious lease sites whereby the cost of turbine deployment, innovative foundation concept as well as O&M may increase.

Due to the associated cost and its contribution to the structural integrity of an OWT, the focus of this research project is narrowed down to the support structure assembly.

## 5.2 Structural assembly analysis

Monopiles are characterised by low stiffness and low natural frequencies relative to a jacket foundation. They are typically designed outside the operational frequencies 1P and 3P (Tempel, 2006) and display sensitivity to dynamic loading by wind and wave loads. Based on engineering design, they are overturning moment resisting structures meant to counter the combined moment generated by the RNA thrust and the environmental loading. These two component moments are highly dependent on the environmental parameters of wind and wave respectively, and therefore, display high spatial and temporal variation. The dynamic design of monopiles is well established, however, the coupling between environmental and structural loads is not well understood. Scaffarczyk (2014) estimates that a wind turbine structure is subjected to 500 million load cycles in the average 20 year lifetime, therefore, the structural integrity may be compromised if the dynamic design is inappropriate for the site conditions.

However, if the monopile is overdesigned, it may contribute to a high LCOE, therefore, reanalysis for lifetime extension of monopiles must be conducted since the wide-scale use of a monopile with generic geometric definition is limited by numerous factors. These include the lack of redundancy in the foundation system which increases chances of single-point failure, the uncertainty associated to the failure of the foundation-transition piece-tower grouted connections and the high installation and manufacturing cost of the piles.

### 5.2.1 CAE simulator inputs

The NREL preprocessing tool TurbSim, aero-hydro-servo-elastic tool FAST and post-processing tools MExtremes and MLife are used to model lifetime accumulated damage at various nodes in the support structure. Each tool has a range of parameter inputs and an insight into the sensitivity of dynamic structural analysis due to variable numerical and physical input parameters provides an increased understanding of parameters relevant to fatigue analysis.

### 5.2.1.1 Environmental parameters

Design assumptions and lumped environmental conditions are adopted from the reduced scatter plots of the K13 shallow water site analysed in the Upwind Design Basis on the method identified by Kühn (2001). This lumped data has been used extensively in load investigations of fixed offshore wind turbines (Aasen et al., 2017; Løken, 2009; Ziegler, 2016) due to its accurate representation of the environmental parameters at the site, while significantly reducing the computational effort as discussed in Chapter 2.

As outlined by Kühn (2001), preliminary lumping of sea states aims to quantify damage for lumped load cases equivalent to all constituent unlumped load cases with increased computational efficiency. Arbitrarily, the number of lumped load cases is limited to twenty with the wind speed discretised to a class width of 1 m/s within the production range of the particular wind turbine and broader class widths near the cut-in and cut-out speeds. Additionally, significant wave height classes of 0.5 m and wave peak period classes of 0.5s are considered.

The relative damage induced by each elementary load case requires the weighting of each environmental parameter. A reasonable prediction under quasi-static, linear response concludes that stress ranges are directly proportional to the standard deviation of the wind speed (consequently the mean wind speed with constant turbulence intensity) and significant wave height and inversely proportional to the zero-crossing period in the elementary load case. While these lumped load cases do not provide an exact match to the cumulative damage from each elementary load case due to simplified assumptions, they provide a computationally inexpensive solution to achieve fatigue life assessment estimates.

With 3-hour average historic data of 22 years and MSL of 21.4m, the K13 site is representative of a typical shallow water site in the Dutch North Sea ideal for deployment of an offshore wind turbine with a monopile substructure. The measured wind speed at 10 m reference height was sheared to the hub-height of 85.16 m above MSL for the UpWind Reference wind turbine (Fischer et al., 2010) using a roughness length of 0.002 for offshore conditions. This wind profile is further sheared to the 90 m hub height of the NREL wind turbine by using Equation. 4.1 (B. J. Jonkman and Kilcher, 2012).

The extracted Lumped Load Cases (LLC) with 17 sets of metocean variables

Table 5.1: Load case metocean parameters based on the K13 shallow water site from the UpWind Project (Fischer et al., 2010).

LLC No.	Wind Speed [m/s]	$H_s$ [m]	$T_p$ [s]	TI %	Occurrence probability
LLC01	2	1.07	6.03	29.2	0.05395
LLC02	4	1.1	5.88	20.4	0.10177
LLC03	6	1.18	5.76	17.5	0.13431
LLC04	8	1.31	5.67	16	0.14768
LLC05	10	1.48	5.74	15.2	0.14288
LLC06	12	1.7	5.88	14.6	0.12459
LLC07	14	1.91	6.07	14.2	0.09917
LLC08	16	2.19	6.37	13.9	0.07259
LLC09	18	2.47	6.71	13.6	0.04910
LLC10	20	2.76	6.99	13.4	0.03079
LLC11	22	3.09	7.4	13.3	0.01793
LLC12	24	3.42	7.8	13.1	0.00972
LLC13	26	3.76	8.14	12	0.00491
LLC14	28	4.17	8.49	11.9	0.00231
LLC15	30	4.46	8.86	11.8	0.00101
LLC16	32	4.79	9.12	11.8	0.00042
LLC17	34-42	4.9	9.43	11.7	0.00024
Aggregate					0.99337

corresponding to significant wave height, wind speed at hub height, peak wave period and turbulence intensity (TI) are shown in Table 5.1.

For LLC17, the corresponding wind speed range is disregarded and the mean wind speed of 38 m/s is chosen for simulating loads on the various subassemblies of the OWT structure. To choose the appropriate turbulence intensity distribution, Fischer et al. (2010) conducted a comparison of various distributions based on IEC 61400-1 (International Electrotechnical Commission, 2005), IEC 61400-3 (British Standards Institution, 2009) and the Nordzeewind project 2008. It was observed that the the first part of IEC 61400 yielded conservative results, whereas, the third part overestimated the turbulence. The Nordzeewind OWEZ project uses

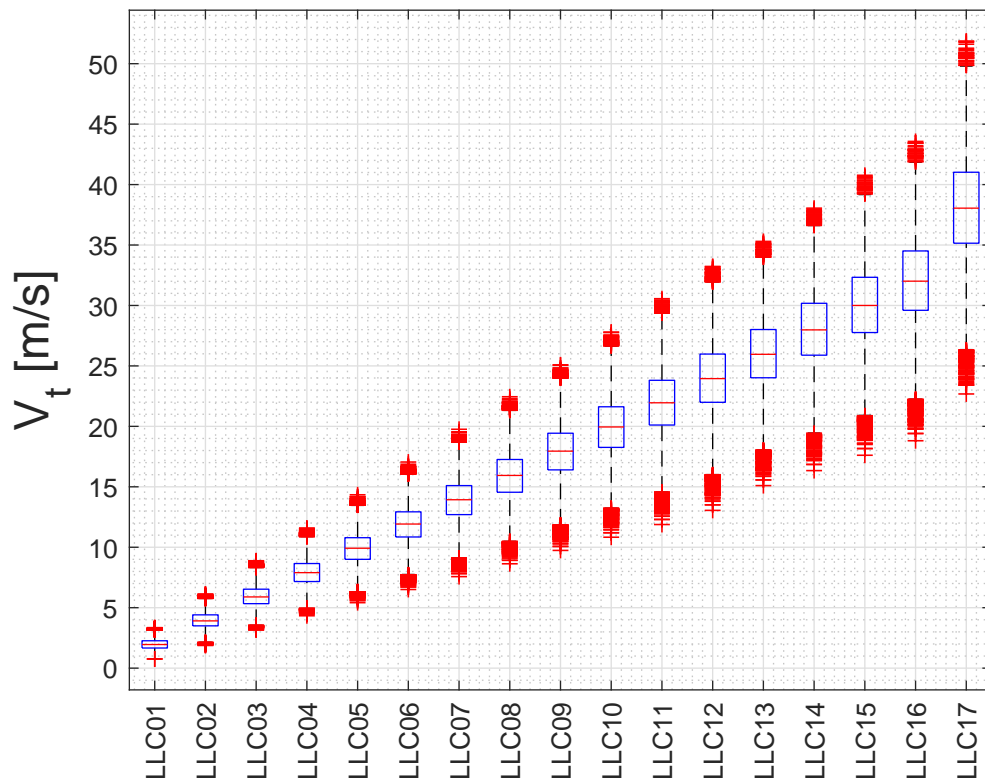
the base IEC 161400-3 distribution but the turbulence is initialised with a different reference intensity taking account of wake. The adapted Nordzeewind distribution provides a good compromise between the two IEC distributions, therefore, was considered most suitable for the UpWind project. However, since the aim of this study is to choose the key subassembly, the available IEC 61400-3 turbulence model in TurbSim is chosen instead of a user-defined spectra. This may yield different fatigue results relative to other fatigue assessments conducted using the UpWind data.

Simulating wind parameters through a Kaimal distribution in TurbSim and wave through the JONSWAP spectrum in the FAST HydroDyn module for each LLC produces metocean parameters with the statistical characteristics shown in Figure 5.1. For each 10 minute period, the wind and waves are assumed to be unidirectional and no directional spreading is introduced, therefore, the most conservative estimate of fatigue life is expected to result from the linear addition of the aero- and hydrodynamic loads. It can be seen that the K13 site is characterised by low  $H_s$  and based on Table 5.1 wind speeds of between 3 m/s - 25 m/s for 90% of the observed period. Since this is the operational range of wind speeds for the 5MW NREL baseline turbine, an ideal turbine deployed at the site is expected to show availability of around 90%.

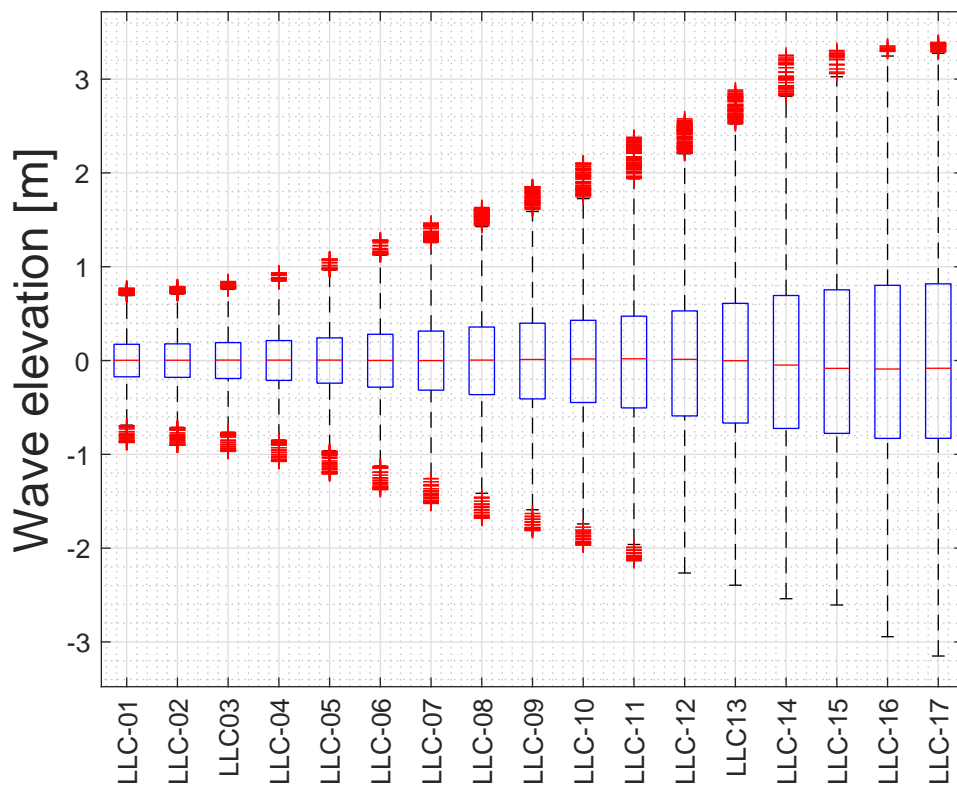
### 5.2.1.2 Choice of DLCs

Considering possible directional effects, operational states and prevalent sea states lead to an offshore wind turbine being exposed to load cases in excess of an order of magnitude relative to an onshore wind turbine. It is unsuitable to account for all possible combinations of external loads, operational conditions and design solutions, therefore, a set of minimum requirements for design driving load cases with a reasonable probability of occurrence is identified to be sufficient for certification purposes.

Available standards (British Standards Institution, 2009) provide a comprehensive matrix of characteristic Design Load Cases (DLC) to be assessed and associated metocean parameters when conducting fatigue or ultimate design analysis using a structural dynamics model for an offshore wind turbine. This matrix incorporates all significant states that influence a wind turbine's structural in-



(a) Wind speed for LLC01 - 17.



(b) Wave elevation for LLC01 - 17.

Figure 5.1: Wind speed and wave elevation statistics for the considered LLCs from the shallow water K13 site in the Upwind project (Fischer et al., 2010).



tegrity through its lifetime, including operation in normal or extreme conditions, fault situations and transient events including start-up or shut-down. Table 1 in the British Standards for design requirements of offshore wind turbines (British Standards Institution, 2009) characterises the DLCs based on the metocean, electrical and other external conditions suggesting appropriate fatigue or ultimate loads analysis for each DLC and providing associated safety factors .

Seven applicable DLCs to assess the fatigue life of an OWT are extracted and presented in Appendix B, however, for the scope of this work only DLC 1.2 and DLC 6.4 are considered. These DLCs provide fatigue load assessment for the power production and idling conditions, respectively. Not only do these DLCs cover the predominant turbine states, they also have low uncertainty associated to the determination of the occurrence probability. Therefore, the aforementioned elementary DLCs are considered sufficient to provide a realistic indicator of the variation in the reliability-informed siting parameter and the remaining DLCs are not considered for this study (Sutherland, 1999).

Early experience with Round I offshore wind turbines shows that average farm availability was 80.2% owing to increase in downtime due to repair and unscheduled maintenance activities (Feng et al., 2010). In these instances and when the wind speed lies outside the operational range, the wind turbine is assumed to be idle. Since lifetime load extrapolation by MLife is performed differently for the power production and parked design load cases, the data is split into its respective design load cases. Considering the selected DLCs (British Standards Institution, 2009) and the range of operational wind speeds (3 m/s to 25 m/s) for an ideal NREL 5-MW turbine with 100% availability, it is determined that LLC02 – LLC12 represent DLC 1.2 Power Production. Whereas, DLC 6.4 Parked and Idling spans over LLC01 and LLC13 – LLC17.

### 5.2.1.3 FAST initialisation parameters

Various parameters in ElastoDyn and ServoDyn must be adapted based on the input wind conditions to ensure numerical stability of the model as well as simulate appropriate design load cases. Based on instructions from the FAST manual (Jason Jonkman and Marshall L Buhl, 2005), a parked OWT for the load cases categorised under DLC 6.4 are simulated by pitching the blades out of the wind, switching off

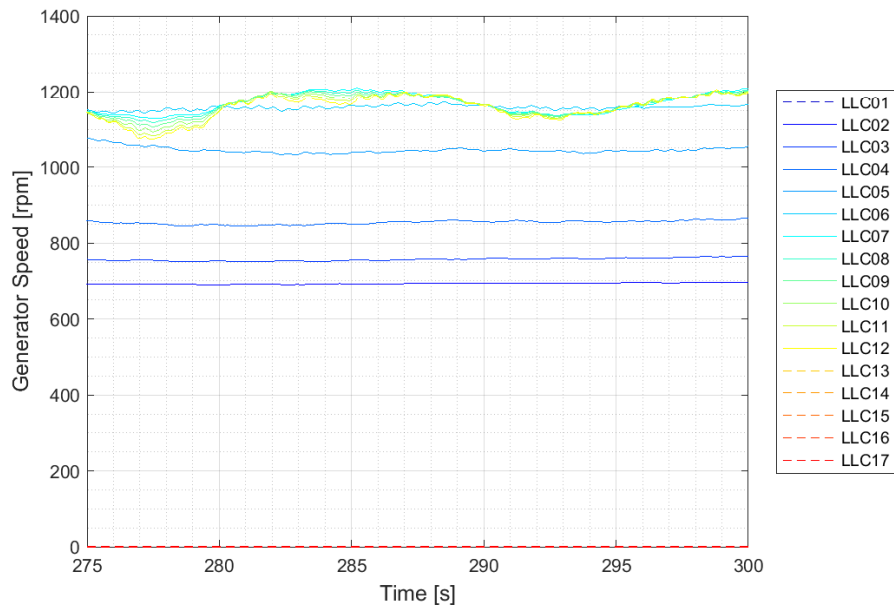
Table 5.2: Appropriate initialisation parameters for ServoDyn and ElastoDyn modules based on (Jason Jonkman and Marshall L Buhl, 2005; Jonkman et al., 2009).

DLC No.	LLC No.	Blade Pitch [degrees]	GenDOF	PCMode	Rotor Speed [rpm]
6.4	LLC01	90	Disabled	0	0
1.2	LLC02	0	Enabled	5	12.1
	LLC03				
	LLC04				
	LLC05				
	LLC06				
	LLC07	3.83			
	LLC08	8.70			
	LLC09	12.06			
	LLC10	14.92			
	LLC11	17.47			
LLC12	19.94				
6.4	LLC13	90	Disabled	0	0
	LLC14				
	LLC15				
	LLC16				
	LLC17				

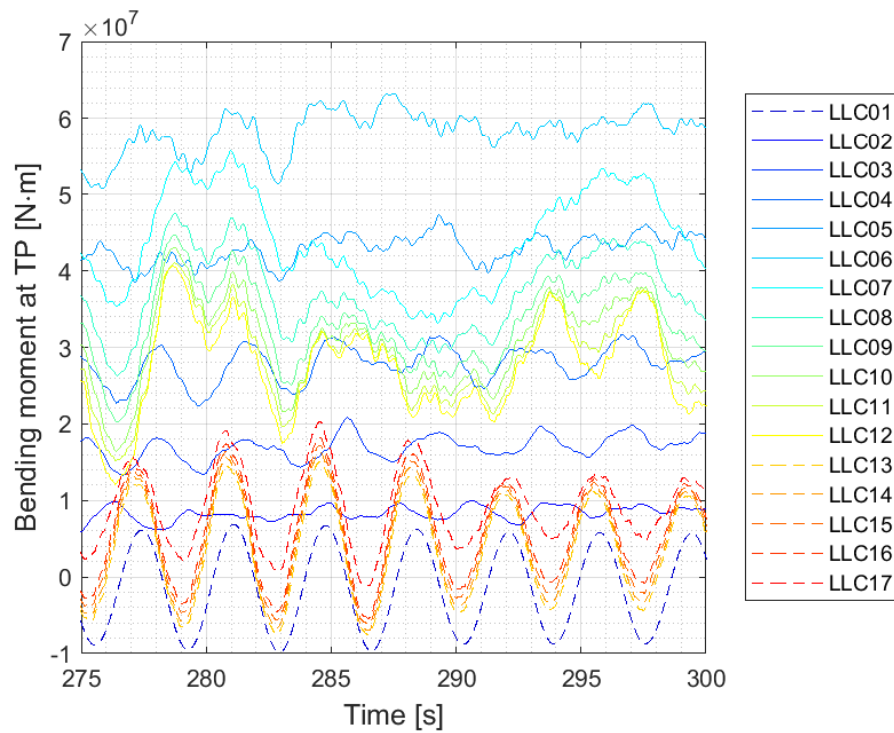
active pitch control, disabling the generator degree of freedom and initialising the rotor speed at 0 m/s. Further details regarding the associated parameters for each LLC can be found in Table 5.2 including (GenDOF) and (PCMode).

### 5.2.2 Turbine dynamic response to various LLCs

Simulating the K13 shallow water site to observe and validate the differences for the turbine power generation and dynamic response between various load cases provides insight into the turbine function. Figure 5.2 shows a section of the simulated 10-minute time series for the generator rotational speed and the bending moment at the transition piece. As seen in Figure 5.2a, the generator is rotating at all load cases between LLC02 to LLC12 (inclusive) operating at full capacity



(a)



(b)

Figure 5.2: OWT generator speed and pitching moment at the transition piece for LLC01 - LLC17 displaying characteristic difference between time series data for operational (DLC 1.2) and parked (DLC 6.4) conditions represented by solid and dashed lines, respectively.

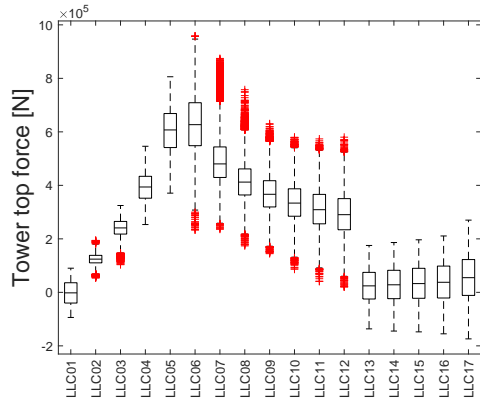
between LLC06 and LLC12, whereas, for load cases outside the  $V_{in} - V_{out}$  range, the generator produces no power. Therefore, the FAST initialisation parameters have successfully modelled a parked wind turbine for wind speeds outside the operational  $V_t$  range.

Time series data for the load cases in Table 5.1 at the various subassemblies of the OWT support structure exhibit an incremental increase until the turbine's rated wind speed is reached, at LLC06 in this case. As an example, this can be seen in Figure 5.2b for the dynamic bending moment at the transition piece in the global inertial coordinate system for the dominant pitch direction. LLCs corresponding to DLC 1.2 display operational natural frequencies, however, for LLCs with wind speeds outside the operational wind speed range, the high frequency moment oscillations are absent since the turbine is in a parked position and only exposed to cyclic environmental loads.

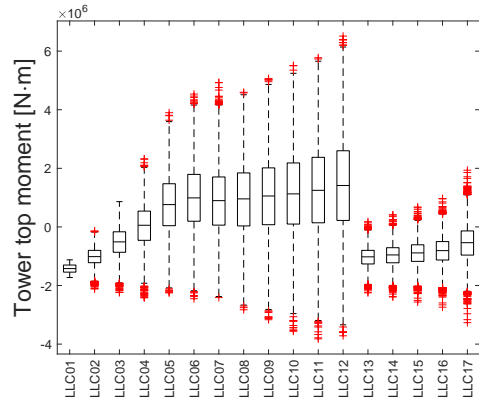
For load cases with wind speeds higher than the rated wind speed but lower than  $V_{out}$ , the rotor motion modulates the induced bending moments due to aerodynamic damping as is characteristic of horizontal axis turbines (Liu et al., 2017). LLC13 - LLC17 for the idling rotor exposed to the strongest wind and wave regimes has highly reduced damping, therefore, high amplitude loading is experienced at the transition piece. The wind loads on the idling turbine with a functioning yaw system are composed mainly of drag forces on the tower and nacelle since the blades are pitched in the wind direction minimising the exposed surface area. The maximum expected wind loads in this condition will be the blade loads perpendicular to the wind direction.

Figure 5.3 shows the basic statistics calculated for all load cases at additional critical locations of the OWT support structure including the tower top, transition piece and substructure for both bending moment and shear force induced loads in the global inertial coordinate system. It can be seen that the extreme loads between the structural subsystems may vary by an order of magnitude and the most extreme loads (for both shear force and bending moment) are experienced by the substructural components at the mudline since they experience a sum of loads by both wind and wave regimes.

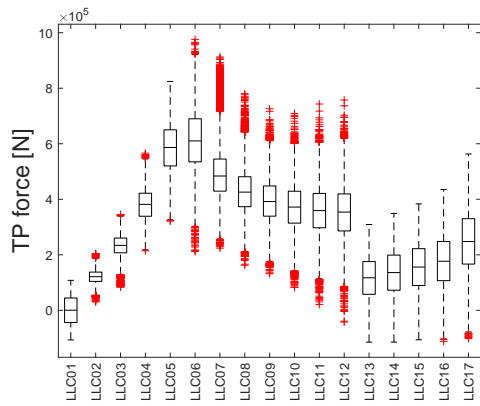
The shear forces at the tower top (Figure 5.3a) and transition piece (Figure 5.3c) display high sensitivity to the turbine operational states at both the rated wind speed and  $V_{out}$ . The maximum loads at the transition piece are at the rated



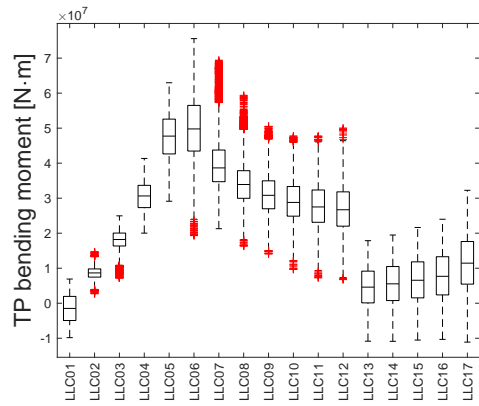
(a) Tower top shear force



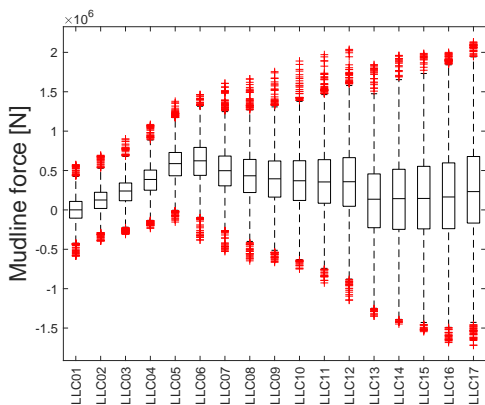
(b) Tower top bending moment



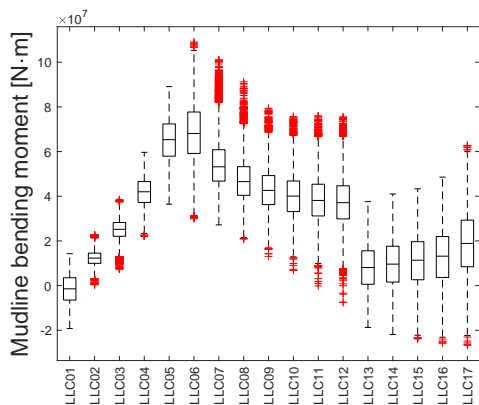
(c) Transition piece shear force



(d) Transition piece bending moment



(e) Mudline shear force



(f) Mudline bending moment

Figure 5.3: Forces and bending moments at various locations on the support structure for multiple LLCs.

wind speed of LLC06 and turbine damping then reduces the loads for further wind speed increase and a sudden decrease is observed at  $V_{out}$ .

The tower top bending moment (Figure 5.3b), which is representative of the shaft loading, displays a differentiated behaviour, displaying negative and positive values for various LLCs. In agreement with existing analysis (Bachynski et al., 2013; Feliciano et al., 2018), the fore-aft tower top bending moments are sensitive to imbalance loads. It is a result of the imbalance between the negative bending moment produced by the rotor weight and positive moment due to the effects of a non-uniform vertical velocity profile if the velocity at the top-half of the rotor disk is larger than that at the bottom-half. Therefore, positive values for the tower top bending moment indicate that the blade imbalance is larger than the weight of the rotor and negative values are observed when the moment is dominated by rotor weight.

Due to the increase in associated wind speed of the LLCs, the tower top bending moment (Figure 5.3b) can be seen to show a steady increase as blade imbalance increases. For LLCs beyond the rated speed, the damping effect attempts to neutralise the loading due to blade imbalance. Once the blades are pitched out of the wind at cut-out speed, the effect of blade imbalance is eliminated and the tower top bending moment becomes dominated by the rotor weight and a drastic load reduction is observed since the only remaining loads acting on the tower top are the wind loads.

For the bending moments at the transition piece (Figure 5.3d) and the mudline (Figure 5.3f), a similar trend as for the shear forces on the transition piece is observed. The bending moments at the tower top and the shear forces at the mudline (Figure 5.3e) do not adhere to this behaviour. The shear forces at the mudline display a very weak correlation with the operational state of the turbine, therefore, the loads at this subassembly can be said to be dominated by the influence of the wave loads.

## 5.3 Choice of critical subassembly

The estimation of the fatigue lifetime of the support structure of an offshore wind turbine requires the identification of critical subassemblies. These critical subassemblies may then be exposed to a large number of time-domain simulations

to account for the range of load conditions that a turbine may experience when deployed at a particular site.

### 5.3.1 Geometric description at support structure nodes

For the nodal analysis of the support structure, the structure is discretised into equally spaced segments (members) which are used for the integration of the elastic forces computed by FAST modules ElastoDyn and SubDyn. Both modules produce load output timeseries at the analysis nodes assigned to the members which can be described as representative data from virtual strain-gauge locations along the length of the support structure. However, ElastoDyn and SubDyn output load data at different points on the member. For the tower modelled in ElastoDyn, nodes are located at the centerpoint of members, whereas in SubDyn, the substructure (including pile and transition piece) load time histories are produced at the edges of the members.

When modelling a non-uniform tower in FAST, at least two locations must be specified, at 0 and 1, respectively, whereby the latter is at the 100% flexible height of the tower. Distributed properties at these stations are specified in the ElastoDyn input and the data is linearly interpolated to the centers or analysis nodes of these members. FAST allows for discretisation of up to a maximum of 100 members, whereby, an increase in the number of members improves the accuracy of the integral with the trade-off of increased computation time. 20 members are recommended as a good compromise between computational efficiency and output accuracy and are therefore, used for this study. The elevation of each analysis node in the undeflected tower (Jason Jonkman and Marshall L Buhl, 2005), relative to the tower base is determined as follows:

$$T_{elev} = \text{Rigid Base Height} + (T - \frac{1}{2}) \times \left( \frac{(T_{Ht} + \text{Tower Draft} - \text{Rigid Base Height})}{\text{Tower Nodes}} \right) \text{ (for } T = 1, 2, \dots, \text{Tower Nodes)}$$
(5.1)

Where,  $T_{elev}$  is the height of the tower analysis node,  $T$  is the serial number of the analysis node and  $T_{Ht}$  is the tower height. Possible values of  $T$  are 1 to the total number of tower nodes, where 1 corresponds to the node closest to the tower base (but not at the base) and a value of Tower Nodes corresponds to the node closest to the tower top. In FAST v8.16.00a-bjj, tower base height has replaced variables

the rigid base height and tower draft with the following relation:

$$\text{Tower Base Height} = \text{Rigid Base Height} - \text{Tower Draft} \quad (5.2)$$

Therefore, adapting Equation. 5.1 to determine node elevation from the mudline produces:

$$T_{elev} = \text{Tower Draft} + \text{Tower Base Height} + \left(T - \frac{1}{2}\right) \times \left(\frac{T_{Ht} + \text{Tower Base Height}}{\text{Tower Nodes}}\right) \quad (\text{for } T = 1, 2, \dots, \text{Tower Nodes}) \quad (5.3)$$

The thickness and diameter of the 5MW NREL turbine tower are assumed to be linearly tapered from base to top with base diameter and thickness of 6m and 0.027m and top diameter and thickness of 3.87m and 0.019m, respectively. With a base height of 10 m, the length of the tubular tower member is 77.6m based on:

$$\text{Tower length} = T_{Ht} - \text{Tower Base Height}$$

The base of the tower is connected to the substructure, a uniform tubular multi-member structure. Unlike the tower discretisation, the members are produced by a single numerical input, the limits for the substructure members are defined by joint coordinates, therefore, member lengths may vary. Each substructure member is further divided into elements with element ends as analysis nodes as seen in Figure 4.9b. The NREL 5MW turbine substructure is modelled as a three member and 3 element per member structure with a uniform diameter and thickness of 6m and 0.06 m, respectively (Jason Jonkman and Musial, 2010) with the first node of member one closest to the mudline and the fourth node of member three at the tower-substructure interface. Similar to the tower discretisation, increasing the number of elements per member may increase accuracy whilst increasing computational time and memory usage.

Based on the above stated discretisation and extrapolation, the investigation into the reliability-critical node utilised five analysis nodes in the tower and four nodes in the substructure. The three critical locations in the support structure, namely, tower top, transition piece and mudline were included. For the tower, analysis outputs were generated for the nodes close to the tower top and tower base and three equidistant nodes in between. Due to the 20 nodes for input parameters, the outputs are generated at analysis node 1, 5, 10, 15 and 20. Similarly, for the substructure, outputs were generated for the node at the mudline and transition piece as well as the interface of the members. Therefore, for the substructure a total



of four nodes at node 1 and 3 of members 1 and 3 were used to generate structural response. Figure 5.4 shows the geometric properties of the chosen analysis nodes in order of increasing height above the mudline. It can be observed that as the distance increases, no change in geometric properties of the monotonic substructure exist, however, the linearly tapered tower shows a decrease in external diameter and a considerable reduction in thickness. This geometric variation may contribute to a consequent high sensitivity of fatigue life to induced loads.

The analysis nodes along with the average shear forces and bending moments for a ten-minute FAST simulation of the OWT in LLC16 at the respective nodes can be seen in Figure 5.5a, Figure 5.5b and 5.5c, respectively. It must be noted, that the plotted mean shear forces and bending moments at the nodes incorporate the influence of the two dominant directional load regimes. Therefore, bending moment output accounts for the simulated local roll and pitch in the element coordinate system for the substructure. Similarly the side-to-side and fore-aft shear forces in the base coordinate system contribute to the estimate of the mean shear force at each tower node.

There is clear indication that for the current LLC, shear forces and bending moments decrease with increase in the height of the analysis node from the mudline. The trends between the shear forces and bending moment, however, vary significantly, with a sharp decrease in the shear forces until J3 in the substructure. Thereafter, the forces plateau until the first node in the tower. For the bending moment, this plateau is reached at the final substructure joint which is closest to the first node of the tower, therefore, similar loads are expected at both points. J3 is the joint at the MSL, therefore, the joints below it are experience higher reaction forces since and are exposed to dynamic wave loads as they are submerged. Analysis for other LLCs yields similar trends in the shear and bending reaction loads to confirm the influence of a combination of the turbine structural and metocean parameters to load outputs.

Figure 5.5 provides the argument for why the support structure is tapered since the structure needs to withstand larger loads at the mudline relative to the tower top.

The bending moments are an order of magnitude higher than the shear forces, therefore, can be considered the limiting factor for the support structure design.

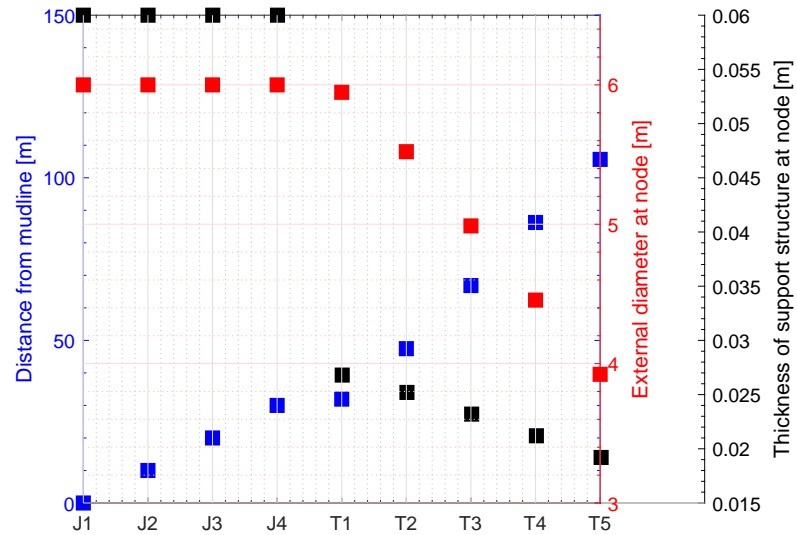


Figure 5.4: Geometric properties of the OWT at the analysis nodes.

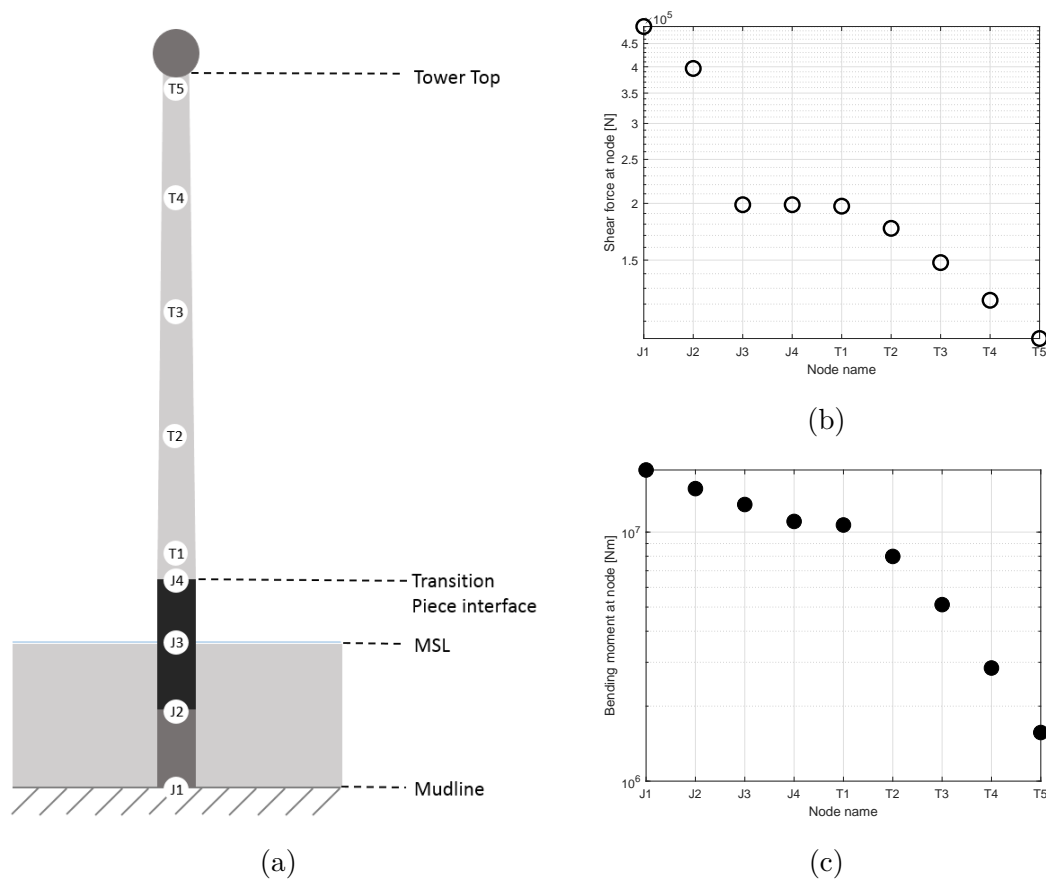


Figure 5.5: Diagrammatic representation of the (a) location of and (b) shear forces and (c) bending moments at the analysis nodes of a fixed OWT for LLC16.

### 5.3.1.1 Turbine performance indicators

Lifetime damage at the analysis nodes of the NREL 5 MW wind turbine can be estimated by the shear or normal stress profile on the structure as discussed in Chapter. 4 for fatigue cycle counting. Ideally, the distortion energy failure theory described in Chapter. 4 should be used to describe failure at the yield criterion since Von Mises stress includes effects from shear and bending loads. However, this requires a detailed finite element analysis of the OWT structure to encapsulate the non-linearities.

The computational efficiency of the linear approach for substructure loads analysis whilst maintaining output fidelity advocates against the use of an FEA analysis for the structure to achieve the aim of this research project (Damiani et al., 2013). FAST provides point load response time-histories for the shear forces and bending moments contributing to these stresses along the support structure which are used for fatigue analysis. While it is at the user's discretion to decide on the methodology for determining the turbine response characteristics based on the aims of the study, confidence established in the FAST simulation outputs by comparison of static analysis results shows sufficient basis to eliminate the need for an FEA analysis.

### 5.3.1.2 Relevant response characteristics for lifetime damage

MLife uses the design lifetime (*DesLife*) and supplied occurrence probability of each bin ( $p_l^v$ ), whether Weibull-generated or user-defined, to estimate the time factor ( $f_j^{life}$ ) for accumulated lifetime damage calculation. Additionally, the availability factor,  $A_f$ , of the wind turbine contributes to the extrapolation factor for time series  $j$  in wind speed bin  $l$  as shown in Equation. 5.4 and Equation. 5.5 for DLC 1.2 and DLC 6.4, respectively. This time factor is used to scale the input ten-minute load simulations from FAST to the proportion of time the turbine experiences the specified loading conditions.

$$f_j^{life} = \frac{DesLife \cdot p_l^v \cdot A_f}{T_l} \quad (5.4)$$

$$f_j^{life} = \frac{DesLife \cdot p_l^v}{T_l} \quad (5.5)$$

$T_l$  is the time spent by each DLC time-series in the particular wind speed bin  $l$ .  $A_f$  informs the percentage of time allocated to the parked and power production states when  $V_t$  is within the operational range, with  $A_f = 1$  indicating that the turbine has no scheduled or unscheduled stops and is always generating electricity when  $V_{in} \leq V_t \leq V_{out}$ . On the contrary,  $A_f = 0$  indicates that the turbine is always offline. Equation. 5.4 is adjusted when the turbine is parked within the operational wind speed range, such that  $A_f$  in is replaced by  $1 - A_f$  for the extrapolation time factor.

Using the bending moment as an input to MLife, the lifetime DELs ( $DEL^{life}$ ) at each node are calculated and represented in Figure 5.6. It can be observed that similar to the loads, the support structure experiences maximum load at the mudline of the support structure. Lifetime damage at the mudline is about five times as much as that at the tower top.

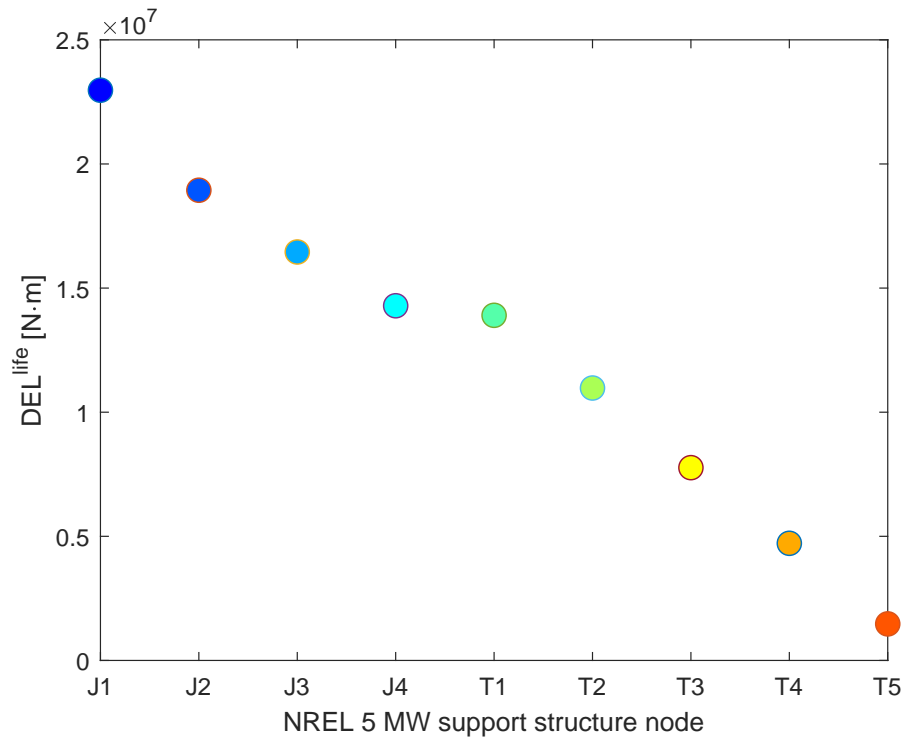


Figure 5.6: Lifetime damage equivalent loads at various nodes of the support structure. Marker colours facilitate comparison with LLC-distributed short-term DELs in Figure 5.7 at the respective nodes.

Furthermore, the short-term DELs ( $DEL^{ST}$ ) are also calculated at each LLC and presented in Figure 5.7 to understand the contribution of individual LLCs on damage. A short-term DEL is the damage equivalent load on the structure based on the input time series only, therefore, the damage induced in the structure during

the 10 minute simulation period. It can be observed that short-term DELs increase until rated speed at all nodes and the highest DELs are at rated speed (between LLC06 - LLC12). Further increase in wind speed reduces the loads to about half the peak value at LLC12 and successive LLCs experience an increase in DEL with increase in wind speed.

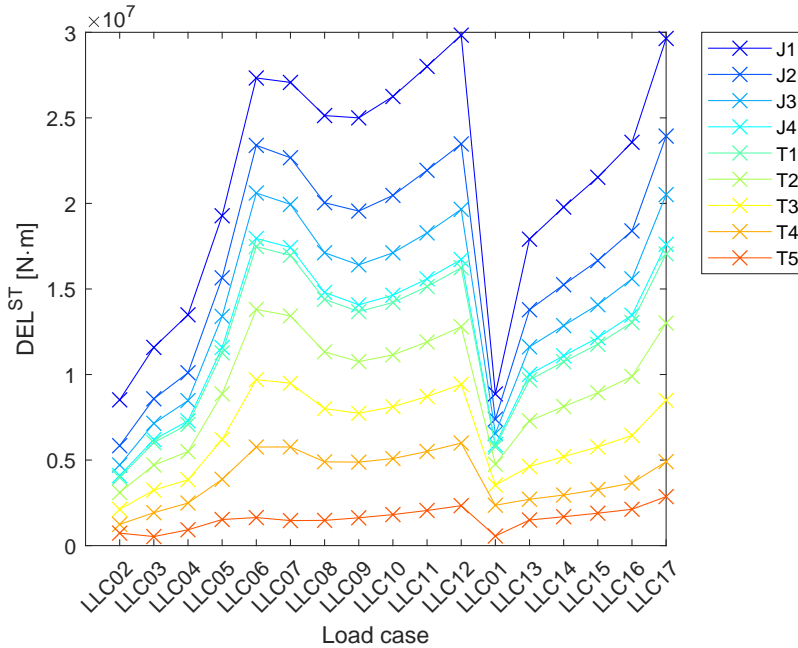


Figure 5.7: Short-term damage equivalent loads at various nodes of the support structure displaying the relative contribution of individual lumped load cases.

### 5.3.2 Power production per unit damage

As observed in Figure 5.7, there are three peaks in the short-term DELs at LLC06, LLC12 and LLC17 for all nodes. While the turbine is in the power production DLC for the two former peaks (with the turbine operating at rated speed at LLC06), it is in the parked DLC for LLC17. J1 is chosen as the reliability-critical node due to the larger shear force, bending moment and short-term and lifetime loads on the structure relative to other nodes that have been investigated in this analysis.

Quantifying the power production per unit damage induced in the structure at J1, it can be seen in Figure 5.8 that load cases under the rated power, namely LLC04 and LLC05, provide optimum generation conditions. Due to the sudden peak in structural loads at rated speed, the feasibility of the turbine operating at rated power between LLC06 - LLC12 is considerably reduced when the risk and

return parameters are combined.

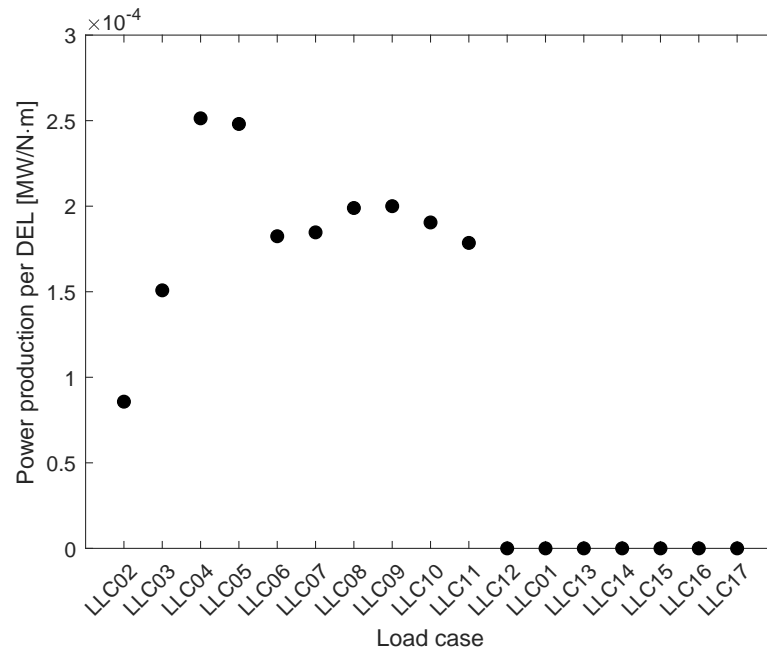


Figure 5.8: Short-term power production per unit damage equivalent load cases at the mudline of the support structure (J1) for the various LLCs.

## 5.4 Sensitivity analysis

Sensitivity analysis is described as the measure of the influence of an input on a given output (Saltelli et al., 2004). Two approaches exist to perform sensitivity analysis, the local and global approach. The former allows for the determination of physical parameters embedded in a complex model from inputs further downstream in the model by exploring only one point in the factors' space. The latter allows to determine which factor needs better determination by identifying the weak link in the chain using regression models. The performance of global sensitivity is poor for non-linear models.

There is a wide range of parameters which may be varied, however, only the parameters expected to have a large impact on fatigue life are considered for the sensitivity analysis in this section. These chosen parameters are summarised in the Table 5.3.

Table 5.3: Rationale and summarised analysis description for structural response sensitivity investigations in FAST.

Parameter	NREL tool	Summary investigation	Rationale
No. of wind seeds	AeroDyn	Explore the need for multiple seeds	British Standards
No. of wave seeds	HydroDyn	for aero- and hydrodynamic modelling	Institution 2009 and Haid et al. (2013)
Simulation length discretisation	Glue code	Determine whether ten minute simulations provide appropriate fatigue estimates	Haid et al. (2013) and Stewart et al. (2013)

### 5.4.1 Aero-hydro-servo-elastodynamic sensitivity

The influence of random realisations and simulation length requirements on the load profile are discussed multiple times in available literature (National Renewable Energy Laboratory, 2018; Haid et al., 2013; DNV GL AS, 2016b; Zwick, 2015). Therefore, this section investigates the sensitivity of the lifetime accumulated damage to these two parameters.

Standard approach (British Standards Institution, 2009; Det Norske Veritas, 2014; DNV GL AS, 2016b) in the offshore wind industry accounts for the inherent uncertainty in the stochastic wind and/or wave model input by conducting a number of random realisations which minimises statistical errors in the simulation results. Arbitrarily, six realisations of ten minute stochastic inputs are considered sufficient to ensure that the simulation results are independent of the seed. However, for certain load cases as outlined in §7.5.4 of the British Standard (British Standards Institution, 2009), simulation requirements may be as intensive as 1 hour simulation length for six random wind and wave seeds.

Additionally, expert recommendations (National Renewable Energy Laboratory, 2018) suggests statistical convergence can not be achieved for simple load cases (like DLC 1.1) with 6 seeds and an additional four seeds must be incorporated. Therefore, to determine the minimum data requirements for fatigue load simulations, a sensitivity analysis of load calculations from FAST to the number of realisations is conducted accounting for wind only, wave only as well as wind and wave effects. This is done for all LLCs from the UpWind project (Table 5.1)

Table 5.4: Simulation conditions for seed-dependence study for fixed offshore wind monopile structures.

Parameters	Units	Wind seed depen- dency	Wave seed depen- dency
No. of DLCs	[#]	17	
DLC types	-	1.1 and 6.4	
Wind parameters	[m/s]	Table 5.1	
$H_s$	[m]	Table 5.1	
$T_p$	[s]	Table 5.1	
$TI$	[%]	Table 5.1	
Simulation length	[s]	660	
No. of $\frac{windseeds}{windbin}$	[#windseeds/bin]	36	1
No. of $\frac{waveseeds}{wavebin}$	[#waveseeds/bin]	1	36
Total $\frac{simulations}{DLC}$	[#]	36	
Total simulations		612	

to account for a range of metocean boundary conditions as well as dominant turbine operational states. Table 5.4 shows the details of the various simulations conducted to determine seed-dependence of the FAST simulations.

#### 5.4.1.1 Aerodynamic load simulation seeds

To incorporate the intrinsic stochastic nature of the environmental parameters and turbine response, random phases and boundary conditions are generated using random numbers. For TurbSim, whilst the first input for stochastic number generation is a random number in the range -2147483648 and 2147483647 (inclusive), the second input in the runtime options provides access to three possible pseudorandom number generators as follows:

- Random number – Integer input in the aforementioned range. This input invokes two intrinsic congruential generators based on an algorithm developed by Pierre L’Ecuyer 1988 with a period of about  $10^{18}$ .
- SNLWIND generator – Invokes the Sandia random number generator



- Luxury pseudorandom numbers – Invokes Level 3 of Lüscher generator (Lüscher, 1994) with an astronomical period ( $10^{171}$ ) which is well suited for large-scale Monte Carlo simulations

Upon recommendation by the user’s guide (B. Jonkman and Marshall L Buhl, 2006), the Lüscher’s generator is used due to its reliability in a range of initial analyses.

As shown in Table 5.4, for each LLC, 36 ten-minute simulations are run with a unique pseudorandom TurbSim seed. Various size groups of the resulting mudline moment are then selected based on possible combinations and the bulk statistics are then compared with statistics for 36 seeds. For example, the use of 6 seeds could yield  ${}^{36}C_6 = 1947792$  combinations. Since a large number of combinations are possible for some size groups, due to the computational intensive nature of generating large combination matrices the number of combinations extracted is limited to an arbitrary 50 combinations chosen randomly. Whilst this limits the analysis since the combinations with the maximum dissimilarity from the mean values may be excluded, however, the available computing power limited more comprehensive calculations. Therefore, the randomness of the sampled seeds is assumed to provide a comprehensive inclusion of the possible seed group combinations.

For the 612 iterations, the influence of aerodynamic loads is isolated through the elimination of hydrodynamic loads by switching off the HydroDyn module of FAST. Figure 5.9 represents the results of the size of the random seed groups plotted against the percent difference from the mean and standard deviation in the FAST mudline moment simulations for 36 seeds. The percentage difference of the mean and standard deviation are calculated as shown in Equations. 5.6 with the latter calculated as the square root of the of each seed group combination since the data size is consistent within the seed groups. The results are categorised based on the OWT operational state with results for LLC01 with  $V_t < V_{in}$ , LLC07 with  $V_{in} < V_t < V_{out}$  and LLC14 with  $V_{out} < V_t$ , respectively.

$$\begin{aligned} \mu &= \frac{\sum_i^S \mu/S - \mu^A}{\mu^A} \cdot 100\% \\ \sigma &= \frac{\sqrt{(\sum_i^S \sigma^S)/S}}{\sigma^A} \cdot 100\% \end{aligned} \tag{5.6}$$

Where, superscript  $S$  indicates that the stastical property refers to the seed group

combination, whereas, superscript  $A$  denotes that the statistical property is for all 36 seeds.

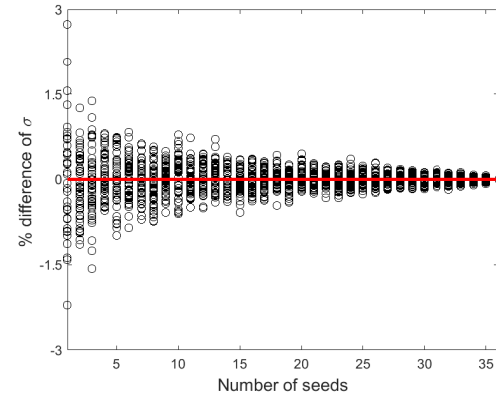
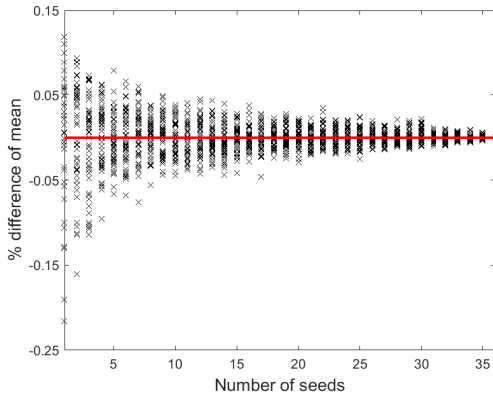
For LLC01 with wind speeds under the cut-in wind speed, the individual mean turbine bending moments at the baseline are observed to be between  $\pm 0.25\%$  of the mean of the 36 seeds. On the contrary, for LLC07 and LLC14 a weaker convergence trend is seen with percentage difference at  $\pm 4\%$ . Therefore, while no significant influence of the turbine operational state can be identified, a clear correlation with the load range can be seen. For higher loads, the realisations show a higher sensitivity to the seed value. The mean falls within 1% of the aggregate mean of 36 seeds for 1 realisation at LLC01, 6 realisations at LL07 and 11 realisations at LLC14.

The percentage difference of the cumulative standard deviation of the realisations increases with the increase in wind speed. Therefore, LLC14 shows the highest percentage difference in standard deviation, whereas, for all seeds in LLC01 data variation is within 4% of the variation observed in 36 realisations.

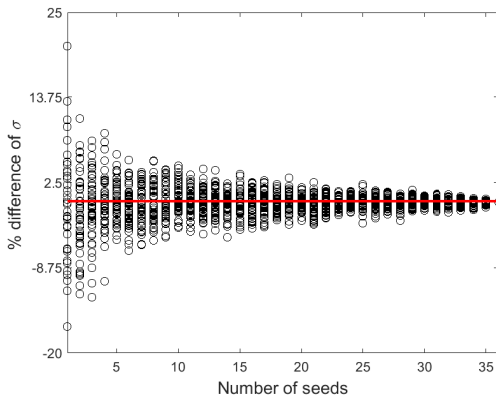
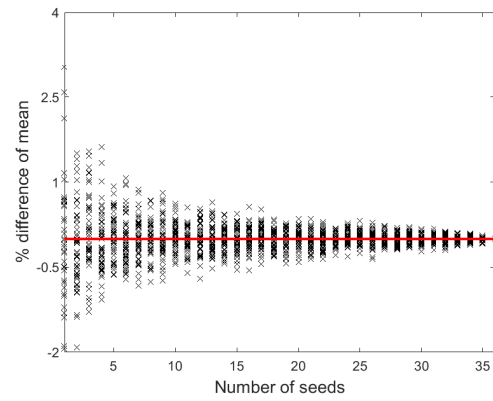
#### 5.4.1.2 Hydrodynamic load simulation seeds

Similarly, as shown in Figure 5.9, to study the effects of wave seeds on convergence of fatigue load simulations, 36 ten-minute realisations for each DLC are conducted with a HydroDyn seed between -2147483648 and 2147483647 (J. M. Jonkman et al., 2015). This influences the internal wave kinematics generated from the wave frequency and direction spectra by changing the phase of the wave time-series. Additionally, the amplitude of the wave frequency spectra is also randomised based on a normal distribution. To isolate the seed dependency on waves, only hydrodynamic loads are computed by switching off the AeroDyn and InflowWind modules. Using Equation. 5.6, the percentage difference in the seed group mean and standard deviation are illustrated in Figure 5.10

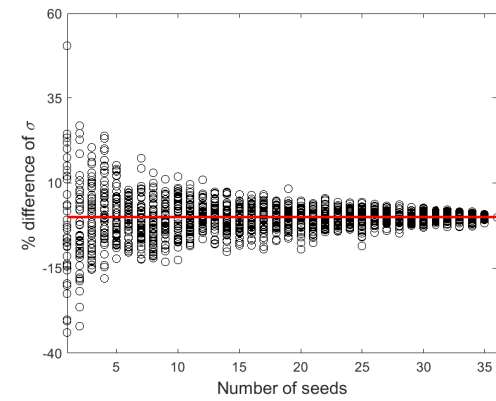
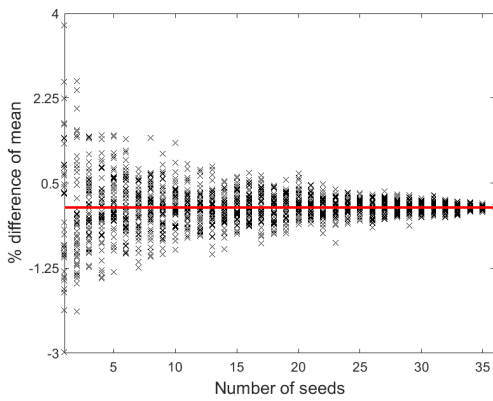
The LLCs for the HydroDyn seed groups display a similar increase to that observed for the TurbSim seed groups in that the mean deviation from the average of 36 seeds increases with increased loads. However, the increase is more gradual since the induced loads are limited to the wave loads with wind and operational loads removed. The mean falls within 1% of the aggregate mean of 36 seeds for 1 realisation at LLC01, 2 realisations at LL07 and 9 realisations at LLC14.



(a) Percent difference of mean at  $V_t < V_{in}$  (b) Percent difference of standard deviation for LLC01

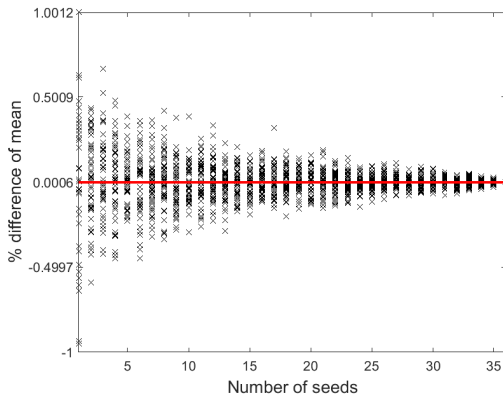


(c) Percent difference of mean for LLC07 (d) Percent difference of standard deviation for LLC07

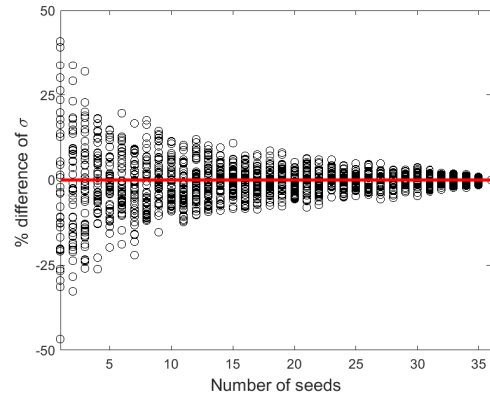


(e) Percent difference of mean for LLC14 (f) Percent difference of standard deviation for LLC14

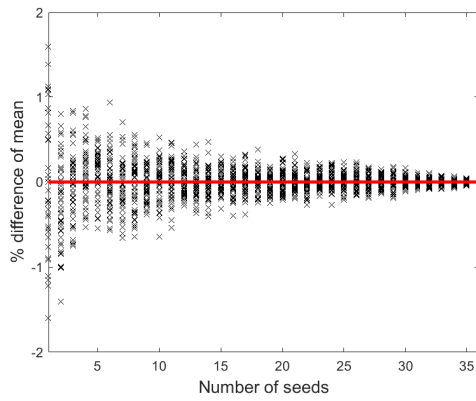
Figure 5.9: Defining TurbSim seed requirements for simulation robustness of an operating OWT using comparison of mean and average standard deviation values relative to 36 seeds for LLC01, LLC07 and LLC14. The horizontal red line corresponds to the average of 36 seeds.



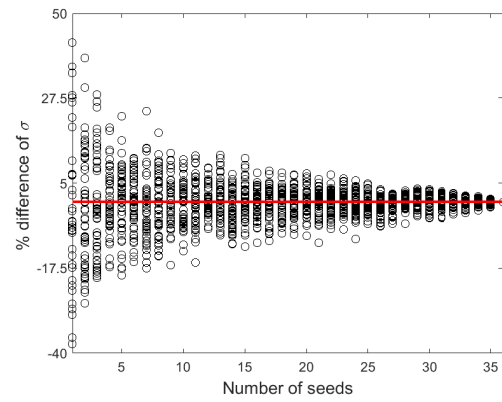
(a) Percent difference of mean for LLC01



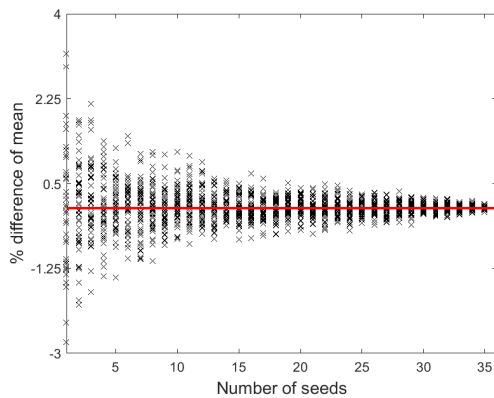
(b) Percent difference of standard deviation for LLC01



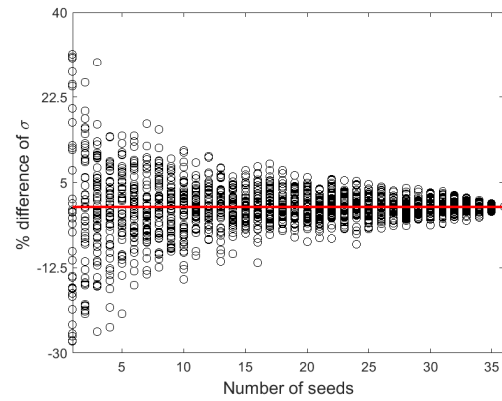
(c) Percent difference of mean for LLC07



(d) Percent difference of standard deviation for LLC07



(e) Percent difference of mean for LLC14



(f) Percent difference of standard deviation for LLC14

Figure 5.10: Defining HydroDyn seed requirements for simulation robustness of an operating OWT using comparison of mean and average standard deviation values relative to 36 seeds for LLC01, LLC07 and LLC14. The horizontal red line corresponds to the average of 36 seeds.

However, trends in the percentage difference of the cumulative standard deviation of the loads for LLCs with increasing wave loads displays no direct correlation with an increase in loads. For all LLCs, the standard deviation for seed groups is between  $\pm 50\%$ .

### 5.4.1.3 Influence of seed on lifetime damage

The largest contribution from wave loads to lifetime accumulated damage is expected at the mudline (Camp et al., 2004), however, due to the stiff support structure and the choice of a shallow water location, this analysis is expected to underestimate the fatigue loads on the mudline.

The lifetime accumulated damage resulting from the load profiles for the 36 wind and wave seeds are plotted in Figure 5.11 and Figure 5.12, respectively. Comparison of the two plots displays that the wave loads have a significantly larger contribution towards the damage accrued over turbine lifetime in the parked/idling state above cut-out speed. The same observation is made for other LLCs with  $V_t$  below cut-in speed and within the turbine operational range as shown in Appendix E. Due to the larger sensitivity of  $D^{life}$  to wave seeds, for an improved assessment of lifetime damage, a larger number of wave seeds must be considered relative to number of wind seeds.

### 5.4.2 Simulation length discretisation requirements

For floating offshore wind turbines, the integrity of the structure cannot be ensured by satisfying design requirements stated in British Standards Institution (2009). After detailed analysis, Haid et al. (2013) identifies that with the use of proper initial conditions and eliminating the effect of start-up transients, the aerodynamic loads are independent of the simulation length, therefore, a set of repeated periodic wind files was recommended to reduce computational effort. Also, Haid et al. (2013) calculated the effect of simulation length on lifetime damage equivalent loads. It was seen that the tension DELs in the fairlead and anchor had an observable increase, however, the sensitivity displayed by the results to the unclosed-cycle counting factor was higher.

Adapting the methodology used for floating OWT (Haid et al., 2013) by fixing the total simulation length, this section simulates ten hour data for each LLC using

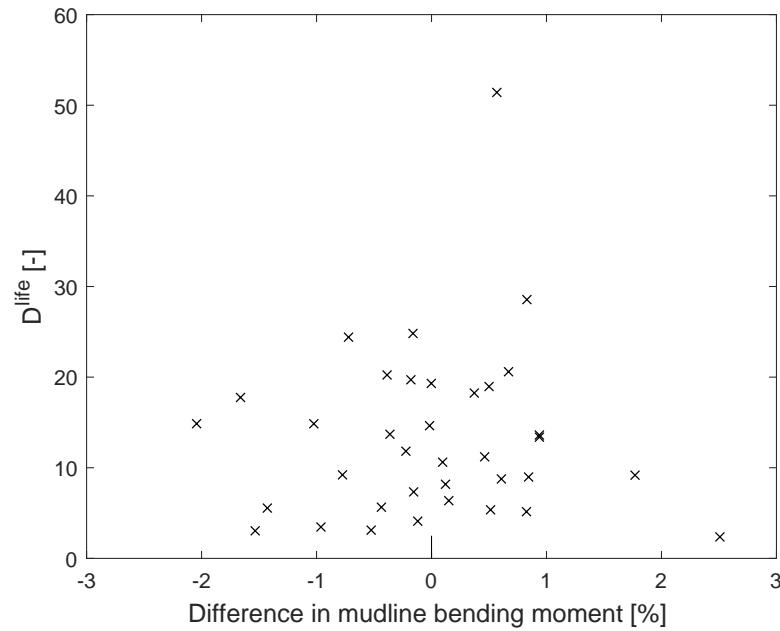


Figure 5.11: Comparison between the influence of the choice of wind seed on the percentage difference from the mean of the bending moment of 36 seeds and associated fatigue damage for LLC17. Structural failure occurs at  $D^{life} = 1$  as denoted by the horizontal red line.

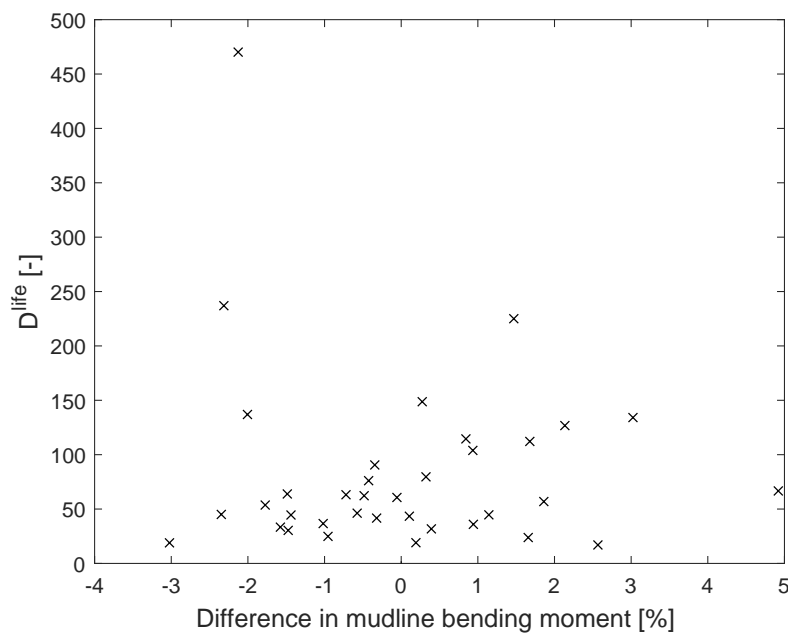


Figure 5.12: Comparison between the influence of the choice of wave seed on the percentage difference from the mean of the bending moment of 36 seeds and associated fatigue damage for LLC17. Structural failure occurs at  $D^{life} = 1$  as denoted by the horizontal red line.

Table 5.5: Computational parameters for investigating simulation length requirements for turbine dynamic response.

Parameter	Simulation parameter					
Transient start-up time [s]	60					
TurbSim simulation length [s]	36000					
HydroDyn simulation length [s]	36000					
Simulation length of each seed set [s]	660	1260	1860	2460	3060	3660
No. of seed sets	60	30	20	15	12	10
Total simulation length [s]	36000					

a variable group of seed-simulation length as shown in Table 5.5.

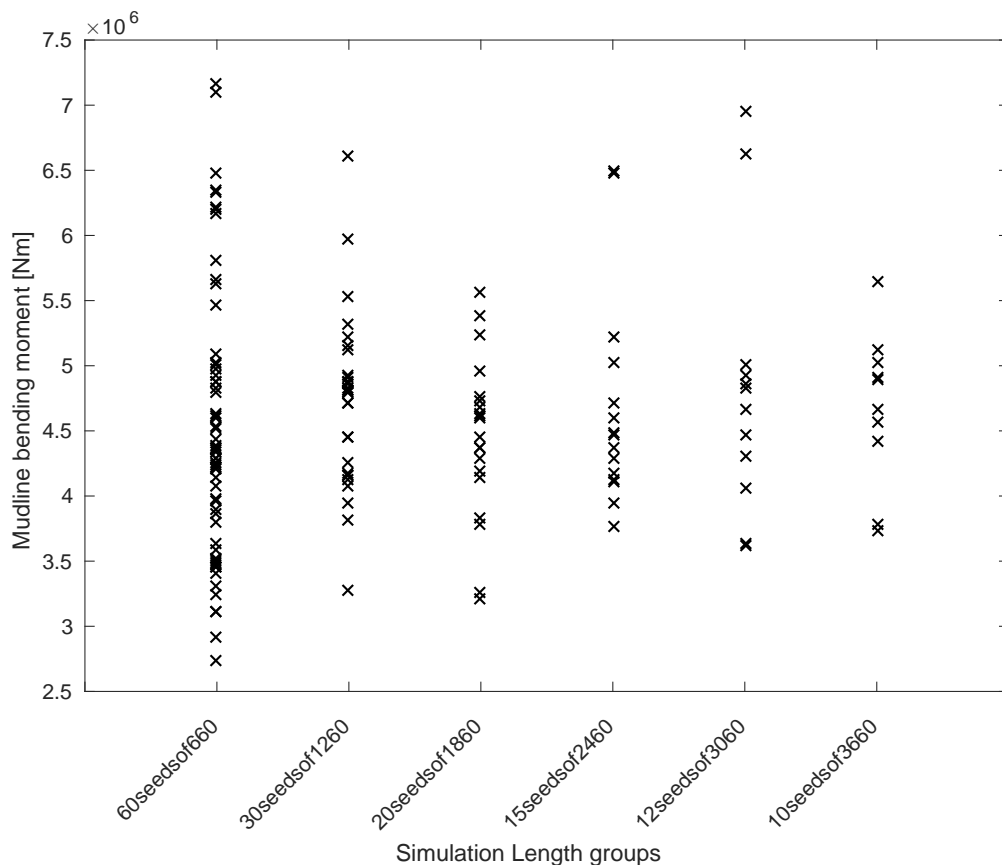
To produce a 10 hour load time history, 10 hour  $H_S$  and  $V_t$  time series are also generated in 60, 30, 20, 15, 12 and 10 sections of 660, 1260, 1860, 2460, 3060 and 3660 seconds, respectively. It is worth reiterating that the initial 60s of the load profile for each simulation are disregarded in the recorded output to remove the influence of the initialisation parameters. The results of the above simulation seed sets are shown in Figure 5.13 for DLC 6.4 and Figure 5.14 for DLC 1.2.

The results indicate that for all 10 hour simulations in each LLC, the resulting mean mudline bending moment is within  $\pm 10^6$ . For the LLCs with higher loads such as LLC07 and LLC14, this contributes to a lower percentage error, however, for LLC01 it could lead to an increase of about 20%. Within each seed-set, the dispersion of the distribution of the seeds shows a generic reduction with increase in simulation length.

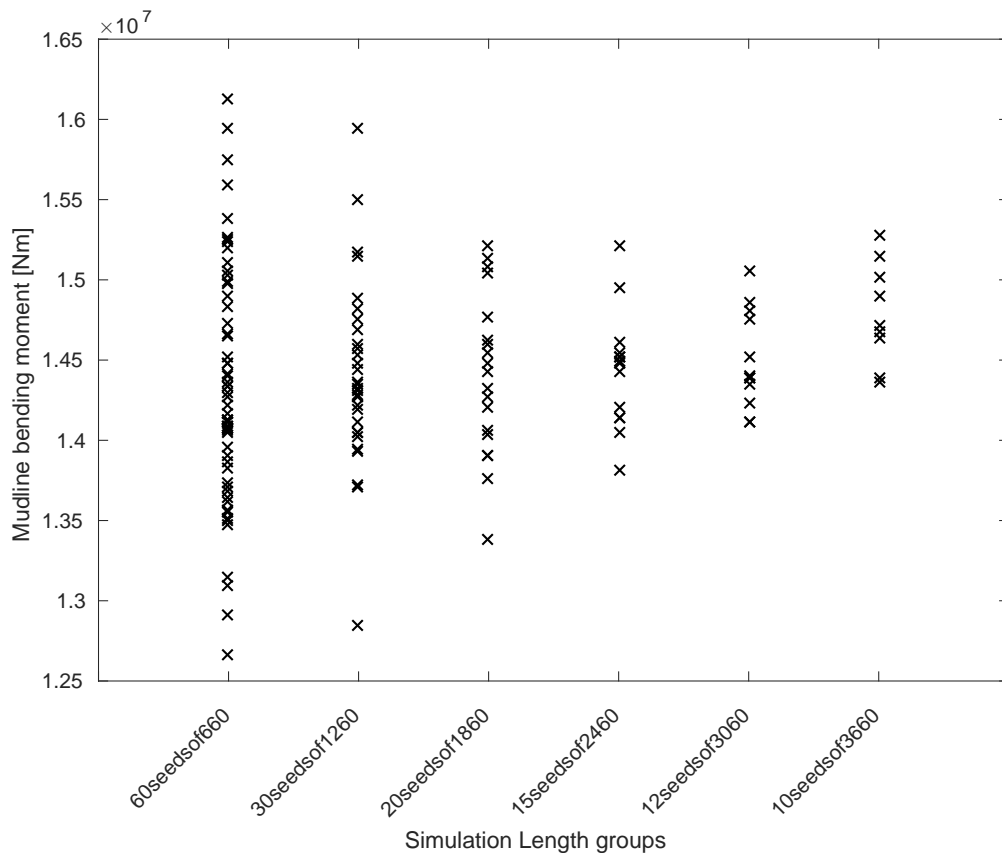
It must be noted that both the TurbSim and HydroDyn modules were enabled and random seeds were generated for both to emulate the variation in results that would result in the realistic simulation conditions. Therefore, the variation in the results also captures the effects arising from the choice of seeds.

### 5.4.3 Damage equivalent loads at the substructure nodes

Using the simulated load profile for damage analysis in MLife, multiple design variables may be adjusted based on the structural and material description. Table



(a)  $V_t < V_{in}$



(b)  $V_{out} < V_t$

Figure 5.13: Simulation length discretisation requirements for the turbine parked state, DLC 6.4, for  $V_t$  below cut-in speed and above cut-out wind speed.



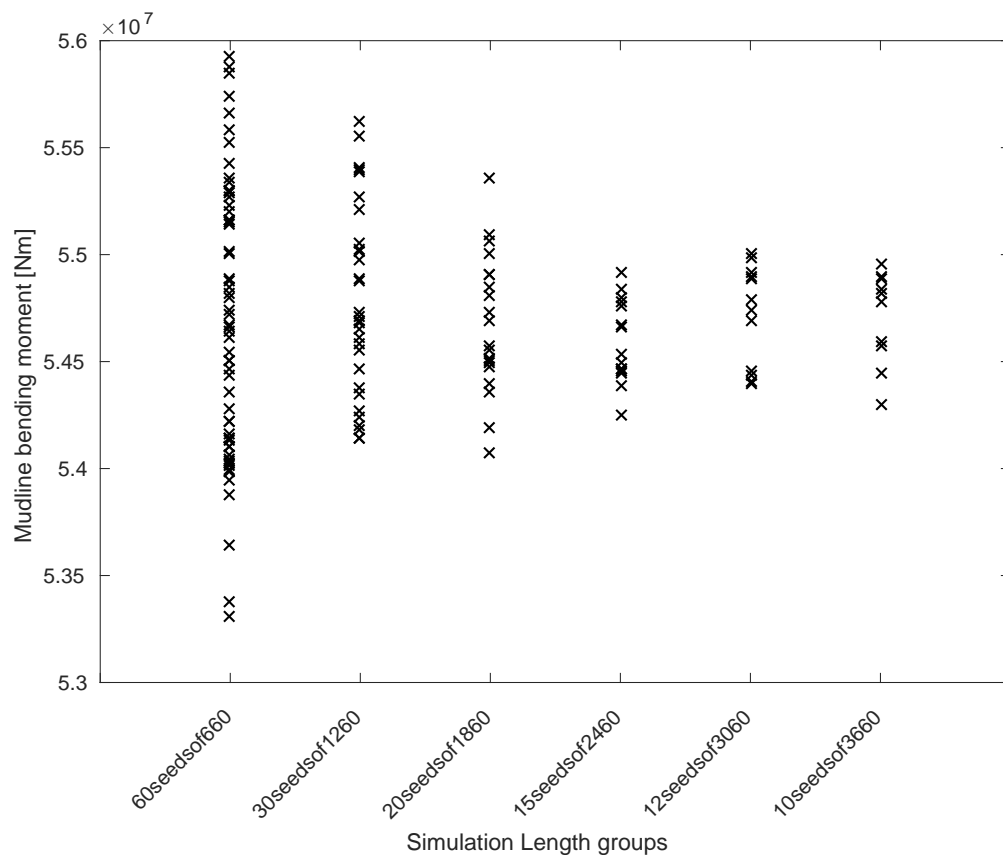


Figure 5.14: Simulation length discretisation requirements for the turbine operational state, DLC 1.2, with  $V_t$  within the operational range.

Table 5.6: Rationale and summarised analysis description for fatigue life sensitivity investigations in MLife.

Parameter	Summary investigation	Rationale
Lifetime load extrapolation distribution	Viability of a user-defined load extrapolation distribution	G. J. Hayman (2012)
Residual cycle counting	Characterise influence of cycle counting method for short simulation data	Stewart et al. (2013), Castro and Oliver (2015), and Marsh et al. (2016)
Goodman correction	Sensitivity of fatigue life to the correction based on the mean load profile	Sutherland (1999) and Marsh et al. (2016)
$L^{Ult}$	Effect of the different methodologies of determining $L^{Ult}$ on accumulated damage	Løken (2009) and G. J. Hayman (2012)
Availability factor	Identify the extent of the influence of operational conditions on fatigue life	G. J. Hayman (2012)

5.6 lists the five parameters investigated in this section and the associated literature recommending these investigations.

#### 5.4.3.1 Lifetime load extrapolation distribution

Using MLife, either the intrinsic Weibull wind distribution or a user-defined distribution based on the frequency of multiple variables can be used for the extrapolation of damage cycle counts to the turbine design lifetime. The occurrence frequency of each sea state depends on the type of probability distribution chosen to define the parameter variability. Loads from both the power production and the parked DLCs are extrapolated for the turbine design life based on the provided distribution.

For both the intrinsic Weibull and user-defined distribution definitions, it is possible to calculate fatigue damage, DELs and unweighted short term damage rates. For the Weibull wind distribution, user-defined wind speed bin width is used to distribute the load time series' solely based on the wind climate. The wind speed bins are then divided into three sections;  $V_0$  to  $V_{in}$ ,  $V_{in}$  to  $V_{out}$  and  $V_{out}$  to  $V_{max}$ , whereby,  $V_{max}$  is the user-defined wind speed maximum determining the upper limit of the final wind speed bin.

For a user-defined distribution, the standard one dimensional Weibull wind

speed generated by MLife is not used for binning the load time series. Instead, up to eight variables may be used to produce a distribution table as input to MLife. For each load time series, MLife accesses the distribution table to extract the associated probability for weighting rainflow count cycles for lifetime fatigue damage calculations. The probability distribution table is stored as a little-endian binary file and is composed of a distribution header and table. The distribution header defines the memory requirements for the floating point variables, distribution name, number of variables with their characteristic number of total bins, bin width and the smallest value of the distribution variable. The table can be a multidimensional matrix specifying the probability density function with a total sum less than or equal to 1.

Since the reduced scatter plot for the K13 site of the UpWind project has one sea state associated to each wind speed bin, the user-defined probability distribution can be simplified to a one dimensional vector with sea state occurrence frequencies associated to the Weibull-fit wind bins chosen from Table 40 in the UpWind report (Fischer et al., 2010) and documented in Table 5.1. To use the latter capability of a Weibull distribution of the wind speed, curve with scale parameter ( $\eta$ ) of 11.85 m/s and shape parameter ( $\beta$ ) of 1.97 is selected to yield the annual mean wind speed of 10.05 m/s (Fischer et al., 2010). For this section of the thesis, a comparison between the user-defined fatigue estimate and Weibull-dependant fatigue estimate is conducted for the K13 shallow water site.

Comparative analysis for an OWT with design lifetime of 20 years is conducted. Unclosed cycles are counted as half-cycles and to reduce computational effort required for the fatigue analysis, the rainflow cycles are not binned. The damage outputs are requested with and without Goodman correction with fixed aggregate mean across all input load time-series calculated intrinsically by MLife.

Figure 5.15 shows that the lifetime damage calculated by both methods produces similar results with an almost negligible higher estimate of lifetime damage by the Weibull distribution. A possible reason for this could be that the sum of the probability distribution frequency of the supplied lumped loads is not equal to one. While isolated the difference is negligible, at a twenty year scale it excludes two days of data. However, the above practice establishes the workability of the user-defined probability distribution frequency for lifetime fatigue calculations. Providing the functionality to allow distribution frequency to account for

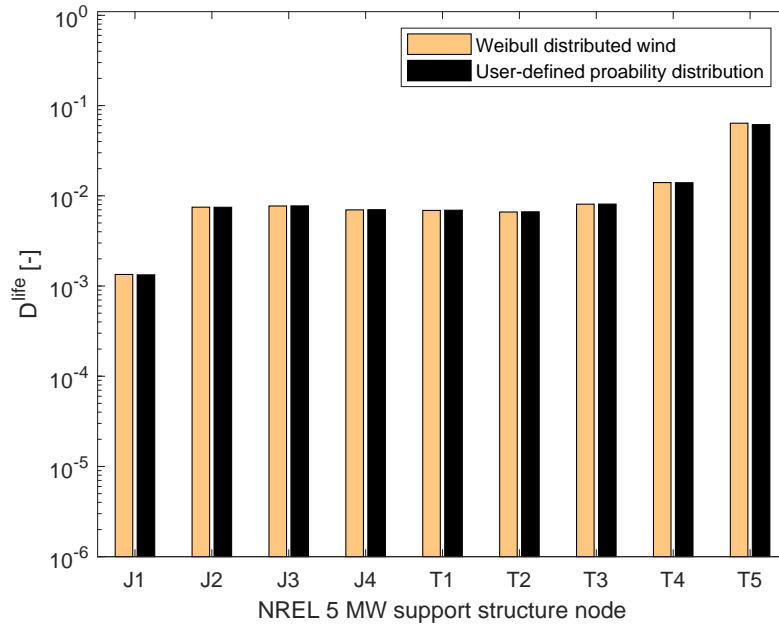


Figure 5.15: Comparison of lifetime damage calculated using a Weibull wind distribution and user-defined distribution with occurrence probabilities as shown in 5.1 at various analysis nodes using the bending moment of the NREL 5MW turbine.

variables in addition to wind gives more flexibility to the user-defined distribution, which is therefore, used for scaling short term loads to lifetime fatigue assessment.

#### 5.4.3.2 Residual cycle counting

MLife uses the one-pass rainflow cycle counting algorithm proposed by Downing and Socie (1982). For short input load time series, it is expected that unclosed cycles may be generated along the length of the timeseries when peaks cannot be matched with equal-amplitude valleys to form a closed hysteresis loop. Since these residual cycles are usually loads with higher amplitudes, therefore, discarding these cycles may overestimate fatigue life for the OWT while counting them as complete cycles may introduce a negative bias in the fatigue life estimate. Therefore, it is industry standard to account for unclosed partial cycles by the half-cycle counting method as recommended by the theory manual (G. J. Hayman, 2012) and existing research (Stewart et al., 2013; Castro and Oliver, 2015).

The sensitivity of the fatigue life to the employed cycle counting approach is investigated. In MLife, counting partial cycles as full cycles attributes a value of 1 to the unclosed cycle count multiplier ( $UCMult$ ), whereas, ignoring the partial cycles uses  $UCMult = 0$ . Figure 5.16 shows the influence of cycle counting on the

damage rate of the NREL 5MW mudline for various LLCs.

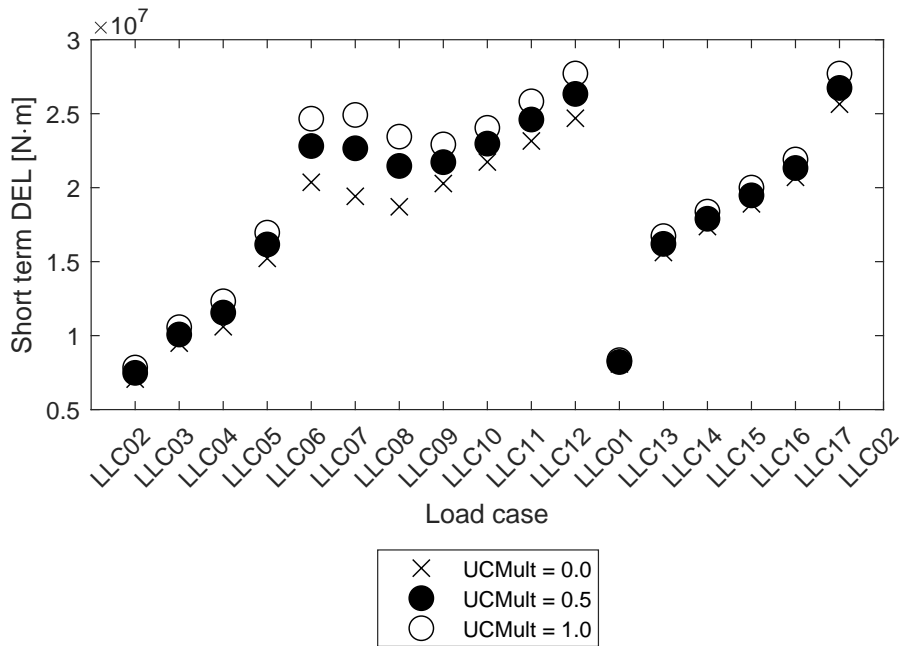


Figure 5.16: Influence of half-cycle counting on the damage rate for various LLCs.

It can be seen that as a general rule, the damage rate is higher when partial cycles are counted as full cycles compared to when their influence of damage is disregarded. Additionally, the influence of partial cycles is much more pronounced in the LLCs with higher fatigue loads particularly within the operational wind speed range of the OWT. As discussed earlier, this is due to the inability of the rainflow counting algorithm to find matching valleys to the recorded peaks to form a closed hysteresis loop. Based on this discussion and existing recommendations, the half cycle counting method is employed to sufficiently capture the influence of these unclosed cycles on fatigue damage for this research.

#### 5.4.3.2.1 Goodman correction

The significance of the Goodman diagram for structural engineering is discussed along with the correction theory applied in MLife in Chapter 4. MLife provides a range of correction methods for load ranges to be employed including correction based on the weighted channel mean, aggregate channel mean as well as user specified value. Short-term DELs for individual LLCs and accumulated lifetime damage are compared at the various OWT analysis nodes using the fixed aggregate channel mean over 17 LLCs to perform the correction. A comparison between the LLCs for the UpWind project using the short term DELs based on the bending

moment is shown in Figure 5.17 as the difference between the short-term DELs with no correction and the Goodman corrected short-term DELs as calculated in Equation. 5.7.

$$DEL_{diff}^{ST} = DEL_{GM}^{ST} - DEL_{NoGM}^{ST} \quad (5.7)$$

Where,  $DEL_{diff}^{ST}$  is the difference in short term DELs for uncorrected ( $DEL_{NoGM}^{ST}$ ) and Goodman corrected DELs ( $DEL_{GM}^{ST}$ ) for DEL estimates based on extrapolated bending moments. For Figure 5.17, data points above the zero level correspond to

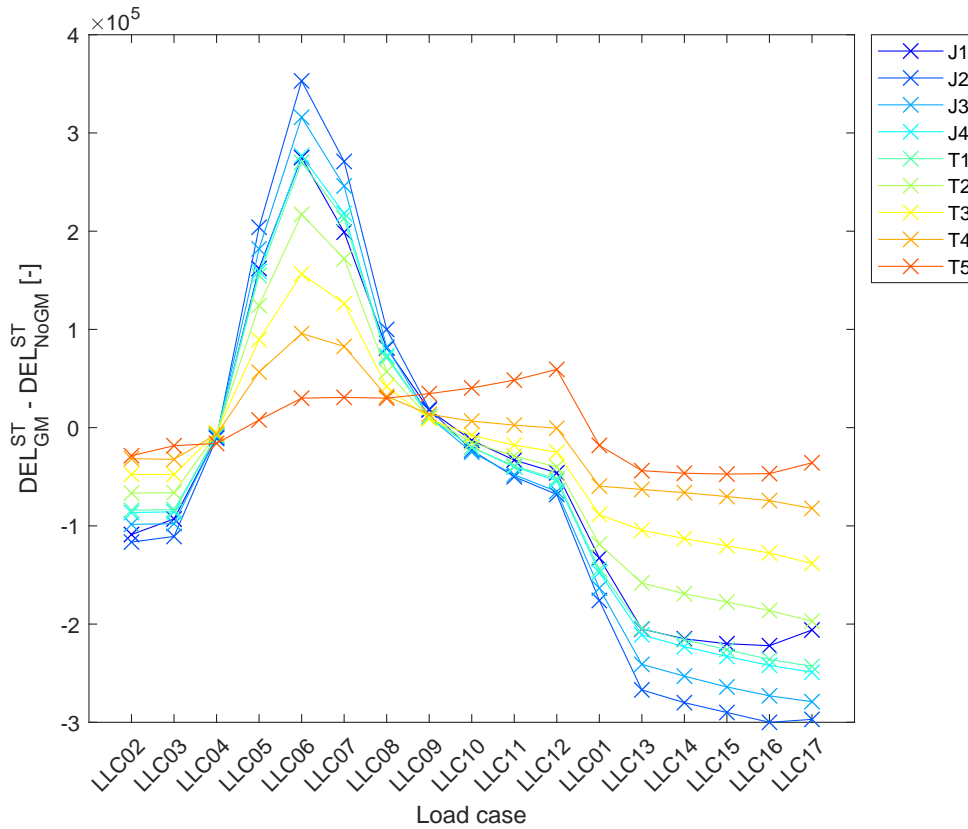


Figure 5.17: Influence of Goodman correction on damage equivalent loads for the short-term ten minute FAST simulations at the analysis nodes.

a lower short-term DEL before the Goodman correction and data points below the level indicate an increase in short-term DELs after application of the correction. It can be observed that the support structure shows the most sensitivity to the Goodman correction at the mudline and the sensitivity of the short-term DELs due to the application of the correction decreases as the height of the analysis nodes from the mudline increases. Similarly, a larger difference between the corrected and uncorrected loads exists for LLCs with higher average loads such as the rated wind speed at LLC06 and LLC17. Shortly, for load cases and turbine subassemblies

with higher loads, short term DELs fluctuate considerably due to the application of the Goodman correction.

Within the operational wind speeds, the short term DELs show a negative bias without the correction, whereas, for parked conditions, the short-term DELs are overestimated without the correction. A possible explanation for this could be the use of the aggregate mean across all LLCs for the correction since an aggregate mean incorporates influences from all load regimes, therefore, having a modulating effect on all LLCs. This effect may be thought of as introducing a new benchmark for the damage to be measured against; for LLCs with higher loads than the benchmark a decrease in DELs is anticipated, whereas, for LLCs with loads below the benchmark, an increase in DELs is anticipated.

Whilst the above analysis only considered the dependence of short-term DELs based on bending moment time-series, Figure 5.18 displays the analysis results incorporating all LLCs for the percentage difference in lifetime damage based on force and bending moment simulations adapting Equation. 5.7 to Equation. 5.8 for accumulated lifetime damage.

$$DEL_{diff}^{life} = \frac{DEL_{GM}^{life} - DEL_{NoGM}^{life}}{DEL_{NoGM}^{life}} \quad (5.8)$$

Where,  $DEL_{diff}^{life}$  is the relative difference in lifetime DELs for uncorrected lifetime DELs ( $DEL_{NoGM}^{life}$ ) and Goodman corrected lifetime DELs ( $DEL_{GM}^{life}$ ). It can be seen that the influence of the Goodman correction on the lifetime damage estimate by shear forces is lower than the estimate using the bending moments particularly for the mudline and tower top node. The application of the correction has the highest impact on lifetime damage estimates at the tower top. At the other end of the spectrum, the lifetime damage is expected to display a lower variability for the nodes in the tower based on whether the correction is applied or not.

#### **5.4.3.2.2 $L^{Ult}$ methodology**

Using the outputs from the FAST simulations at various support structure analysis nodes, an investigation into the dominant loads is conducted. A Weibull distribution is used to scale fatigue loads from the 10-minute time series to the design lifetime of 20 years with the Wöhler exponent of 4. The results are corrected using the Goodman fit at the aggregate mean of the FAST simulation output across all

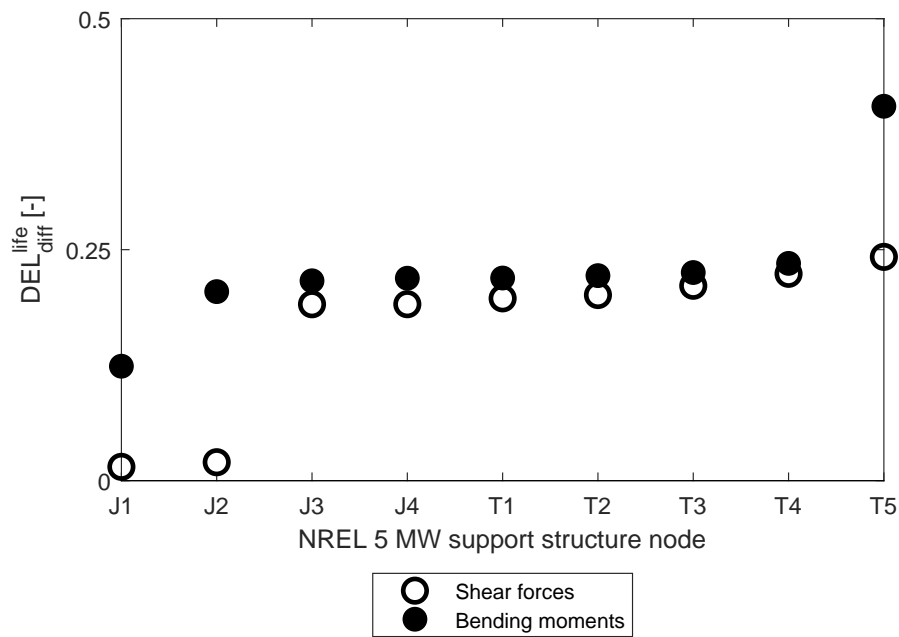


Figure 5.18: Influence of Goodman correction on lifetime damage equivalent loads at the analysis modes.

17 LLCs.  $L^{Ult}$  estimates using an extreme event analysis are used to determine the material strength. The results for the comparative fatigue life at the various nodes using bending moment and shear force time-series are shown in Figure 5.19.

Based on the Miner's rule of linear damage accumulation, a cumulative lifetime damage of 1 indicates subassembly failure during design lifetime. For the individual analysis nodes, it can be seen that the lifetime damage varies based on the type of FAST output channel considered, namely, force or bending moment. In the real life scenario the accumulated damage will be a combination of both. Although the chart displays a variability of lifetime damage estimates between analysis nodes, this comparison between analysis nodes does not conform to the theoretical shear and moment experienced by an idealised cantilever beam. The variance in the environmental parameters is stronger than the variation in the model.

A material can withstand a maximum stress before failure, namely the ultimate strength. Therefore, engineers introduce a safety factor to ensure that during its service lifetime, the material is only stressed to a fraction of its ultimate strength. Once exposed to stress beyond the ultimate strength, the material is expected to experience sudden failure. As described in Chapter 4, the ultimate load at a structural subassembly may be determined by an analytical approach or using an arbitrary multiplicative factor to extrapolate the maximum loads that the structure



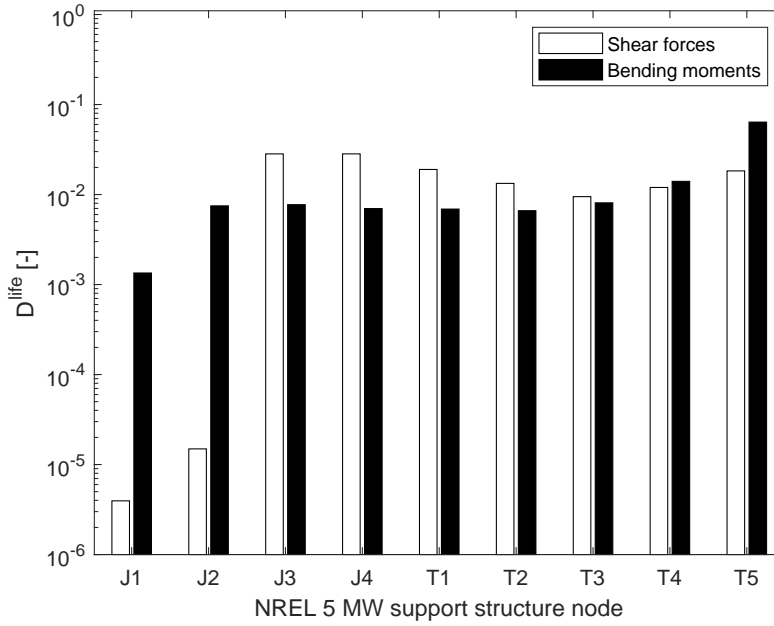


Figure 5.19: Comparison of the lifetime damage accumulated due to the shear forces and the bending moments at various analysis nodes of the NREL 5-MW wind turbine using a Weibull distribution with  $\beta = 1.97$ ,  $\eta = 11.85$  and mean wind speed of 10.5 m/s. Structure fails at  $D^{life} = 1$ .

withstands onshore and/or offshore from available simulation results. The two proposed methods for determining  $L^{Ult}$  are compared in this section.

An analysis of the extreme loads on the substructural components from 13340 simulations conducted for the look-up table in Chapter 7 provides a value of 498.6 MNm for  $L^{max}$  of the bending moment at node 1 of member 1 of the substructure of the 5 MW NREL baseline turbine. Therefore,  $L^{Ult}$  can be calculated using:

$$L^{Ult} = L^{max} \times ULF$$

$$\therefore L^{Ult} = 498\text{MNm} \times ULF,$$

$$\text{where, } ULF = 1.25, 2.5, 5, 10, 20$$

The extracted  $L^{max}$  values for the various subassemblies are recorded in Table 5.7. For the analytical description prescribed in existing literature (Løken, 2009), the flexure stress formulation in Equation. 4.12 and the maximum shear stress calculated from the Timoshenko derivation in Equation. 4.14 are used in conjunction with the geometric configuration of the support structure and  $L^{max}$  at the analysis node documented in Table 5.7. Consequent results for the damage life of the various nodes are plotted in Figure 5.20. The damage life is seen to be limited by bending moments at all analysis nodes, with the tower displaying larger

Table 5.7: Material properties of the tower and substructure analysis nodes used as MLife input.

Analysis node	Load type *	$L^{max}$ ( $10^6$ )	$L^{Ult}$ ( $10^6$ )	ULF
J1	F	40.50	405.0	10
	M	498.60	4986.0	
J2	F	28.72	287.2	
	M	294.00	2940.0	
J3	F	2.94	29.4	
	M	253.90	2539.0	
J4	F	2.94	29.4	
	M	224.85	2248.5	
T1	F	2.94	29.4	
	M	219.35	2193.5	
T2	F	2.94	29.4	
	M	174.59	1745.9	
T3	F	2.87	28.7	
	M	118.83	1188.3	
T4	F	2.72	27.2	
	M	64.82	648.2	
T5	F	2.51	25.1	
	M	15.34	153.4	

\* F = Shear force loads, M = Bending moment loads

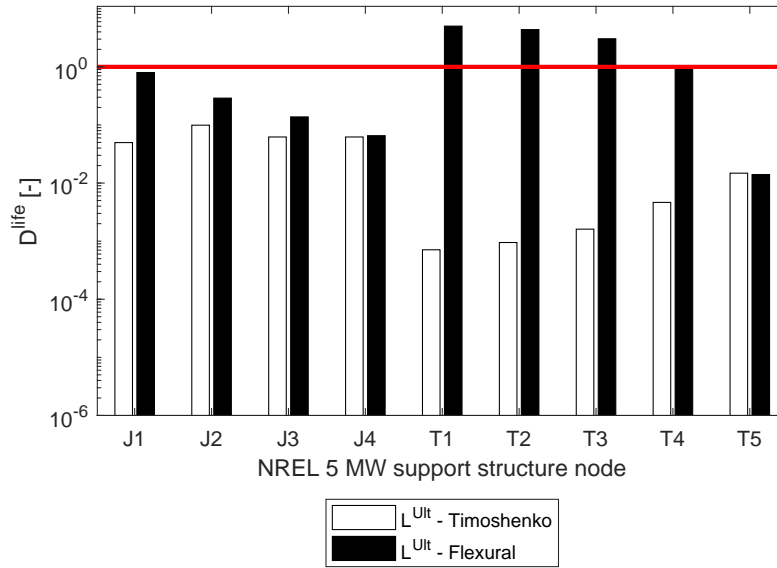


Figure 5.20: Damage life calculated using analytical  $L^{Ult}$  for bending moment and shear stress. Structural failure occurs at  $D^{life} = 1$  as denoted by the horizontal red line.

bending stresses than the substructure. Figure 5.20 suggests that the substructure experiences higher shear stresses than the tower and shear stresses on the tower increase with height. This trend, again, is absent in Figure 5.19 but validates the theoretical framework of wave loads inducing larger stresses than wind loads and increasing stress at the analysis nodes with increase in height due to shear effects.

Comparison of the damage life estimates using normal stress with  $L^{Ult}$  values based on the analytical approach and arbitrary multiplicative factors (ULF) for each analysis node are plotted in Figure 5.21. The damage life estimates using the flexural formula are in strong contrast with those calculated using the arbitrary multiplicative factor of 10 for  $L^{max}$ . However, they show a general agreement with the loads analysis at various LLCs: nodes with higher bending moment experience higher normal stress par when the geometric variations are introduced as in the case of the tower.

Finally, to determine whether the recommendation (Matha et al., 2010) of the application of onshore loads by Jason Jonkman (2007) to offshore turbines provides an accurate representation of the ultimate loads, a comparative study between the two is performed. For fatigue failures associated to the overturning moment at the mudline in the baseline turbine, comparative accumulated lifetime damage

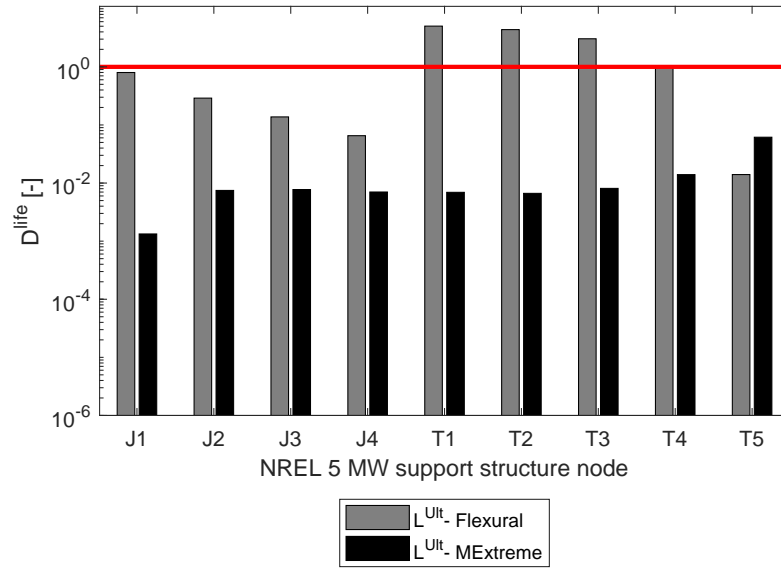


Figure 5.21: Damage life of an NREL 5MW OWT at the K13 shallow water site based on the analytical and simulated  $L^{Ult}$  values. Structural failure occurs at  $D^{life} = 1$  as denoted by the horizontal red line.

between the two  $L^{max}$  sources for a range of ULF values is shown in Figure 5.22. While the selection of the source for  $L^{max}$  is seen to have an effect on the lifetime damage, it is not the only source of variation in results. This is displayed by the large influence of the choice of ULF on the fatigue life estimates, with the highest ULF value leading to a decrease in accumulated damage up to the order of  $10^7$ .

### 5.4.3.3 Availability factor

Based on early experience at the Round I offshore wind sites over a three year period, a range of system availability is observed with a minimum of 67.4% at Barrow and maximum of at 87.7% for North Hoyle (Feng et al., 2010). Both the extremes of the availability lie in the same regional belt of the Irish Sea. Using the system availability to characterise the NREL 5 MW turbine, this subsection discusses the contribution of this key performance indicator on the lifetime damage.

Based on Equation. 2.2, 100% turbine production-based availability is assumed, that is, for all wind speed bins within the operational  $V_t$  range, the turbine is generating electricity. This allows the damage estimates to fully account for all states the OWT experiences during its lifetime simulated by FAST and represented by DLCs identified earlier in this chapter. MLife weighs the availability

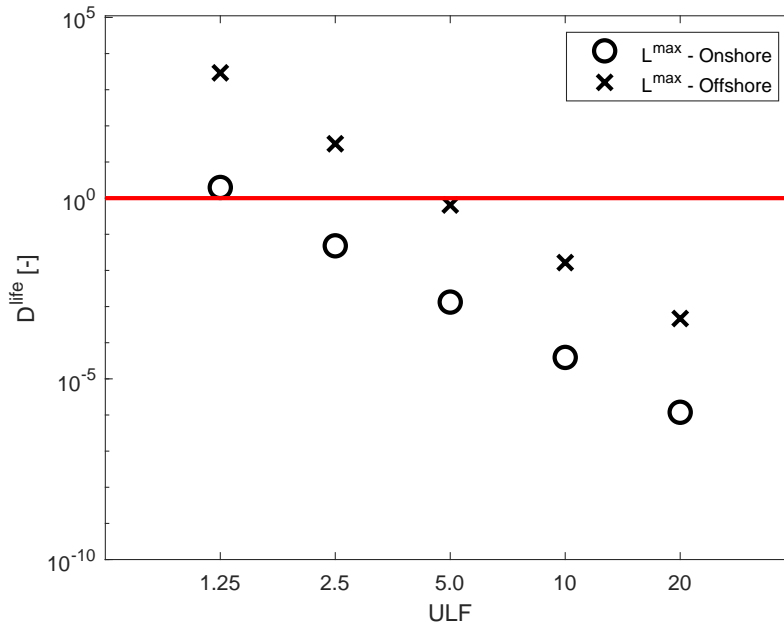


Figure 5.22: Damage life of NREL 5MW OWT based on overturning moment at the mudline based on the  $L^{Ult}$  values generated by the  $L^{max}$  for onshore and offshore locations. Structural failure occurs at  $D^{life} = 1$  as denoted by the horizontal red line.

using Equation. 5.4 to determine the extrapolation of loads to the design lifetime of the OWT. Using a range of availability between 60% to an ideal availability of 100%, damage estimates are produced for the NREL 5 MW OWT and displayed in Figure 5.23. The accumulated lifetime damage for an OWT displaying the average availability from early experiences in offshore wind energy in the UK (Feng et al., 2010) is highlighted in black.

It can be observed that for each iteration with increasing availability, the lifetime damage displays a linear increase. For an ideal wind turbine always in the power production state, the lifetime damage can be said to be twice as much as a turbine with half the availability.

## 5.5 Suitable parameters for spatial reliability distribution

The support structure at the mudline is identified as the critical component to be used as a representative subassembly for developing the mapping methodology

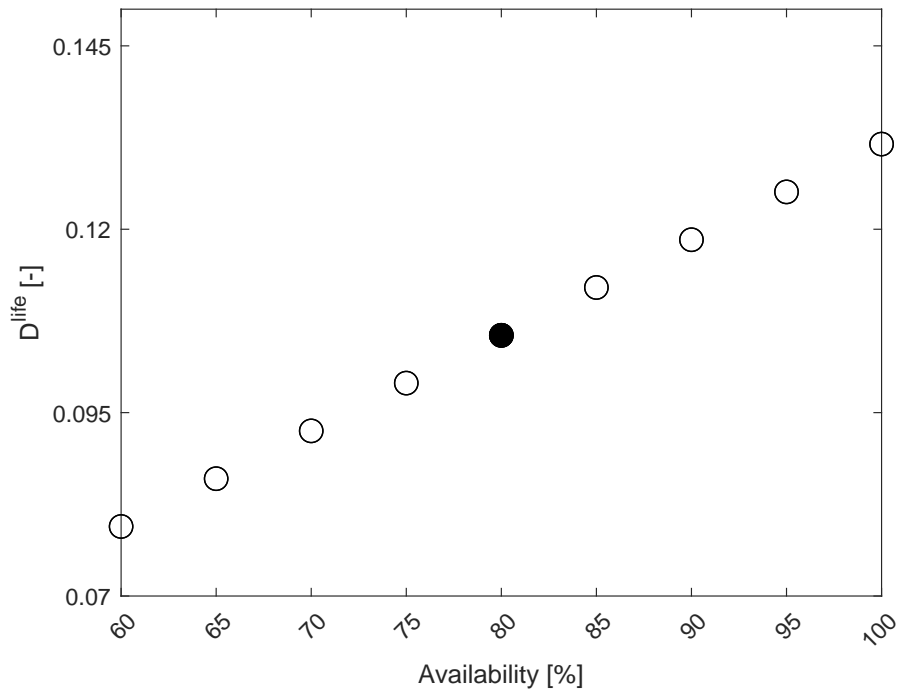


Figure 5.23: Damage life of an NREL 5MW OWT at the K13 shallow water site based on the availability of the turbine.

for reliability indicators. At the mudline, the support structure has to provide resistance to the large horizontal loads applied at an arm of up to 90 m causing high bending moments. Furthermore, the structural integrity and the stability of the support structure has a large bearing upon system safety (Aasen et al., 2017).

The structure experiences small vertical loads relative to the horizontal shear loads and bending moments (Byrne and Houlsby, 2003), therefore, only horizontal loads will be considered for further studies.

Additionally, based on the sensitivity analysis conducted in this chapter, parameters described in Table 5.8 will be used for the spatial reliability distribution analysis.

## 5.6 Chapter summary

This chapter applies the Stream 2 methodology to an OWT deployed at the K13 shallow water site in the Dutch North Sea. Figure 5.24 summarises the analyses undertaken in this chapter.

At the outset, the support structure of the OWT is chosen as an illustrative assembly based on the sensitivity of turbine manufacturing cost to the said assembly. The Stream 2 methodology is applied to various nodes in the support structure

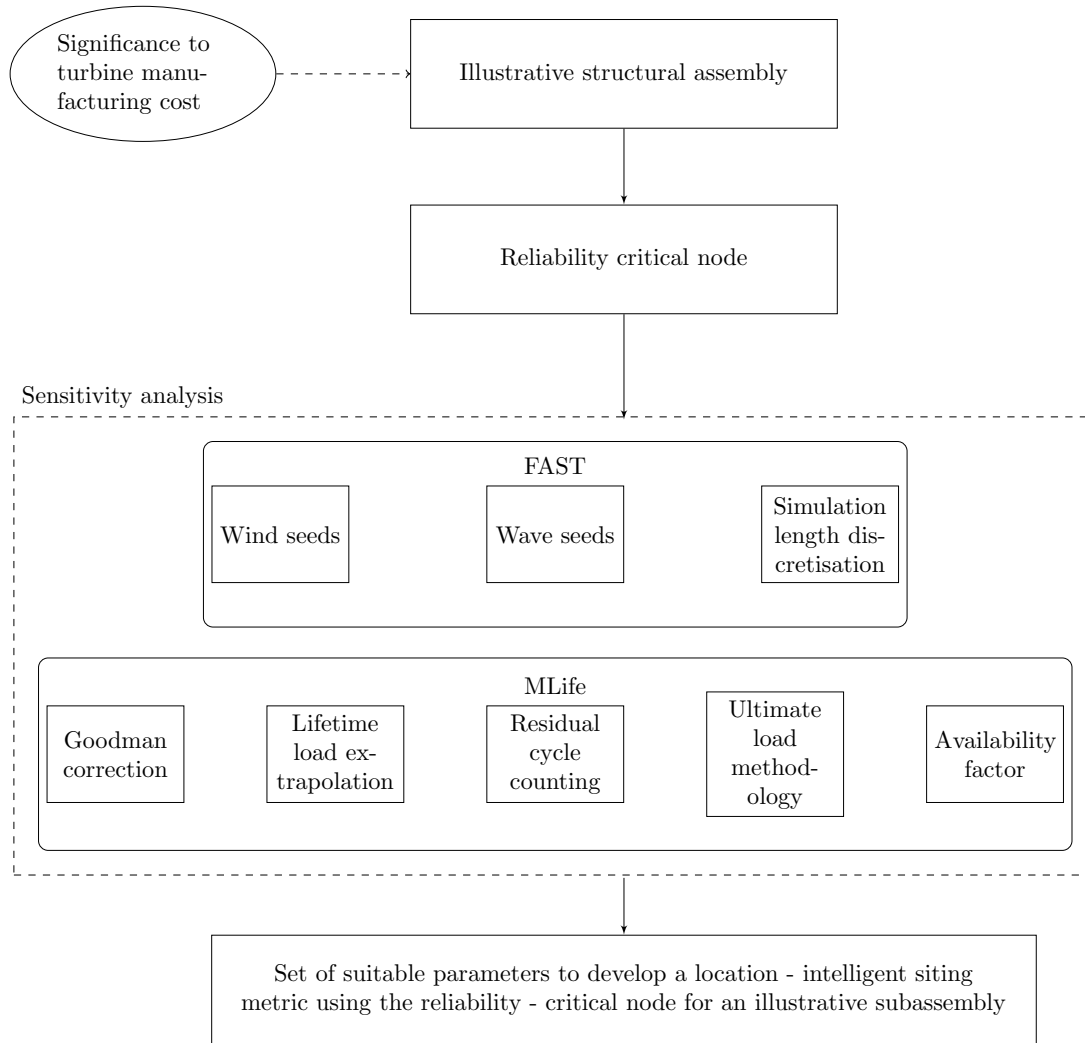


Figure 5.24: Flowchart summarising the analyses conducted for selection of the reliability-critical node in the illustrative assembly and a suitable set of physical, numerical and material parameters to develop the methodology for improved quantification and visualisation of OWT deployment sites.

Table 5.8: Suitable values of the parameters used for determining spatial reliability distribution for the NREL 5 MW turbine based on loads at the mudline of the substructure.

Parameter	Value
No. of wind seeds	One wind seed
No. of wave seeds	One wave seed
Simulation length discretisation	660s truncated at the beginning by 60 s to eliminate transient effects
Lifetime load extrapolation distribution	User-defined frequency distribution for modelled $H_s$ , $T_p$ and $V_t$ data
Residual cycle counting	Half-cycle counting method
Goodman correction	Damage estimate based on the weighted mean of each time series
$L^{Ult}$	$L^{max} \times ULF$ using offshore estimates
Availability factor	A = 1

to identify the reliability-critical node using the two most significant load cases for the fatigue limit state analysis and suitable FAST initialisation parameters. Based on the shear force, bending moment and short - term DELs at all LLCs, the mudline is determined as the reliability-critical node for the support structure. Uncertainties introduced in the modelled results due to the possible adoption of a range of physical, numerical and material characteristics lead to the requirement of a sensitivity analysis which facilitates the determination of a suitable set of parameters to be used for the spatial analysis. A set of suitable parameters is then chosen to deliver a robust location-intelligent siting metric whilst reducing the computational effort required to implement the method.





## Part III

# Site-specific Performance

## Indicators



# Chapter 6

## Sub-regional Characterisation for OWE Deployment

Assessment and improvement of the intrinsic reliability is significant to establish that wind farms installed at different offshore locations will be cost effective. Therefore, site characterisation is not only vital to determine the resource, but also to gauge possible influences on reliability.

Exposed to variable environmental conditions, LCOE reduction of OWTs garners interest from utility owners. To this end, site characterisation tools with the capability to inform maintenance strategies and estimate remaining lifetime could provide useful information for lifetime extension decisions. This chapter aims to apply the fatigue life calculation of the support structure using site-specific environmental conditions at the various sub-regions in the UKCS and adjoining areas to provide a spatial assessment of reliability metrics. To achieve this aim, three main objectives are set out:

- Simulating relevant structural response characteristics post-processed for fatigue life estimation and recorded in a look-up table;
- Extracting suitable fatigue life estimates from the look-up table based on site-specific environmental conditions to compare various sub-regions in the UKCS;
- Presenting the argument for a performance metric based on metocean parameters.

To fulfill the first objective, the structural response of the OWT is simulated for

a range of environmental conditions likely to be experienced in the UKCS. Then an extreme event analysis is conducted by post-processing the FAST simulation outputs to identify the maximum loads experienced at the mudline of the OWT substructure to inform the material strength for determination of fatigue life. The computed material strength is used to generate a look-up table for fatigue assessment displaying the damage for each set of metocean conditions. The table is then extended by the associated energy production for a turbine exposed to the respective set of environmental conditions.

For the second objective, fatigue lifetime analysis is conducted for the same 5 MW NREL turbine deployed at various sub-regions in the UKCS to identify whether a correlation between sites and structural reliability exists.

Lastly, a metocean-centric site characterisation metric is produced based on reliability and energy production for the analysis data points in the sub-regions. A basic cost analysis of a 500 MW wind farm at grid points in each sub-region is conducted to provide an estimate of site-dependent cost of energy.

### 6.1 Look-up table approach

A look-up table consists of an array of input data mapped to useful output values that enable swift execution of a process. For fatigue damage data, look-up tables can facilitate computationally inexpensive data accessibility to expedite the cumulative damage calculation process. Preliminary research (Hart et al., 2016) indicates the potential of a look-up table approach for wind turbine fatigue loading for reliability calculations using a range of field measurements of wind.

The benefits of increased instrumentation of an OWT to capture an increased volume of data pertaining to operation and environment are offset by the increase in investment required to install the devices. Computational tools provide a potential for the estimation of significant operational parameters such as structural fatigue with little to no increase in individual project costs. However, the outputs from the aero-hydro-servo-elastodynamic tools are highly specific to the design, size, rating and age of turbine. To fully account for all these variables, a large number of load cases tailored for each class of turbines must be conducted.

There is a range of outcomes that may be presented in the look-up table. As suggested (Hart et al., 2016), this includes fatigue life predictions by computationally-

intensive FEA analysis to provide a more definitive result or the DELs which may be cumulatively totalled to indicate lifetime estimates. Conducting a structural analysis using additional variables such as material strength leads to an increase in the associated uncertainty. For the scope of this project, the damage estimates are calculated in terms of the short-term damage rate which can be then used in conjunction with site-specific metocean data and probability occurrence to calculate lifetime DELs and post-processed using material properties in a structural analysis tool to estimate the fatigue life.

### 6.1.1 Load cases

For this work, the NREL 5 MW fixed base turbine is considered and the definition of failure is limited to the fatigue limited state, thereby, failure in a structure is anticipated when the accumulated damage reaches the damage equivalent of  $D^{life} = 1$ .

The developed look-up table in this thesis incorporates effects of DLC1.2 Normal operation and DLC6.4 Parked/ Idling turbine since they have a reduced dependence on the controller (Castro and Oliver, 2015). Multiple additional DLCs including transient events and fault conditions are also significant for fatigue life calculation, however, current practices in OWE do not allow for accurate prediction and simulation of fault conditions (Kusiak and Li, 2011; Simani, 2015). Once suitable fatigue damage estimates are available for the fault conditions along with their associated occurrence frequency, they should also be readily appended to this table for inclusion in the structural analysis.

### 6.1.2 Environmental parameters

While the table aims to provide a comprehensive coverage of possible sea states, incorporating all possible sea states is a computationally expensive task, therefore, aero-elastic-hydro simulations are run for bins of metocean parameters. This reduces the number of total simulations required whilst incorporating the influence of metocean variability of structural loads for effective fatigue life analysis. The industrial standard for the binning of environmental parameters dictates that demarkations for  $V_t$ ,  $H_s$  and  $T_p$ , be at intervals of 2 m/s, 0.5 m and 0.5 s respectively (Bierbooms, 1994). This standard approach is followed for  $H_s$  and  $V_t$ , however,

Table 6.1: Characteristics of the binning parameters of the look-up table data.

Parameter Name	Symbol	Units	Parameter Range	Bin Width	# of Bins
Wind speed	$V_t$	[m/s]	$0 \leq V_t < 40$	2	20
Significant wave height	$H_s$	[m]	$0 \leq H_s < 14.5$	0.5	29
Peak period	$T_p$	[s]	$0 \leq T_p < 23$	1	23

the bin width for  $T_p$  is increased to 1 s. The simulated loads are taken to be representative of all metocean input parameters in the corresponding bin.

FAST simulations for wind speeds between 0 - 40 m/s with bin width of 2 m/s at midpoints of each bin are run. For each wind speed bin,  $H_s$  ranges between 0 - 14.5 m with a binwidth of 0.5 m and the input  $H_s$  parameter in FAST is at the midpoint of the bin. Finally for each wave height bin within the wind speed bin,  $T_p$  ranges between 0 - 23 s with a bin width of 1 s and FAST inputs are at the middle of each bin. As an example, for a sea state characterised by  $V_t = 22.5$  m/s,  $H_s = 5.1$  m and  $T_p = 9.3$  s, data from the table with  $V_t = 23$  m/s,  $H_s = 5.25$  m and  $T_p = 9.5$  s is used. Regarding the number of simulations performed, for each wave height bin in a particular wind speed bin, 23 simulations were performed. Each wind speed bin is composed of 29 wave bins, therefore a total of 667 simulations were performed per wind bin. The Gallos high performance cluster with 256 CPU cores, 1024GB RAM and 3TB storage giving a performance rating of 2.5 teraflops is used to run a cumulative total of 13340 ten-minute FAST simulations to produce the look up matrix. Table 6.1 provides details of the range, bin width and number of bins for the simulations conducted to produce the look-up Table

Since wind speed varies with height, a general industrial standard is to adjust data to represent the wind flow at 10 metres above MSL or effective ground level. In order to facilitate the use of the look-up table for various databases, all wind speed inputs to the TurbSim model are at 10 m above MSL, the model then uses a diabatic logarithmic profile to scale the wind along the 160 m grid height to produce the wind field used for calculating wind-induced loads on the OWT. In this research, aligned unidirectional wind and wave loading is considered to produce the matrix. Since the environmental loads are aligned with each other,

this produces the most extreme scenario for the loads outside of the operational  $V_t$  range with the most conservative fatigue life estimate.

### 6.1.3 $L^{Ult}$ analysis

As discussed in Chapter 2 and expanded in Chapter 4, for fatigue life estimation of an OWT deployed at various sites around the UK, it is important to have an estimate of the extreme bending moments and shear forces experienced by the structure. To this purpose, the NREL post-processing software MExtremes (G. Hayman, 2015) is used to establish the maximum and minimum values for relevant loads. Table 6.2 tabulates the resulting extreme loads for the bending moment and shear force at the mudline of the NREL 5 MW OWT. The combined loads are calculated as the vector sum of the roll and pitch for bending moment and the surge and sway for the shear forces. Similar tables are generated for all investigated nodes to identify suitable  $L^{Ult}$  estimates for individual nodes.

The loads at the mudline are dominated by the fore-aft forcings and pitching moment due to the use of the unidirectional incident wind and waves. It is observed that the extrema extracted by MExtremes are predominantly experienced during parked/idling conditions. These load cases are either characterised by high wind speeds outside the operational  $V_t$  range of the OWT, large waves and/or wind and wave frequencies close to the natural frequency of the structure.

Also, it can be seen that in agreement with the outputs of Chapter 5, the maximum combined bending moment is almost ten times larger than the combined shear force. Therefore,  $L^{Ult}$  is determined as the maximum combined bending moment and is used in conjunction with the ULF, Wöhlers exponent and the FAST simulation output to estimate the damage rate at the mudline of the 5 MW baseline OWT exposed to various environmental conditions.



Category	Parameter	Type	Shear force			Bending moment			Combined Loads			Other parameters		
			Fore-aft [MN]	Side-to-side [MN]	Roll [MN.m]	Pitch [MNm]	Shear forces [MN]	Bending moment [MN.m]	Wind [m/s]	Wave ele- vation [m]	$T_p$ [s]	GenPwr [MW]		
Shear force	Fore-aft	Minimum	-43.56	0.01	-1.36	-501.30	43.56	501.30	2.51	-40.44	22.50	0		
		Maximum	9.98	-0.003	4.35	212.40	9.98	212.44	11.44	-6.63	5.50	5.03		
	Side-to-side	Minimum	-0.20	-0.79	64.79	50.73	0.82	82.29	64.90	0.59	3.50	0		
		Maximum	0.27	0.90	-73.00	25.50	0.94	77.33	54.10	-0.41	22.50	0		
Bending moment	Roll	Minimum	0.88	0.74	-73.41	70.70	1.15	101.92	66.25	0.37	5.50	0		
		Maximum	0.23	-0.69	71.49	43.42	0.73	83.64	66.00	0.46	5.50	0		
	Pitch	Minimum	-43.56	0.01	-1.36	-501.30	43.56	501.30	2.51	-40.44	22.50	0		
		Maximum	9.12	0.02	-1.28	334.10	9.12	334.10	1.27	0.91	3.50	0		
Combined loads	Shear forces	Minimum	-0.000002	-0.000002	-0.04	-1.89	0.000003	1.89	1.34	0.005	1.50	0		
		Maximum	-43.56	0.01	-1.36	-501.30	43.56	501.30	2.51	40.44	22.50	0		
	Bending moment	Minimum	0.05	0.0004	-0.0009	-0.0001	0.05	0.0009	0.95	0.28	1.50	0		
		Maximum	-43.56	0.01	-1.36	-501.30	43.56	501.30	2.51	-40.44	22.50	0		

Table 6.2: Load cases with the largest structural response at the mudline from the 13340 simulations with associated environmental parameters and power output appended. The highlighted cells correspond to the maximum and minimum values for the bending moments and shear forces at the mudline of an NREL 5 MW monopile in the fore-aft and side-to-side directions as well as the combined loads in the two directions.

### 6.1.4 Sample outputs from look-up table

Mlife is used to calculate basic statistical parameters, such as minimum value, mean, maximum value, standard deviation, skewness, kurtosis, range and associated damage rate of each FAST simulation for a Wöhler exponent of  $m = 4$ ,  $ULF$  of ten using Goodman correction based on the weighted mean of each time series input.

The combined bending moment at the mudline is used to calculate the damage rate for the OWT at the mudline. For the range of considered  $H_s$  and  $T_p$  parameters for the  $V_t$  bin at 11 m/s, the bending moment is represented in Figure 6.1.

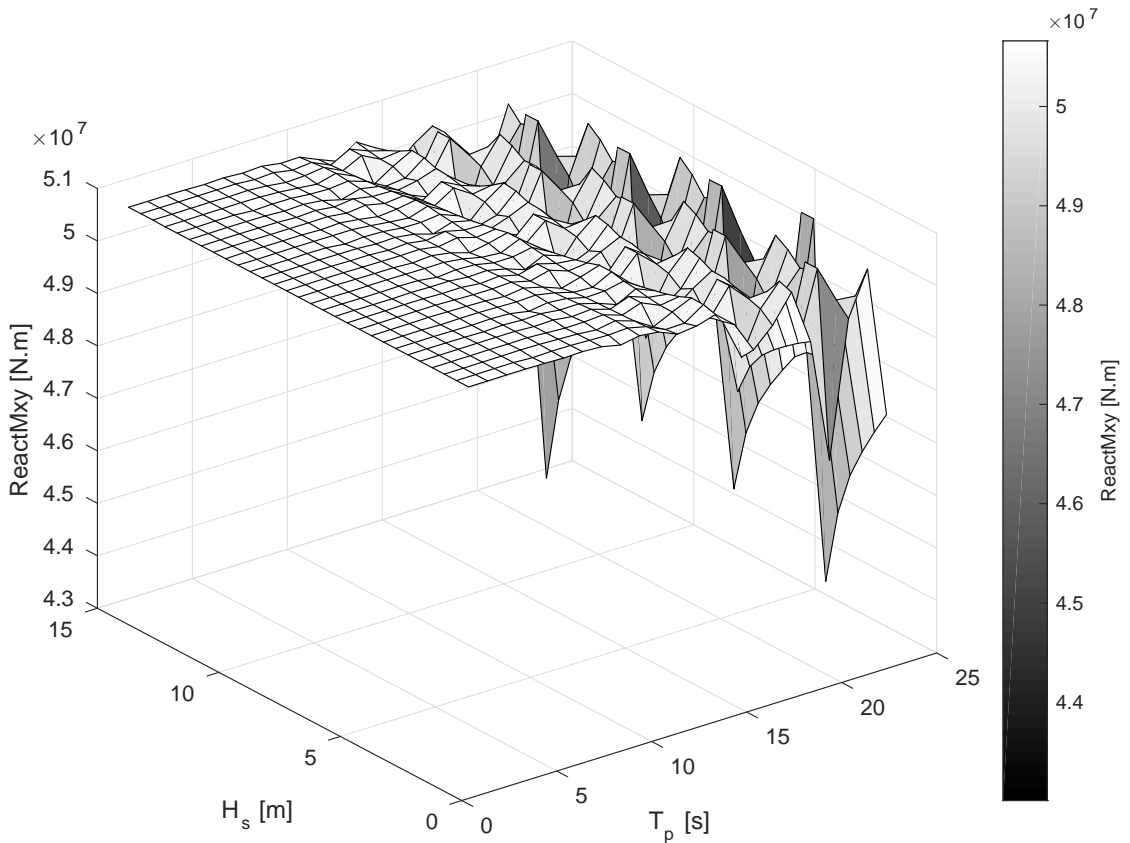


Figure 6.1: Bending moments for all  $H_s - T_p$  combinations for  $V_t = 11$  m/s

It can be observed that within the same wind speed bin, variation in wave parameters leads to changes in loads of upto  $7 \text{ MN}\cdot\text{m}$ . The reduction in loads is mainly observed due to an increase in the  $T_p$  of the incident waves, however, the reduction varies for different significant wave heights.

The second main component of the look-up table is the power output. The theoretical extractable power (assuming 100% efficiency of the gearbox and gener-

ator), for a given wind profile is shown in Figure 6.2a for the range of wind speeds used in the look-up Table

Figure 6.2b shows the mean extracted power at each wind speed bin based on Equation. 2.4 and is seen to emulate the power curve for the NREL 5 MW baseline turbine.

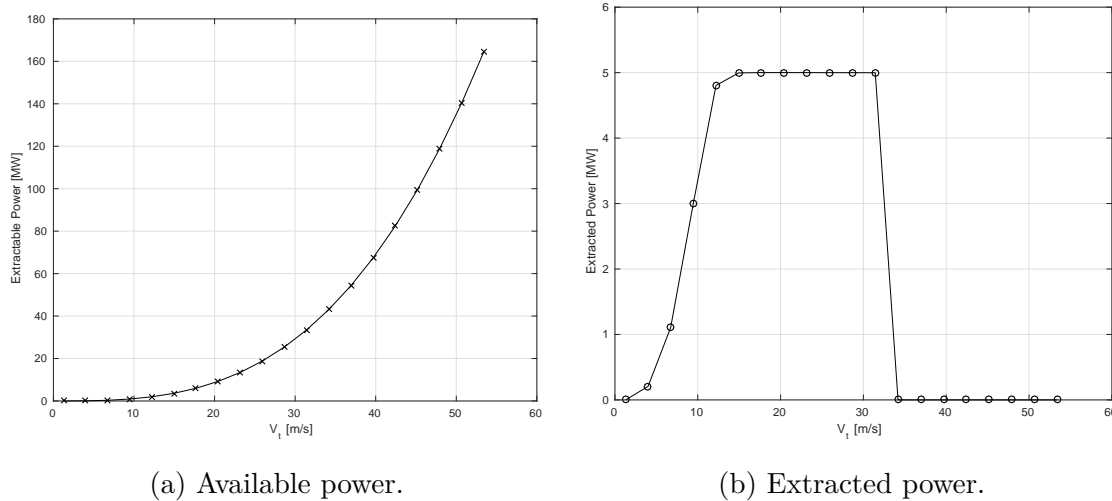


Figure 6.2: Available and extracted power plots for the NREL 5 MW OWT.

The load profiles at the structural nodes, generated through FAST, are post-processed using the  $L^{Ult}$  values from MExtremes to produce damage estimates. When plotted for all  $H_s - T_p$  combinations for  $V_t = 11$  m/s, the damage rate can be seen to increase with an increase in  $H_s$  as shown in Figure 6.3.

There are two observed peaks in the damage rate within the same wind speed bin; for very steep and long period waves. Therefore, while the resource is constant within each wind speed bin, variable damage can be observed based on the predominant wave climate. Although the offshore wave climate is largely governed by the wind conditions, this indicates that OWTs may experience site-specific damage variability due to additional factors influencing the wave climate such as bathymetric considerations.

The results of the structural response, fatigue damage and power production tabulated in the look-up table are further used to achieve the second objective of this study in the next section by performing fatigue life estimation for various sub-regions in the UKCS and adjoining areas.

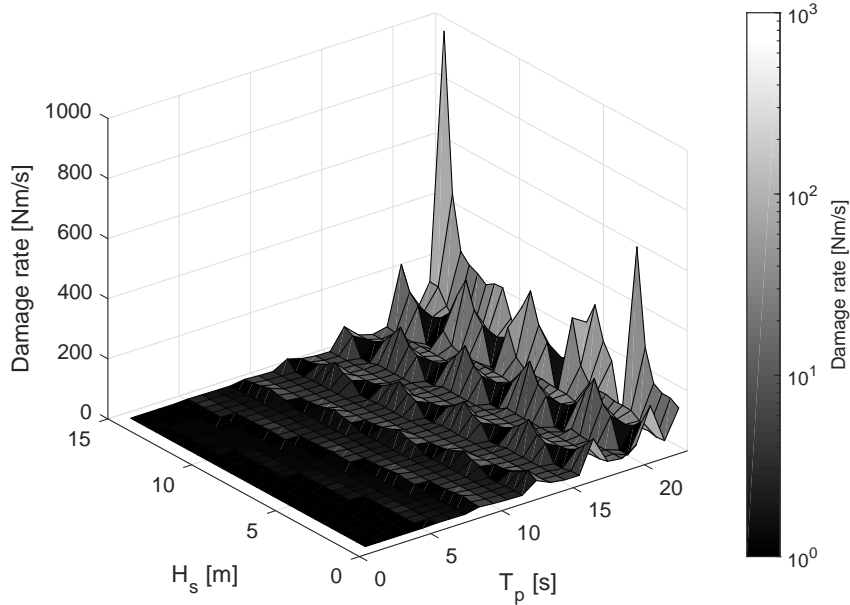


Figure 6.3: Damage rate for all  $H_s - T_p$  combinations for  $V_t = 11$  m/s

## 6.2 Sub-regional characterisation for UKCS

To establish the rationale for a UKCS-wide parametric study, this section works with select Grid Points (GPs) in various sub-regions of the EEZ. A select eight sub-regions due to their representative set of conditions in the UKCS are considered, including the Northern North Sea, Central North Sea, Southern North Sea, English Channel, Celtic Sea, Irish Sea, Hebrides Shelf and West Shetland Shelf. The work presented here assumes the turbine under discussion is installed in all locations, as it allows to isolate the influence of metocean parameters on providing an estimate of site-dependent reliability variations for the turbine.

### 6.2.1 Environmental data

The North European Storm Study (NESS) was developed to fulfill the requirement of quality hindcast metocean data (Health and Safety Executive, 2005). It was based on wind fields provided by the UK Meteorological Office and the Norwegian Meteorological Institute. Using the spectral HYPAS wave model and a coarse grid for the North Atlantic and finer grid resolution for the North European shelf of 150 km and 30 km, respectively, the advanced NEXT wave model by GKSS Forschungszentrum produces a robust hindcast database. For the southern North

Sea, a data resolution of 10 km was used to account for the influence of the highly variable topography. The hydrodynamic modelling, determining the tide and surge parameter, was done using the System 21 developed by Danish Hydraulic Institute which embeds a finer 10 km grid within the 150 km coarse grid.

However, the usefulness of the NESS model is limited by the lack of continuity in the data and the short-comings of the first- and second-generation wave models used. It was run for the winter period only between 1964 to 1989 except the years 1977-9, where the model was run for the summer period as well. Owing to this, the hindcast drew criticism for poor representation of metocean conditions in the UKCS, the NEXT hindcast data was produced which incorporated a third generation wave model, additional wind fields provided by National Oceanic and Atmospheric Administration (NOAA) and an extended hydrodynamic model. This added a continuous period of data to the NESS database from 1989-1995 including the summer period. However, inconsistent wind field inputs led to unfavourable comparison of the NEXT dataset with North Sea measurements at four locations during storm conditions. This includes a comparison between the K13 site (extensively discussed in Chapter 5) and NEXT GP15514. Therefore, an improved NEXT Re-Analysis (NEXTRA) hindcast database was produced.

However, use of the NEXTRA database is restricted to the NESS user group and associated contractors. Used widely for OWT structural model inputs in the DOWEC study (Ponterotto et al., 1995; Bierbooms, 1994), the NEXT data set is extensively researched and its viability for the determination of OWT structural response and weather windows for O&M activities established. Therefore, to establish this methodology, available NEXT data from the Fugro GEOS (2001) report is utilised. The report provides sufficient data integrity for non-storm conditions and seeks to improve data reliability by discarding any data which is considered inaccurate.

This report details environmental data published for forty sites around the British Isles using the hindcast wind and wave time series from the NEXT model (Fugro GEOS, 2001). The presented data is used in this chapter for the estimation of subassembly reliability in various sub-regions of the UKCS. The report aims to provide the data to inform offshore operation decisions but can be used for fatigue estimates of OWTs deployed in the UKCS. The data spans over nine years for the combined periods between January 1977 to December 1979 and January 1989 to

December 1994. Of the provided metocean data, the joint frequency distribution tables for  $H_s - V_t$  and  $H_s - T_p$  are used to characterise each location of interest while information regarding the directionality of the wind and wave parameters is not incorporated. The report divides the UKCS into eight zones with a variable number of GPs in each zone as can be seen in Figure 6.4.

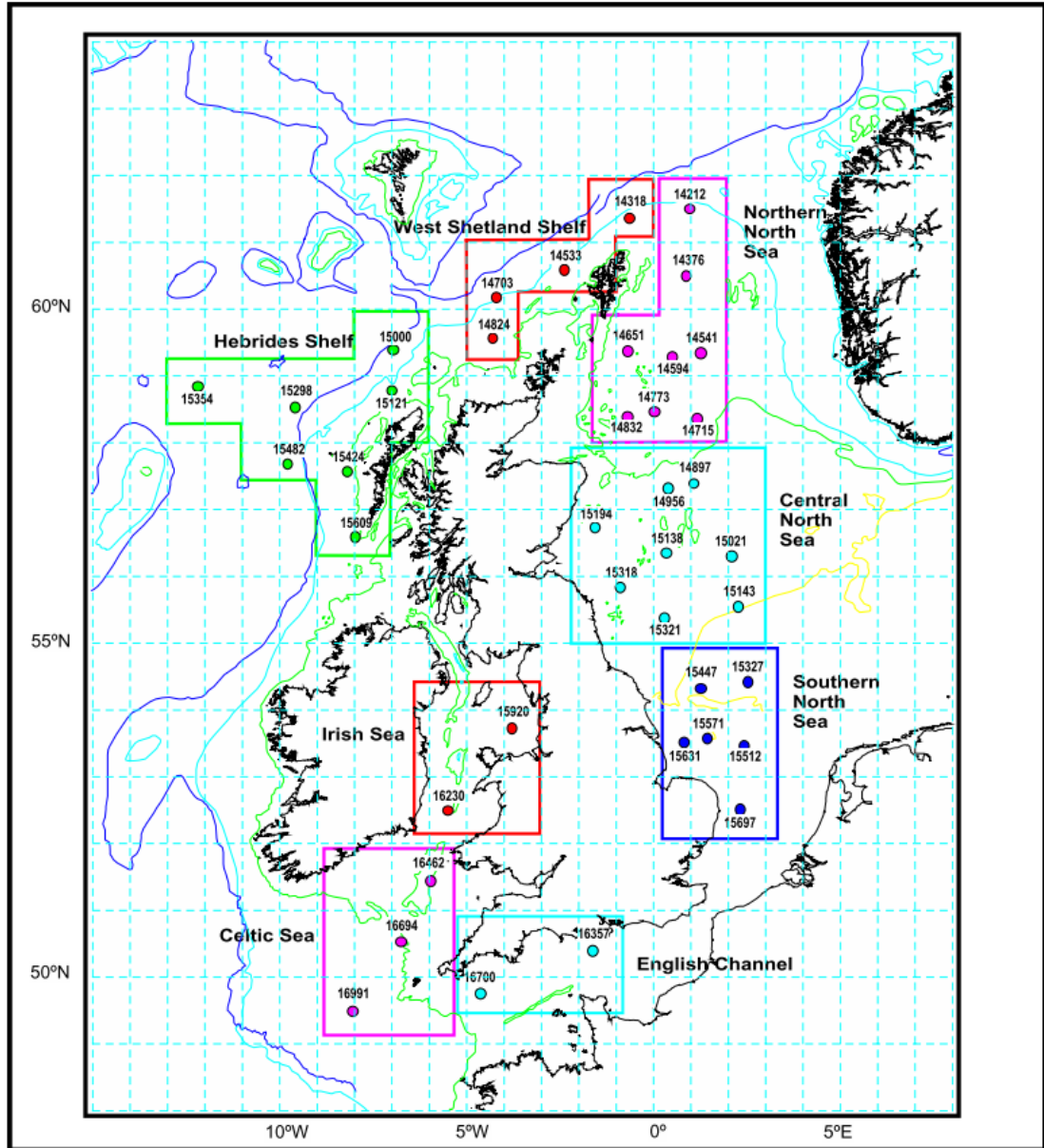


Figure 6.4: Sub-regional division and location of the NEXT data GPs for which comprehensive data is publicly available (Fugro GEOS, 2001).

The NEXT hindcast model provides an estimate of wind parameters within the surface boundary layer, where the wind speed shows variation with increase in distance from the ground, however, the wind direction is not impacted by the change of hub height relative to the reference height. The wind speed parameter

from the NEXT database corresponds to a 1-hour average wind speed at a height of 10 metres above sea level.

The database provides average annual wind and wave frequency distributions showing the frequency of the joint occurrence of  $H_s$  and  $V_t$  conditions irrespective of the  $T_p$  for an average year derived from the nine year data. The  $H_s$  bin width is 0.5 m up to a wave height of 8.5 metres equivalent to 1% exceedance level. All wave occurrences with  $H_s$  greater than the 1% exceedance level are allocated to the last  $H_s$  bin with the cut-off at  $V_{max}$  to indicate that although the data for the storm conditions exists, it is not considered sufficiently representative of the actual conditions. The wind bins are of variable length, each bin corresponding to the lower limit of the equivalent wind range associated to the Beaufort Force as seen in Table 2.1.

### 6.2.2 Processing metocean data for $D^{life}$ estimates

This sub-section presents the methodology followed to identify possible differences in structural fatigue using the available outputs from the look-up table for all GPs in the sub-regions. A brief outline of the methodology followed to determine lifetime accumulated damage for the support structure at the mudline is presented in Figure 6.5.

In order to adapt the NEXT data to utilise the simulation outputs from the look-up table, the width of all bins for the environmental variables must be homogenised particularly the Beaufort-discretised wind bins. Additionally, since data points in the tail of the distribution are to be included in the analysis to account for the influence of dynamic wave conditions on fatigue life, the existing bin width (upwards of 6 m) is divided into 0.5 m bins to distribute the data into definitive sections and the occurrence data distributed uniformly between the bins. Similarly, wind speed data is regenerated by a uniform distribution of the occurrence data in each wind speed bin from the available NEXT scatter plots. This regenerated data is then binned into standard bin width of 2 m/s between 0 m/s to an arbitrarily chosen upper limit of 34 m/s.

To use the HornSea offshore wind farm as a reference site to demonstrate the methodology, GP15571 of the Southern North Sea is chosen since it is in the closest proximity to the HornSea project, falling within the same grid cell 1° - 2° E and

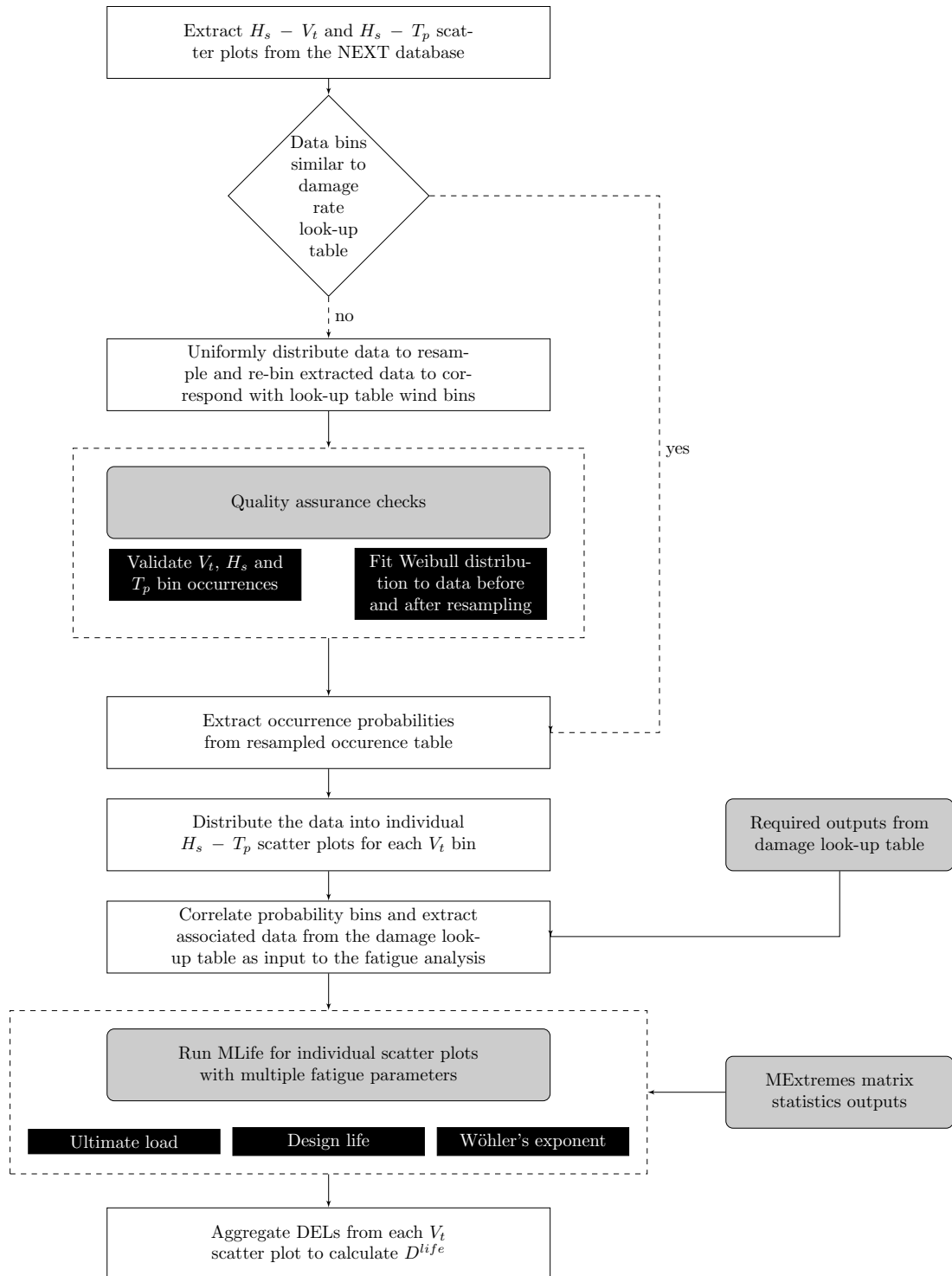


Figure 6.5: Methodology flowchart for conducting fatigue analysis at the sites identified in Figure 6.4 for various sub-regions in the UKCS.



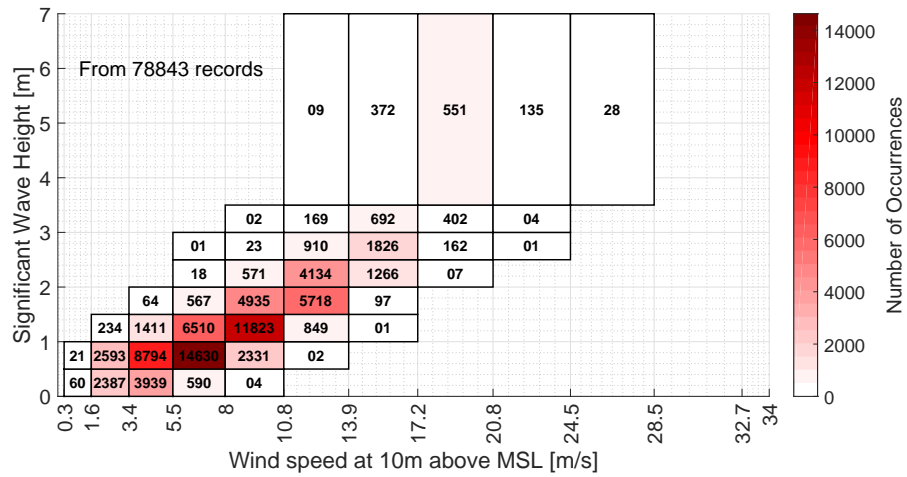
53° - 54° N. Figure 6.6a shows the extracted data from the report for GP15571 at 53.587°N, 1.422°E in the Southern North Sea, while Figure 6.6b shows the data after it has been rebinned into standard wind speed and wave height bins. The available scatter plot provides the number of occurrences of 1-hour intervals of each bin in the 9 year data period. This is translated into the percentage occurrence for the produced scatterplot Figure 6.6b and percentage occurrence of less than 0.1 are shown as the number of occurrences in the respective bin.

The peak period data is then appended to the wind and wave data from the joint frequency distribution available in the FUGRO report. The  $H_s - T_p$  scatterplot can be seen in Figure 6.7 for GP15571.

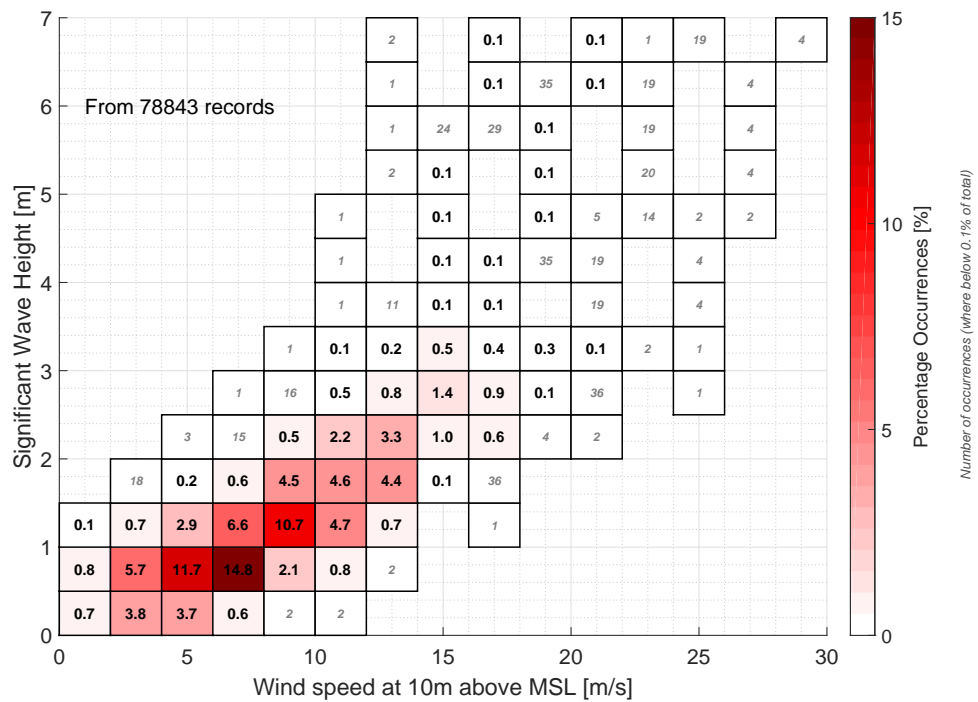
Since all required data has now been extracted, two checks are made for quality assurance of the resampled data. Firstly, the total occurrences for the resampled data are aggregated and the expected outcome is 78843 occurrences. This is because the aggregate of hourly data points for nine years (with 1 year = 365 days) produces a record of 78843 data points. Secondly, a comparison is made between the data fit to a Weibull distribution pre- and post-resampling, particularly in the low frequency tail of the distribution, to observe if the resampled data displays any differences due to the resampling process. For GP15571, this can be seen in Figure 6.8, where for wind speed the data regeneration and rebinning does not alter the shape and scale parameters of the Weibull fit.

Frequency distribution data for  $H_s - T_p$  is then separated for the 2 m/s wind bins and fatigue analysis run for each wind bin separately. Figure 6.9 shows sample scatter plots generated for GP15571 for the first six bins. MLife is used to perform fatigue analysis separately on each scatter plot by translating the occurrence into a user-defined distribution table input.

Running MLife for scatterplots associated with each wind speed bin yields lifetime damage equivalent loads based on the bending moment of the piled OWT. OWT availability input factor of MLife is varied for each scatterplot based on the  $V_t$  falls within the operational wind speed range or not. For environmental conditions outside the operation wind speed range of the OWT, an availability of zero is used, whereas an availability of 1 is used if all load cases fall within the operational wind speed range. Therefore, the 5 MW NREL turbine is assumed to be exposed to the ideal conditions of 100% availability and no downtime due to maintenance activities.



(a) Available scatter plot from the NEXT database for GP15571 at 53.587°N, 1.422°E based on the Beaufort scale for wind. The large bin width for  $H_s \geq 3.5$  groups all wave occurrences with  $H_s$  greater than the 1% exceedance level to indicate that although the data for the storm conditions exists, it is not considered sufficiently representative of the actual conditions



(b) Produced scatterplot for the FUGRO database after resampling the data in bins of equal length.

Figure 6.6: Comparison between the available scatterplot binning of the NEXT data in the Fugro GEOS (2001) report to the resampled data for fatigue life analysis.

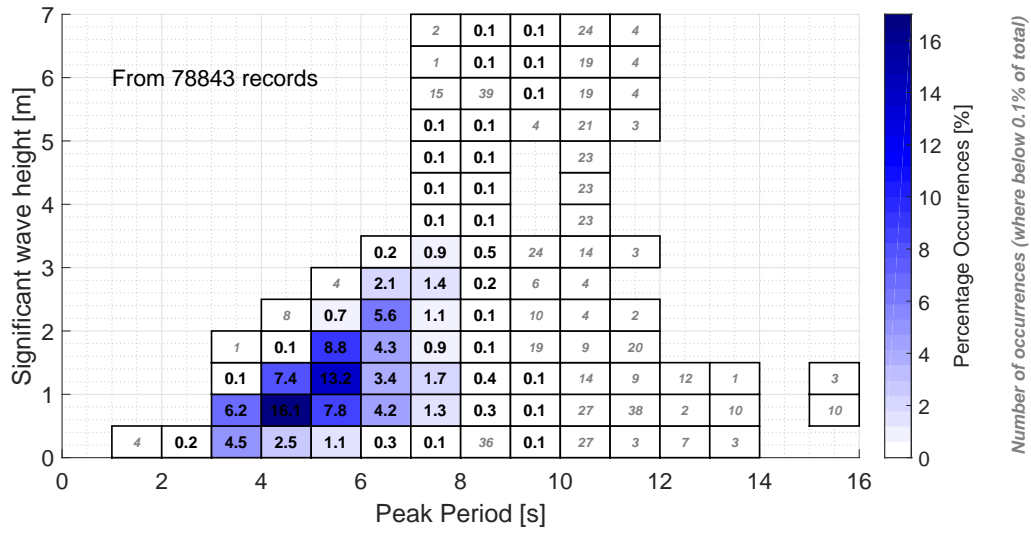


Figure 6.7: Resampled  $H_s - T_p$  scatter plot for all wind speeds at GP15571.

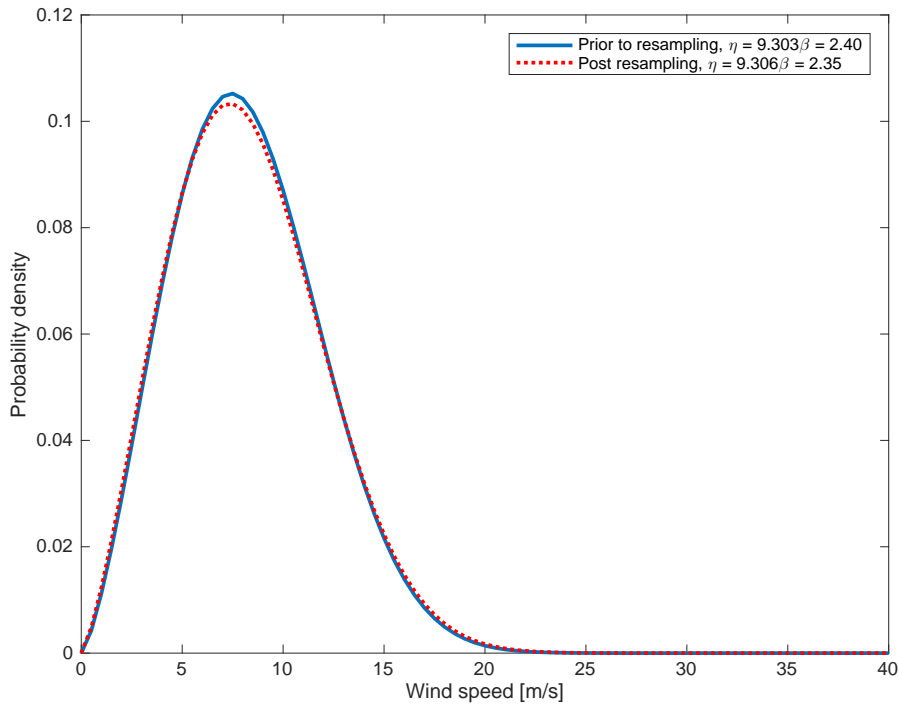


Figure 6.8: Weibull fitted wind data from the provided (Fugro GEOS, 2001) and resampled data.

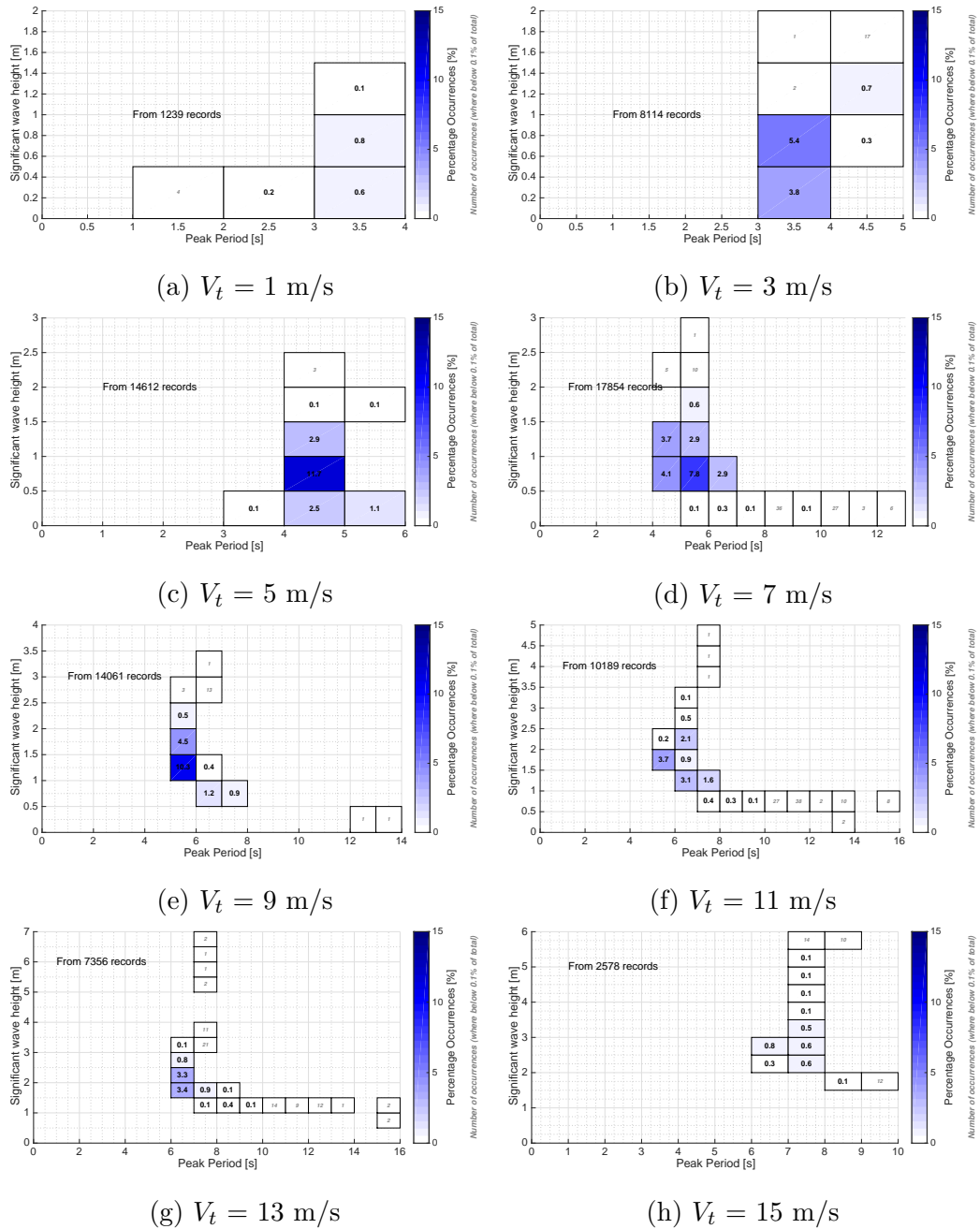


Figure 6.9: Scatter plots for  $0 \leq V_t < 15$  for GP15571

Mlife uses the supplied occurrence probability of each  $H_s - T_p$  bin, the availability factor and associated design lifetime ( $DesLife$ ) to estimate the time factor ( $f_j^{life}$ ) to extrapolate fatigue damage to structural lifetime.

Figure 6.10 shows the distribution of the time-weighted lifetime damage across the wind speed bins for GP15571 when a  $DesLife \approx 20$  years and a Wöhler exponent of 4 is chosen for longitudinal welds in steel at the mudline of the support structure. The ultimate strength is chosen to be 5 times  $L^{max}$  extracted from MExtreme as discussed in Chapter 6.1.3.

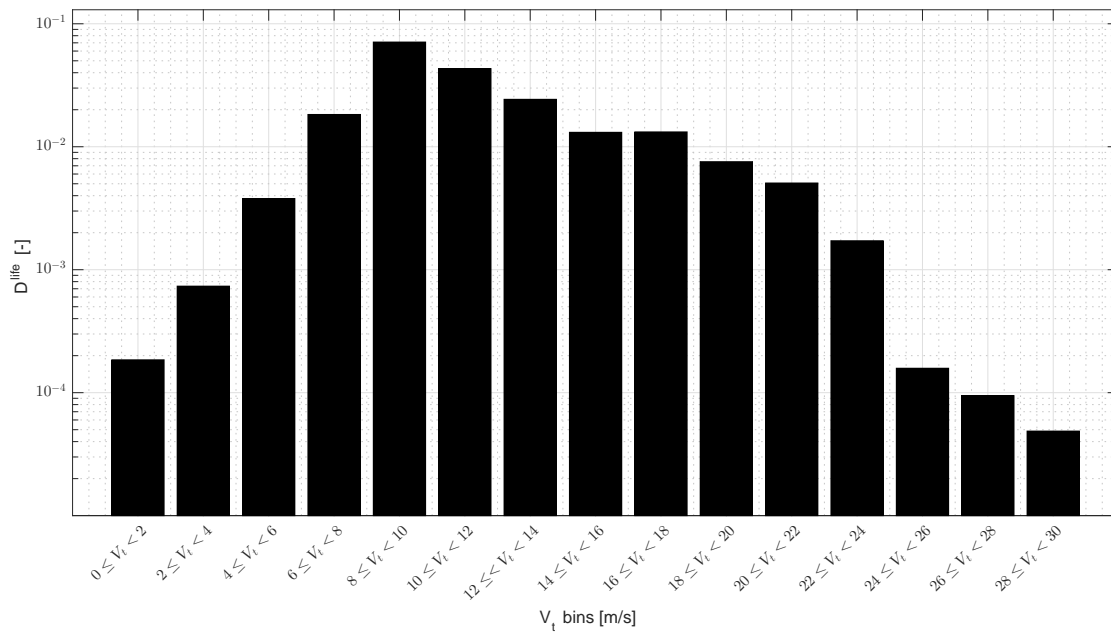


Figure 6.10: Lifetime accumulated damage within each wind speed bin at GP15571 with  $L^{Ult} = 5 \times L^{max}(ReactMxyss)$ ,  $m = 4$  and  $DesLife = 20$  years. An aggregate of all  $V_t$  bins at this site yields a  $D^{life}$  of 0.202 with the maximum damage at  $8 \leq V_t < 10$  m/s.

The time-weighted accumulated fatigue damage for wind speeds shows that damage within the power production DLC increases until the rated wind speed is reached. Of the total  $D^{life}$  (estimated as an aggregate of individual wind bin  $D^{life}$ ) at 0.202, the highest contribution to damage is within the power production phase of the OWT. Maximum damage occurs at  $8 \leq V_t < 10$  m/s; this is associated to the large number of recorded occurrences at 1406 in the redistributed binned data in the scatter plots in Figure 6.9e as well as this bin being representative of the rated speed once the  $V_t$  is sheared to hub height based on Equation. 4.1.

To further investigate the distribution of the accumulated damage life between

the wind speed bins for all GPs, a scatterplot is produced and displayed in Figure 6.11.

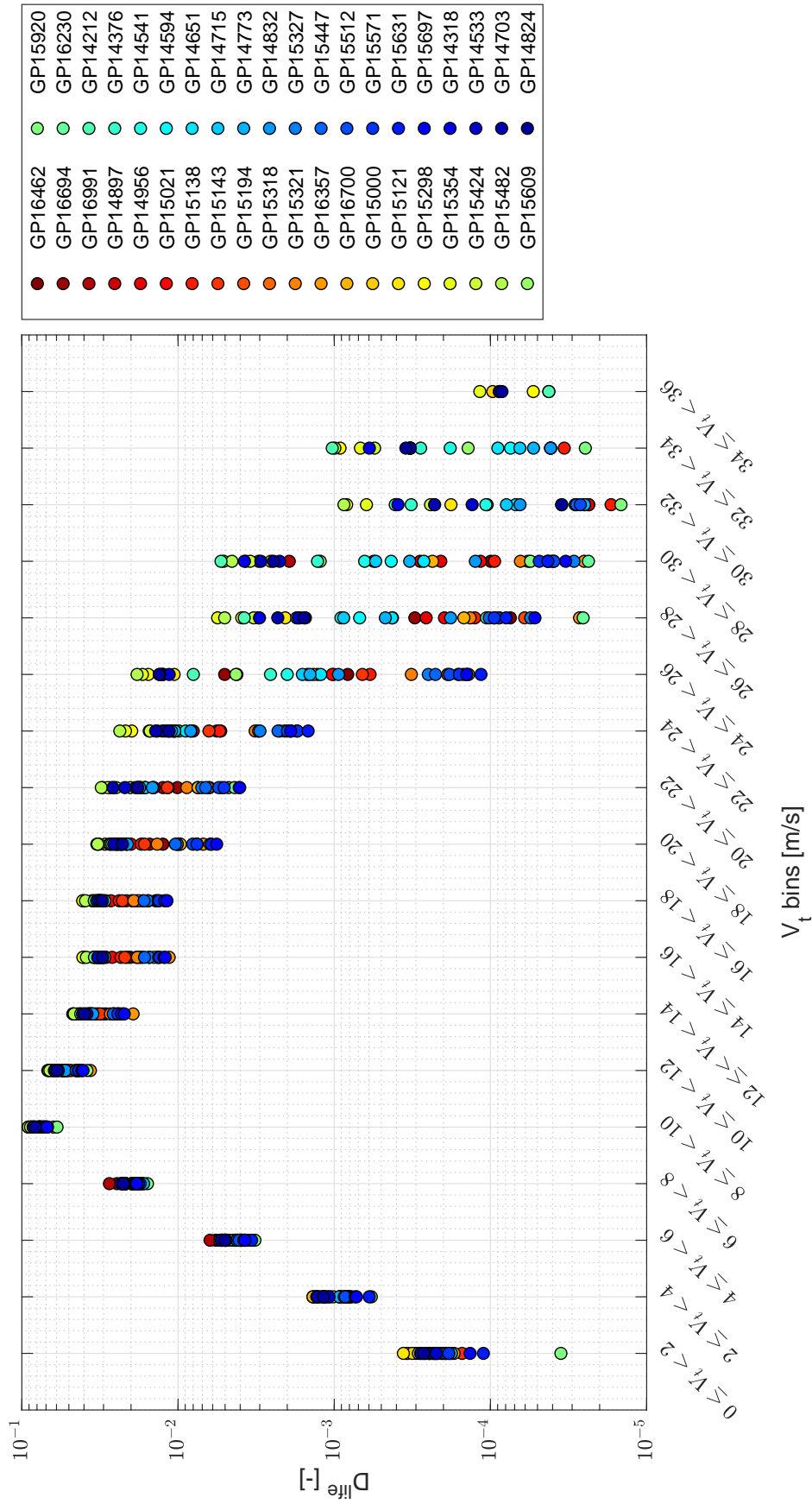


Figure 6.11: Distribution of accumulated lifetime damage for each wind speed bin at the 40 investigated GPs.

It is observed that the relative contribution of individual  $V_t$  bins to  $D^{life}$  at all GPs is similar with the peak at  $8 \leq V_t < 10$  m/s. Structural damping after this peak reduces the damage, however, a progressively larger variation in damage is seen after cut-in speed. This spread becomes more pronounced after the cut-out speed and may be attributed to the larger uncertainty attached to the input metocean parameters from the NEXT database for storm conditions.

### 6.2.3 Structural fatigue analysis outputs

As the aim of this research project is not to provide deterministic estimates for fatigue life of the OWT in various locations in the UKCS. Therefore, an investigation into factors influencing fatigue is conducted to display possible variability in results which can be attributed to factors in addition to the loads on the structure.

#### 6.2.3.1 Sensitivity Analysis

A local sensitivity analysis is conducted to evaluate the contribution of key variables, that is, design life, ultimate load and Wöhler exponent on the lifetime fatigue damage. To this purpose, at each iteration of the analysis only one parameter is varied while the other parameters remain unchanged. Using a range of possible values for the variables outlined in Table 6.3 for  $L^{Ult}$ ,  $DesLife$  and Wöhler exponent, MLife simulations are run for each grid point from the NEXT database. The range of values are colour-coded, where, a darker colour corresponds to an input value with lower fatigue life. Therefore, 90 simulations for each GP are conducted to provide the range of possible fatigue life estimates that can be generated for the same point.

The range of values for the Wöhler exponent are based on the generally prescribed values for steel structural components in wind turbines (DNV GL AS, 2016a), offshore structures (Det Norske Veritas, 2005; API, 2014) and OWT standards (British Standards Institution, 2009). For  $L^{Ult}$ , the recommended values for the  $ULF$  (National Renewable Energy Laboratory, 2018) are used in conjunction with the maximum bending moment extracted from the matrix in Chapter 6.1.3 using MExtremes.

For design life, the following values are chosen: 5 years (157680000s), 10 years (315360000s), 15 years (473040000s), 20 years (630720000s), 25 years (788400000s)



and 30 years (946080000) at each GP. Based on the O&M regime employed at the site, the components may be serviced and restored to as-good-as-new status and the design life is taken to be indicative of such maintenance activities. As an example, a design life of 5 years postulates that the component was serviced every 5 years during a preventive maintenance activity to a degree that it is restored to its initial conditions.

Using data from all 90 iterations at GP15571 assumed to represent the HornSea project, Figure 6.12 shows the envelope of possible lifetime fatigue damage.

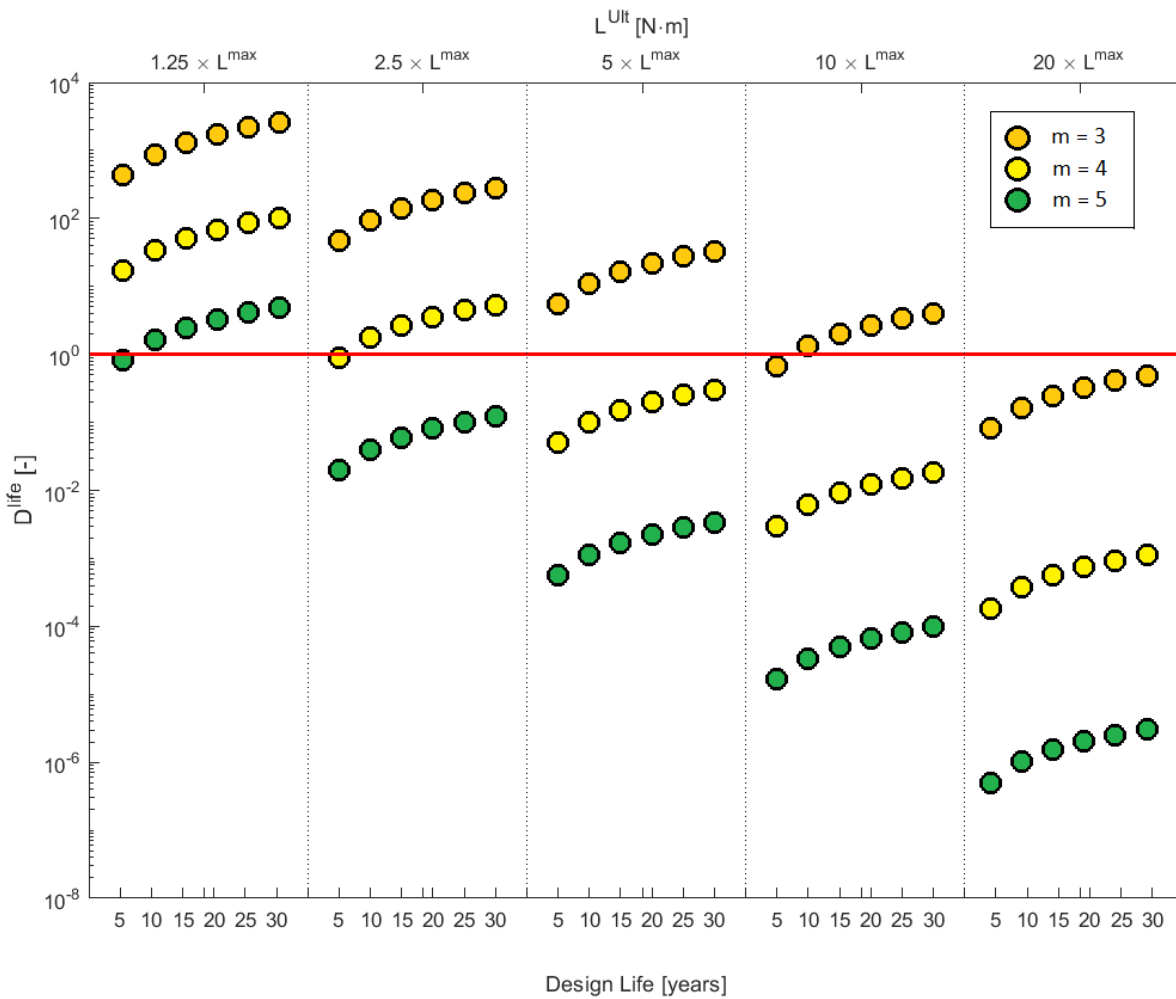


Figure 6.12: Lifetime fatigue damage envelope for the HornSea site using the NEXT model data.

It can be observed that the lifetime accumulated damage can vary in the order of 10 based on the strength and design specifications used in MLife. Correlating the input parameters from Table 6.3 and the  $D^{life}$  scatter in Figure 6.12, it can be seen that both show agreement. That is,  $D^{life}$  is seen to decrease with an increase in  $m$  and  $L^{Ult}$  and a decrease in  $DesLiFE$ . To determine that the influence of the

Table 6.3: Colour-coded MLife input parameters for which the fatigue analysis is performed at the NEXT GPs; a darker colour corresponds to an input value with higher fatigue damage.

Parameter	Input					Units
$m$	3		4		5	-
$L^{Ult}$	$1.25 \times L^{max}$	$2.5 \times L^{max}$	$5 \times L^{max}$	$10 \times L^{max}$	$20 \times L^{max}$	N.m
DesLife	5	10	15	20	25	30
						years

input parameters is uniform across all GPs,  $D^{life}$  at all GPs is determined for the 90 combinations of input parameters. Lifetime accumulated damage across each sub-region is then calculated as the average of the  $D^{life}$  of constituent GPs and plotted in Figure 6.13, Figure 6.14 and Figure 6.15 to explore the sensitivity to  $L^{Ult}$ ,  $DesLife$  and  $m$ , respectively.

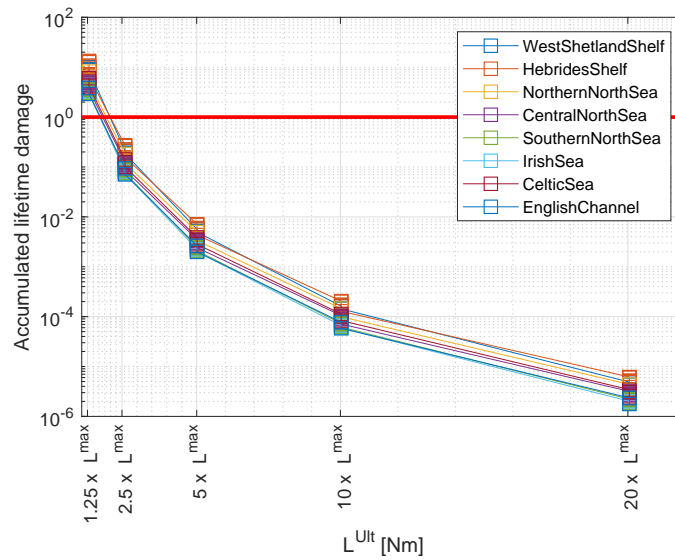


Figure 6.13: Influence of the  $L^{Ult}$  values of on calculated damage equivalent load estimates for fatigue life analysis.

Conducting the sensitivity analysis, it can be observed once again that in agreement with the expectations laid out by the colour codes in Table 6.3, lifetime damage is positively correlated to  $L^{Ult}$  and the Wöhler exponent and is inversely linked to the assigned DesLife for all sub-regions. The influences are more pronounced if a linear y-axis is used instead of the log axes in Figure 6.13 - Figure 6.15.

The key factor for accumulated lifetime damage is determined to be the Wöhler

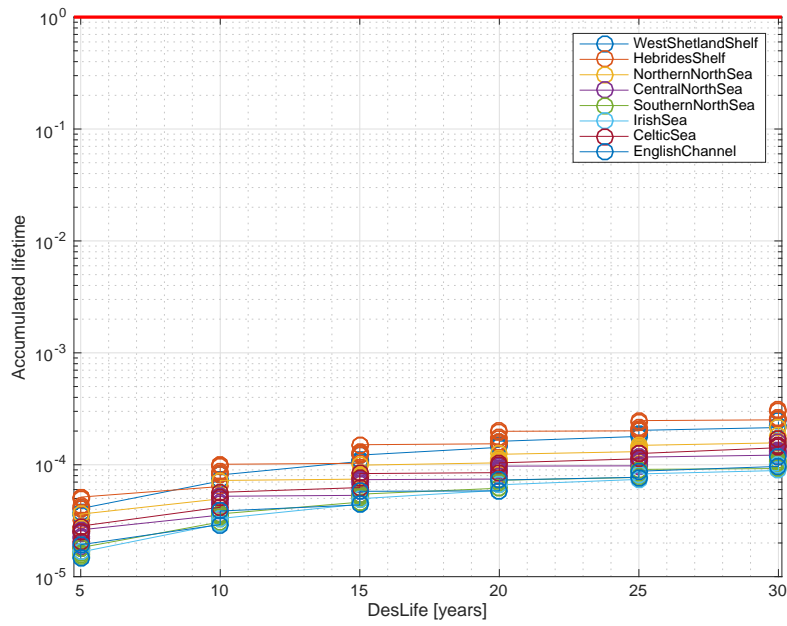


Figure 6.14: Influence of the design life values of 5, 10, 15, 20, 25 and 30 years on calculated damage equivalent load estimates for fatigue life analysis.

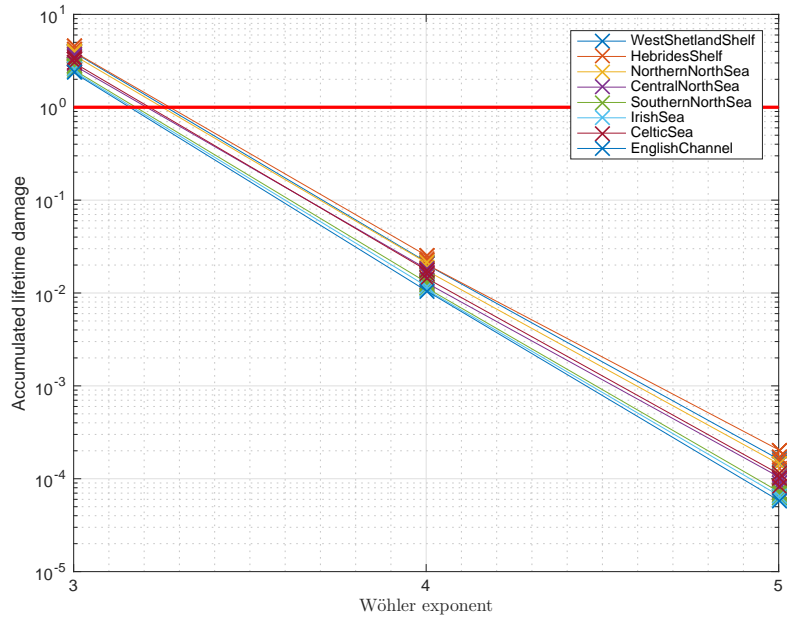


Figure 6.15: Influence of the Wöhler exponent values of 3, 4 and 5 on calculated damage equivalent load estimates for fatigue life analysis.

exponent since an increase by a factor of 1.7 leads to a five order of magnitude change in  $D^{life}$ . An increase in  $L^{Ult}$  parameter with a factor of 16 leads to an increase in lifetime accumulated damage of six orders of magnitude. Finally, for an increase in  $DesLife$  from 5 to 30 years, the resulting  $D^{life}$  at the mudline of the support structure increases by 1.5 orders of magnitude making it the least significant parameter of the three parameters investigated for  $D^{life}$ .

Furthermore, it can be observed the more dynamic sites, such as the Hebrides Shelf, West Shetland Shelf and Northern North Sea show consistently higher damage than more benign sites such as the Southern North Sea and Irish Sea for all chosen values of  $L^{Ult}$ ,  $m$  and  $DesLife$ , therefore, any combination of values for these parameters is suitable for determining the sub-regional differences in lifetime accumulated damage.

To achieve a better understanding of the degree of influence of the various combinations of fatigue calculation parameters on lifetime damage, three scenarios may be considered. Appendix F provides the  $m$ ,  $DesLife$  and  $ULF$  values for the three scenarios. The best-case scenario, where the calculated damage is minimal and the worst-case scenario, where the calculated damage is maximum, show us the envelope of the possible values. Simultaneously, the mean-case scenario provides a measure of the average accumulated lifetime damage estimates.

A mean scenario and associated error bars in Appendix F provide a visual representation of the difference in results based on the inputs described in Appendix F.

For each analysed scenario, all grid points experience accumulated fatigue damage within the same order of magnitude. However, between scenarios, the magnitude of the worst-case characteristic damage is  $10^7$  as much as the best-case scenario. For the worst-case scenario at all locations with the low grade steel and no maintenance for the 30 year lifetime, failure at the mudline occurs during the design life. On the contrary, for all locations with high grade steel and perfect preventative maintenance, the turbine is exposed to lower risk. Risks are within the acceptable range for medium strength steel and a restorative maintenance action every 15 years.

## 6.2.3.2 Sub-region fatigue DELs at mudline

The trends followed by OWTs located at different sites in the UKCS are similar and the variability may be attributed to the change in fatigue life calculation variables. Due to the uniform influence of the variables in Table 6.3 across the sites, any set of parameters may be used for site- comparison. Figure 6.16 shows the distribution of accumulated lifetime damage across 40 sites in the UKCS using the NEXT metocean data with Wöhler's exponent = 4, design life = 15 years and  $L^{Ult} = 5 \times L^{max}$ .

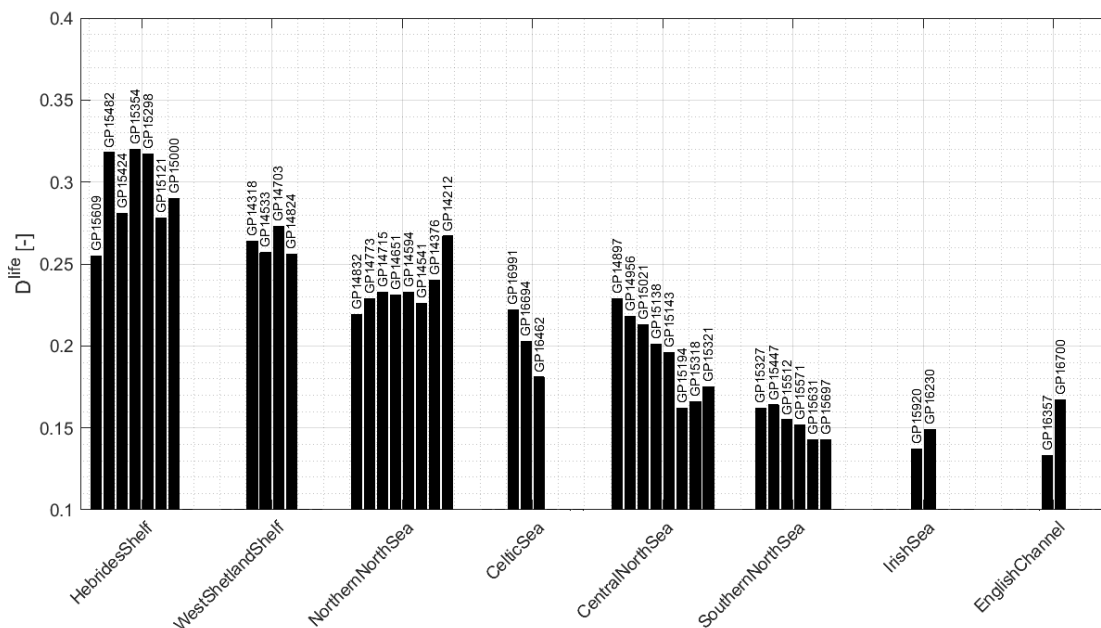


Figure 6.16: Distribution of  $D^{life}$  categorised based on GP locations across the UKCS with  $m = 4$ ,  $DesLife = 15$  years and  $L^{Ult} = 5 \times L^{max}$ .

The accumulated lifetime damage results for the support structure at the mudline display a distinct difference for turbines on the more exposed west coast relative to the sheltered east coast. The Hebrides Shelf and the West Shetland Shelf can be seen as the locations with the highest accumulated fatigue damage, whereas, damage at the Celtic Sea is noticeably lower. Damage to structures deployed at the Southern North Sea is approximately half of the damage experienced by structures in the Hebrides Shelf. And as the GPs move further down the latitudes towards the Central and Southern North Sea, accumulated damage further decreases.

The sheltered Irish Sea indicates the highest lifetime expectancy, almost two times that of structures in the dynamic Hebrides Shelf. Finally, insufficient GPs

are available to make an informed judgement about fatigue loads in the English Channel, therefore, fatigue analysis at additional locations in the English Channel must be conducted. Within each site, the distribution of accumulated lifetime damage at GPs shows a general agreement, except GP14212 in the northern North Sea which experiences larger damage relative to the other GPs in the Northern North Sea. This is expected since the geographical location of GP14212 (refer to Figure 6.4) makes it susceptible to more dynamic conditions generated by the increased fetch for the predominantly southwesterly winds over the North Atlantic (Neill and Hashemi, 2013).

### 6.2.3.3 Energy production

As can be seen in the scatter plot for GP15571 in Figure 6.7, the percentage occurrence of wind speeds within the power production range is over 95%. Therefore, for an ideal wind turbine with no scheduled maintenance stops or failures throughout its lifetime, power production is expected to continue over this period using the descriptive power curve in Figure 6.2b.

For each site, there is nine years or 78843 hours of metocean data available, therefore, to calculate the total annual energy output  $E^{ann}$  for an OWT installed at the site, Equation. 6.1 is used.

$$E^{ann} = \sum_{i=1}^{TotBins} \frac{p_i^v}{100} \times \frac{T^{scat}}{T_{years}^{scat}} \times P \quad (6.1)$$

where,  $i$  is the bin index from 1 to TotBins total number of bins in the rebinned scatter plot,  $p_i^v$  is the probability occurrence percentage for the respective bin,  $T^{scat}$  is the length of time for each record over the analysed period and  $T_{years}^{scat}$  is the time length of the data in years.

Since the power output is solely dependant on the wind flow input from the metocean scatterplots, a simplified one dimensional scatterplot with wind speed bins can be used for energy production analysis. Figure 6.17 shows the resulting power output at all GPs in the various sub-regions displaying a higher annual power output for regions with a higher resource.

Currently populated regions of the UKCS, namely the Irish Sea and Southern North Sea do not provide the incentive of a relatively larger output despite the consideration of an ideal turbine with 100% availability. Thus, it may be inferred that the turbines deployed in these regions spend a higher proportion of time

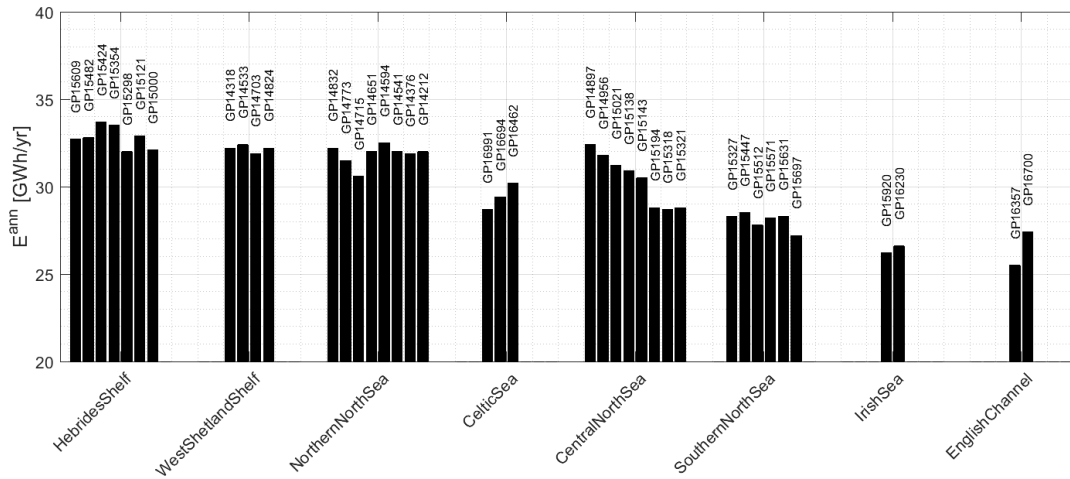


Figure 6.17: Annual energy production at the various sub-regions of the UKCS.

below the the rated wind speed or above  $V_{out}$  which consequently limits the power output. Using the annual energy production output for an ideal turbine with no downtime due to failure or maintenance activities, theoretical capacity factors at the different sub-regions in the UKCS are calculated through Equation. 2.3. The subsequent results are presented in Figure 6.18.

Since the same turbine with a 5 MW rating is assumed to be deployed at all sites, the resulting capacity factors are higher for locations with higher annual power output. As seen in Figure 6.18, ideal capacity factors lie between 58 - 77% for a turbine that is always in DLC 1.2 when the wind speed is in the operational range. However, realistic turbines experiencing downtime due to O&M activities within the operation range of wind speeds are expected to exhibit lower capacity factors. Recorded fleet-wide average capacity factors for OWTs have demonstrated an increase from 30% in 2005 to almost 40% in 2018 with some individual projects achieving up to 50% (The Crown Estate, 2019).

### 6.3 Metocean-centric metric for sub-regions

To fulfill the final objective of this research to support the usefulness of a site-dependant KPI, the interaction between the two drivers, namely, energy production and the accumulated damage at all grid points is investigated. This is done by employing the portfolio analysis methodology for strategic management to characterise the returns and associated risks for current and future deployments in the

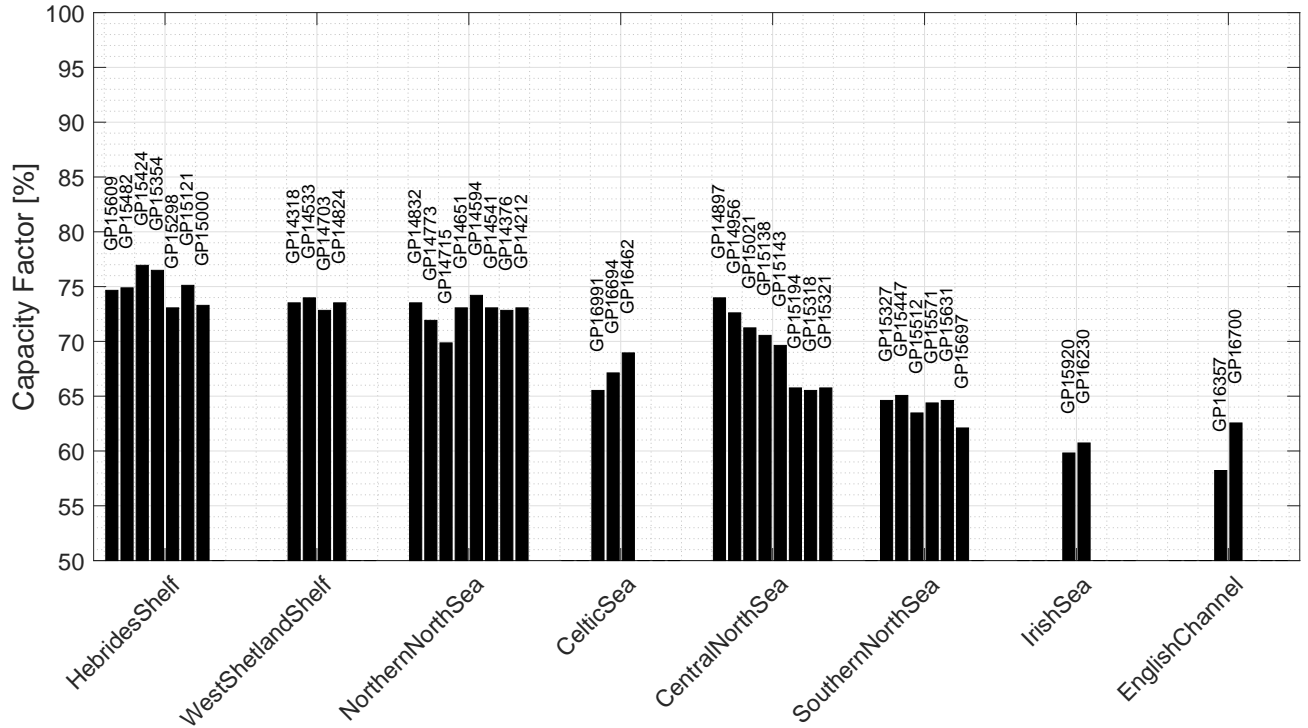


Figure 6.18: Theoretical capacity factors at various sub-regions of the UKCS discounting downtime due to factors outside of metocean conditions.

UKCS. Assuming that the return on investment can be measured solely in terms of power production and project risk defined in terms of lifetime accumulated structural damage, the portfolio analysis allows for the identification of the most risk efficient locations in the UKCS (Chapman and Ward, 1996). To perform the portfolio analysis, the plot area is divided into four quadrants with the characteristics outlined in Table 6.4.

Since, the aim of each deployment is to reduce the accumulated damage while increasing the power production, therefore, RIV provides the best opportunity for

Table 6.4: Risk and return portfolio analysis for the 5 MW baseline turbine deployed in the UKCS and adjoining areas.

Quadrant	Return	Risk
RI	High	High
RII	Low	High
RIII	Low	Low
RIV	High	Low



OWE installations with maximum return and reduced risk. Figure 6.19 displays the relationship between the accumulated lifetime damage and energy production for the various sub-regions in the UKCS using the quadrants in Table 6.4.

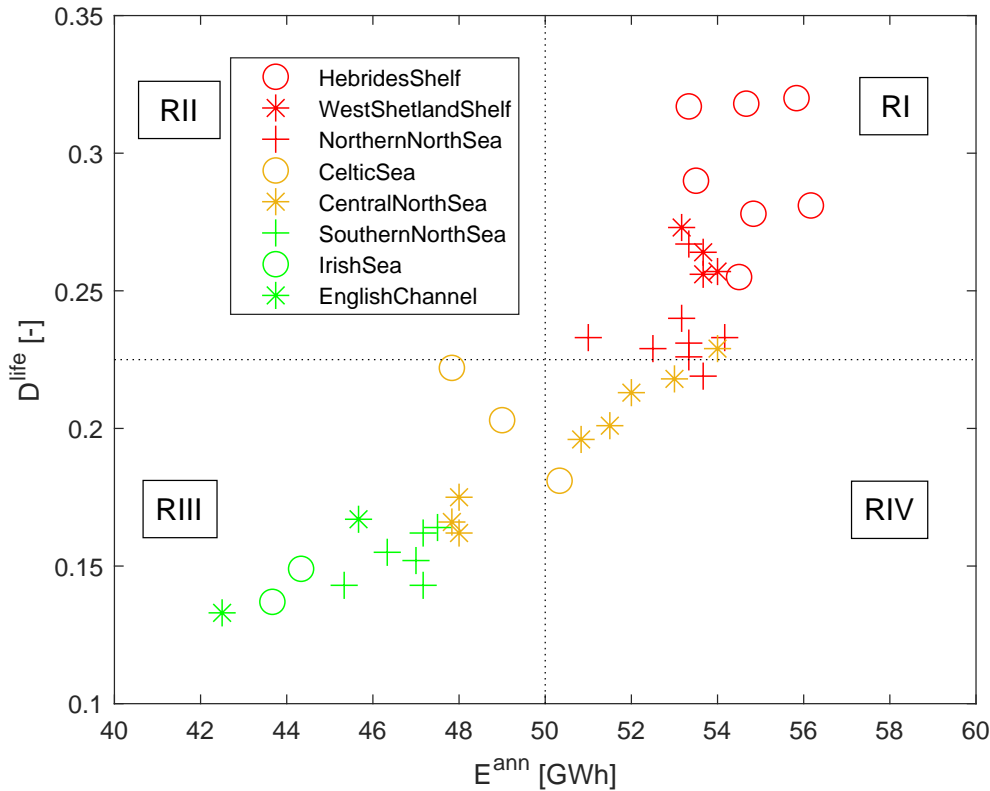


Figure 6.19: Relationship between the annual energy production and damage for the 5 MW NREL turbine deployed at various sub-regions in the UKCS.

RI is populated by GPs from West Shetland Shelf and Hebrides Shelf as well as GP14212 in the Northern North Sea. These locations provide abundant resource potential at the cost of higher damage to the structure. GP14212 has been discussed previously (refer to Chapter 6.2.3.2) due to its deviation from the general damage estimates in the Northern North Sea.

RIII is populated by GPs with low annual power production and consequently low lifetime accumulated damage. These characteristics are exhibited by the Southern North Sea, Irish Sea and English Channel.

The GPs in the Celtic Sea lie at the cusp of RIII and RIV, whereas, those in the Central North Sea are spread throughout RIII and RIV. Therefore, while the damage incurred at the Celtic Sea and Central North Sea is low, the former is characterised by moderate power production, whereas, the latter has a large

range of power production. Locations in the Northern North Sea predominantly lie in RIV, therefore, the GPs of the Northern North Sea can be characterised by an improved power production at the cost of a relatively smaller increase in accumulated lifetime damage.

The combined influence of both performance metrics at each grid point in the various sub-regions of interest is estimated using simple normalisation as shown in Equation. 6.2.

$$K^{DP} = \frac{D^{life}}{E^{ann} \cdot DesLife} \quad (6.2)$$

Where,  $K^{DP}$  is the performance indicator that can assist with offshore wind farm siting based on the accumulated lifetime damage normalised by the energy production. It is a function of the design life ( $DesLife$ ), lifetime accumulated damage ( $D^{life}$ ) and annual energy production ( $E^{ann}$ ).  $K^{DP}$  does not incorporate the influence of variables effecting balance of plant such as water depth, distance to shore and type of soil bed.

Figure 6.20 shows the results for  $K^{DP}$  for GPs in the various sub-regions of the UKCS.

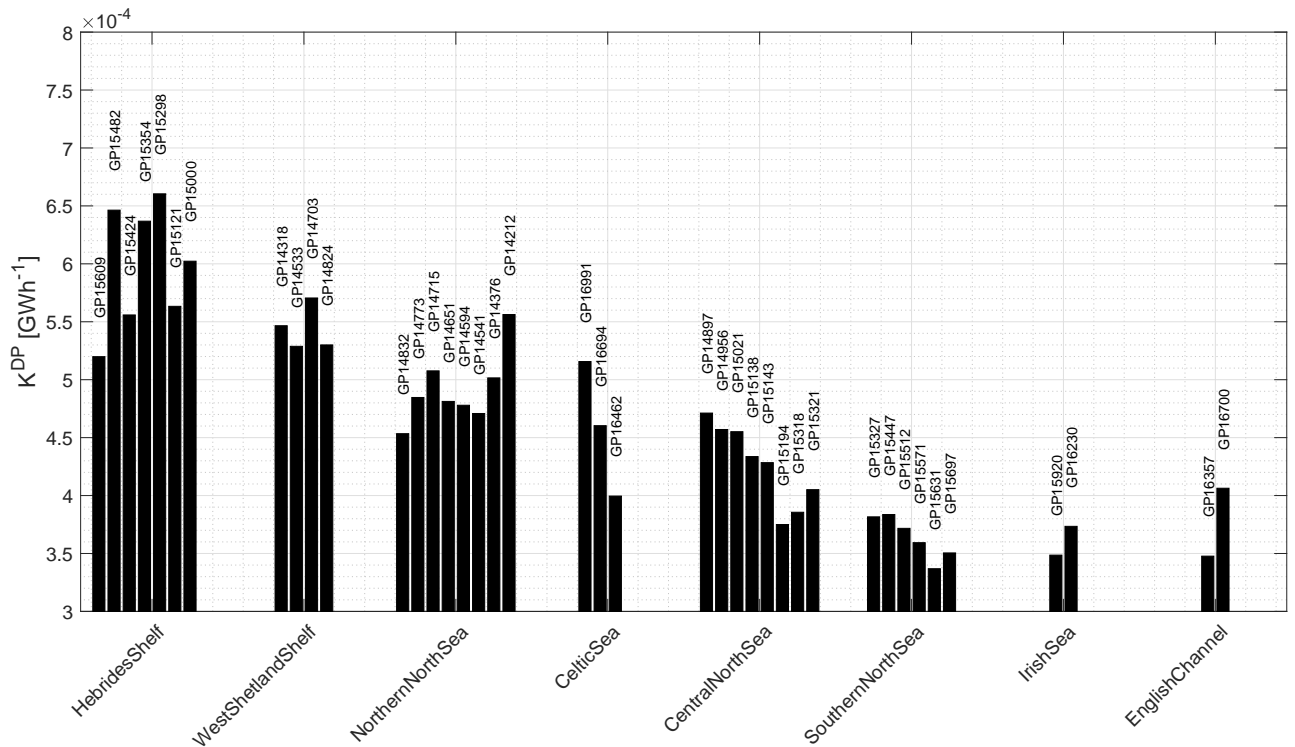


Figure 6.20:  $K^{DP}$  performance indicator combining the influence of energy production weighted by accumulated fatigue damage at the various sub-regions of the UKCS.

The bar chart shows that  $K^{DP}$  as a performance indicator for the 5 MW baseline turbine highlights the suitability of the sub-regions differently compared to  $E^{ann}$ ; the most lucrative sites for energy production are not the most attractive sites for OWT deployment. Instead, benign locations such as the Southern North Sea and Irish Sea appear to be more attractive for siting of OWT installations from a fatigue reliability perspective.

### 6.4 Cost of energy in the UKCS sub-regions

A simplistic cost of energy (COE) analysis using modelled estimates for CAPEX, OPEX and D&D (Shafiee et al., 2016) is used to provide an estimate of the COE for a 500-MW baseline wind farm centered at each GP populated by 100 5-MW NREL piled OWTs. The said LCC model uses a comprehensive cost breakdown structure incorporating all five phases of the OWT lifecycle including pre-development and consenting, production and acquisition, installation and commissioning, O&M and the D&D phase for the cost analysis. Additionally, when compared with other models (Laura and Vicente, 2014; Cantú, 2011; Ioannou et al., 2018; Snyder and Mark J. Kaiser, 2009; Myhr et al., 2014) and experimental results (Mark J Kaiser and Snyder, 2011), the model shows high agreement and can, therefore, be regarded as a robust input for the COE analysis.

While the analysis framework of the LCC model provides estimates for an offshore wind farm with a design life of 25 years, its results are extrapolated for use in the 30 year lifecycle in this study. Additionally, the fixed OWTs considered in the LCC have jacket foundations deployed at a depth of 45m, and as discussed in Chapter 2, cost estimates for the pile and jacket structures vary considerably for various water depths. Comparison of monopile to jacket substructure (Damiani et al., 2016) shows that a 35% reduction in support structure cost can be achieved for an OWT with a monopile foundation in 20 m water depth relative to an OWT with a jacket structure in 45 m water depth. Meanwhile, the overall balance of system (BOS) cost difference is only 10% with the offshore support structure fabrication, transportation, installation and other pertinent ancillary costs as it is a major component. Other research (Nielsen, 2003) argues that there is a 2% increase in support structure material costs for every additional meter of water depth regardless of what foundation concept is used. Since, the LCC allocates

Table 6.5: Extracted and adjusted LCC model data for the CAPEX, OPEX and D&D of a 500 MW offshore wind farm based on (Shafiee et al., 2016).

Cost element	Cost			Adjusted cost		
	Wind farm [bil	Per	installed	Wind farm [bil	Per	installed
	£]	MW	[mil	£]	MW	[mil
		£/MW]			£/MW]	
CAPEX	1.45	2.90		1.41	2.83	
OPEX	0.079	0.16				
D&D	0.20	0.40				

25.2% of its production and acquisition costs to the substructural component of the BOS, therefore, the 10% reduction for the overall BOS is considered as a sufficient adjustment factor for the cost.

$$\text{CAPEX}^{\text{adj}} = \text{CAPEX} - (\text{CAPEX} \cdot C_{ss} \cdot \text{BOS}^{\text{adj}}) \quad (6.3)$$

Where,  $\text{CAPEX}^{\text{adj}}$  is the adjusted CAPEX,  $C_{ss}$  is the percentage of CAPEX attributed to the substructural BOS and  $\text{BOS}^{\text{adj}}$  is the reduction factor of 0.1 for the BOS based on research (Damiani et al., 2016).

Table 6.5 tabulates the extracted and adjusted cost inputs for the model on a per wind farm as well as per unit of installed power basis.

A simplified calculation of the COE can be performed using Equation 6.4 adapted from Feng et al. (2010)

$$\text{COE} = \frac{\text{CAPEX} \cdot \text{FCR} + \text{OPEX} + \text{D\&D}}{E^{\text{ann}}} \quad (6.4)$$

where FCR is the annual fixed charge rate (%). The simplistic formulation yields the same results as the LCOE cost used in the Wind energy annual report (International Energy Agency, 2005), where the parameter FCR is a function of the discount rate (Feng et al., 2010). The discount rate is the aggregate of the interest and inflation, therefore, if inflation effects are removed from the analysis, the discount rate is solely represented by the interest rate. The FCR has high bearing upon the cost of energy since it contributes to the reduction of the highest cost component, namely, the CAPEX; with a 1% reduction in interest rate, the LCOE is expected to reduce by 5.3% (Shafiee et al., 2016) - 7% (Feng et al., 2010). Available data regarding FCR suggests that a 10% discount rate is an appropriate

estimate, therefore, this is used for further cost of energy analysis for the 500 MW wind farms.

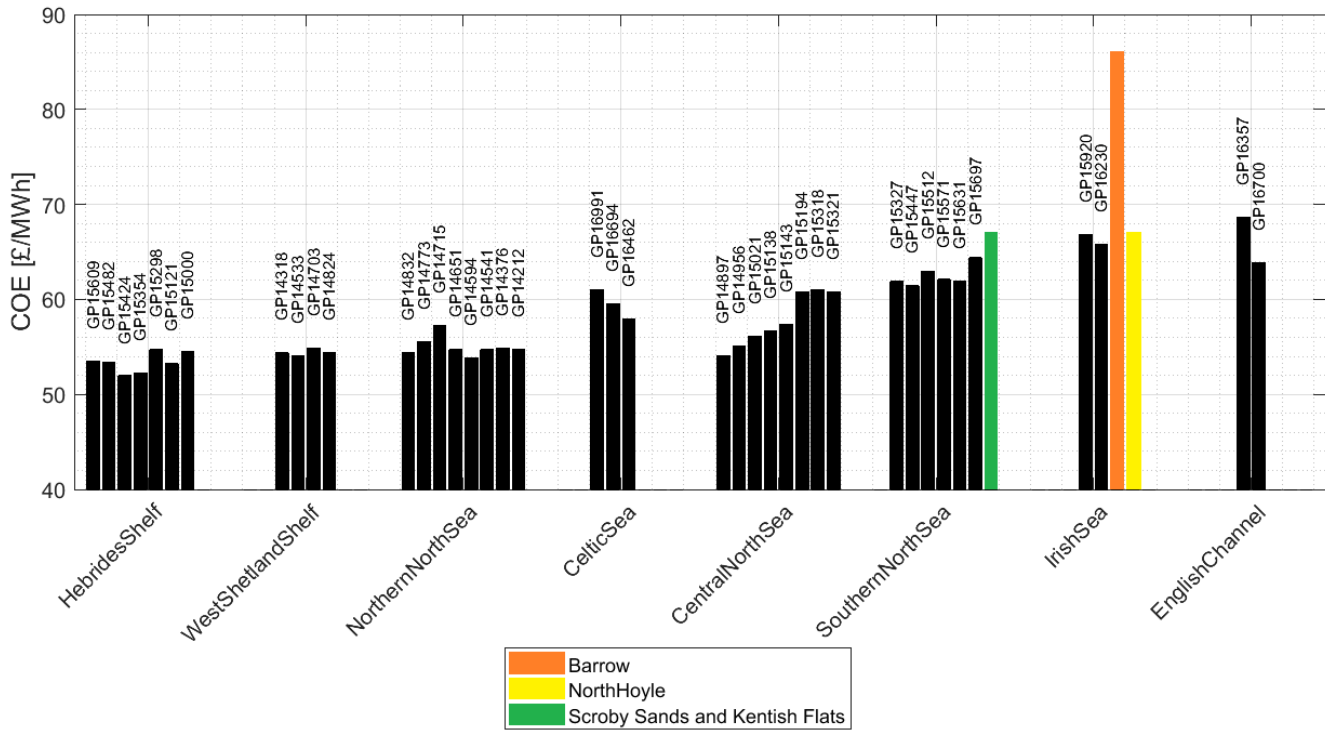


Figure 6.21: Comparison of reported COE by Feng et al. (2010) with the expected sub-regional COE distribution based on cost estimates for the CAPEX, OPEX and D&D by Shafiee et al. (2016).

Figure 6.21 shows the COE for a 500 MW wind farm composed of 100 5 MW fixed-bottom turbines deployed at each of the GPs in the FUGRO database. The range of COE at all sites is compared with those reported by Feng et al. (2010) for existing OWFs; two in the Irish Sea and the remaining in the Southern North Sea. While a general agreement is seen for both sub-regions, the COE reported by Feng et al. (2010) is higher for Barrow. This anomaly can be attributed to the gearbox replacements in 2007 that increased OPEX and reduced the power produced by the turbines considerably whilst the replacement activities were being conducted.

The comparison between the sub-regions in Figure 6.21 indicates that existing locations of OWE deployment are less lucrative than sub-regions with more dynamic conditions such as the Hebrides Shelf. This can, of course, be attributed to the higher energy production by each turbine as can be seen in Figure 6.17, which when scaled to farm-level increases by a factor of 100.

It is imperative to reiterate that these values are only meant to serve as an

indicator since numerous additional variables influence BOS and COE including, but not limited to, distance to shore, depth, design concept, wind farm effects and the maintenance strategy applied by the farm operators.

To incorporate the influence of fatigue damage in the COE, it is assumed that all subassemblies and components undergo an increase in duty cycles to the same extent and experience the same level of damage as the substructure. This simplification enables the damage to be translated directly to the CAPEX and OPEX.

### 6.4.1 Interaction between OPEX and revenue

To demonstrate the interaction of revenue and CAPEX,  $E^{ann}$  and  $D^{life}$  estimates for individual sites plotted in Figure 6.19 are used. The revenue generation is estimated by lifetime energy production of the turbine at each location exploring the lifetime extension possibilities as shown in Equation 6.5.

$$\text{Lifetime energy generation (TWh)} = \frac{E^{ann} \times DesLife}{D^{life} \times 1000} \quad (6.5)$$

The product of the adjusted CAPEX per unit installed capacity from Table 6.5 and variable FCR is used to provide an indicator for site-specific CAPEX adjustment based on the risk metric  $D^{life}$ . Variation in FCR is introduced based on the site-specific risk; locations with high risk are characterised by high FCR relative to locations with low  $D^{life}$ . The range of FCR is determined to be between 10% (Feng et al., 2010) and 12.6% (Stehly et al., 2016). These are fed into Equation 6.6 and are used to calculate CAPEX per unit power weighted by FCR which is plotted in Figure 6.22 against the lifetime energy generation for the various sub-regions.

$$\text{Risk-weighted CAPEX} = \frac{\text{Range of FCR} \cdot (D^{life} - \text{Minimum } D^{life})}{\text{Range of } D^{life}} + \text{Minimum FCR} \quad (6.6)$$

The large sensitivity of the CAPEX, and consequently the LCOE, to FCR can be observed since for a change of 2.6% in FCR, the CAPEX per unit installed power fluctuates by 30%. Benign locations with low  $E^{ann}$ , have a higher lifetime energy production due to lifetime extension if the turbine is assumed to function until it fails. They are also characterised by lower FCR due to the lower risk. For the more dynamic locations, improved revenue generation can be achieved by deploying larger turbines and reduction in FCR due to informed risk taking.

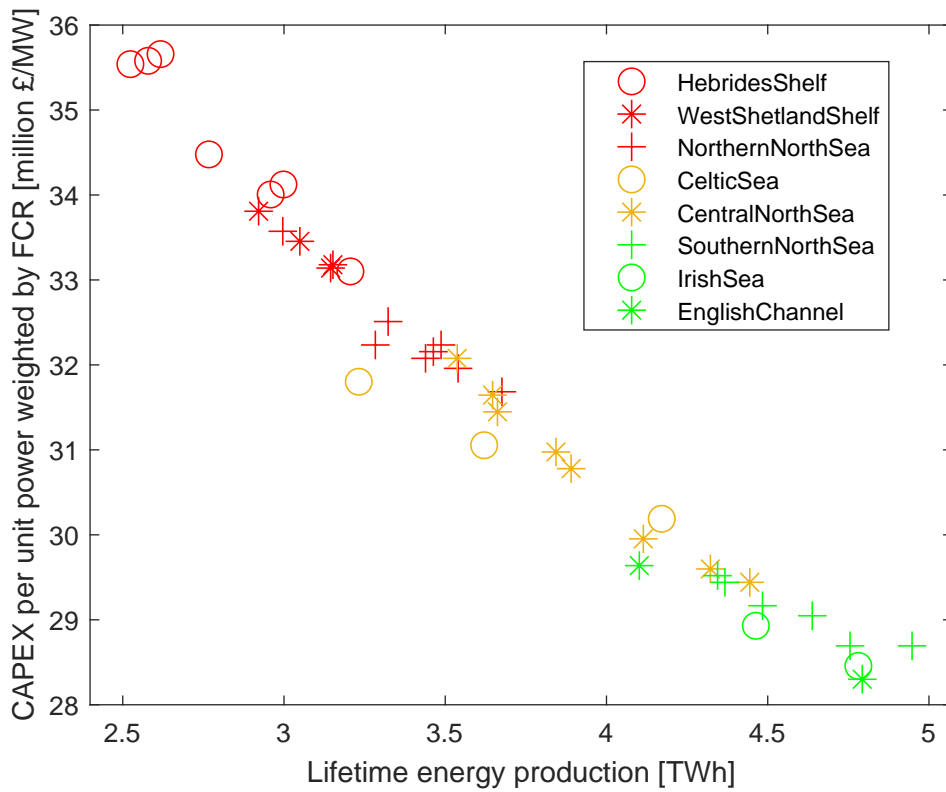


Figure 6.22: Revenue and CAPEX per unit power weighted by FCR for various sub-regions in the UKCS based on annual energy production and lifetime accumulated damage estimates.

### 6.4.2 OPEX adjustments

The quoted OPEX in Table 6.5 is divided into two major parts, the operation and maintenance, where the rental lease, insurance and transmission charges constitute the former while the latter is composed of direct and indirect maintenance costs. The employed maintenance regimes for the LCC are broadly categorised into the corrective and the proactive maintenance. As indicated by the names, corrective maintenance is carried out once the system has failed, whereas, proactive maintenance is a preventive measure to keep the device in a good enough state to avoid failure. Ideally, OWT asset managers should proactively maintain the structures to reduce the risk of failure, however, this would increase the cost of the overall O&M and a consequent increase in LCOE. Therefore, an efficient proactive maintenance strategy is significant to achieve cost-effectiveness.

Based on the the estimates by Shafiee et al. (2016), 43% of the overall OPEX is determined to display sensitivity to the maintenance frequency. This includes the proactive (19.8%) and corrective (16.9%) maintenance as well as the indirect cost (6.3%) of port fee, vessel cost and labour costs.

The damage at each site is normalised based on the average damage at all sites to acquire an adjustment factor for the OPEX as shown in Equation 6.7.

$$\text{OPEX}_{\text{adj}} = \text{OPEX} \times \frac{K^{DP} \text{ at GP}}{\text{Mean } K^{DP} \text{ across all sites}} \quad (6.7)$$

Figure 6.23 shows that fatigue normalised OPEX does not influence the COE significantly. This could be attributed to the relatively lower impact of OPEX to the COE relative to the  $E^{ann}$  and the CAPEX. Also, the adjustment factor does not discriminate between major and minor failures or replacement activities, therefore, has inherent assumptions due to the simplification of the process.

The comparison of modelled and empirical maintenance data for a population of 350 OWTs (Carroll et al., 2015) administered over a five year period shows a disconnect between the repair cost and failure rates, with a positive bias in the modelled data. Therefore, the above OPEX adjustments should be validated by the use of site specific data in the various sub-regions of the UKCS. To produce more comprehensive estimates, a complete RAMS database must be used with additional data within the methodology framework proposed by existing research (Hameed et al., 2011).



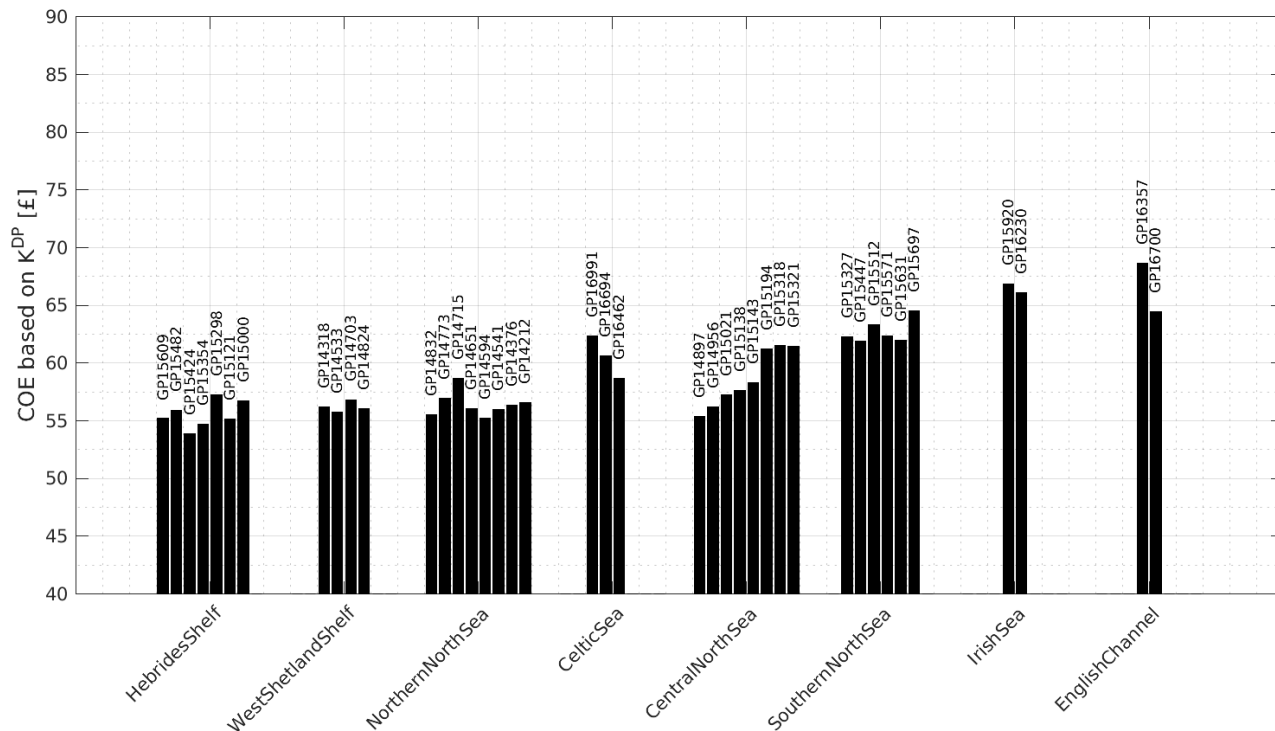


Figure 6.23: Sub-regional COE with fatigue-based OPEX costs factored in.

## 6.5 Chapter summary

This chapter promotes and implements the idea of a look-up table approach to facilitate damage calculations in the OWE industry. Structural response simulations for a  $20 \times 29 \times 23$  matrix with binned  $V_t$ ,  $H_s$  and  $T_p$  are run using FAST. The extrema from the simulation results are extracted using MExtremes. Long - term environmental characteristics for 40 sites in eight sub-regions of the UKCS are extracted from the NEXT database and the data is redistributed and rebinned to be consistent with the binning practice employed in the look-up table generation. Using the maximum load extracted by MExtremes and the occurrence probability of individual sea states in conjunction with the structural response generated by FAST, lifetime accumulated damage for each wind speed bins is calculated. The damage for individual  $V_t$  bins is aggregated to provide estimates for  $D^{life}$ .

A metocean - centric site selection metric, namely  $K^{DP}$ , is calculated as the damage per unit energy produced. This, in addition to annual energy production and lifetime accumulated damage, is used to quantify and visualise the spatial distribution of expected OWT performance in the eight sub-regions of the UKCS. Results indicate that the dynamic locations, such as the Hebrides Shelf provide

large energy generation potential but are also characterised by higher damage and  $K^{DP}$  in contrast to benign locations such as the Irish Sea. To conclude, a preliminary financial assessment is conducted to investigate the influence of higher damage on site-specific COE.



# Chapter 7

## Geospatial Mapping of Site Characteristics

Since a correlation between offshore location and lifetime damage is observed for various sub-regions in the UKCS in Chapter 6, this chapter presents the cumulative damage assessment at the mudline of a fixed OWT for the expanse of the UKCS and its adjoining areas. The analysis uses site-specific occurrence probability distributions from the ECMWF-ERA Interim database and the loads based on simulation outputs from the aero-servo-hydro-elastic tool FAST recorded in the look-up table. The aim is to produce thematic maps focusing on the spatial distribution of lifetime accumulated damage in the UKCS which is considered one of the main research contributions of this thesis.

Using this in conjunction with the power production at individual sites, the metocean-centric parameter is used to characterise the UKCS and its adjoining areas. A comparison of the accumulated damage and power production potential with the metocean-centric metric shows that the developed metric encapsulates the influence of both parameters sufficiently for site characterisation across the region.

### 7.1 Site-specific metocean characteristics

Spatial parameters of wind and wave from the ECMWF database are used to characterise the UKCS and its adjoining areas and contribute to the estimation of site characterisation parameters such as power production, accumulated damage

and  $K^{DP}$  (as described in Equation. 6.2). While the aggregated power from the FAST simulations in conjunction with the wind scatter plots provides information for the geospatial distribution of the energy produced, the accumulated damage is calculated by the methodology highlighted in Figure 6.5. Normalising the resulting damage by the energy production yields the metocean-centric metric  $K^{DP}$  for characterising the damage per GWh generated in various regions of the UKCS.

### 7.1.1 Input environmental parameters

The ECMWF's ERA - 40 database has been widely used for informing metocean conditions at offshore renewable energy sites (Barstow et al., 2009; Trøen, 2014) with data available from 1957 - 2002. This was an improvement on the ERA-15 reanalysis database from 1979 - 1993, however, the ERA-40 had a coarse grid of  $1.5^\circ$  reducing its usefulness in some locations.

For the scope of this project, however, metocean data from the extent of the UKCS is extracted from the ECMWF ERA - Interim database. ERA - Interim is the reanalysis of global atmosphere covering the period since 1979 continuing in real time to provide open-source data. The project was initiated in 2006 by improving key aspects of the ERA-40 with the vision of working towards a next-generation extended reanalysis. Reanalysis data is the analyses of the atmospheric and oceanographic quantities performed by processing available data using state-of-the-art forecasting models and assimilation techniques. This eliminates possible effects from variable analysis systems which may occur in operational analysis, however, influences of altered coverage and biases in the observing system are not eliminated.

The ERA-Interim reanalysis data by ECMWF provides global best estimates of numerous atmospheric and oceanographic parameters through a combination of modelled and observed data. Gridded multivariate data for 3-hourly parameters is available for a spatial resolution of  $0.75^\circ \times 0.75^\circ$ .

It conducts a four dimensional variational analysis and couples an atmospheric model to an ocean-wave model. Updated every month with a lag of two months to ensure quality assurance, the data can be downloaded as a batch using the provided Python script. The data may be downloaded at time 00:00:00 with a minimum of 6-hourly intervals for a wide selection of environmental parameters.

This provides a lower temporal resolution than the NEXT database, however, this is compensated by extending the period of the data record used from nine years to 10 years.

The chosen parameters relevant to calculation of structural loading for OWTs include:

- x- and y-components of the  $V - t$  vector at 10 m above MSL
- $H_s$  of combined wind waves and swell
- $T_p$
- 10 metre wind gust since previous post-processing

As discussed in Chapter 4, the dominant environmental parameters for fatigue analysis are  $V_t$ ,  $H_s$  and  $T_p$ , therefore, for this site characterisation study the influence of gust are not considered. Using the ECMWF's Meteorological Archival and Retrieval System, GRIB files are retrieved for the said parameters and  $V_t$  is calculated using the Pythagorean theorem for each pair of x- and y-components of wind speed velocity.

Since the ERA-Interim database allows only for the extraction of a rectangular grid, therefore, the extracted dataset is in the range of latitudes 48°N to 64°N and longitudes 24°W to 4°E defining the extrema for the scope of the UKCS. Furthermore, since the data is available in the finest resolution of up to 0.75° latitude and 0.75° longitude, therefore to achieve compatibility, the area is increased by 0.5° in the northern and eastern directions. The result is a grid with 23 rows and 39 columns with the following associated parameters:  $V_t$  at 10 m above MSL,  $H_s$  of combined wind waves and swell and  $T_p$ . It must be noted that the metocean parameters are point values extracted from the model at the geometrical centroid of the grid points, therefore, the parameters vary throughout grid cell but such variations have not been accounted for in this initial project.

Figure 7.1 a, c and e map the average of these parameters for Week 1 of 2017. The displayed parameter values are merely averages for the said week; they are in no way indicative of the extreme ocean conditions that the devices might be exposed to at these sites. It can be seen that the offshore wind resource is more abundant off the west coast relative to the east coast with wind speeds displaying an increase as the distance from shore increases. Similar trends can be observed

for the wave parameters of  $H_s$  and  $T_p$ , however, the distinction between the wave climate off the two coasts is more marked than the dominant wind conditions with  $H_s$  on the west coast about twice as much as that off the east coast. While the relatively benign wave climate off the east coast can be attributed to the lower wind speeds, the limited fetch also plays an important in limiting wave height. The locations of current OWE deployment, namely Southern North Sea and Irish Sea experience moderate wind resource accompanied by lower waves of around 2.5 m.

The mean peak period for the week indicates that while the western half of the UKCS is swell dominated with  $T_p$  of up to 10 s, the eastern half is mostly characterised by wind waves and local or regional swells with lower  $T_p$ .

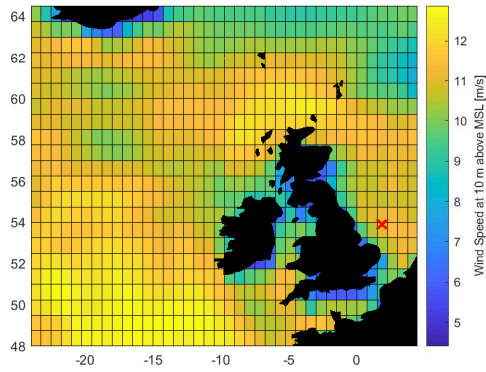
While  $V_t$  data is available for all locations of interest, due to the coarse mesh of the ERA - Interim dataset,  $H_s$  and  $T_p$  data in the territorial waters is sparse. As highlighted in Chapter 5, wave loads are highly significant for the determination of loads on offshore structures, therefore, the regions with no wave data are excluded from the analysis.

### 7.1.2 Comparison of the ECMWF and NEXT databases for site characterisation

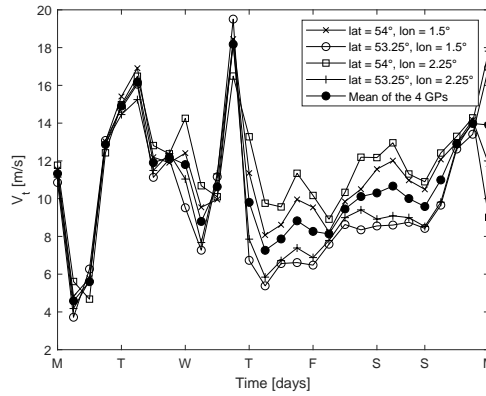
To highlight the differences in site characterisation parameters stemming from database selection, the HornSea Offshore wind project at  $53.883^\circ$  N and  $1.922^\circ$  E in the Southern North Sea is used as an illustrative example. The project lies in the ECMWF cell with margins at  $53.25^\circ$ - $54^\circ$ N and  $1.5^\circ$ - $2.25^\circ$ E.

To extract timeseries data for a point between the ECMWF grid points, deterministic (phase-revolving) models or spectral (phase-averaged) models may be used. A commonly used nearshore, shallow water model is the Simulating WAVes Nearshore (SWAN) (Holthuijsen et al., 2006) developed by Delft University of Technology. However, for this analysis of the comparison of the ECMWF and NEXT database, a rudimentary method is used to reduce computational effort. The GP with the least deviation from average metocean values of the four encircling grid points is considered to provide sufficient environmental information for the HornSea deployment site.

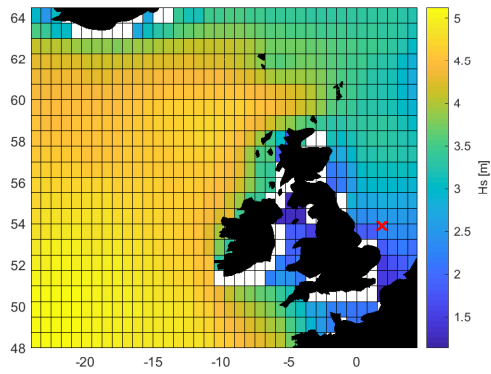
Figure 7.1b, d and f show the  $V_t$ ,  $H_s$  and  $T_p$  values at all four grid points for



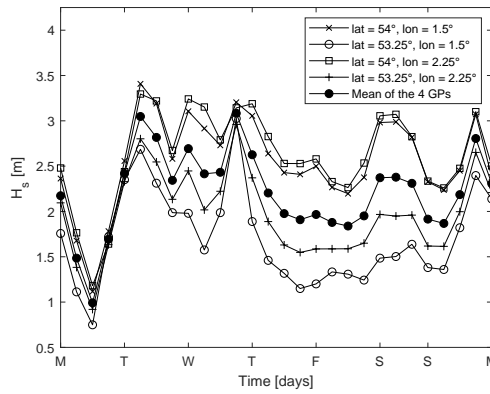
(a) Mean weekly  $V_t$  at 10 m above MSL



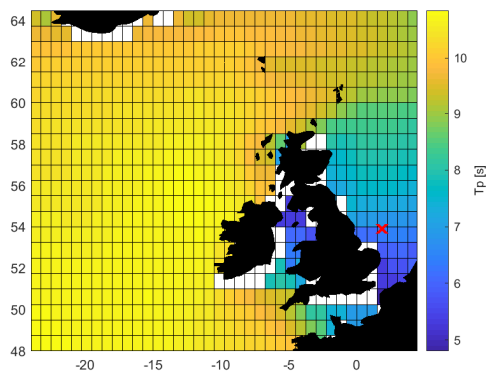
(b)  $V_t$  timeseries for select GPs



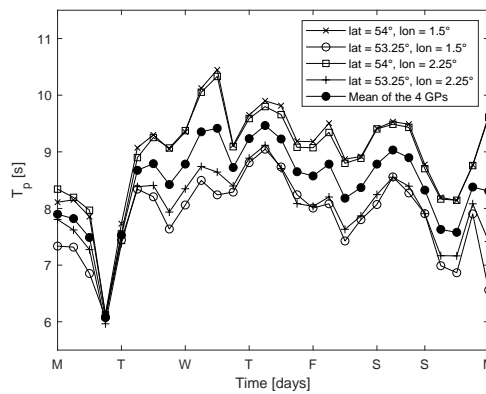
(c) Mean  $H_s$  for Wk 1, 2017



(d)  $H_s$  timeseries for for select GPs



(e) Mean  $T_p$  Wk 1, 2017



(f)  $T_p$  timeseries for select GPs

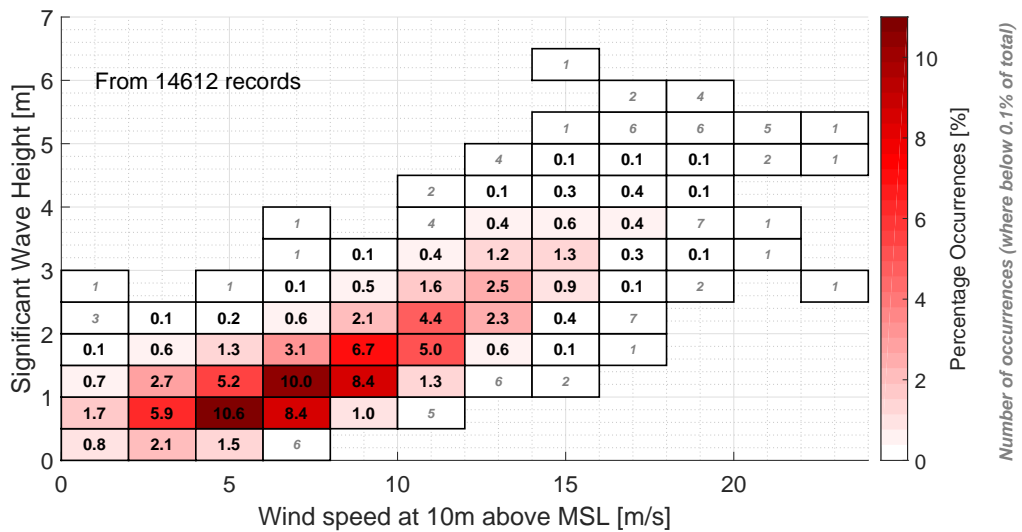
Figure 7.1: Mapped mean metocean parameters for Week 1, 2017 in the UKCS extracted from the ECMWF ERA-Interim dataset with time series at GPs around the HornSea offshore wind farm site. The farm site is marked by a red cross off the east coast of the UK.



week 1 of January 2017 for the site along with the mean for all four grid points. For the scope of this study, the metocean parameters at 54°N and 1.50°E are considered to be the best representation for all metocean parameters extracted from the ECMWF database for the lifetime damage assessment due to their proximity to the mean value of the enclosing GPs.

As discussed in Chapter 2, it is common practice in the offshore industry to express wave climate data as a 2-dimensional scatter diagram showing the probability of number of occurrences of each combination of  $H_s$  and  $T_p$ . Additionally, for the OWE industry,  $V_t$  must also be accommodated as a third dimension into the plots.

The ECMWF timeseries data for  $V_t$ ,  $H_s$ , and  $T_p$  are binned based on the binning parameters described in Table 6.1. The binning is performed to attribute midpoints to the data bins; as an example, for a  $V_t$  bin of 3 m/s, all values in the range  $\geq 2$  m/s and  $< 4$  m/s are included. Similarly, a  $H_s$  bin of 0.5 m includes all occurrences ranging from  $\geq 0.25$  m and  $< 0.75$  m. The resulting  $H_s - V_t$  scatterplot with 12  $V_t$  bins and 13  $H_s$  bins is presented in Figure 7.2.



renders a direct comparison of record numbers inappropriate. Therefore, a comparison between the percentage occurrence probability within each  $V_t$  bin between the two databases is tabulated in Table 7.1 and plotted in Figure 7.3. Without

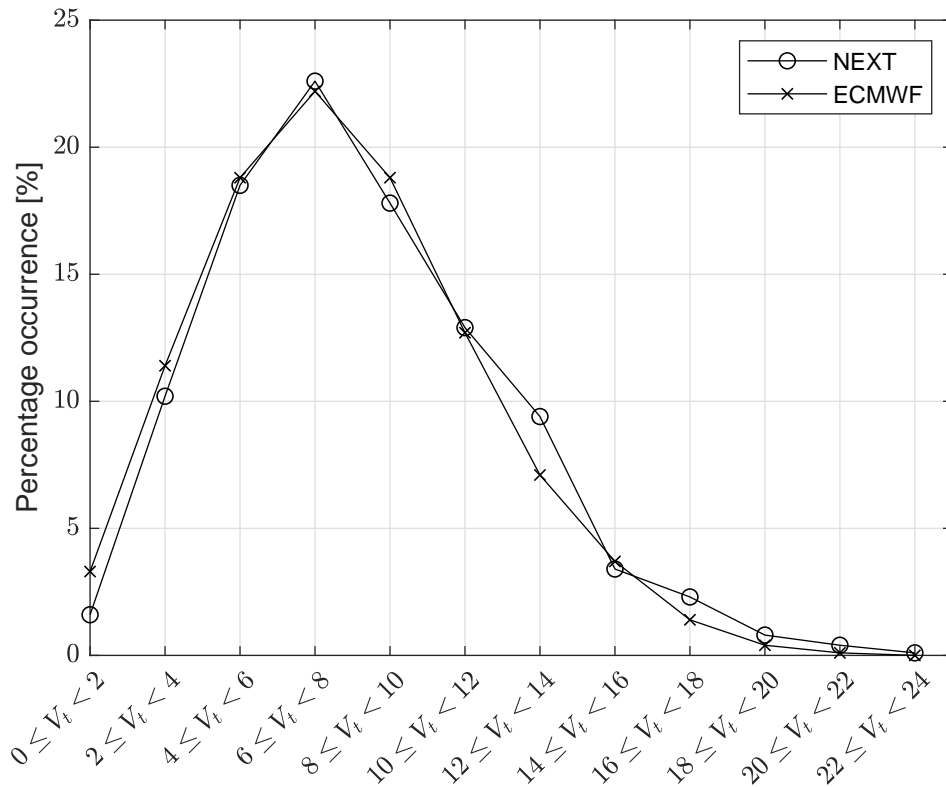


Figure 7.3: Comparison of the  $H_s - V_t$  scatter plot for the percentage occurrence probability of sea states for the HornSea site.

consideration of cells in the scatterplot with occurrences of less than 0.1%, the cumulative total for the NEXT database is 99.7%, whereas, that for the ECMWF database is 99.6%. For bins with an estimated number of occurrences above 78.8 and 14.6 for the NEXT and ECMWF databases, respectively, an additional 0.1% is added to the percentage bin occurrence.

The ECMWF database is seen to overestimate the occurrence probability of lower wind speeds while underestimating higher load cases; for the medium wind speeds, both databases show good agreement. As seen in Figure 6.10, lifetime damage at the mudline is dominated by damage incurred at moderate and high wind speeds. Therefore, the ECMWF database is expected to slightly underestimate the accumulated lifetime damage relative to the NEXT database.

Figure 7.4 shows the distribution of the damage incurred for the various wind speed bins at  $54^\circ\text{N}$  and  $1.50^\circ\text{E}$  of the ERA - Interim database representing the

Table 7.1: Comparison of the  $H_s - V_t$  scatter plot for the percentage occurrence probability of sea states for the HornSea site.

$V_t$ bin [m/s]	NEXT [%]	ECMWF [%]	$V_t$ bin [m/s]	NEXT [%]	ECMWF [%]
$0 \leq V_t < 2$	1.6	3.3	$12 \leq V_t < 14$	9.4	7.1
$2 \leq V_t < 4$	10.2	11.4	$14 \leq V_t < 16$	3.4	3.7
$4 \leq V_t < 6$	18.5	18.8	$16 \leq V_t < 18$	2.3	1.4
$6 \leq V_t < 8$	22.6	22.2	$18 \leq V_t < 20$	0.8	0.4
$8 \leq V_t < 10$	17.8	18.8	$20 \leq V_t < 22$	0.4	0.1
$10 \leq V_t < 12$	12.9	12.7	$22 \leq V_t < 24$	0.1	0.0

HornSea offshore wind site overlaying the outputs generated using the NEXTE database as previously shown in Figure 6.10.

The damage induced in the structure by the ERA - Interim database is seen to be distributed for wind speed bins of up to a maximum of 23 m/s relative to the 29 m/s for the NEXTE database, therefore, the ECMWF database does not account for these damaging load cases. The last three bins of the produced scatter plot from the NEXTE database in Figure 6.6b have an aggregate of 49 occurrences. While the occurrence probability of these high wind speed events is extremely low ( $\approx 0.06\%$ ), they have a relatively significant contribution to the accumulated damage, therefore, their influence should not be discounted in damage calculations.

The maximum damage-inducing wind speed bin is at 9 m/s in Figure 7.4 which may be attributed to the combined influence of a high probability of occurrence as seen in Figure 7.3 as well as a high load induced in the structure due to the wind speeds being close to the rated wind speed as discussed in Chapter 7. This is in agreement with the damage calculations performed using the NEXTE database.

It is noteworthy, that the damage induced by wind speeds below cut-in speed are also underestimated by the ECMWF database, by an order of magnitude. This does not agree with the higher occurrence probability of events in this  $V_t$  bin for the ECMWF (3.3%) than the NEXTE database (1.6%) as well as higher associated  $H_s$  of up to 3 m/s compared to 1.5 m/s for the NEXTE database. However, when the  $H_s - T_p$  scatter plots of the two databases for this wind speed are queried in Figure 7.5, it can be seen that the lower damage in the  $V_t = 1$  m/s bin for the

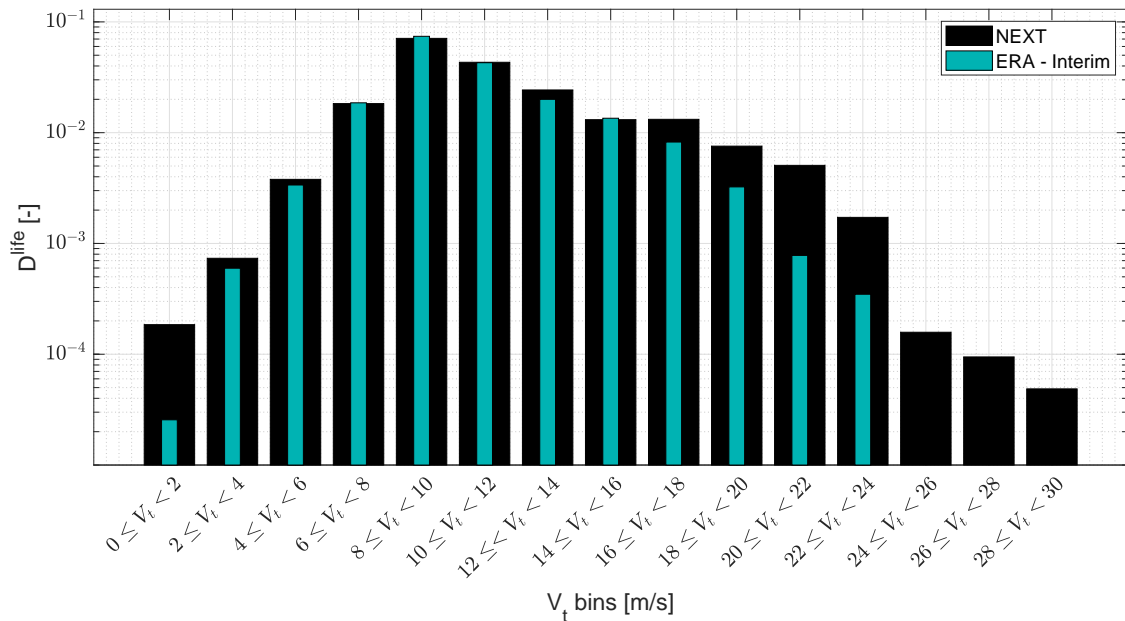


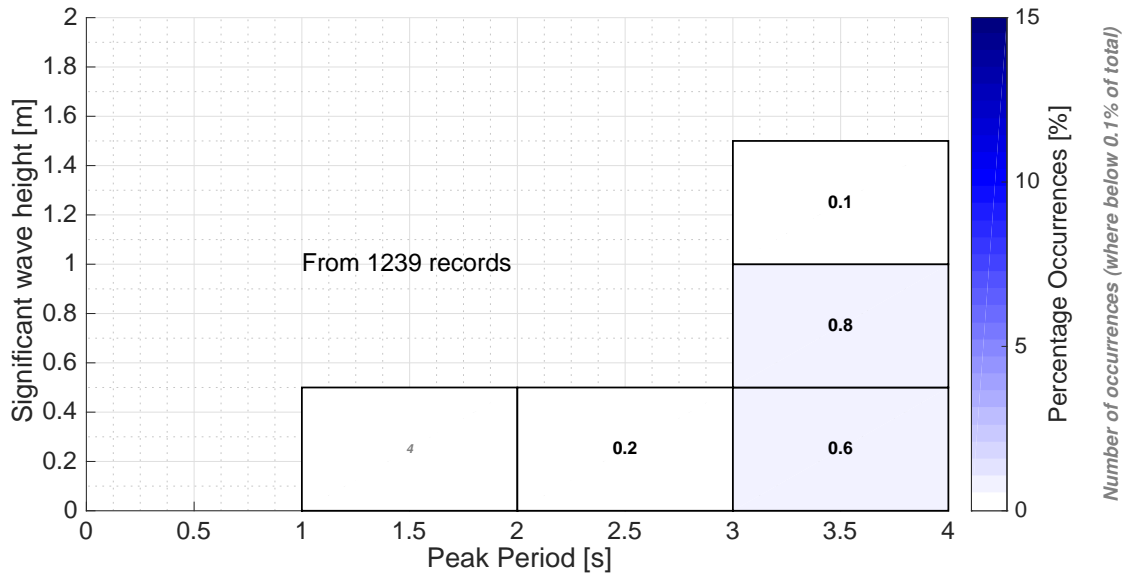
Figure 7.4: Comparison of the binned accumulated damage at the mudline for an NREL baseline turbine deployed at the HornSea OWF site with  $m = 4$ ,  $DesLife = 20$  and  $L^{Ult} = 5 \times L^{max}$  using the ECMWF-ERA Interim and the NEXT databases.

ECMWF data can be attributed to the generally higher  $T_p$  values associated to the  $H_s$  data.

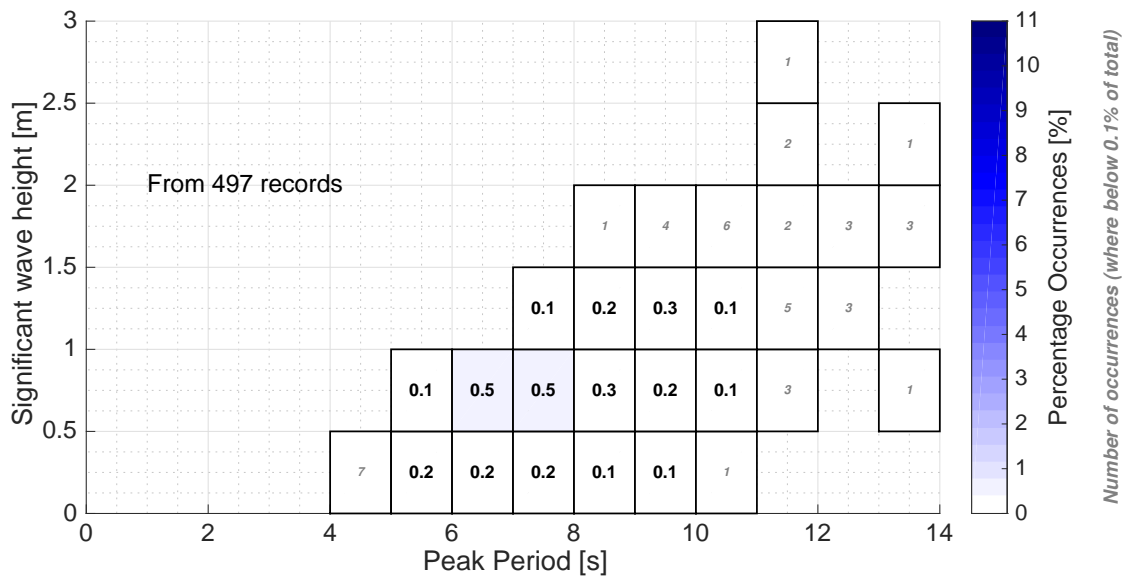
Figure 7.5 shows that for this  $V_t$  bin, the probability of  $H_s$  is mainly concentrated at bins of up to 1.25 m for both databases. However, the  $T_p$  values are observed to be considerably different with the NEXT database modelling a dominant  $T_p$  of about 3.5 s, whereas, the ECMWF database predicting higher values with larger spread between 5.5 - 9.5 s. Referring back to Figure 6.3, it can be seen that damage within the same  $H_s$  bin peaks at  $T_p$  of 4 s and 23 s which corresponds to the data distribution in the NEXT database. Therefore, the  $T_p$  distribution can be the cause of higher resultant damage for the wind speed bin under cut-in speed in the NEXT data relative to the ECMWF data.

The comparison of the accumulated damage for all wind speed bins between the two databases is shown for the best-, worst- and mean-case scenario in Table 7.2.

All scenarios are generated based on Table 6.3 for the range of MLife inputs that may be used for damage accumulation calculations. Comparing the accumulated damage estimates at the mudline of the NREL 5 MW baseline turbine in Table 7.2, it can be seen that for all combinations of  $m$ ,  $DesLife$  and  $L^{Ult}$  the NEXT



(a) NEXT data at GP 15571



(b) ECMWF data at 54°N and 1.50°E

Figure 7.5:  $H_s - T_p$  scatter plot for  $V_t = 1$  m/s using the NEXT and ECMWF databases for comparing the mudline damage at the HornSea offshore wind site.

Table 7.2: Comparison of the accumulated lifetime damage at the HornSea site based on the ECMWF and NEXT metocean datasets for the best-, worst- and mean scenarios generated by the fatigue variables.

Scenario	m	DesLife	$L^{Ult}$	ECMWF	NEXT	Percentage difference [%]
	[-]	[yrs]	[Nm]	[-]	[-]	
Best case	5	30	$20 \times L^{max}$	$2.79 \cdot 10^6$	$3.02 \cdot 10^6$	7.6
Mean case	4	15	$5 \times L^{max}$	0.139	0.152	8.6
Worst case	3	5	$1.25 \times L^{max}$	397	435	8.7

database overestimates the accumulated damage by about 7 - 9%. This can mainly be attributed to the general overestimation of occurrence probabilities in wind speed bins above rated wind speed by the NEXT database as seen in Figure 7.3.

For damage incurred due to wind speed bins above 24 m/s, this difference arises due to the lumped metocean data provided for these storm conditions in the NEXT database since this is not considered sufficiently representative of the prevalent environmental conditions. For wind speeds between the turbine rated speed and 28 m/s, the underestimation of the ECMWF may be due to the reduced temporal data resolution. The estimates are based on different temporal resolutions, using 6 hour metocean datasets to simulate structural fatigue damage potentially does not cover all events with higher loads relative to the hourly data available from the NEXT dataset.

## 7.2 Characterisation of UKCS and adjoining areas

Using the metocean data with a spatial resolution of  $0.75^\circ$  margining at the UKCS between  $48^\circ\text{N}$  to  $64.5^\circ\text{N}$  and longitudes  $24^\circ\text{W}$  to  $4.5^\circ\text{E}$  spanning over the decade from 2008 - 2017 with a temporal resolution of 6 hours, thematic maps for relevant parameters for OWE site characterisation are produced. These parameters include:

- Energy production
- Component - level lifetime accumulated damage

- Component - level  $K^{DP}$

Although wind data exists for all GPs, 129 coordinates do not have any associated wave data due to land cover. Therefore, of the total 897 coordinates, only 768 are further processed for extraction of these parameters.

As it was observed in Figure 7.1, there is a marked difference between the wave climate off the east and west coast of the UK, therefore, a comparative study of turbine siting off both coasts is also conducted with a demarcation at 2.5°W.

### 7.2.1 Resource characterisation

The energy potential at each grid point is calculated using the produced scatter plots for the wind occurrence probability in conjunction with the methodology established in Chapter 6.2.3.3 with adjustments for the 6 hour resolution of each record of the ECMWF database. Equation. 6.1 is used with  $T^{scat}$  adjusted as shown in Equation. 7.1:

$$T^{scat} = Occ_i^{tot} \times \Delta t \quad (7.1)$$

Where,  $Occ_i^{tot}$  is the number of records in the period under consideration and  $\Delta t$  is the temporal resolution of each record in the database.

Average energy production estimates for all the coordinates at offshore locations is conducted and presented as a heat map in Figure 7.6.

The total annual energy production for the 5 MW baseline turbine deployed at any location in the UKCS and its adjoining areas ranges between 12 to 34 GWh. As anticipated, the wind resource is seen to rapidly increase as the distance from the shore increases in Figure 7.6. While the North Sea and Irish sea display low resource potential, the abundant resource at the Hebrides Shelf and West Shetland Shelf lead to an increase in the energy produced from the same turbine located at these sites. Deployment sites off the east coast are observed to produce less energy relative to the sites off the west coast. This is expected since the power production is a function of the wind speed, therefore, the power production thematic map reproduces the patterns observed in the wind speed thematic map.

It is observed that energy production for the same turbine deployed across the UKCS can display a threefold increase depending on the chosen site. As a high level observation, the energy produced reduces as the site shifts from west

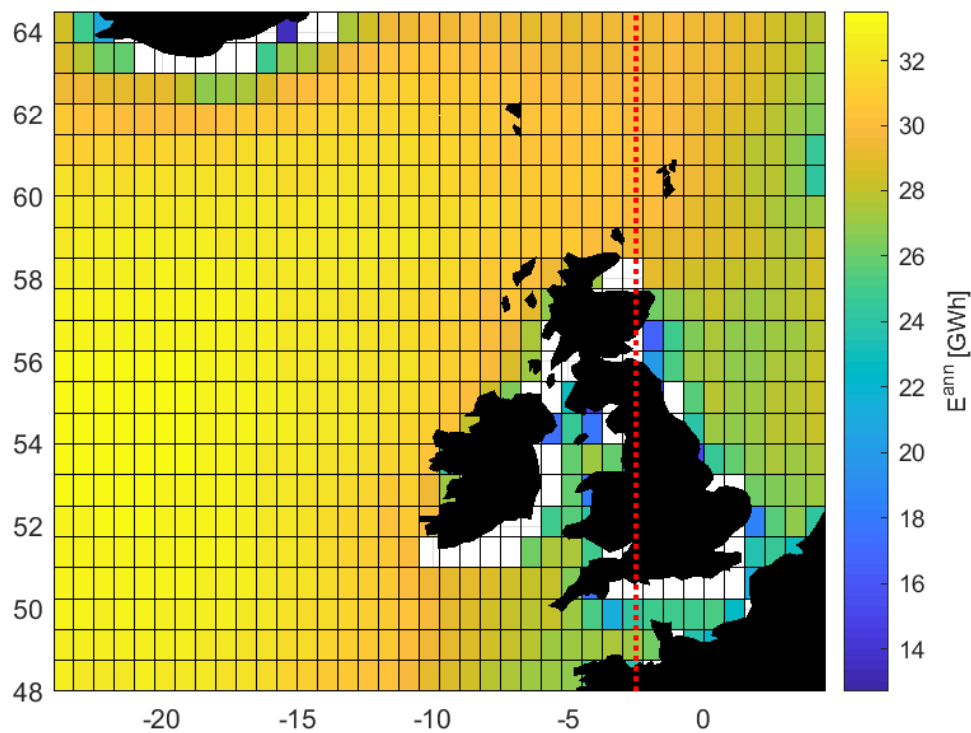


Figure 7.6: Heat map displaying the spatial distribution of  $E^{ann}$  for the NREL 5 MW baseline turbine deployed at the UKCS and its adjoining areas with the east and west coast demarcated at  $2.5^\circ\text{W}$ .



to east. The line segregating the energy production estimates off the east and west coast shows that while the energy production increases while moving from north to south off the west coast, trends are reversed for the east coast. The most sheltered regions in the UKCS, therefore, lie off its south-east coast. Most current installations populate this low energy production region of the UKCS in addition to the highly sheltered Irish Sea. Also, it can be seen that the spread in the power production data increases towards the east. Therefore, while the east coast provides a range of power production potential, the sites off the west coast display less variation in expected energy generation.

The next section presents a damage characterisation in order to supplement the geospatial resource and energy generation estimates.

### 7.2.2 Damage characterisation

The damage characterisation presented in this section is relevant for longitudinal welds at the mudline of the fixed NREL 5 MW baseline turbine. A Wöhler exponent of 4, design life of 15 years and ultimate load five times of  $L^{max}$  are chosen in continuation of the analysis performed for the grid points using NEXT data in Chapter 6. The resulting damage for each wind speed bin at each site is aggregated and represented in Figure 7.7 for characterisation of damage at the turbine mudline at various sites.

The accumulated lifetime damage distribution ranges between 0.04 to 0.26 at the UKCS and exhibits similar trends as the power production, with increased damage as the distance from shore increases as displayed by Figure 7.7. OWTs deployed at the Hebrides and West Shetland shelves are expected to be exposed to highly damaging environmental parameters whereas those in the North Sea and Irish Sea are expected to experience considerably lower damage. The difference between the damage envelopes off the east and west coasts is not as strong as that displayed by the energy production metric, however, the sites off the east coast can generally be characterised by a lower lifetime damage estimate relative to those off the west coast.

The scatter of the lifetime accumulated damage in Figure 7.7 shows that damage can display an increase of about five times relative to the three times increase in power production based on the allocated site of the OWT. A decrease in damage

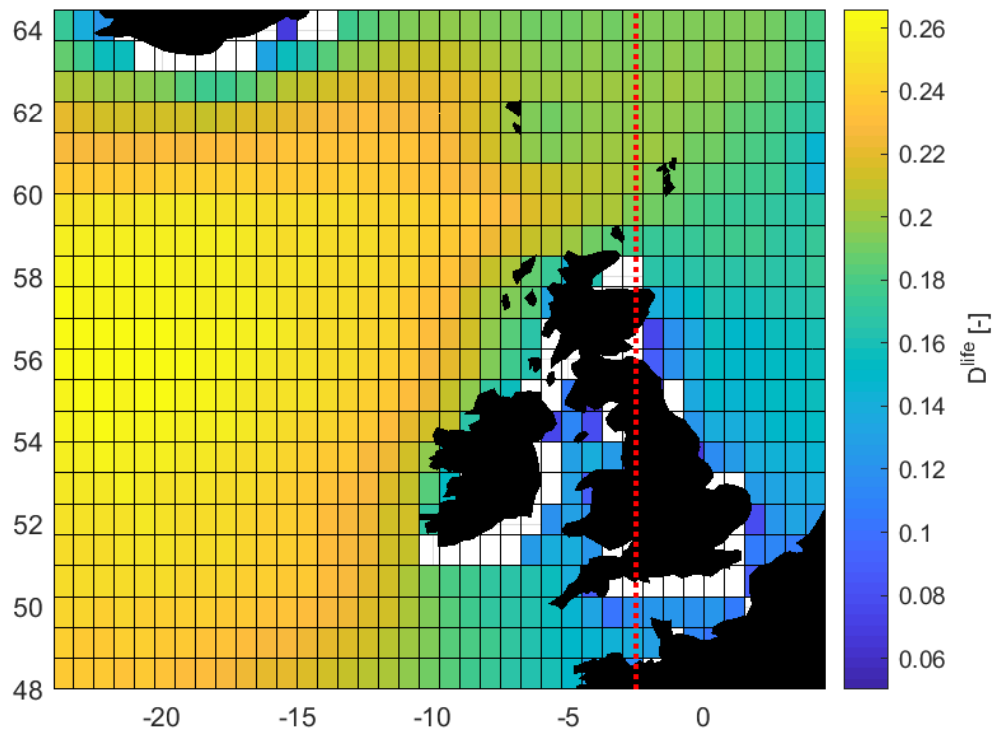


Figure 7.7: Heat map for the spatial distribution of  $D^{life}$  at the OWT mudline for the UKCS and adjoining areas using  $m = 4$ ,  $DesLife = 15$  years and  $L^{Ult} = 5 \times L^{max}$  with the east and west coast demarcated at  $2.5^\circ W$ .

life is observed for grid points moving east, however, the gradient of this decrease is higher than that for the energy production scatter. Similar to the energy production scatter, a reversal of the damage rate is observed between the sites off the east and west coast; the former characterised by an increase in damage with an increase in latitude and the latter displaying reduced accumulated lifetime damage.

The next section explores the relationship between the expected annual energy production and accumulated lifetime damage for various sites to establish their combined influence.

### 7.2.3 Combined power and damage characterisation

The importance of a metocean-centric site characterisation parameter has been discussed in Chapter 6 with the development of  $K^{DP}$  to compare the various sub-regions in the UKCS. The proposed methodology is suitable for representing the site-specific performance of an OWT deployment across the UKCS and its adjoining regions.

Prior to the presentation of the  $K^{DP}$  metric incorporating the influence of energy production and accumulated damage, the relationship between the two parameters is investigated.

#### 7.2.3.1 Correlation between power and damage

As displayed in Figure 7.6 and Figure 7.7, the energy produced and damage incurred by the fixed NREL baseline turbine are positively correlated. To further understand this relation and the influence of longitudinal coordinates, Figure 7.8 plots this relation based on the longitude of each site employing the portfolio analysis discussed in Chapter 6.3.

The two performance metrics are seen to be positively correlated, that is, an increase in energy production at the site is accompanied by an increase in fatigue damage to the turbine. The maximum density of GPs is found in RI and these locations are characterised by high energy production and associated increase in accumulated lifetime damage. A significant number of offshore sites also reside within RIII and RIV. Continuing the demarcation of the east and west coast at  $2.50^\circ$  W, it is seen that regions off the west coast predominantly lie in RI, whereas, moving east reduces the damage at a higher rate than reduction in power

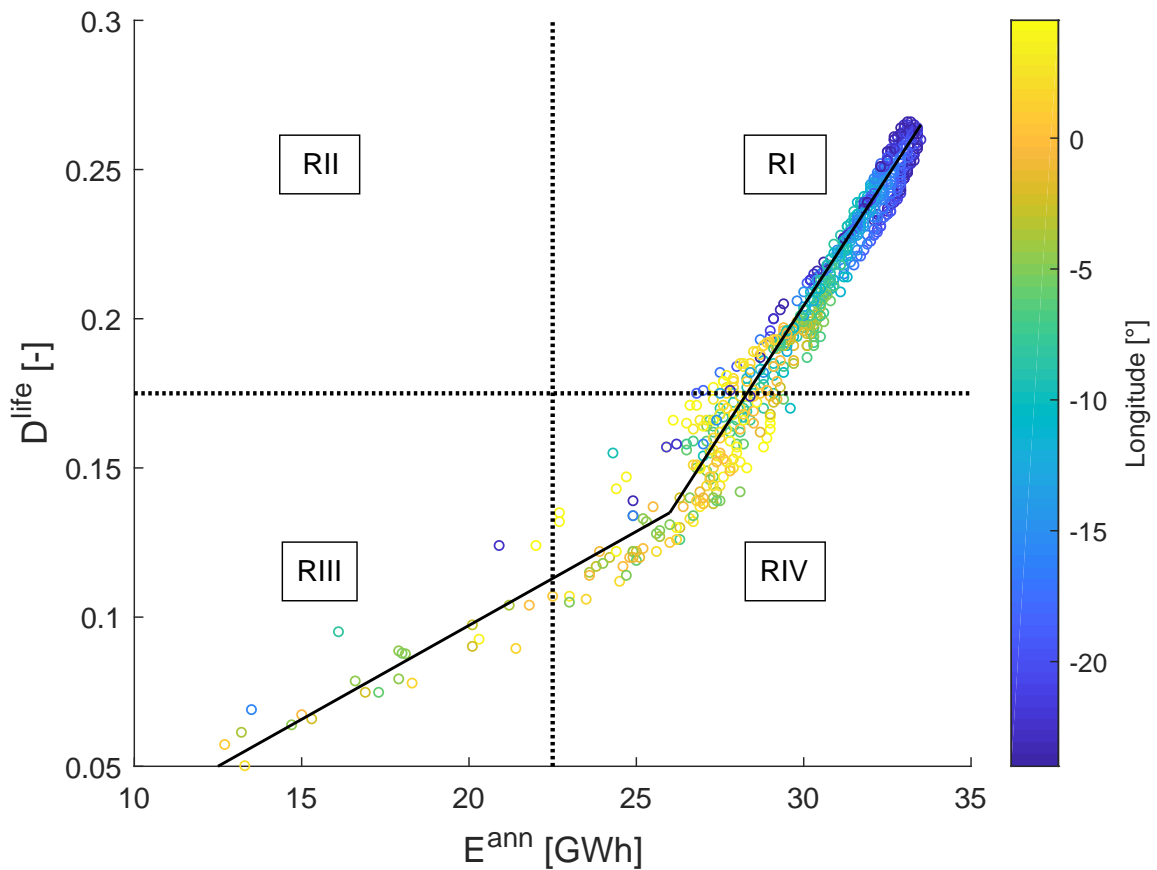


Figure 7.8: Portfolio analysis for the accumulated lifetime damage at the mudline and annual energy production for the NREL 5 MW turbine deployed at the UKCS and its adjoining areas. The bilinear relationship between  $E^{ann}$  and  $D^{life}$  is also highlighted.

production. Therefore, the deployment sites at the east could generate higher energy yields for the same unit damage.

### 7.2.3.2 Spatial distribution of the $K^{DP}$ parameter

Amalgamating the influence of the energy production and lifetime damage accumulation characteristics to produce a performance metric presenting the damage per unit of power generated provides an improved site characterisation parameter. Therefore, using the formulation in Equation. 6.2,  $K^{DP}$  for each offshore coordinate is estimated to provide an approximation of the influence of metocean parameters on OWT siting. The resulting spatial distribution of  $K^{DP}$  is displayed in Figure 7.9.

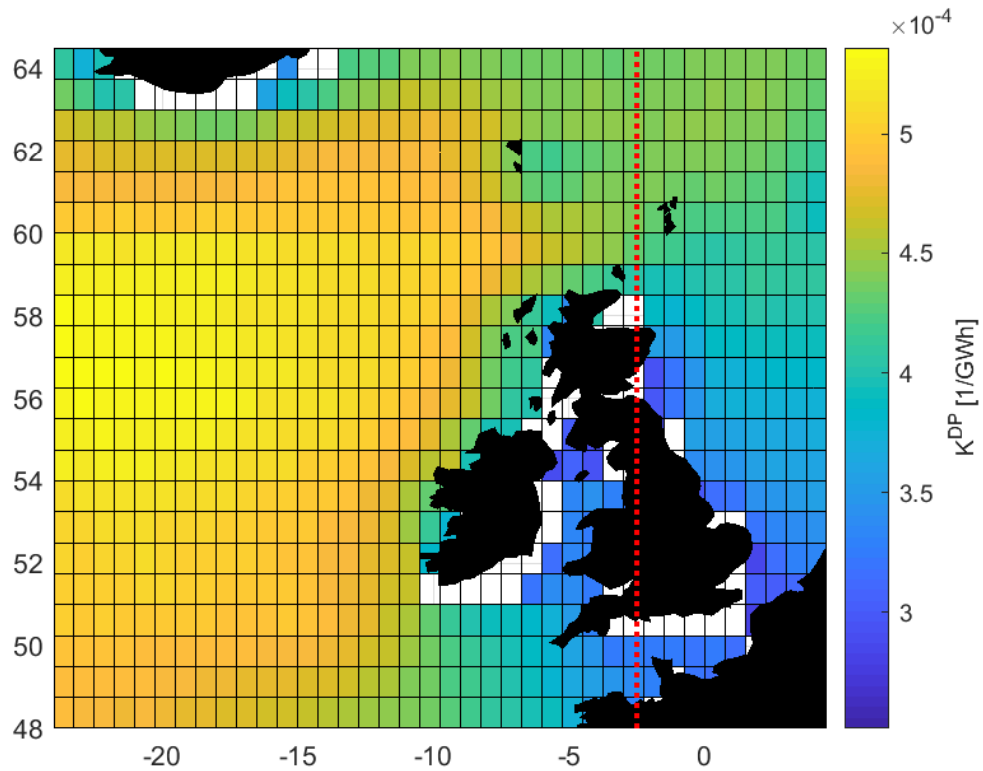


Figure 7.9: Heat map for the spatial distribution of  $K^{DP}$  for a 5 MW turbine with design lifetime of 15 years at the UKCS and its adjoining areas with the east and west coast demarcated at  $2.5^\circ\text{W}$ .

As the sites move further away from the shore, they are marked by higher  $K^{DP}$ , therefore, have a higher damage per unit energy produced. Additionally, the regions off the east coast are characterised by lower  $K^{DP}$  relative to those off the west coast by up to a factor of two.

The maximum and minimum  $K^{DP}$  for the UKCS and adjoining regions can only be differentiated by a factor of two. As seen in Figure 7.9, the  $K^{DP}$  distribution shows high correlation with the damage profile of the mudline across the UKCS and adjoining regions. The next section further investigates the dependence of  $K^{DP}$  on the environmental parameters to identify the key metocean parameter for this risk-return metric.

### 7.3 Dependence of $K^{DP}$ on the environmental parameters

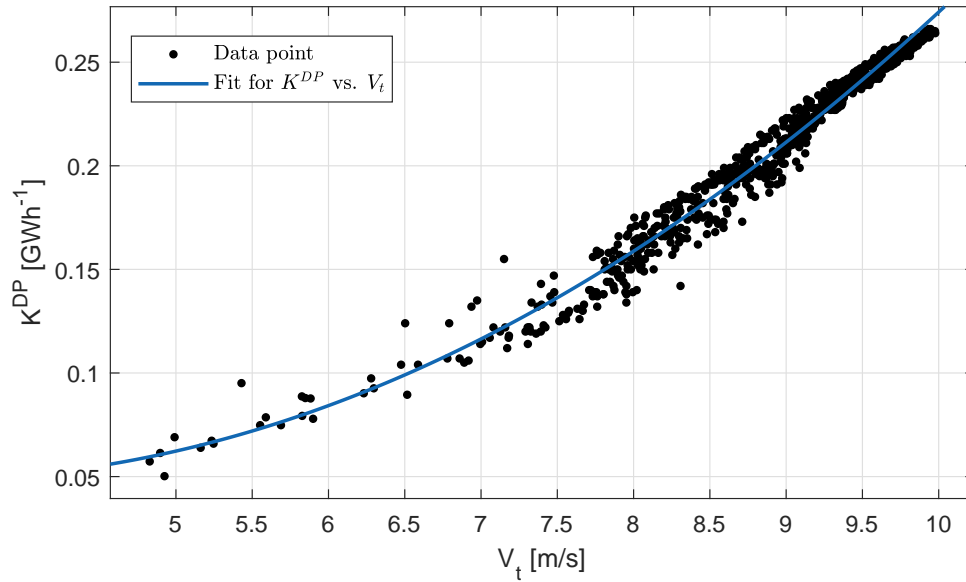
Energy production from an OWT depends on site windspeed, whereas, the structural damage is characterised by wind and wave loads at the site. Therefore, it is of interest to quantify the dependence of damage per unit energy on the metocean characteristics of the deployment location. Figure 7.10a and 7.10b describe the influence of average annual wind speed and significant wave height on  $K^{DP}$  at sites across the UKCS and its adjoining areas, respectively.

$K^{DP}$  is observed to be positively correlated and is expected to increase non-linearly with an increase in both environmental parameters. However, there is a stronger influence of wind speed on the damage per unit energy production than wave height; the increase in  $K^{DP}$  is similar when  $V_t$  is doubled or  $H_s$  is increased over threefold. The larger dependence on wind speed may be explained by the contribution of  $V_t$  to both the energy production from and damage inducing loads on the OWT.

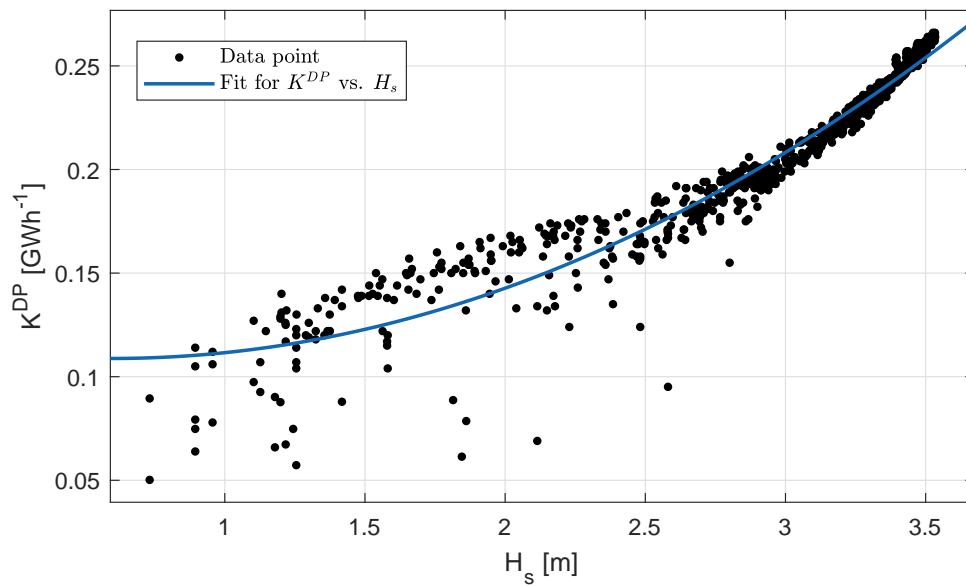
The  $K^{DP} - V_t$  fit has a root mean square error of 0.007 relative to 0.011 for the  $K^{DP} - H_s$  fit, therefore, both  $H_s$  and  $V_t$  can be used for  $K^{DP}$  estimation. However, the residuals resulting from fitting a quadratic distribution to both parameters in Appendix G show that the  $K^{DP} - V_t$  model is better suited for estimation of damage per unit energy produced than  $K^{DP} - H_s$ .

### 7.4 Chapter summary

Observing differences in location - specific OWT performance indicators for various sub-regions in the UKCS in the previous chapter, the Stream 2 methodology is



(a) Distribution and fit of  $K^{DP}$  on the annual  $V_t$ .



(b) Distribution and fit of  $K^{DP}$  on the annual  $H_s$ .

Figure 7.10: Dependence of the damage per unit energy on the annual average  $V_t$  and  $H_s$  at sites across the UKCS and its adjoining regions.

applied to metocean data from the ERA - Interim database for the UKCS and adjoining areas in this chapter. A comparison between the occurrence probability and consequent lifetime damage estimates using the ECMWF and NEXT data highlights the sensitivity of the site characterisation metric to the input metocean data. While both databases experience maximum damage in the same wind speed bin, the NEXT database overestimates lifetime accumulated damage for most wind speed bins.

The three location - dependant performance metrics, namely  $E^{ann}$ ,  $D^{life}$  and  $K^{DP}$ , replicate similar trends between sub-regions as observed in Chapter 6. There are discernible differences between deployment locations off the east relative to the west coast and the parameters also exhibit a change as the distance-to-shore increases. The chapter concludes with the investigation of the dependance of  $K^{DP}$  on wind and wave parameters.





## **Part IV**

### **Discussion and Conclusion**



# Chapter 8

## Discussion and Concluding Remarks

Currently, the OWE industry relies on mapping techniques for resource assessment, bathymetric analysis and identifying project locations. With reliability identified as a crucial issue for the advancement of the OWE industry in the UKCS, this thesis proposes the extension of mapping methods for the representation of reliability parameters. The contributions of this thesis are discussed in this chapter, together with the main limitations of the work. Furthermore, recommendations are made for future research that may be performed building on this thesis.

### 8.1 Discussion of research outcomes

At the outset of the thesis in Chapter 3, the lack of suitable site-specific failure rate data was identified and the aim to quantify site-specific failure rates was established as a consequence. While a generic reliability assessment using OWE industrial failure rates allows farm operators to compare the performance of their installations to industrial benchmarks, it does not provide the comprehensive understanding of failure rate variation between various locations. Therefore, improved quantification of failure rates for OWTs using maintenance logs, strain-gauge measurements or modelled load profiles based on the variable environmental conditions is significant to encapsulate regional influences.

### 8.1.1 Site-specific structural response

Structural elements of an offshore wind turbine experience loading by metocean parameters of wind, wave and tidal currents. The quantification of the lifetime loading and duty cycles for structural subsystems can allow for a more informed quantitative reliability assessment. To improve the reliability estimates based on site-specific conditions, a comprehensive dynamic response analysis of the structural components is conducted in Chapter 5. Using LLCs for site specific data from the K13 shallow water site, the turbine is simulated for elementary DLC 1.2 and 6.4 based on the incident wind speed. Possible influence on turbine lifetime from transient events and fault conditions is not accounted since the influence from these events is highly dependent on user-defined occurrence frequencies as discussed in Chapter 4.

No power production occurs for LLCs within DLC 6.4, whereas, an increasing amount of power is generated for LLCs above cut-in speed (LLC02) until the output power stabilises at rated power (LLC06). Figure 5.3 displays that the dominant loads on the support structure are due to the bending moment which exceed the shear forces by at least an order of magnitude at the tower top, transition piece as well as at the mudline.

Since fatigue for wind turbines can be characterised by DELs (Løken, 2009), an investigation into the short-term DELs induced by bending moment in Figure 5.7 shows that for all investigated nodes, LLC06, LLC12 and LLC17 experience higher DELs. Whilst the first two LLCs experience operational loads since they lie within the operational  $V_t$  range for the turbine, the DELs at LLC17 are purely due to the increased wind and wave loading. Within the operational  $V_t$  range, DELs display a uniform increase until LLC06 whereby the  $V_t$  gets close to the turbine's rated speed of 11.4 m/s, further increase in wind speed leads to reduced DELs due to the damping effect of turbine operation up to LLC09. Thereafter, the offset in DELs due to operational damping is overcome until the DELs experience their highest peak right before  $V_{out}$ .

Weighting the power production of the OWT by the fatigue characteristics shows that the most favourable LLCs for the turbine operation are below rated speed with the maximum power production per unit damage as seen in Figure 5.8. Therefore, due to the reduced damage per unit energy produced, the reliability-

centered OWT performance with regard to the DEL is optimum at wind speeds lower than rated speed. This is an interesting finding, as it is counter intuitive to the yield-centered generation optimum.

### 8.1.2 Identification of reliability-critical subassembly

An increase in structural reserves at the end of the turbine design lifetime is observed by the deployment of the structure in relatively benign conditions compared to the nominal design.

As seen in Figure 5.3, Figure 5.5 and Figure 5.6 the loads and consequent DELs show a considerable reduction for components of the support structure as the distance increases from the mudline. The shear forces at the tower top display a reduction by a factor of three, bending moments by an order of magnitude and lifetime DELs by a factor of 16 compared to mudline. Load characterisation on the mudline is in accordance with previous research findings (Løken, 2009; Jason Jonkman, 2007) showing that the two load peaks occur, first at the LLC closest to the rated power and the second at the LLC with the highest  $V_t$  and  $H_s$ . LLCs within DLC 6.4 display no operational natural frequencies in the dynamic response of the support structure but may be characterised by high amplitude cyclic response for  $V_t > V_{out}$ .

Summarising these results over turbine lifetime, Figure 5.6 shows that the support structure at the mudline experiences lifetime DELs of about ten times as much as the tower top. Existing literature (HBM Test and Measurement, 2016; Tempel, 2006) also identify the region just above and below the seabed as critical design drivers for support structures since these are areas of greatest strain in the structure.

From a financial perspective, it is anticipated that innovations in support structure may contribute to a 4% reduction in LCOE. Since the OWT foundation contributes to approximately 70% of the support structure cost (BVG Associates, 2012), therefore, fatigue analysis at the mudline of the support structure is used as a representative case to establish the proposed methodology.

### 8.1.3 Sensitivity analysis of turbine response characteristics and fatigue life

Based on recommendations by existing research, as identified in Table 5.3 and 5.6, numerous variables are investigated for their influence on the turbine damage at the mudline including:

- Wind and wave seeds - Alternately varying the wind and wave seeds shows that the distribution of damage life for the OWT has a higher spread based on the variation of wave seeds than wind seeds. With a standard deviation of 0.365 for the lifetime damage estimates for 36 wind seeds (Figure 5.11) compared to 0.462 for the wave seeds (Figure 5.12), Section. 5.4.1.3 shows that for the selected set of environmental variables, the significance of the number of wave seeds is higher for the modelled structural system lifetime estimates.
- Simulation length discretisation - Load estimates for the fore-aft bending moment of the support structure at the mudline show negligible improvement for a simulation length of 10 hours divided into seed sets of 10 to 60. Therefore, if the total time is kept constant, there is limited value in the distribution allocated to the number of seeds run. However, for the consequent fatigue life, longer simulations with lower number of seed sets deliver the advantage of reducing the number of residual cycles (Haid et al., 2013). Therefore, the fatigue life calculated for a 10 hour simulation is expected to have improved representation when performed in 10 sets of 1-hour long simulations than 60 sets of 10-minute simulations.
- Lifetime load extrapolation distributions - For single parameter fatigue calculations, the Weibull distribution of the wind speed may be used effectively in the absence of the probability of individual load cases as seen for the K13 shallow water site in Figure 5.15. However, for a comprehensive assessment based on site conditions, a multi-parameter distribution must be used accounting for the variation of both wind and wave parameters using the occurrence probability associated to each sea state.
- Residual cycle counting - Rainflow counting for the fatigue analysis of a typ-

ical wind turbine is not expected to have a large number of partial cycles (G. J. Hayman, 2012), since either longer load history time series are considered or multiple short time-series are concatenated so that most cycles are expected to be closed (Sutherland, 1999). However, for the 10-minute simulations considered in Figure 5.16, short term DELs for LLCs between the rated and cut-out wind speed show significant sensitivity to the method employed to account for unclosed cycles. With possible  $DEL^{ST}$  variation of up to 25% between counting residual cycles as full cycles or discarding their influence, the half-cycle approach is found to be a good compromise for residual cycle counting.

- Goodman correction - The influence of mean loads on the fatigue life of the support structure at different nodes shows considerable variation and should therefore, be accounted in the fatigue analysis. While the tower top displays the highest influence of the correction with a 40% increase in DEL estimates, a significantly reduced change (of 10%) is seen in DELs at the mudline in Figure 5.18 with the Goodman fit. Therefore, the structure experiences close to fully reversed bending at the mudline with a low mean stress for all amplitudes.
- $L^{Ult}$  methodologies - For determination of the  $L^{Ult}$  for the lifetime accumulated damage, three methods are compared. The limitations associated to each method are as follows:
  - Application of  $L^{max}$  from onshore data - Inherent limitation due to the use of onshore data can be overcome by the choice of  $ULF$  as shown in Matha et al. (2010). However, the heuristic determination of  $ULF$  between the recommended value of 1.25 - 20 introduces an uncertainty in the order of six for estimates of accumulated lifetime damage estimates as displayed in Figure 5.22.
  - Application of  $L^{max}$  from offshore data - As seen in Figure 5.22, fatigue life calculated using offshore data exhibits a logarithmic offset in the order of three from that calculated using onshore data for the same  $ULF$ . Similar to the application of  $L^{max}$  from onshore data, uncertainty associated to the determination of  $ULF$  effects the results.  $ULF$  influences



onshore- and offshore-determined  $L^{Ult}$  to the same extent since the offset between  $D^{life}$  estimates remains constant across all  $ULF$  values.

- Application of the formulations for normal and axial strength - The flexure formula (Equation. 4.12) only applies to a simple beam undergoing pure bending, whereas, the the maximum stress formulation (Equation. 4.14) is for a beam undergoing shear forces only. However since an OWT support structure is exposed to a combination of both shear forces and bending moments, therefore, the application of this method can only be applied under the assumption of isolated loads.

Therefore, for an improved estimation of fatigue life from structural response simulations, a cross-sectional analysis for a complicated multi-component stress state including effects of axial, shear and bending forces should be performed. Particularly,  $L^{Ult}$  for nonaxisymmetric cross sections of anisotropic material should be calculated through analysis methods such as FEA of the cross section of the component being investigated.

- Availability factor - Due to the contribution of operational loads to the fatigue life of an OWT, the utilisation of a site-specific availability factor can improve the robustness of damage estimates. As Figure 5.23 depicts, wind turbines located at an ideal site with  $V_t$  speeds always within the operational range have a higher system availability and can be categorised with a higher capacity factor, however, they provide limited scope for lifetime extension of turbines due to higher incurred damage over the design lifetime.

The sensitivity analyses in Chapter 5 is supplemented by further analysis in Chapter 6 through the sensitivity analysis based on structural design input parameters such as the Wöhler exponent ( $m$ ),  $L^{Ult}$  and the prescribed design lifetime ( $DesLife$ ). A considerably larger variation in lifetime accumulated damage is seen when structural design input parameters are varied relative to the parameters listed above. Therefore,  $m$ ,  $L^{Ult}$  and  $DesLife$  are the dominant parameters for fatigue damage calculation of an OWT.

Figure 8.1 summarises the influence of these three parameters on  $D^{life}$  of the support structure at the mudline. The material properties of the steel, namely  $m$  and  $L^{Ult}$ , have maximum bearing on the lifetime accumulated damage. Therefore,

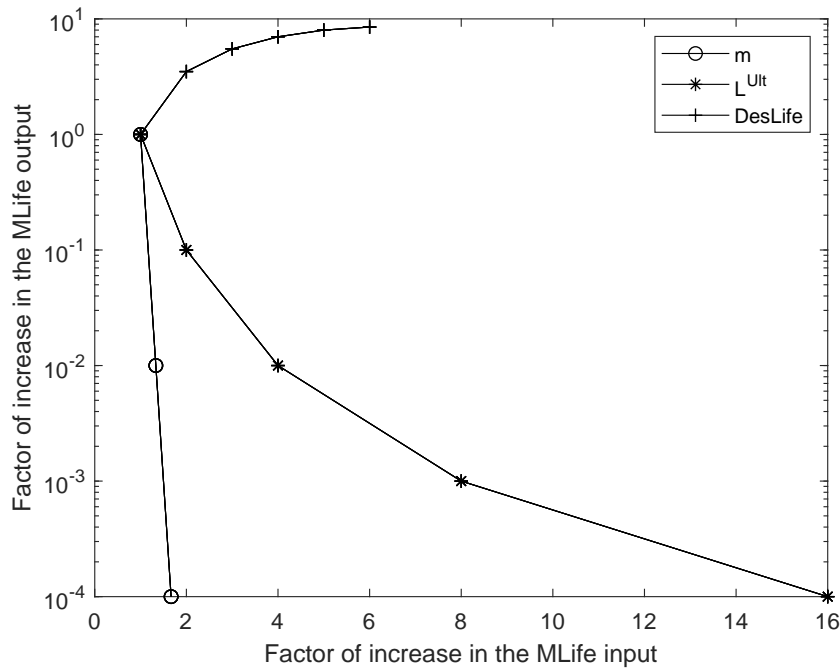


Figure 8.1: Relative influence of the design input parameters such as  $m$ ,  $L^{Ult}$  and  $DesLife$  on the lifetime accumulated damage estimates by MLife showing that  $D^{life}$  displays the maximum sensitivity to the Wöhler exponent  $m$ .

the material properties must be appropriately quantified based on the steel grade, component/subassembly design and the environmental conditions (Det Norske Veritas AS, 2012).

#### 8.1.4 Ideal support structure design

For an ideal support structure design, the accumulated damage at each structural node should be less than one to satisfy the Miner's rule. Based on Figure 5.19, OWT designs deliver a safe support structure, however, the significantly lower damage at the submerged nodes, namely J1 and J2, implies that the structure has higher safety factors at these nodes to account for large uncertainties in soil-structure interaction. Existing research has shown that a reduction in monopile wall thickness causes a moderate increase in bending moments, but a considerable increase in fatigue damage (Løken, 2009) thereby leading to possible fatigue failure or buckling of the structure. While such structural decisions require detailed analysis at individual sites, outcomes of this thesis allow for the identification of potential sites.

### 8.1.5 Look-up table approach for reliability assessment

For accurate data-based fatigue quantification of an OWT, the system must be instrumented with an array of strain gauges, displacement transducers and accelerometers. Retrofitting measurement instruments on a substantial number of existing turbines requires a large investment consequently increasing the LCOE, therefore, offsetting gains possible through the improved understanding of structural dynamics (Hart et al., 2016). Consequently, fatigue predictions rely on the aero-hydro-elasto-servodynamic modelling of the structural response due to the lower associated cost of computational methods which have been validated for representative cases.

For a comprehensive fatigue analysis, all possible design load cases must be accounted for in conjunction with all sea states, however, the computational effort required for such an analysis is large. To improve the computational efficiency of the process, common industry practice is the binning of environmental parameters. For a specific turbine configuration, the DELs due to a particular sea state can be considered to be constant regardless of the deployment location for a constant water depth. Therefore, it is proposed that the DELs of a particular OWT should be simulated and recorded for a range of sea states. These recorded DELs can be used to assess the damage for a similar structure deployed at different locations, thereby, reducing the computational effort required. Therefore, 13340 ten-minute structural response simulations and their associated DELs were calculated and recorded in a lookup table to allow for repeated use at all locations in the UKCS assuming uniform depth.

While the look-up table represents structural loads for the 20m baseline depth, DELs at the mudline are expected to display strong dependency to variation in water depth (Ziegler et al., 2015). The increase in combined effect of wave loads due to a larger moment arm and the decrease in the natural frequency of the structure leads to underestimation of the DELs for deep water sites while the opposite is true for shallow water sites.

### **8.1.6 Sub-regional characterisation of performance indicators**

OWTs are characterised by high availability during moderate winds since increase in  $V_t$  increases the production at the cost of inducing higher structural loads which may contribute to increase in failures, downtime and loss of energy (DNV GL, 2017). These environmental conditions at the considered sites form the design basis of the proposed OWT by informing the turbine class decision (British Standards Institution, 2009). Furthermore, the characterisation of site-specific wind conditions may also improve the availability by restriction of the repair and maintenance activities to low-wind conditions for reduction of the unavoidable loss of energy due to a parked turbine during the O&M activities.

Research conducted by SPARTA performs a rudimentary dimensional breakdown of installed wind turbines based on deployment region (SPARTA, 2018). Broadly dividing the existing deployments into the East and West categories, with the former corresponding to the installations in the North Sea and the latter to those in the Irish Sea, multiple KPIs are compared for April 2017 to March 2018. While the dominant environmental conditions between the East and West coast do not show considerable monthly variation, with an annual average wind speed of 8-9m/s at hub height and  $H_s$  of 0.8-1.0m, the East Coast has half as many transfers and 30% fewer non-access days than the West coast. Consequently, the East coast was seen to perform better with a higher average production based availability. Therefore, existing lease sites awarded under the first three rounds represent improved performance of deployments in the North Sea relative to the Irish Sea.

Using an improved categorisation of the UKCS into distinct geographic sub-regions based on environmental parameters reported in Fugro GEOS (2001), Chapter 6 produces reliability-centric KPIs for OWE siting in eight sub-regions. The site-specific metocean parameters for a set of 40 GPs are utilised from the NEXT database to produce reliability and power production estimates for comparison between the sub-regions.

Based on the range of environmental conditions, the North Sea is divided into three regions suitable for offshore installations. The environmental conditions at each GP are characterised by the occurrence probability of each sea state

determined by the  $H_s - V_t$  and  $H_s - T_p$  scatter plots at the site. Performing damage calculations for each wind speed bin, and noting that the highest bending moment on the structural components occurs at the turbine rated speed, the OWT is seen to display the highest accumulated damage levels at  $8 \leq V_t < 10$  for all GPs as displayed in Figure 6.11.

The scatter in the  $D^{life}$  due to higher wind speeds between various GPs is in accordance with observations made by C. H. Lange and Winterstein (1996). They show that the data contained in a representative scatter plot of a site provides good agreement for the main body of the load distribution. However, uncertainties associated to the extreme loads in the high-stress tail of the distribution are higher. This is reiterated in the data source (Fugro GEOS, 2001) whereby, the occurrence frequency of extreme environmental conditions is summarised in a single large bin, indicating the availability of data but also highlighting reduced confidence in its representation of storm conditions.

The aggregate for the lifetime accumulated damage for all wind speed bins at a site yields the characteristic  $D^{life}$  at the GP used as an indicator for OWT performance. When grouped based on the sub-region in Figure 6.16, northwestern, northern and northeastern sub-regions of the UKCS, namely the Hebrides Shelf, West Shetland Shelf and the Northern North Sea, are the locations with the highest damage to the support structure at the mudline. The southwestern and eastern sub-regions, namely the Celtic and Central North Sea, provide a moderate potential for lifetime extension of the support structure. From a reliability perspective, sheltered locations such as the Irish Sea, English Channel and the Southern North Sea are the ideal location for OWT deployment. Summarily, dynamic locations in the north, northwest and northeast of the UKCS are characterised by lower reliability, whereas, OWTs deployed in the sheltered and southeasterly parts of the UKCS can be expected to have higher structural reliability assuming a like for like turbine design, control and O&M regime.

The second performance indicator is the annual energy production as shown in Figure 6.17 with the associated turbine capacity factors plotted in Figure 6.18. With an expected increase in annual energy production of around 5GWh/year/turbine for dynamic locations in the north of the UKCS relative to the benign and sheltered locations, it can be seen that the distribution of  $E^{ann}$  is related to the accumulated lifetime damage; locations with high power production experience higher damage,

therefore, have less potential for lifetime extension.

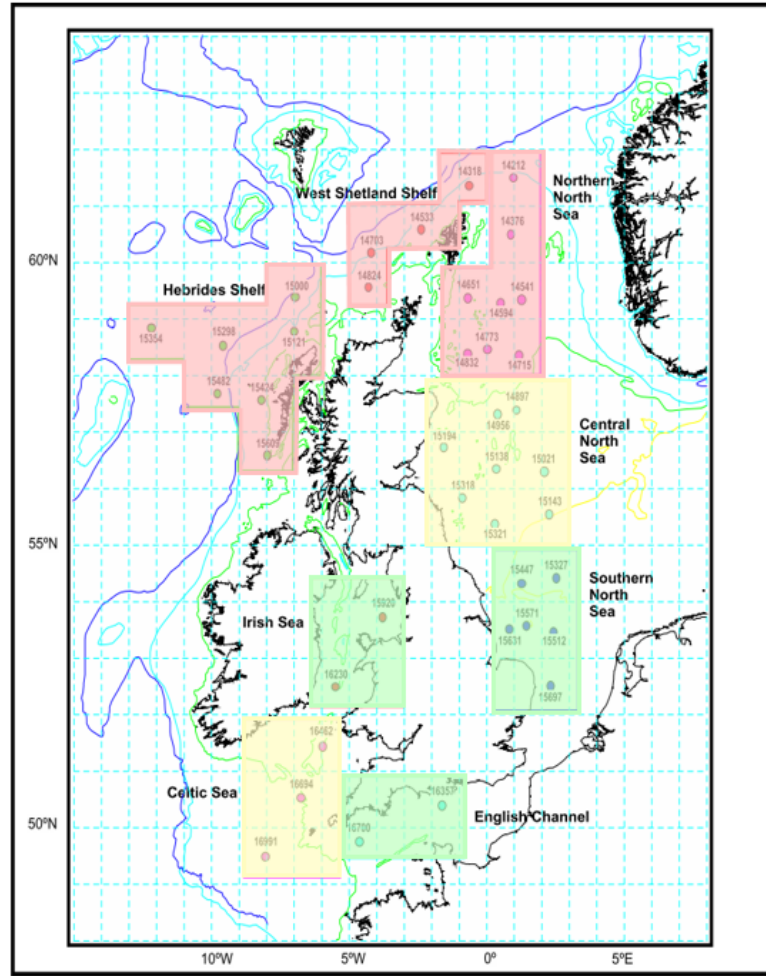
Due to the low damage for structures in RIII based on the portfolio analysis in Figure 6.19, these GPs provide a reduced risk for the OWE industry in its initial stages to establish design solutions. However, assuming equivalent CfD pricing, these locations may provide lower economic incentive due to reduced power production and consequently a lower revenue generation. Commercial farm siting under all existing lease rounds has been concentrated in these regions. The Northern North Sea is identified as the most advantageous location for OWE deployment regarding the combined effect of both site decision parameters, namely energy generation and damage accumulation. Therefore, future installations in the UKCS can provide the highest annual power production at the expense of low structural damage in the Northern North Sea.

### 8.1.7 Development of a met-ocean centric KPI

Some OWF operators are setting performance targets for OWFs such as technical availability and energy production per unit installed power. As with all KPIs, care has to be taken in their evaluation and ranking, as an example the differences in O&M strategy can cause significant bias. An alternative objective for operators could be the determination of the optimal O&M cost for project cost-effectiveness which will be subject to variation between projects due to deployment location (P. Tavner, 2012).

Here, a new production-normalised damage metric,  $K^{DP}$ , is proposed. The derivation of a metric that characterises the damage induced in the structure per megawatt generated is useful to highlight the alternative site-specific differences for OWT deployment locations.

Site comparisons of the  $K^{DP}$  performance indicator for various subregions of the UKCS in Figure 8.2a is tabulated in Figure 8.2b. It shows that the benign locations such as the Irish Sea, English Channel and the Southern North Sea display consistently low damage per GWh. This is in agreement with the portfolio analysis of Figure 6.19, therefore,  $K^{DP}$  is seen to be an acceptable KPI to evaluate the suitability of a site for OWE deployments by incorporating the combined effect of power production and damage incurred.



(a) Map of the UKCS showing sub-regions colour-coded based on the risk-return factor,  $K^{DP}$  with corresponding to the ranking tabulated below.

Risk-return ranking	$K^{DP}$ value ( $\times 10^{-4}$ ) [ $\text{GWh}^{-1}$ ]	Sub-region name
High	$>5$	Hebrides Shelf West Shetland Shelf Northern North Sea
Moderate	4-5	Celtic Sea Central North Sea
Low	$<4$	Southern North Sea Irish Sea English Channel

(b) Tabulated ranking of the sub-regions in the UKCS. A high value corresponds to higher damage per unit energy produced than locations with a lower ranking.

Figure 8.2: Mapped and tabulated ranking of sub-regions in the UKCS based on the risk-return metric calculated using the NEXT database. OWTs with higher structural integrity should be deployed at locations with a higher ranking for similar design lifetimes.

### 8.1.8 Geospatial mapping of performance metrics for UKCS and adjoining regions

Currently, most offshore wind deployment is located in the shallow waters of the Irish Sea and the Southern North Sea, with depths less than 50m as highlighted in Figure 8.3. The distribution of deployments in Europe for 2018 continued to populate the same regions with 77% focused in the North Sea and Irish Sea (WindEurope Business Intelligence, 2019). Of these, installations in the UK included Galloper, Beatrice 2, Race Bank, Aberdeen OWF in the North Sea, Walney Extension East and West in the Irish Sea and Rampion in the Atlantic. Existing and planned offshore wind projects as seen in Figure 8.4 off the east of England have resulted in considerable economic activity for the region, however, with the maturation and rapid development of the OWE industry, this concentrated activity will expand to other regions in the UKCS.

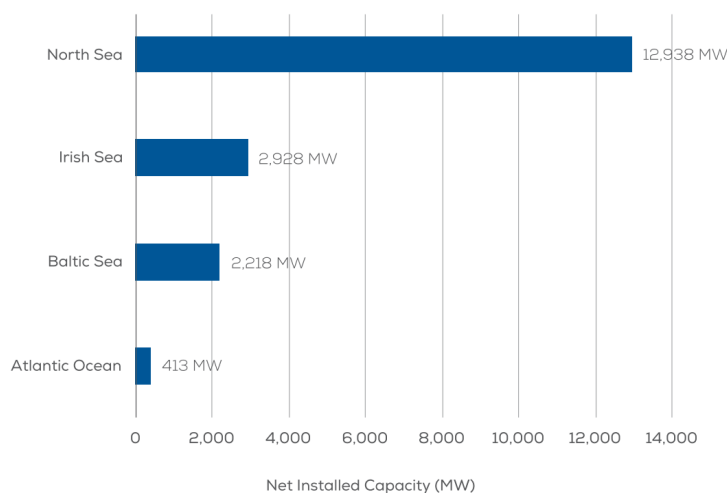


Figure 8.3: Cumulative OWE installations by sea basin across Europe (WindEurope Business Intelligence, 2019).

Requests for information useful in identifying technically and commercially suitable regions for OWE deployment within the UKCS by The Crown Estate 2018 shows that there is scope for improved identification of future lease sites. Current resource and constraints analysis performed by The Crown Estate (2018c) for identifying characterisation areas for the future lease rounds provides limited reliability information to developers.

Using the methodology established for characterisation of sub-regional performance indicators, a UKCS - wide analysis was conducted for resource, damage and



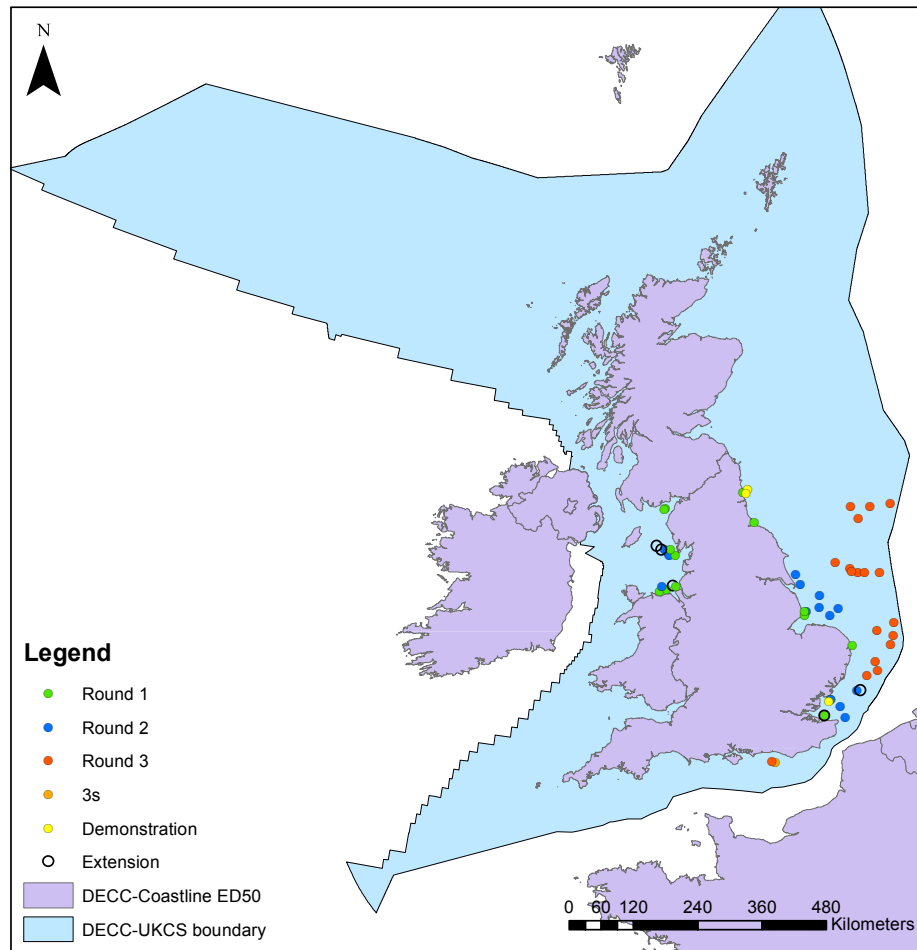


Figure 8.4: Map showing the distribution of the UK offshore wind farm lease sites by round within the UKCS boundary.

$K^{DP}$  characterisation. As seen in Figure 8.5a, with current installations focused close to shore in the benign locations of the Southern North Sea and the Irish, the exploited wind resource is limited. The lifetime structural damage in these regions is also significantly lower than more dynamic locations such as the Hebrides Shelf in the north west, therefore, they provide a larger potential for lifetime extension. A visualisation of  $K^{DP}$  for the UKCS and adjoining regions in Figure 8.6 shows that the North Sea and Irish Sea are characterised by lower damage per unit energy produced. Consequently, the risk is lower for every unit return and these locations are ideal for the OWE industry to fine-tune their technology whilst maintaining profitability to facilitate future deployments in high risk locations.

With annual energy production of up to twice as much, the offshore regions off the west coast of the UK provide a higher energy potential that can be exploited by the deployment of OWTs. Use of the same 5 MW wind turbine in locations with a higher distance to shore, particularly on the west coast can improve turbine capacity factors by increasing annual energy production by up to 15 GWh. There is further scope of improved power production in these regions by deployment of larger turbines with a higher rated power.

Similar to the annual power production, contours of the lifetime accumulated damage for the OWT support structure at the mudline depict an increase in  $D^{life}$  with an increase in distance to shore. However, it must be observed that the rapid increase in power production with increase in the distance of site to the shore is not directly translated into the damage behaviour; a more gradual increase is observed in Figure 8.5b. It can, therefore, be concluded that while the benefits of the improved power production can be achieved at relatively low distance from the shore, the consequent increase in damage is lower leading to a belt of optimum OWF sites around the UK characterised by moderate power production but low lifetime damage. Examples of such locations exist in the Northern and Central North Sea.

The white spaces in the contour plots of Figure 8.5 are due to the limitations of the database spatial coverage. These regions were not incorporated in the current analysis due to the lack of wave data provided by the ERA-Interim database for near-shore regions and the inherent significance of wave loads to lifetime accumulated damage as discussed in Chapter 5.

Reperforming the portfolio analysis from Chapter 6 shows that the optimum

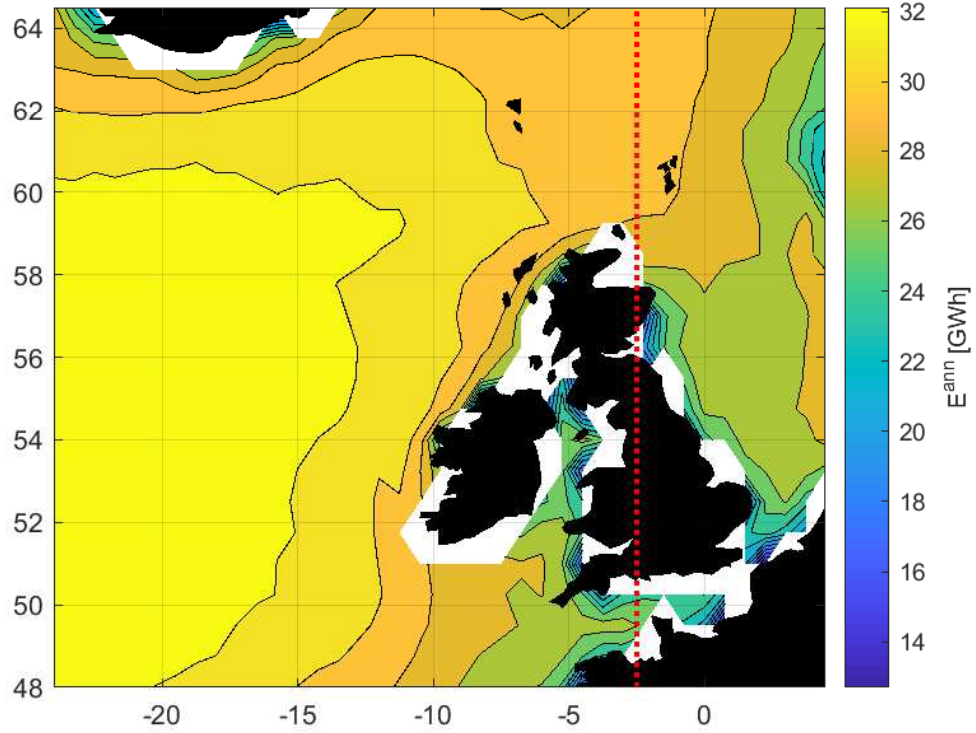
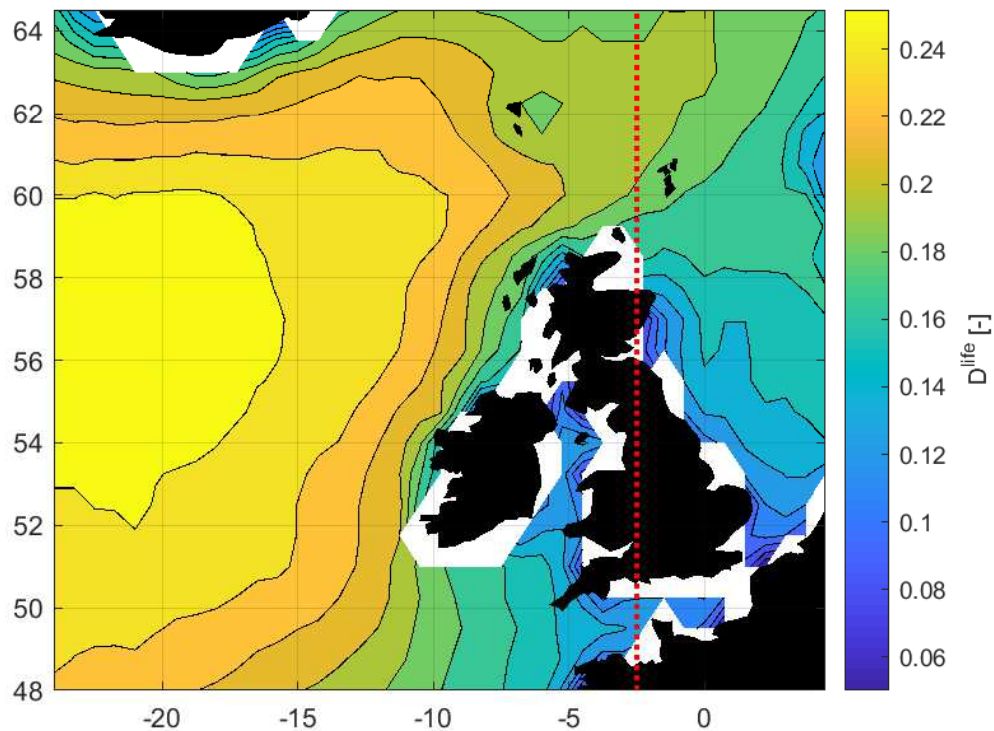
(a)  $E^{ann}$  contour plot.(b)  $D^{life}$  contour plot using  $m = 4$ ,  $DesLife = 15$  years and  $L^{Ult} = 5 \times L^{max}$ .

Figure 8.5: Spatial distribution of annual energy production and accumulated lifetime damage at the OWT mudline for the UKCS and adjoining areas with the east and west coast demarcated at  $2.5^\circ\text{W}$ .

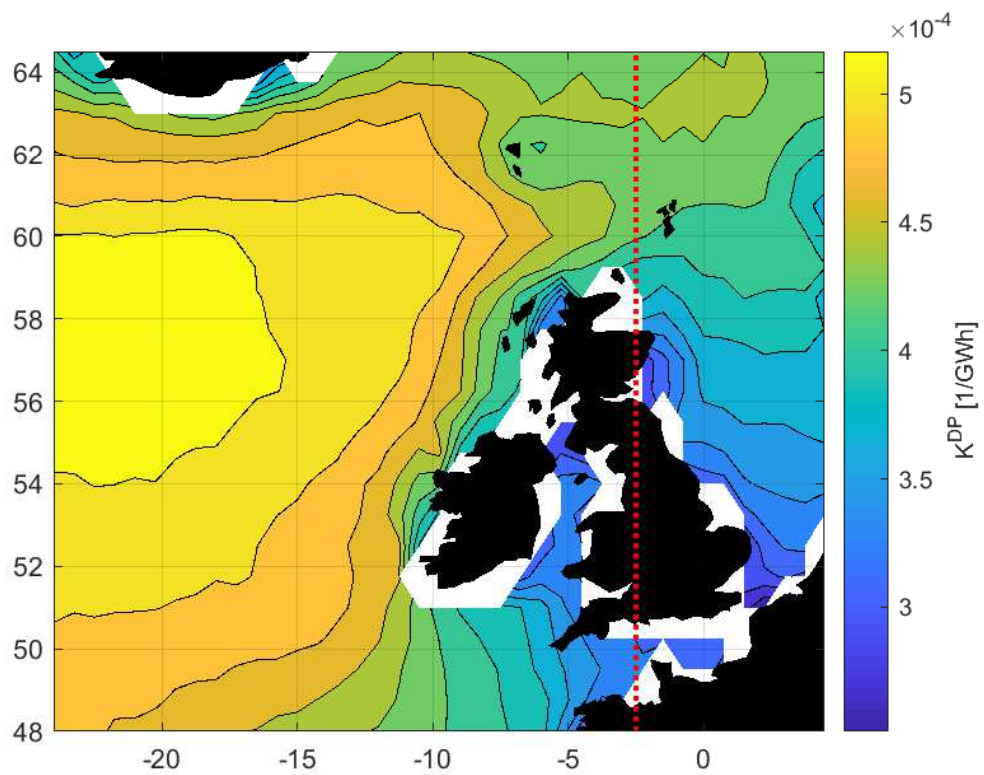


Figure 8.6: Contour map of  $K^{DP}$  with the east and west coast demarcated at  $2.5^\circ\text{W}$ .

siting locations for OWFs are at and around the intersection of the bilinear slope of the accumulated lifetime damage and annual energy production in Figure 7.8. The analysis also confirms the hypothesis that the deployment sites further off the east coast could generate higher energy for the same unit damage relative to wind farms in the west since they are characterised by a lower  $K^{DP}$ . The contour plot of the spatial distribution of  $K^{DP}$  in Figure 8.6 shows agreement with this observation.

The distribution of  $K^{DP}$  with reference to the  $D^{life}$  and  $E^{ann}$  is represented in Figure 8.7 showing the influence and relationship of both on  $K^{DP}$ .

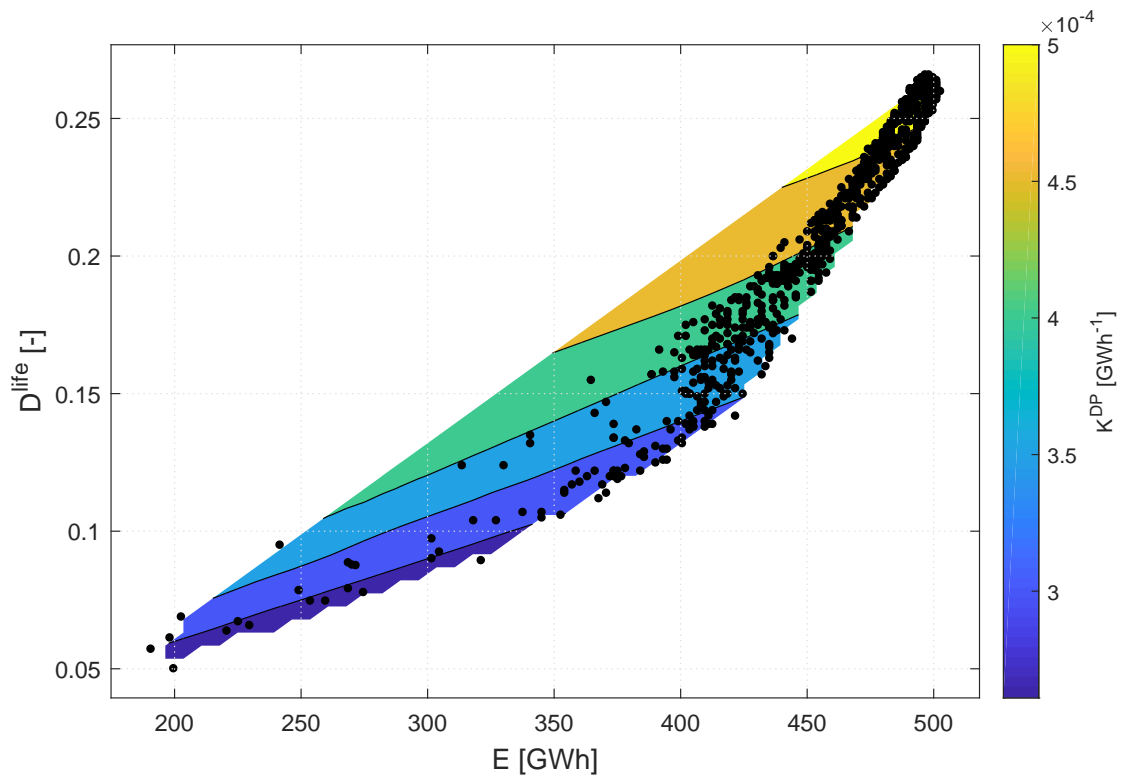


Figure 8.7: Lifetime energy production and accumulated damage scatter plot with associated  $K^{DP}$  characteristics for an NREL 5 MW turbine deployed at the UKCS and its adjoining regions with a lifetime of 15 years.

$K^{DP}$  favours low risk locations as it is heavily influenced by  $D^{life}$ ; the increased dependence of  $K^{DP}$  on accumulated lifetime damage with higher energy production is evident in Figure 8.7. The locations with the highest damage and power production display higher  $K^{DP}$ . When compared to Figure 7.8, it can be seen that a correlation between the longitudinal coordinates and  $K^{DP}$  leads to locations further west being characterised by a higher  $K^{DP}$ . Therefore, as the turbines

are deployed at locations further west, the damage per unit power generated is expected to increase, thereby, reducing the possibility for lifetime extension relative to existing deployment locations off the east coast.

### 8.2 Limitations

The rationale for this research project has been to develop and present a methodology to provide an improved mapping technique incorporating influences of turbine reliability. The usefulness of the methodology depends on the accuracy and completeness of the input parameters as well as the quality of the models. Numerous numerical methods have been applied to facilitate this task. In the process, however, limitations were introduced to improve computational efficiency. Future research will aim to address these limitations to improve the robustness of the methodology to yield more accurate results as required.

**Turbine type and rating** This methodology is established for the geared NREL 5 MW turbine since a majority of the installations at the conception of this research project were of similar rating and concept. It must be noted, however, that the extracted power is limited by the rating of the OWT, therefore, if a turbine of larger rating is deployed in locations with higher potential, the power production is expected to increase significantly. Therefore, as OWE moves further offshore into deeper waters, the turbine rating is expected to increase to harvest the improved energy potential. Similarly, the suitability of novel turbine concepts for the energy-rich offshore locations is subject of ongoing research efforts. This may include, but is not limited to, a switch to direct-drive (H. Polinder et al., 2007; Scott Semken et al., 2012), multi-rotors (Jamieson and Branney, 2014) or vertical axis installations (B. Owens et al., 2013; B. C. Owens et al., 2014).

Current installations in the UKCS predominantly rely on monopiles as a cost-effective and reliable foundation solution, therefore, this research project utilised a fixed base turbine to develop and explore the validity of the mapping methodology. While fixed turbine concepts are suitable for the shallower waters of the Irish and Southern North Sea, their economic viability is limited to waters of up to 60m (LEANWIND, 2017). Utilisation of the wind resource in the deep sea regions will rely heavily on deployment of floating wind concepts such as the Hywind farm off the coast of Aberdeenshire. With exploration of the larger resource potential

in deeper waters, floating OWTs may reach commercial maturity, therefore, additional turbine foundation models should also be investigated using the developed methodology to identify the suitability of various concepts at all sites in the UKCS.

**Fixed foundation modelling** The fixed base model does not fully incorporate the influence of the foundation flexibility since the FAST SubDyn module is currently limited to rigid connections between the substructure and the seabed. To address this problem, it is possible to use the apparent fixity model to simulate a flexible monopile foundation. The apparent fixity method reproduces the stiffness of the soil-pile system by producing a fictive cantilever beam fixed at its lower end below the mudline to provide an improved soil - structure interaction. It has been found that the use of the fixed base model underestimates the structural dynamics and consequent lifetime accumulated damage in the order of 20% relative to a flexible foundation (Løken, 2009) modelled using the apparent fixity method.

**Metoccean characterisation database** The use of two different metoccean databases, namely, the NEXT and ECMWF - ERA Interim databases highlights that there are various contributing factors to the difference of damage estimates using the NEXT and ECMWF databases as discussed in Section. 7.1.2. Load cases with higher wind speeds and wave heights must be adequately quantified due to their large impact on fatigue analysis relative to their occurrence probability. In consideration of the approximation made by the NEXT data when quantifying the larger wind speeds by assigning them to one bin, an inherent error is introduced in the fatigue life assessment using the data, whilst the ECMWF database does not provide sufficient information about these low frequency events.

Another possible cause of the disparity may be the different time periods of data used for both the NEXT (combined period of Jan 1977 to Dec 1979 and Jan 1989 to Dec 1994) and ECMWF databases (2008 - 2017). While a 9 - 10 year period is expected to provide a reasonable coverage in terms of seasonal variation (e.g. due to El Niño and La Niña events), the difference arising due to database length should be investigated. This can be done by using similar data periods of the same length for comparison of the metoccean database for use in damage estimates.

**Simulation of environmental parameters** The simulation of wind and wave profiles using the metoccean database was performed by introducing uniformity in most environmental input parameters. Parameters of particular interest include

the water depth, wind turbulence intensity and wave spectral model.

The purpose for using a uniform depth across the UKCS was to allow the isolation of wind and wave effects on damage per unit power generation. While water depth is also expected to have an effect of wave height, this is indirectly covered through the  $H_s$  data. It is expected that as the distance to shore increases, the depth of the seabed also increases leading to an increase in support structure length. The consequent moment arm of the forces also increases compounding the damage incurred at further offshore locations. This would lead to a further increase in  $K^{DP}$  for deep water sites further offshore. Future work accounting for site-specific variation in the depth should be supplemented with sufficient adjustment to the support structure design to explore the structural integrity in more detail.

The exclusion of site-specific turbulence intensity may prove limiting for certain subassemblies. P. Tavner et al. (2011) observed greater cross-correlations between failures and the wind speed turbulence coefficients than mean wind speed or wind speed standard deviation for the pitch mechanism.

The use of the JONSWAP spectral model for all locations in the UKCS may also introduce limitations in the results since the applicability of the model to deep water sites is reduced. Instead, a deep water model such as the Bretschneider spectrum 1952 could be utilised for improved quantification of wave loads at deep water sites.

**Directionality of metocean loads** An assessment of the combined effect of aerodynamic, wave and structural damping under misaligned wind and wave conditions is significant for the structural response in the operational DLCs. The influence of aerodynamic damping is restricted to the wave excitation from the fore-aft direction only, therefore, the wave loads in the lateral direction are assumed to have negligible influence of aerodynamic damping. Consequently, the highest fatigue damage is expected for a  $90^\circ$  angle of misalignment (Trøen, 2014). Since wind direction is generally expected to agree with dominant wave regimes, the occurrence probability of load cases with high misalignment between the two loads is generally expected to be low. However, discounting the influence of these load cases may provide an underestimation of accumulated lifetime damage for regions with high directional misalignment. Therefore, the directionality of the loads should be incorporated into future site-specific assessments.

**Variables for lifetime damage accumulation** For the scope of this project,



the structural fatigue life at the mudline is considered to be limited by normal stresses since the bending moment is higher than the shear forces by an order of magnitude. For structures subjected to combined axial loads and bending moments, the fatigue life should be estimated by the linear accumulation of both loads for the Miner formulation as shown in Equation. 8.1.

$$\sum \frac{\text{load effects}}{\text{resistance}} \leq 1.0 \quad (8.1)$$

Whereby, the load effects are the shear forces and bending moments with associated resistance due to the axial strength and nominal bending strength of the structure, respectively.

In addition to the structural response analysis, fatigue calculation is highly dependant on the governing parameters, therefore, point value estimation of fatigue life requires input parameters derived from the OWTs structural, material and geometric properties. Whilst the absence of turbine-specific fatigue input parameter values limits the direct applicability of the estimated damage values, it provides sufficient information for a comparative analysis of various locations in the UKCS to determine the extent of influence of site characterisation parameters on the viability of a offshore wind project.

The thesis does not aim to provide point values for fatigue damage of the 5 MW NREL turbine at various locations in the UKCS since a perfunctory choice of the calculation parameters is a hindrance for producing point values for reliability. However, using a consistent set of parameters is sufficient for site reliability comparison.

**Metoccean database spatial coverage** While power production can be estimated for the UKCS, a lack of wave data for near-shore locations in the ECMWF database limits the spatial scope of this thesis. This is noteworthy, since the sites of most existing wind farms lie within these near-shore grid points. Near shore lease sites include regions where tidal flows are concentrated such as straits between islands, however, the ECMWF model poorly captures the metoccean parameter variation in these areas. This highlights the significance of acquiring high resolution model or field data to attain a better understanding of the leased sites for OWT deployment through site. The use of a database with improved data availability for near-shore locations could provide lifetime damage estimates for existing deployments which may allow for the validation of the methodology using

project-specific reliability data.

### 8.3 Concluding remarks

The aim of this research was to investigate the following question:

Can an improved quantification and visualisation of site-specific OWT performance inform location-intelligent decisions for farm siting?

To address this research question, a methodology has been developed to demonstrate the spatial distribution of the suitability for OWE deployment. The new approach uses the power production and the lifetime accumulated damage at the support structure at the reliability-critical mudline node as a representative example. The results of this research show that a combined risk and return parameter can enable further location-intelligent decisions in the OWE industry to facilitate improved siting of OWEs.

This contribution to knowledge has widespread implications in the OWE industry and the academic community which are further discussed in Section 8.3.1. However, due to the large computational effort required to address the research question, limitations were introduced in the project as discussed in Section 8.2. These limitations provide avenues for future research by the academic community to encompass a larger range of parameters to further tailor results to individual sites. Some recommendations for future work are provided in Section 8.3.1.4.

#### 8.3.1 Implication of thesis

The mapping methodology allows for location-intelligent decision making for OWE siting and has implications across the project lifecycle from the conception stage, through the operation and all the way to decommissioning.

##### 8.3.1.1 Application to manufacturing

The proposed methodology supports the argument for the facilitation of access to load data at earlier design stages to reduce the possibility of under- or over-designing the turbine and achieving consequent economic advantages. Existing design processes in the OWE industry aim to improve the performance of each

turbine by increasing component reliability. However, with the maturation of the industry, existing project operators predict that further cost reduction can be achieved by informed lifetime extension decisions (The Crown Estate, 2012). Therefore, the turbines tend to follow a conservative design for their respective sites. The presented method can support early design decisions by informing additional decision factors including risk/cost-benefit analyses.

Currently, the targeted OWT lifetime is between 20 to 25 years followed by the decommissioning of the system. Improved extreme and fatigue damage forecasts for the system based on the site-specific environmental conditions could allow a CAPEX reduction for certain subassemblies. As an example, the geometric properties of the installations on the east coast may be altered to reduce the design lifetime to the expected lifetime or the design lifetime for the existing structures may be increased following detailed site specific assessment and, where possible, the analysis of load histories.

#### 8.3.1.2 Application to wind farm siting

This thesis presents maps displaying structural fatigue for a 5 MW NREL fixed turbine in the UKCS and adjoining locations using the ECMWF-ERA Interim data. An additional map with the production-fatigue metric is also drawn (as shown in Figure 8.6) to show the degree of influence of turbine siting on the OPEX. The combination of both metrics yields the damage per GWh generated by the wind turbine and may be used for an improved understanding of OWT performance. These performance metrics may provide useful information to farm operators for current installations and planning future deployments.

**Current installations** Based on the learnings from the power production weighted by lifetime damage, the two regions with higher deployment intensity also exhibit the highest achieved balance between power production and fatigue damage. Therefore, the North Sea and the Irish Sea are the most attractive sites for current deployments.

The structural damage per GWh for other components and subassemblies of existing installations can be calculated by following the methodology established in Chapter 7. Environmental data with improved resolution from nearshore, shallow water models such as SWAN could be employed for the fatigue life analysis in the

Southern North Sea and Irish Sea.

The analytical outputs of this research, parallel studies regarding site-specific lifetime assessment of other structural subassemblies may be used along with turbine inspection and maintenance logs (DNV GL, 2016a) to inform lifetime extension decisions for these installations.

**Future installations** Improved site characterisation based on reliability metrics can support the siting of future OWE deployments, exploring the trade-off between risk and performance. The existing risk and return analysis can help to identify risk-efficient boundaries (Chapman and Ward, 1996) to:

- manage expectations of the project by identifying the expected risk and return;
- explore desirable change in OWF planning by conducting an analysis of project limitations and identifying possible changes to reduce risk;
- facilitate and encourage risk taking which has the potential to improve profitability in the long run.

Anticipated to be twice the size of the fixed OWE industry, the key aim for floating wind energy industry is to achieve economic viability at a faster rate than fixed concepts by drawing on the learnings of the fixed OWT industry. The regions with suitable water depth for deployment of floating offshore include the areas off the Scottish, Welsh and Cornish coasts. In Chapter. 6 it was observed that for a fixed turbine concept, the Celtic Sea and the Central North Sea there is a higher production to damage ratio relative to the Hebrides and West Shetland Shelf regions. While this may be an indicator for the increased suitability of the Celtic Sea and Central North Sea for floating concept deployment, fatigue analysis for floating models must be conducted to achieve a more applicable understanding of turbine behaviour in these regions.

### 8.3.1.3 Operation and maintenance companies

Promoting the argument and the development of a methodology for deriving and mapping the damage-dependent site characterisation parameter may provide useful information to turbine operators to reduce OPEX. Instead of having a universal

O&M regime, the key players in the OWE industry may customise their maintenance plans based on the considered sites. A rigorously improved preventative maintenance at more dynamic sites, while reduction in maintenance efforts at benign sites may provide cost reduction opportunities for individual projects.

#### 8.3.1.4 Research community/Future work

Whilst addressing the research question, the required computational effort was reduced by limiting the research scope and introducing modelling assumptions. Therefore, the proposed methodology in this project can be improved by further contribution from the research community to allow for an increased confidence in the application of this methodology and utilisation of results. Identified avenues for subsequent further research are suggested below:

- Extension of the developed methodology to other structural and mechanical components, so that a site-specific aggregate system lifetime assessment may be conducted. Applying this methodology to various turbine concepts would provide design-specific reliability estimates for improved location-intelligent siting. Additional design load cases for fatigue and extreme design analysis may also be incorporated into future work.
- Exploration of the aggregate force and moment effect on the design lifetime of subassemblies may provide better understanding of the reliability-critical components. Furthermore, incorporating load directionality may provide a more comprehensive fatigue analysis since the current assessment provides conservative estimates of reliability based on unidirectional forces.
- Inclusion of farm-wide variables such as the wake deficits, wind-farm super controllers and ambient wind in addition to aero-hydro-servo-elastic dynamics of the turbines to develop problem-specific farm reliability metrics.
- Incorporating the influences of additional environmental parameters, particularly bathymetric conditions, since they are significant design and cost drivers. Turbine foundation concepts could be employed based on the depth profile of each site for improved application of the methodology. Also of significance is the distance to shore since this contributes heavily to the OPEX, therefore, is of fundamental importance to the resulting LCOE.

- To conduct a robust reliability-based site characterisation, a range of empirical environmental, structural and economic data is required. Data availability for OWE, due to its associated competitive advantage, is still a key limitation for research in the sector. To validate the methodology developed in this thesis, data from OWE project reliability databases, structural response measurements and metocean records would be highly useful. Validation of the methodology can be achieved by using strain gauge data at existing offshore wind project sites in conjunction with the conventional design and admission procedure developed by Veldkamp (2006).
- Attribute tables of the wind farm shape files may be appended by farm characteristics, environmental, resource potential and reliability metrics to provide a more comprehensive database for existing installations. Free and publicly accessible sources for farm characteristics from the UK Wind Energy Database by RenewableUK RenewableUK (2015) and 4C Offshore *4C Offshore - Offshore wind farm database* (2015), provide wind farm details including region, (proposed) date of commissioning, farm capacity, number of devices, device rating, foundation type (offshore wind), distance to shore, O&M port, number of offshore substations (if applicable) and expected life.

The work presented in this thesis has led to some interesting findings pertaining to the site characterisation based on a risk-return metric for the UKCS and its adjoining regions. By classifying deployment sites based on the damage per unit energy produced, this thesis displays the trade-off between risk and performance at existing and future installations to inform location-intelligent decisions in the OWE industry. It is hoped that this proves useful for the academic community as well as industry practitioners in order to further develop the offshore wind sector in the UK and beyond.



# References

- 4C Offshore - Offshore wind farm database* (2015). URL: <https://www.4coffshore.com/windfarms/windfarms.aspx?windfarmId=UK36> (visited on 08/01/2015).
- Aasen, Steffen et al. (2017). “Effect of foundation modelling on the fatigue lifetime of a monopile-based offshore wind turbine”. In: *Wind Energy Science* 2.2, pp. 361–376. ISSN: 2366-7451. DOI: 10.5194/wes-2-361-2017. URL: <https://www.wind-energ-sci.net/2/361/2017/>.
- ABP Marine Environmental Research Ltd (2008). *Atlas of UK Marine Renewable Energy Resources : Technical Report*. Tech. rep. Department for Business, Enterprise & Regulatory Reform.
- ABPmer (2008). *Atlas of UK Marine Renewable Energy Resources*. URL: <http://www.renewables-atlas.info/> (visited on 03/31/2015).
- Alesbe, Israa, Moustafa Abdel-Maksoud, and Sattar Aljabair (2017). “Analysis of unsteady flow over Offshore Wind Turbine in combination with different types of foundations”. In: *Journal of Marine Science and Application* 16.2, pp. 199–207.
- Almarnaess, A (1985). *Fatigue handbook: offshore steel structures*. URL: <https://www.osti.gov/biblio/5095889>.
- Ambühl, Simon, Morten Kramer, and John Dalsgaard Sørensen (2015). “Different Reliability Assessment Approaches for Wave Energy Converters”. In: *Proceedings of the 11th European Wave and Tidal Energy Conference*, pp. 1–9.
- Andrawus, Jesse Agwandas (2008). “Maintenance optimisation for wind turbines.” PhD thesis. The Robert Gordon University. URL: <https://openair.rgu.ac.uk/handle/10059/268>.
- Andrews, John and Nick Jelley (2017). *Energy science: principles, technologies, and impacts*. Oxford university press.



- Angelov, Ivo (2018). “Dynamic response of the tower of a NREL 5MW wind turbine generator”. In: *MATEC Web of Conferences* 234, p. 04008. DOI: 10.1051/mateconf/201823404008.
- API (2014). *API RP 2A - Recommended Practice for Planning, Designing, and Constructing Fixed Offshore Platforms — Working Stress Design* API RP 2A - Recommended Practice for Planning, Designing, and Constructing Fixed Offshore Platforms — Working Stress Design. Tech. rep.
- ArcelorMittal (2012). *HISTAR - Innovative high strength steels for economical steel structures*. Tech. rep.
- Arent, Douglas et al. (2012). *Improved Offshore Wind Resource Assessment in Global Climate Stabilization Scenarios* Improved Offshore Wind Resource Assessment in Global Climate Stabilization Scenarios. Tech. rep.
- Artigao, Estefania et al. (2018). “Wind turbine reliability: A comprehensive review towards effective condition monitoring development”. In: *Applied Energy* 228.May, pp. 1569–1583. ISSN: 03062619. DOI: 10.1016/j.apenergy.2018.07.037.
- Bachynski, Erin E. et al. (2013). “Dynamic analysis of floating wind turbines during pitch actuator fault, grid loss, and shutdown”. In: *Energy Procedia* 35.December, pp. 210–222. ISSN: 18766102. DOI: 10.1016/j.egypro.2013.07.174.
- Barstow, Stephen et al. (2009). “WorldWaves wave energy resource assessments from the deep ocean to the coast”. In: *Proceedings of the 8th European Wave and Tidal Energy Conference, Uppsala, Sweden*, pp. 149–159. ISSN: 1934-8975.
- Barthelmie, R J et al. (2008). “Flow and wakes in large wind farms in complex terrain and offshore”. In: *European Wind Energy*, p. 10. ISSN: 10954244. DOI: 10.1002/we.408. URL: [http://www.upwind.eu/Shared%20Documents/WP8%20-%20Flow/AWEA2008%7B%5C\\_%7DUpwindWP8-barthelmie.pdf](http://www.upwind.eu/Shared%20Documents/WP8%20-%20Flow/AWEA2008%7B%5C_%7DUpwindWP8-barthelmie.pdf).
- Basquin, O. H. (1910). “The exponential law of endurance tests”. In: *American Society for Testing and Materials Proceedings* 10.
- Becker, Dennis E (1996). “Eighteenth Canadian Geotechnical Colloquium: Limit States Design For Foundations. Part I. An overview of the foundation design process”. In: *Canadian Geotechnical Journal*.
- BEIS (2017). *Contracts for Difference Second Allocation Round Results*. Tech. rep. September, pp. 1–3. URL: [https://www.gov.uk/government/uploads/system/uploads/attachment%7B%5C\\_%7Ddata/file/643560/CFD%7B%5C\\_](https://www.gov.uk/government/uploads/system/uploads/attachment%7B%5C_%7Ddata/file/643560/CFD%7B%5C_)

- %7Dallocation%7B%5C\_%7Dround%7B%5C\_%7D2%7B%5C\_%7Doutcome%7B%5C\_%7DFINAL.pdf.
- Bierbooms, W. (1994). “Offshore wind and wave design conditions based on the NEXT database”. In: *World Wind Energy Conference*, pp. 1–4.
- Blanco, María Isabel (2009). “The economics of wind energy”. In: *Renewable and Sustainable Energy Reviews* 13.6-7, pp. 1372–1382. ISSN: 13640321. DOI: 10.1016/j.rser.2008.09.004.
- Bloomberg (2018). *Offshore Wind Farms Offer Subsidy-Free Power for First Time*. URL: <https://www.bloomberg.com/news/articles/2017-04-13/germany-gets-bids-for-first-subsidy-free-offshore-wind-farms> (visited on 03/29/2018).
- Bosch, Jonathan, Iain Staffell, and Adam D Hawkes (2018). “Temporally explicit and spatially resolved global offshore wind energy potentials”. In: *Energy*. ISSN: 0360-5442. DOI: 10.1016/j.energy.2018.08.153. URL: <https://doi.org/10.1016/j.energy.2018.08.153>.
- Bretschneider, C. L. (June 1952). “The generation and decay of wind waves in deep water”. In: *Transactions, American Geophysical Union* 33.3, p. 381. ISSN: 0002-8606. DOI: 10.1029/TR033i003p00381. URL: <http://doi.wiley.com/10.1029/TR033i003p00381>.
- British Standards Institution (2009). *BS EN 61400-3: Wind turbines — Part 3: Design requirements for offshore wind turbines*. Tech. rep. URL: [http://www.homepages.ucl.ac.uk/~%7B~%7Ducesaug/Fluids2/Wind%7B%5C\\_%7DTurbines/Codes%7B%5C\\_%7Dand%7B%5C\\_%7DManuals/BS%7B%5C\\_%7DEN%7B%5C\\_%7D61400-3%7B%5C\\_%7D2009.pdf](http://www.homepages.ucl.ac.uk/~%7B~%7Ducesaug/Fluids2/Wind%7B%5C_%7DTurbines/Codes%7B%5C_%7Dand%7B%5C_%7DManuals/BS%7B%5C_%7DEN%7B%5C_%7D61400-3%7B%5C_%7D2009.pdf).
- Brondsted, Povl and Rogier P. L. Nijssen (2013). *Advances in wind turbine blade design and materials*. Woodhead Publishing, p. 461. ISBN: 9780857097286.
- Buhl, M. L. (2009). *MCrunch Theory Manual for Version 1.00*. Tech. rep., NREL/TP-500-xxxxx. URL: [www.nrel.gov](http://www.nrel.gov).
- Burton, Tony, David Sharpe, and Nick Jenkins (2001). *Handbook of wind energy*. John Wiley & Sons.
- BVG Associates (2012). *Offshore wind cost reduction pathways - Technology work stream*. Tech. rep. URL: <http://www.thecrownstate.co.uk/media/305086/BVG%20WCRP%20technology%20work%20stream.pdf>.

- (2019). *A Guide to an Offshore Wind Farm*. Tech. rep. DOI: 10.1016/S0029-5493(00)00422-2. URL: [http://www.thecrownestate.co.uk/guide%7B%5C\\_%7Dto%7B%5C\\_%7Doffshore%7B%5C\\_%7Dwindfarm.pdf](http://www.thecrownestate.co.uk/guide%7B%5C_%7Dto%7B%5C_%7Doffshore%7B%5C_%7Dwindfarm.pdf).
- BVGassociates (2017). *The surprising results from the latest UK CfD auction*. URL: <https://bvgassociates.com/the-surprising-results-from-the-latest-uk-cfd-auctions/> (visited on 03/18/2018).
- BWEA, Garrad Hassan (2009). “Charting the Right Course: Scenarios for Offshore Capital Costs for the Next Five Years”. In: *British Wind Energy Association, London*.
- Byrne, B. and G. Houlsby (2003). “Foundations for offshore wind turbines.” In: *Philosophical transactions. Series A, Mathematical, physical, and engineering sciences* 361.2003, pp. 2909–30. ISSN: 1364-503X. DOI: 10.1098/rsta.2003.1286. URL: <http://www.ncbi.nlm.nih.gov/pubmed/14667305>.
- Camp, T. et al. (2004). *Design Methods for Offshore Wind Turbines at Exposed Sites Final*. Tech. rep. Garrad Hassan and Partners Ltd., p. 71. DOI: EUJouleIIIPROJECTJ0R3-CT98-0284.
- Cantú, Héctor Trevino (2011). “Life-Cycle Cost Analysis for Offshore Wind Farms: Reliability and Maintenance.” PhD thesis. Gotland University, p. 47. URL: [http://uu.diva-portal.org/smash/record.jsf?pid=diva2%7B%5C\\_%7D3A691609%7B%5C\\_%7Ddswid=-2036](http://uu.diva-portal.org/smash/record.jsf?pid=diva2%7B%5C_%7D3A691609%7B%5C_%7Ddswid=-2036).
- Carbon Trust (2008). *Offshore wind power : big challenge , big opportunity*. Tech. rep. Carbon Trust.
- Carroll, James, Alasdair McDonald, and David Mcmillan (2015). “Failure rate , repair time and unscheduled O & M cost analysis of offshore wind turbines”. In: *Wind Energy*. DOI: 10.1002/we.
- Carta, José A., Sergio Velázquez, and Pedro Cabrera (2013). “A review of measure-correlate-predict (MCP) methods used to estimate long-term wind characteristics at a target site”. In: *Renewable and Sustainable Energy Reviews* 27, pp. 362–400. ISSN: 13640321. DOI: 10.1016/j.rser.2013.07.004. URL: <http://dx.doi.org/10.1016/j.rser.2013.07.004>.
- Castro, Oscar Gerardo and Christian Oliver (2015). “Comparing Fatigue Life Estimations of Composite Wind”. In: *Proceedings of the 20th International Conference on Composite Materials*.

- Cavazzi, S. and A. G. Dutton (2016). “An Offshore Wind Energy Geographic Information System (OWE-GIS) for assessment of the UK’s offshore wind energy potential”. In: *Renewable Energy*. ISSN: 18790682. DOI: 10.1016/j.renene.2015.09.021. URL: <http://dx.doi.org/10.1016/j.renene.2015.09.021>.
- Chapman, Chris and Stephen Ward (1996). *Project risk management: processes, techniques and insights*. John Wiley.
- Collins, Jack (1993). *Failure of materials in mechanical design : analysis, prediction, prevention*. Wiley, p. 654. ISBN: 9780471558910. URL: <https://www.wiley.com/en-us/Failure+of+Materials+in+Mechanical+Design%7B%5C%7D3A+Analysis%7B%5C%7D2C+Prediction%7B%5C%7D2C+Prevention%7B%5C%7D2C+2nd+Edition-p-9780471558910>.
- Crabtree, C. J., D. Zappala, and S. I. Hogg (2015). “Wind energy: UK experiences and offshore operational challenges”. In: *Proceedings of the Institution of Mechanical Engineers, Part A: Journal of Power and Energy*. ISSN: 0957-6509. DOI: 10.1177/0957650915597560. URL: <http://pia.sagepub.com/lookup/doi/10.1177/0957650915597560>.
- Craik, Alex D.D. (2004). “The Origins of Water Wave Theory”. In: *Annual Review of Fluid Mechanics* 36.1, pp. 1–28. ISSN: 0066-4189. DOI: 10.1146/annurev.fluid.36.050802.122118. URL: <http://arjournals.annualreviews.org/doi/abs/10.1146%7B%5C%7D2Fannurev.fluid.36.050802.122118>.
- Crown Estate Scotland (2018). *New offshore wind leasing for Scotland*. Tech. rep.
- Dallyn, Paul et al. (2017). “Prediction of Wear in Grouted Connections for Offshore Wind Turbine Generators”. In: *Structures* 10, pp. 117–129. ISSN: 23520124. DOI: 10.1016/j.istruc.2017.02.001. URL: <http://dx.doi.org/10.1016/j.istruc.2017.02.001>.
- Damiani, Rick, K. Dykes, and G. Scott (2016). “A comparison study of offshore wind support structures with monopiles and jackets for U.S. waters”. In: *Journal of Physics: Conference Series*. ISSN: 17426596. DOI: 10.1088/1742-6596/753/9/092003.
- Damiani, Rick, Jason Jonkman, and G J Hayman (2015). *SubDyn User’s Guide and Theory Manual*. Tech. rep. March.
- Damiani, Rick et al. (2013). “Assessing the Importance of Nonlinearities in the Development of a Substructure Model for the Wind Turbine CAE Tool FAST”. In: *International Conference on Ocean, Offshore and Arctic Engineering*. March.

- Nantes. ISBN: 978-0-7918-5542-3. DOI: 10.1115/OMAE2013-11434. URL: [http://www.osti.gov/bridge?:%7B%5C%7D5Cnhttp://www.ntis.gov/help/ordermethods.aspx%7B%5C%7D5Cnhttp://www.scopus.com/inward/record.url?eid=2-s2.0-84893069932%7B%5C%7DpartnerID=40%7B%5C%7Dmd5=f5d4e49387abf94f389db8612da66420%7B%5C%7D5Cnhttp://proceedings.asmedigitalcollection.asme.org/proceeding.a](http://www.osti.gov/bridge/?%7B%5C%7D5Cnhttp://www.ntis.gov/help/ordermethods.aspx%7B%5C%7D5Cnhttp://www.scopus.com/inward/record.url?eid=2-s2.0-84893069932%7B%5C%7DpartnerID=40%7B%5C%7Dmd5=f5d4e49387abf94f389db8612da66420%7B%5C%7D5Cnhttp://proceedings.asmedigitalcollection.asme.org/proceeding.a).
- Davidson, John and C Hunsley (1994). “The Reliability of Mechanical Systems, Mech. Guides for the Process Industries”. In: *Mechanical Engineering Publications Limited for The Institution of Mechanical Engineers, London (1988.)*, ISBN: 0 8529.8881, p. 8.
- DECC (2009). *UK Offshore Energy Strategic Environmental Assessment*. Tech. rep.
- (2011). *UK Renewable Energy Roadmap*. Tech. rep. DOI: 10.1021/es00108a605. URL: <http://www.decc.gov.uk/en/content/cms/meeting%7B%5C%7Denergy/renewable%7B%5C%7Dener/re%7B%5C%7Droadmap/re%7B%5C%7Droadmap.aspx>.
- (2012). *Offshore Wind Cost Reduction Task Force Report*. Tech. rep. June.
- (2016). *UK Offshore Energy Strategic Environmental Assessment*. Tech. rep.
- Delorm, T. M., D. Zappala, and P. J. Tavner (2012). “Tidal stream device reliability comparison models”. In: *Proceedings of the Institution of Mechanical Engineers, Part O: Journal of Risk and Reliability* 226, pp. 6–17. ISSN: 1748-006X. DOI: 10.1177/1748006X11422620.
- Department for Business Energy & Industrial Strategy (2019). *Contracts for Difference Scheme for Renewable Electricity*. Tech. rep. January.
- Department of Defence (1991). *Military Handbook - Reliability prediction of electronic equipment*. Tech. rep.
- (2011). *Military Handbook - Reliability Growth Management*. Tech. rep.
- Department of Energy (2018). *IEA Research Study Extended To Improve Accuracy of Offshore Wind Systems Design Tools*. URL: <https://www.energy.gov/eere/wind/articles/iea-research-study-extended-improve-accuracy-offshore-wind-systems-design-tools%7B%5C%7Dvalidation%7B%5C%7Dprojects> (visited on 11/03/2018).
- Det Norske Veritas (2005). *DNV-RP-C203: Fatigue design of offshore steel structures*. Tech. rep.

- Det Norske Veritas (2010). *DNV-RP-C205: Environmental conditions and environmental loads*. Tech. rep. October, pp. 9–123. DOI: 10.1109/INTLEC.1993.388591.
- (2014). *DNV-OS-J101: Design of Offshore Wind Turbine Structures*. Tech. rep.
- Det Norske Veritas AS (2012). *DNV-OS-B101: Metallic Materials*. Tech. rep. October.
- (2014). *DNV-OS-C101: Design of Offshore Steel Structures , General ( LRFD Method )*. Tech. rep.
- Dinwoodie, I., F. Quail, and D. McMillan (2012). “Analysis of Offshore Wind Turbine Operation and Maintenance Using a Novel Time Domain Meteo-Ocean Modeling Approach”. In: *Proceedings of ASME Turbo Expo*, p. 847. DOI: 10.1115/gt2012-68985.
- DNV GL (2016a). *DNVGL-ST-0262: Lifetime extension of wind turbines*. Tech. rep.
- (2016b). *WIN WIN - WIND-powered Water INjection*. URL: <https://www.dnvgl.com/energy/feature-articles/win-win-wind-powered-water-injection.html> (visited on 05/24/2019).
- (2017). *Definitions of Availability Terms for the Wind Industry*. Tech. rep.
- DNV GL AS (2016a). *DNVGL-ST-0126: Support structures for wind turbines*. Tech. rep.
- (2016b). *DNVGL-ST-0437: Loads and site conditions for wind turbines*. Tech. rep. November.
- Downing, S. D. and D. F. Socie (1982). “Simple rainflow counting algorithms”. In: *International Journal of Fatigue* 4.1, pp. 31–40. ISSN: 01421123. DOI: 10.1016/0142-1123(82)90018-4.
- DTU Wind Energy (2018). *Danish research to strengthen the design of floating wind turbines*. URL: <https://www.vindenergi.dtu.dk/english/news/2018/10/danish-research-to-strengthen-the-design-of-floating-wind-turbines?id=23405be2-139c-4db2-9411-d1ab57949294> (visited on 05/24/2019).
- Dupont, Elise, Rembrandt Koppelaar, and Hervé Jeanmart (2018). “Global available wind energy with physical and energy return on investment constraints”. In: *Applied Energy*. ISSN: 0306-2619. DOI: 10.1016/j.apenergy.2017.09.085. URL: <https://doi.org/10.1016/j.apenergy.2017.09.085>.

- Ehrnberg, Daniel (2017). *Dynamic turbine system by SeaTwirl*.
- Emeis, Stefan and T Matthias (2007). “Comparison of Logarithmic Wind Profiles and Power Law Wind Profiles and their Applicability for Offshore Wind Profile”. In: *Wind energy*. ISBN: 9781909327078. DOI: 10.1007/978-3-540-33866-6.
- Energy Voice (2018). *UK seventh most attractive country for renewables*. URL: <https://www.energyvoice.com/otherenergy/170280/uk-seventh-most-attractive-country-for-renewables/> (visited on 06/24/2018).
- Ernst & Young (2017). *RECAI - The retail energy revolution*. Tech. rep. 50. URL: <https://emeia.ey-vx.com/4864/93958/landing-pages/recai-50-all-pages-interactive-dps-view.pdf>.
- European Commission (2017a). “Proposal for a directive of the European Parliament and of the council on the promotion of the use of energy from renewable sources (recast)”. In: *Official Journal of the European Union*. URL: [http://eur-lex.europa.eu/resource.html?uri=cellar:3eb9ae57-faa6-11e6-8a35-01aa75ed71a1.0007.02/D0C%7B%5C\\_%7D1%7B%5C%7Dformat=PDF%7B%5C%7D0Ahttp://eur-lex.europa.eu/legal-content/EN/TXT/?uri=CELEX:52016PC0767R%7B%5C%7D2801%7B%5C%7D29](http://eur-lex.europa.eu/resource.html?uri=cellar:3eb9ae57-faa6-11e6-8a35-01aa75ed71a1.0007.02/D0C%7B%5C_%7D1%7B%5C%7Dformat=PDF%7B%5C%7D0Ahttp://eur-lex.europa.eu/legal-content/EN/TXT/?uri=CELEX:52016PC0767R%7B%5C%7D2801%7B%5C%7D29).
- (2017b). *Third Report on the State of the Energy Union*. Tech. rep. URL: [https://ec.europa.eu/commission/sites/beta-political/files/third-report-state-energy-union%7B%5C\\_%7Den.pdf](https://ec.europa.eu/commission/sites/beta-political/files/third-report-state-energy-union%7B%5C_%7Den.pdf).
- European Environmental Agency (2009). *Europe’s onshore and offshore wind energy potential*. Tech. rep.
- European Parliament (2009). “Directive 2009/28/EC of the European Parliament and of the Council of 23 April 2009”. In: *Official Journal of the European Union* 140.16, pp. 16–62. ISSN: 02870827. DOI: 10.3000/17252555.L\_2009.140.eng. arXiv: 534.
- Evans, Simon (2017). *Analysis: UK auction reveals offshore wind cheaper than new gas*. URL: <https://www.carbonbrief.org/analysis-uk-auction-offshore-wind-cheaper-than-new-gas> (visited on 07/23/2018).
- Faulstich, S, P Lyding, and P J Tavner (2011). “Effects of Wind Speed on Wind Turbine Availability”. In: *Proceedings of European Wind Energy Conference & Exhibition 2011 (EWEC 2011)*.

- Faulstich, Stefan and Berthold Hahn (2009). *Comparison of different wind turbine concepts due to their effects on reliability*. Tech. rep.
- Faulstich, S et al. (2009). “Reliability of offshore turbines – identifying risks by onshore experience”. In: *Proceedings of European Offshore Wind*.
- Federal Maritime and Hydrographic Agency (2007). *Standard - Design of Offshore Wind Turbines*. Tech. rep.
- Feliciano, J. et al. (2018). “Generalized analytical displacement model for wind turbine towers under aerodynamic loading”. In: *Journal of Wind Engineering and Industrial Aerodynamics* 176.March, pp. 120–130. ISSN: 01676105. DOI: 10.1016/j.jweia.2018.03.018.
- Feng, Y., P.J. Tavner, and H. Long (2010). “Early experiences with UK Round 1 offshore wind farms.” In: *Proceedings of the Institution of Civil Engineers* November, pp. 167–181. ISSN: 1751-4223. DOI: 10.1680/ener.2010.163.4.167. URL: <http://dx.doi.org/10.1680/ener.2010.163.4.167>.
- Ferguson, M.C. and M. Kühn (1998). *Opti-OWECS Final Report Vol. 4: A Typical Design Solution for an OWECS*. ISBN: 9076468052.
- Finkelstein, Maxim (2008). *Failure rate modelling for reliability and risk*. Springer Science & Business Media.
- Fischer, T, W de Vries, and B Schmidt (2010). *Upwind Design Basis - WP4: Offshore Foundations and Support Structures*. Tech. rep., p. 139.
- Forristall, G. Z. (1978). “On the statistical distribution of wave heights in a storm”. In: *Journal of Geophysical Research* 83.C5. ISSN: 0148-0227. DOI: 10.1029/JC083iC05p02353.
- Fraunhofer Institute for Energy Economics and Energy System Technology (2018). *Wind Monitor*. URL: [http://windmonitor.iee.fraunhofer.de/windmonitor%7B%5C\\_%7Den/index.html](http://windmonitor.iee.fraunhofer.de/windmonitor%7B%5C_%7Den/index.html) (visited on 09/30/2018).
- Fraunhofer IWES (2013a). *Description of the Load Cases and Output Sensors to be Simulated in the OC4 Project under IEA Wind Annex 30*. Tech. rep.
- (2013b). *Wind Energy Report 2013*. Tech. rep.
- (2015). *Use of steel for towers of wind turbines and support structures Wingerde*. Tech. rep.
- Fugro GEOS (2001). *Wind and Wave Frequency Distributions for Sites around the British Isles*. Tech. rep. DOI: o1001303.
- Gandhi, Umesh (2010). *Investigation of anisotropy in elastic modulus of steel*.



- Gelaro, Ronald et al. (2017). “The modern-era retrospective analysis for research and applications, version 2 (MERRA-2)”. In: *Journal of Climate*.
- Gonzalez, Elena et al. (2017). “Key Performance Indicators for Wind Farm Operation and Maintenance”. In: *Energy Procedia* 137, pp. 559–570. ISSN: 18766102. DOI: 10.1016/j.egypro.2017.10.385.
- Haid, Lorenz et al. (2013). “Simulation-Length Requirements in the Loads Analysis of Offshore Floating Wind Turbines (Preprint)”. In: *Ocean Renewable Energy*. Vol. 8. June, V008T09A091. ISBN: 978-0-7918-5542-3. DOI: 10.1115/OMAE2013-11397. URL: <http://proceedings.asmedigitalcollection.asme.org/proceeding.aspx?articleid=1786780>.
- Hameed, Z., J. Vatn, and J. Heggset (2011). “Challenges in the reliability and maintainability data collection for offshore wind turbines”. In: *Renewable Energy* 36.8, pp. 2154–2165. ISSN: 09601481. DOI: 10.1016/j.renene.2011.01.008. URL: <http://dx.doi.org/10.1016/j.renene.2011.01.008>.
- Harman, Keir, Ross Walker, and Michael Wilkinson (2008). “Availability Trends Observed At Operational Wind Farms”. In: *European Wind Energy Conference*. Brussels. ISBN: 9781615671151 (ISBN).
- Harrabin, Roger (2017). *Offshore wind power cheaper than new nuclear - BBC News*. URL: <https://www.bbc.co.uk/news/business-41220948> (visited on 07/23/2018).
- Hart, E, M Keegan, and D McMillan (2016). “A lookup table approach to determining wind turbine operational fatigue loading from wind field measurements”. In: *ASRANet International Conference on Offshore Renewable Energy*.
- Hassan, Garrad (2003). *GH Bladed - Theory Manual*. Tech. rep. September.
- Hasselmann, K. et al. (1973). *Measurements of wind - wave growth and swell decay during the Joint North Sea Wave Project (JONSWAP)*. Tech. rep.
- Hau, Erich (2013). *Wind turbines: fundamentals, technologies, application, economics*. Third edit. Springer Science & Business Media.
- Haver, Sverre (2001). “Application of stochastic methods in structural design-The offshore experience”. In: *20th ASME Wind Energy Symposium*.
- Hayman, G J (2012). *MLife Theory Manual for Version 1.00*. Tech. rep. October, p. 12.
- Hayman, G.J. (2015). *MExtemes Manual Version 1.00*. Tech. rep. September.

- HBM Test and Measurement (2016). *Foundation monitoring – resistive versus fiber-optical strain gauge systems*. Tech. rep.
- Health and Safety Executive (2005). *Wave mapping in UK waters*. Tech. rep. PhysE Ltd. URL: <http://scholar.google.com/scholar?hl=en%7B%5C%7DbtnG=Search%7B%5C%7Dq=intitle:Wave+mapping+in+UK+waters%7B%5C%7D0>.
- Hearn, E. N. and L. Edgers (2010). “Finite Element Analysis of an Offshore Wind Turbine Monopile”. In: *GeoFlorida 2010: Advances in Analysis, Modeling & Design*, pp. 1857–1865. DOI: 10.1061/41095(365)188.
- Hermans, K W and J M Peeringa (2016). *Future XL monopile foundation design for a 10 MW wind turbine in deep water*. Tech. rep. December. ECN.
- Hill, Roger R et al. (2008). *Wind Turbine Reliability : A Database and Analysis Approach*. Tech. rep. February. Sandia National Laboratories, p. 60.
- HM Government (2010). *2050 Pathways Analysis*. Tech. rep. July, pp. 1–252. DOI: Ref:10D/764. arXiv: 764 [URN 10D].
- Holthuijsen, L. H. (2010). *Waves in oceanic and coastal waters*.
- Holthuijsen, L. H. et al. (2006). *User manual SWAN - Version 41.20*. Tech. rep., p. 137. URL: <http://iod.ucsd.edu/~%7B%7Dfalk/modeling/swanuse.pdf>.
- Hong Kong Offshore Wind Limited (2006). *Hong Kong Offshore Wind Farm in Southeastern Waters*. Tech. rep. April. URL: <http://www.epd.gov.hk/eia/register/profile/latest/esb146.pdf>.
- Infrastructure and Projects Authority (2017). *Analysis of the National Infrastructure and Construction Pipeline*. Tech. rep.
- International Electrotechnical Commission (2005). *IEC 61400-1: Wind turbines*. Tech. rep. 3rd edition. DOI: 10.5594/J09750.
- (2014). *IECRE OD-50: Project Certification Scheme*. Tech. rep., pp. 1–30.
- International Energy Agency (2005). *Wind Energy annual report*. June. ISBN: 0978638301.
- Ioannou, Anastasia, Andrew Angus, and Feargal Brennan (2018). “A lifecycle techno-economic model of offshore wind energy for different entry and exit instances”. In: *Applied Energy* 221.March, pp. 406–424. ISSN: 03062619. DOI: 10.1016/j.apenergy.2018.03.143. URL: <https://doi.org/10.1016/j.apenergy.2018.03.143>.

- Jacobsen, Vagner and Morten Rugbjerg (2005). “Offshore Wind Farms – the Need for Metocean Data”. In: *The Offshore Wind Energy Conference*. Copenhagen, pp. 1–13.
- Jamieson, P. and M. Branney (2014). “Structural considerations of a 20MW multi-rotor wind energy system”. In: *Journal of Physics: Conference Series* 555.1. ISSN: 17426596. DOI: 10.1088/1742-6596/555/1/012013.
- Johnston, G.O (1982). “A review of probabilistic fracture mechanics literature”. In: *Reliability Engineering* 3.6, pp. 423–448. ISSN: 01438174. DOI: 10.1016/0143-8174(82)90035-X.
- Jonkman, Bonnie J and Jason Jonkman (2016). *FAST v8.16.00a-bjj*. Tech. rep.
- Jonkman, Bonnie J and Levi Kilcher (2012). *TurbSim User’s Guide: Version 1.06.00*. Tech. rep.
- Jonkman, Bonnie and Marshall L Buhl (2006). *TurbSim User’s Guide*.
- Jonkman, Jason (2007). *Dynamics modeling and loads analysis of an offshore floating wind turbine*. Tech. rep. November.
- Jonkman, Jason M, Amy N Robertson, and Greg J Hayman (2015). *HydroDyn User’s Guide and Theory Manual*. Tech. rep. National Renewable Energy Laboratory.
- Jonkman, Jason and Marshall L Buhl (2005). *FAST User’s Guide*. Tech. rep. DOI: 10.2172/15020796. URL: <http://www.ncbi.nlm.nih.gov/pubmed/21564034>.
- Jonkman, Jason and W Musial (2010). *Offshore code comparison collaboration (OC3) for IEA task 23 offshore wind technology and deployment*. Tech. rep. DOI: NREL/TP-5000-48191.
- Jonkman, Jason et al. (2008). *Offshore Code Comparison Collaboration within IEA Wind Annex XXIII : Phase II Results Regarding Monopile Foundation Modeling*. Tech. rep. January, p. 15. DOI: NREL/CP-500-42471.
- Jonkman, J et al. (2009). *Definition of a 5-MW Reference Wind Turbine for Offshore System Development*. Tech. rep. February.
- Kaidis, Christos (2012). “Wind turbine reliability prediction - A SCADA processing and reliability estimation tool”. PhD thesis. ISBN: 9781619423299.
- Kaiser, Mark J and Brian Snyder (2011). *Offshore Wind Energy Installation and Decommissioning Cost Estimation in the U . S . Outer Continental Shelf Authors*. Tech. rep. Bureau of Ocean Energy Management, Regulation and Enforcement.

- Kaldellis, J. K. and M. Kapsali (2013). “Shifting towards offshore wind energy- Recent activity and future development”. In: *Energy Policy* 53, pp. 136–148. ISSN: 03014215. DOI: 10.1016/j.enpol.2012.10.032. URL: <http://dx.doi.org/10.1016/j.enpol.2012.10.032>.
- Kallehave, Dan et al. (2015). “Optimization of monopiles for offshore wind turbines”. In: *Philosophical Transactions of the Royal Society A: Mathematical, Physical and Engineering Sciences* 373.2035. ISSN: 1364503X. DOI: 10.1098/rsta.2014.0100.
- Kasinatha Pandian, P et al. (2010). “An overview of recent technologies on wave and current measurement in coastal and marine applications”. In: *Journal of Oceanography and Marine Science* 1.1, pp. 1–10. URL: <http://www.academicjournals.org/joms>.
- Khalid, F., P. R. Thies, and L. Johanning (2015). “Reliability assessment of tidal stream energy : significance for large-scale deployment in the UK”. In: *Proceedings of the 3rd International Conference on Renewable Energies Offshore (RENEW 2018)*. ISBN: 9781138626270.
- Kougioumtzoglou, Maria A. and Iraklis Lazakis (2015). “Developing a Risk Analysis and Decision Making Strategy for an Offshore Wind Farm”. In: *Ship Operations, Management and Economics (SOME)*.
- Kühn, M (2001). “Dynamics and design optimization of offshore wind conversion systems”. PhD thesis. Technische Universiteit Delft. ISBN: urn:isbn:90-76468-07-9.
- Kusiak, Andrew and Wenyan Li (2011). “The prediction and diagnosis of wind turbine faults”. In: *Renewable Energy* 36.1, pp. 16–23. ISSN: 09601481. DOI: 10.1016/j.renene.2010.05.014. URL: <http://dx.doi.org/10.1016/j.renene.2010.05.014>.
- L’Ecuyer, Pierre (1988). “Efficient and Portable Combined Random Number Generators”. In: *Communications of the ACM*.
- Lange, C H and S R Winterstein (1996). “Fatigue design of wind turbine blades: Load and resistance factors from limited data”. In: *American Society of Mechanical Engineers*.
- Lange, Michael, Michael Wilkinson, and Thomas Van Delft (2011). “Wind Turbine Reliability Analysis”. In: *German Wind energy Conference DEWEC*. Bremen,

- pp. 1–4. URL: [http://www.gl-garradhassan.com/assets/downloads/Wind%7B%5C\\_%7DTurbine%7B%5C\\_%7DReliability%7B%5C\\_%7DAnalysis.pdf](http://www.gl-garradhassan.com/assets/downloads/Wind%7B%5C_%7DTurbine%7B%5C_%7DReliability%7B%5C_%7DAnalysis.pdf).
- Lantz, Eric (2013). “Operations Expenditures : Historical Trends And Continuing Challenges”. In: *AWEA Wind Power Conference, Chicago*.
- Laura, Castro Santos and Diaz Casas Vicente (2014). “Life-cycle cost analysis of floating offshore wind farms”. In: *Renewable Energy* 66, pp. 41–48. ISSN: 09601481. DOI: 10.1016/j.renene.2013.12.002. URL: <http://dx.doi.org/10.1016/j.renene.2013.12.002>.
- Lazakis, Iraklis and Maria A. Kougioumtzoglou (2017). “Assessing offshore wind turbine reliability and availability”. In: *Proceedings of the Institution of Mechanical Engineers Part M: Journal of Engineering for the Maritime Environment* November 2017. ISSN: 20413084. DOI: 10.1177/1475090217735413.
- LEANWIND (2017). *Driving Cost Reductions in Offshore Wind*. Tech. rep. 614020. URL: <http://www.leanwind.eu/>.
- Levin, Mark A, Ted T Kalal, and Ed Kalal (2003). *Improving product reliability: strategies and implementation*. Vol. 1. John Wiley & Sons.
- Liu, Xiong et al. (Oct. 2017). “Effects of aerodynamic damping on the tower load of offshore horizontal axis wind turbines”. In: *Applied Energy* 204, pp. 1101–1114. ISSN: 0306-2619. DOI: 10.1016/J.APENERGY.2017.05.024. URL: <https://www.sciencedirect.com/science/article/pii/S0306261917305135>.
- Løken, Ingrid Bye (2009). “Dynamic Response of Offshore Wind Turbines”. In: *Wind Engineering* 17.5, pp. 238–246. URL: <file:///localhost/Users/jonlewis/Documents/Papers/1993/Wastling/Dynamic%20Response%20of%20offshore%20Wind.pdf>.
- Lombardi, Domenico (2010). “Dynamics of Offshore Wind Turbines”. PhD thesis. University of Bristol.
- Lu, Xi, Michael B Mcelroy, and Juha Kiviluoma (2009). “Global potential for wind-generated electricity”. In: *Proceedings of the National Academy of Sciences*.
- Lüscher, Martin (1994). “A portable high-quality random number generator for lattice field theory simulations”. In: *Computer Physics Communications* 79.1, pp. 100–110. ISSN: 00104655. DOI: 10.1016/0010-4655(94)90232-1. arXiv: 9309020 [hep-lat].
- Lynn, Paul A (2012). *Onshore and offshore wind energy: an introduction*. John Wiley & Sons.

- Madsen, Peter Hauge (2008). *Introduction to the IEC 61400-1 standard*. Tech. rep. National Laboratory for Sustainable Energy.
- Manuel, Lance, Paul S. Veers, and Steven R Winterstein (2001). “Parametric Models for Estimating Wind Turbine Fatigue Loads for Design”. In: *Journal of Solar Energy Engineering* 123. DOI: 10.1115/1.1409555.
- Mari, Author and Ellen Kerr (2018). “Effect of Government Policy on the Development of Renewable Generation in the UK”. PhD thesis. University of Strathclyde, pp. 1–106.
- Marijuán, Alberto R (2017). “Analysis of a solution for motion mitigation”. PhD thesis. KTH Royal Institute of Technology.
- Marsh, Gabriel et al. (2016). “Review and application of Rainflow residue processing techniques for accurate fatigue damage estimation”. In: *International Journal of Fatigue*, pp. 757–765. ISSN: 0142-1123. DOI: 10.1016/j.ijfatigue.2015.10.007. URL: <http://dx.doi.org/10.1016/j.ijfatigue.2015.10.007>.
- Martin, Rebecca et al. (2016). “Sensitivity analysis of offshore wind farm operation and maintenance cost and availability”. In: *Renewable Energy* January, pp. 1226–1236. ISSN: 18790682. DOI: 10.1016/j.renene.2015.07.078. URL: <http://dx.doi.org/10.1016/j.renene.2015.07.078>.
- Matha, D. et al. (2010). “Model Development and Loads Analysis of a Wind Turbine on a Floating Offshore Tension Leg Platform”. In: *European Offshore Wind Conference* February, pp. 1–10. URL: <http://www.nrel.gov/docs/fy10osti/46725.pdf>.
- McCrone, Angus et al. (2018). *Global trends in renewable energy investment 2018*. Tech. rep. Frankfurt School of Finance & Management gGmbH. URL: <http://fs-unep-centre.org/sites/default/files/publications/gtr2018v2.pdf>.
- Miner, M A (1945). “Cumulative Damage in Fatigue”. In: *Journal of Applied Mechanics*.
- Moriarty, P J, W E Holley, and S P Butterfield (2004). *Extrapolation of Extreme and Fatigue Loads Using Probabilistic Methods*. Tech. rep. November.
- Moubray, John (1997). *Reliability-centered maintenance*. Industrial Press Inc.
- Musial, Walter and Bonnie Ram (2010). *Large-Scale Offshore Wind Power in the United States: Assessment of Opportunities and Barriers*. Tech. rep. September.

- NREL (National Renewable Energy Laboratory). URL: [http://www.osti.gov/bridge:%7B%5C%7D5Cnhttp://www.ntis.gov/ordering.htm](http://www.osti.gov/bridge/%7B%5C%7D5Cnhttp://www.ntis.gov/ordering.htm).
- Musial, Walter et al. (2016). *Offshore Wind Energy Resource Assessment for the United States*. Tech. rep. National Renewable Energy Laboratory.
- Myhr, Anders et al. (2014). “Levelised cost of energy for offshore floating wind turbines in a life cycle perspective”. In: *Renewable Energy*, pp. 714–728. ISSN: 09601481. DOI: 10.1016/j.renene.2014.01.017. URL: <http://linkinghub.elsevier.com/retrieve/pii/S0960148114000469>.
- Nagababu, Garlapati et al. (2016). “Application of OSCAT satellite data for offshore wind power potential assessment of India”. In: *Energy Procedia*. ISSN: 1876-6102. DOI: 10.1016/j.egypro.2016.11.173. URL: <http://dx.doi.org/10.1016/j.egypro.2016.11.173>.
- Natarajan, Anand (2016). “Design load basis for offshore wind turbines”. PhD thesis. Technical University of Denmark. ISBN: 9788793278998.
- National Renewable Energy Laboratory (2018). *National Wind technology Center - Forum*. URL: <https://wind.nrel.gov/forum/wind/> (visited on 05/18/2018).
- Neill, Simon P. and M. Reza Hashemi (2013). “Wave power variability over the northwest European shelf seas”. In: *Applied Energy* 106, pp. 31–46. ISSN: 03062619. DOI: 10.1016/j.apenergy.2013.01.026. URL: <http://dx.doi.org/10.1016/j.apenergy.2013.01.026>.
- Niclas, Matti et al. (2017). “Influence of statistical uncertainty of component reliability estimations on offshore wind farm availability”. In: *Reliability Engineering and System Safety*. DOI: 10.1016/j.ress.2017.05.021.
- Nielsen, Per (2003). “Offshore wind energy projects, feasibility study guidelines”. In: *SEAWIND-Altener project-Feasibility Study Guidelines (EMD)*.
- NoordzeeWind (2010). *Operations Report 2009*. Tech. rep. November, pp. 1–32.
- NordzeeWind (2008). *Operations report 2007*. Tech. rep.
- OGP-IPIECA (2015). *OSR-JIP Review of Models and Metocean Databases*. Tech. rep., p. 75. URL: <http://oilspillresponseproject.org/sites/default/files/uploads/WP3%20and%20WP4%20REVIEW%20OF%20MODELS%20AND%20METOCEAN%20DATABASES.pdf>.
- Okulov, Valery L and Gijs A M Van Kuik (2012). “The Betz – Joukowsky limit : on the contribution to rotor aerodynamics by the British , German and Russian scientific schools ”. In: *Wind Energy*. DOI: 10.1002/we.

- Owens, Brian C., D. Todd Griffith, and John E. Hurtado (2014). “Modal Dynamics and Stability of Large Multi-megawatt Deepwater Offshore Vertical-axis Wind Turbines: Initial Support Structure and Rotor Design Impact Studies”. In: *32nd ASME Wind Energy Symposium*. January, pp. 1–21. DOI: 10.2514/6.2014-0518.
- Owens, Brian et al. (2013). “Aeroelastic Modeling of Large Off-shore Vertical-axis Wind Turbines: Development of the Offshore Wind Energy Simulation Toolkit”. In: *54th AIAA/ASME/ASCE/AHS/ASC structures, structural dynamics, and materials conference*, pp. 1–14. DOI: 10.2514/6.2013-1552.
- Palmgren, A (1924). “Die Lebensdauer von Kugellagern. Z. VDI 68”. In: *S339–S341*.
- Parliament of the United Kingdom (2004). *Energy Act 2004*.
- Passon, P. et al. (2007). “OC3 – Benchmark Exercise of Aero-Elastic Offshore Wind Turbine Codes (Preprint)”. In: *EAWC Special Topic Conference: The Science of Making Torque from Wind*.
- Peters, Valerie A, Alistair B Ogilvie, and Cody R Bond (2012). *Continuous Reliability Enhancement for Wind ( CREW ) Database : Wind Plant Reliability Benchmark*. Tech. rep. September. Sandia National Laboratories.
- Pettersson, Lasse, J-o Andersson, and Cecilia Orbert (2010). *RAMS-database for Wind Turbines*. Tech. rep. August. Elforsk.
- Pierson, Willard J and Lionel Moskowitz (1964). “A Proposed Spectral Form for Fully Developed Wind Seas Based on the Similarity Theory of S . A . Kitaigorodskii”. In: *Journal of Geophysical research* 69.24.
- Platt, Andy, Bonnie Jonkman, and Jason Jonkman (2016). *InflowWind User’s Guide*. Tech. rep.
- Polinder, H. et al. (2007). “10 MW wind turbine direct-drive generator design with pitch or active speed stall control”. In: *Proceedings of IEEE International Electric Machines and Drives Conference, IEMDC 2007 2*, pp. 1390–1395. DOI: 10.1109/IEMDC.2007.383632.
- Polinder, Henk et al. (2006). “Comparison of direct-drive and geared generator concepts for wind turbines”. In: *IEEE Transactions on Energy Conversion* 21.3, pp. 725–733. ISSN: 08858969. DOI: 10.1109/TEC.2006.875476.



- Ponterotto, J. G.. et al. (1995). “Determination of wind and wave design conditions based on the NEXT database”. In: *Offshore Wind Energy - Special Topic Conference*. Vol. 55. 6. Brussels, pp. 1016–1031.
- Rademakers, L.W.M.M et al. (2003). “Assessment and optimisation of operation and maintenance of offshore wind turbines”. In: *Proc. EWEC*, pp. 8–12. ISSN: 0046-9580. DOI: 10.5034/inquiryjrnl\_40.2.210.
- Ragan, Patrick and Lance Manuel (2007). “Comparing Estimates of Wind Turbine Fatigue Loads Using Time-Domain and Spectral Methods”. In: *Wind Engineering* 31.2, pp. 83–99. ISSN: 0309-524X. DOI: 10.1260/030952407781494494. URL: <http://journals.sagepub.com/doi/10.1260/030952407781494494>.
- Ramboll Group (2018). *150 Monopiles in the North Sea push offshore wind into deeper waters - Ramboll UK Limited*. URL: <http://www.ramboll.co.uk/projects/re/150-monopiles-in-the-north-sea-push-offshore-wind-into-deeper-waters> (visited on 05/28/2018).
- Rausand, Marvin and Arnljot Høyland (2003). *System Reliability Theory: Models, Statistical Methods, and Applications, 2nd Edition*, p. 664. ISBN: 047147133X. URL: <http://www.amazon.com/dp/047147133X>.
- ReliaSoft (2007). *Reliability, availability and Optimization*. Tech. rep.
- RenewableUK (2015). *Wind Energy Projects*. URL: <https://www.renewableuk.com/page/UKWEDSearch> (visited on 08/01/2015).
- (2018). *Wind Energy Statistics*. URL: <http://www.renewableuk.com/page/UKWEDhome> (visited on 05/16/2018).
- (2010). *State of the Industry Report - Onshore and offshore wind : a progress update*. Tech. rep.
- (2017). *Offshore Wind Project Timelines*. Tech. rep.
- RenewableUK and BVG Associates (2011). *Offshore Wind Forecasts of future costs and benefits*. Tech. rep.
- Rivkin, David A and Laurel Silk (2013). *Wind turbine systems*. Jones & Bartlett Publishers.
- Robertson, A et al. (2015). *OC5 Project Phase I : Validation of Hydrodynamic Loading on a Fixed Cylinder Preprint*. Tech. rep. April.
- Rubert, T., D. McMillan, and P. Niewczas (2018). “A decision support tool to assist with lifetime extension of wind turbines”. In: *Renewable Energy* 120,

- pp. 423–433. ISSN: 18790682. DOI: 10.1016/j.renene.2017.12.064. URL: <https://doi.org/10.1016/j.renene.2017.12.064>.
- Rychlik, Igor (1987). “A new definition of the rainflow cycle counting method”. In: *International journal of fatigue* 9.2, pp. 119–121.
- S. Faulstich, B. Hahn, P. Tavner (2010). “Wind turbine downtime and its importance for offshore deployment”. In: *Wind Energy* 17.July 2010, pp. 657–669. DOI: 10.1002/we. URL: <http://onlinelibrary.wiley.com/doi/10.1002/we.1608/full>.
- Sakagami et al. (2015). “Effects of turbulence, wind shear, wind veer, and atmospheric stability on power performance: a case study in Brazil”. In: *EWEA Annual Event*, pp. 1–6.
- Saltelli, Andrea et al. (2004). “Sensitivity analysis in practice: a guide to assessing scientific models”. In:
- Sandia National Laboratories (2013). *Definition of a 5MW/61.5m Wind Turbine Blade Reference Model*. Tech. rep. Sandia Report.
- Scaffarczyk, Alois (2014). *Understanding Wind Power Technology: Theory, Deployment and Optimisation*.
- Scott Semken, R. et al. (2012). “Direct-drive permanent magnet generators for high-power wind turbines: benefits and limiting factors”. In: *IET Renewable Power Generation* 6.1, p. 1. ISSN: 17521416. DOI: 10.1049/iet-rpg.2010.0191.
- Seebregts, A J, LWMM Rademakers, and B A Van Den Horn (1995). “Reliability analysis in wind turbine engineering”. In: *Microelectronics Reliability* 35.9-10, pp. 1285–1307.
- Seidel, Marc and Sebastian Kelma (2012). “Stochastic modelling of wind and wave induced loads on jacket piles”. In: *Stahlbau* 81.9, pp. 705–710. ISSN: 00389145. DOI: 10.1002/stab.201201599.
- Seyr, Helene and Michael Muskulus (2016). “Value of information of repair times for offshore wind farm maintenance planning”. In: *Journal of Physics: Conference Series*. ISSN: 17426596. DOI: 10.1088/1742-6596/753/9/092009.
- Shafiee, Mahmood, Feargal Brennan, and Inés Armada Espinosa (2016). “A parametric whole life cost model for offshore wind farms”. In: *The International Journal of Life Cycle Assessment*, pp. 961–975. ISSN: 0948-3349. DOI: 10.1007/

- s11367-016-1075-z. URL: <http://dx.doi.org/10.1007/s11367-016-1075-z>.
- Sharma, J N, R G Dean, et al. (1981). “Second-order directional seas and associated wave forces”. In: *Society of Petroleum Engineers Journal* 21.01, pp. 129–140.
- Simani, Silvio (2015). “Advanced issues of wind turbine modelling and control”. In: *Journal of Physics: Conference Series* 659.1. ISSN: 17426596. DOI: 10.1088/1742-6596/659/1/012001.
- SMart Wind Limited (2013). *Hornsea Offshore Wind Farm - Project One*. Tech. rep.
- Snyder, Brian and Mark J. Kaiser (2009). “Ecological and economic cost-benefit analysis of offshore wind energy”. In: *Renewable Energy* 34.6, pp. 1567–1578. ISSN: 09601481. DOI: 10.1016/j.renene.2008.11.015. URL: <http://dx.doi.org/10.1016/j.renene.2008.11.015>.
- SPARTA (2018). *2017/18 Portfolio Review*. Tech. rep.
- Spinato, F. et al. (2009). “Reliability of wind turbine subassemblies.” In: *IET Renewable Power Generation* 3.January 2008, pp. 387–401. ISSN: 17521416. DOI: 10.1049/iet-rpg.2008.0060. URL: <http://dx.doi.org/10.1049/iet-rpg.2008.0060>.
- Stehly, Tyler, Donna Heimiller, and George Scott (2016). *2016 Cost of Wind Energy Review*. Tech. rep. December. URL: <https://www.nrel.gov/docs/fy18osti/70363.pdf>.
- Stewart, G et al. (2013). “Assessing Fatigue and Ultimate Load Uncertainty in Floating Offshore Wind Turbines Due to Varying Simulation Length”. In: *11th International Conference on Structural Safety and Reliability* NREL/CP-5000-58518.
- Sutherland, J (1999). *On the Fatigue Analysis of Wind Turbines*. Tech. rep. Sandia National Laboratories.
- Tavner, P J et al. (2010). “Study of Effects of Weather & Location on Wind Turbine Failure Rates”. In: *Ewec 2010* Ewec.
- Tavner, Peter (2012). *Offshore wind turbines: reliability, availability and maintenance*. The Institution of Engineering and Technology.
- Tavner, Peter, Jiangping Xiang, and Fabio Spinato (Jan. 2007). “Reliability analysis for wind turbines”. In: *Wind Energy* 10.1, pp. 1–18. ISSN: 10954244. DOI: 10.1002/we.204. URL: <http://doi.wiley.com/10.1002/we.204>.

- Tavner, Peter et al. (2011). “The Correlation Between Wind Turbine Turbulence and Pitch Failure”. In: *European Wind Energy Conference*, pp. 2–6.
- Tempel, Jan Van der (2006). *Design of Support Structures for Offshore Wind Turbines*. ISBN: 9076468117.
- The Crown Estate (2017). *OWE map and GIS data*. URL: <http://www.thecrownestate.co.uk/energy-and-infrastructure/downloads/maps-and-gis-data/%7B%5C%7D0A> (visited on 05/05/2017).
- (2012). *Offshore Wind Cost Reduction Pathways Study*. Tech. rep.
- (2014). *Energy and infrastructure outlook 2014-15 - Offshore wind*. Tech. rep.
- (2015). *SPARTA : The performance data exchange platform for offshore wind*. Tech. rep.
- (2018a). *Interim regions refinement report*. Tech. rep.
- (2018b). *Offshore Wind Constraints Analysis and Characterisation Review*. Tech. rep.
- (2018c). *Resource and Constraints Assessment for Offshore Wind - Interim Regions Refinement Report*. Tech. rep.
- (2019). *Offshore wind operational report 2018*. Tech. rep. December.
- The Renewables Consulting Group (2018). *Global Renewable Infrastructure Project (GRIP) database*. URL: <https://grip.thinkrcg.com/> (visited on 05/26/2018).
- The Royal Society for the Protection of Birds (2010). *Offshore wind farms and birds : Round 3 zones , extensions to £ Scottish Territorial Waters*. ISBN: 9781905601257.
- Thies, P R, J Flinn, and G H Smith (2009). “Is it a showstopper ? Reliability assessment and criticality analysis for Wave Energy Converters”. In:
- Thies, Philipp (2012). “Advancing reliability information for Wave Energy Converters”. PhD thesis.
- Torsethaugen, Knut, Turid Faanes, and Sverre Haver (1985). *Characteristics for extreme sea states on the Norwegian continental shelf*. Tech. rep.
- Trøen, Tine Louise (2014). “Fatigue Loads on Large Diameter Monopile Foundations of Offshore Wind Turbines in Shallow Water”. PhD thesis.
- Turner, Rodney (2012). *Handbook of project-based management*. McGraw-Hill Publishers.
- UK Department of Energy and Climate Change (2013). *A Comparison of Emissions Factors for Electricity Generation*. Tech. rep.

- UK Energy Research Centre (2010). *Great Expectations: The cost of offshore wind in UK waters – understanding the past and projecting the future*. Tech. rep. DOI: 10.1586/erm.10.83. URL: <http://www.ncbi.nlm.nih.gov/pubmed/20964599>.
- UK Green Investment Bank (2018). *Offshore wind fund*. URL: <http://greeninvestmentgroup.com/funds/offshore-wind-fund/> (visited on 05/17/2018).
- UK Hydrographic Office (2015). *UK, UK Overseas Territories and UK Crown Dependencies Maritime Limits and Law of the Sea*. URL: <https://www.gov.uk/guidance/uk-maritime-limits-and-law-of-the-sea%7B%5C#%7Dhistory> (visited on 07/11/2017).
- UKNDA (2016). *Protection of the UK 's EEZ and Territorial Seas : Does the Government care ?* Tech. rep.
- UNFCCC (2015). “Paris Agreement”. In: *Conference of the Parties on its twenty-first session* December, p. 32. ISSN: 1098-6596. DOI: FCCC/CP/2015/L.9/Rev.1. arXiv: arXiv:1011.1669v3. URL: <http://unfccc.int/resource/docs/2015/cop21/eng/109r01.pdf>.
- United Kingdom Met Office (1927). *Marine Observer's Handbook*. Tech. rep. Fourth Edition.
- United Nations (2001). *United Nations Convention on the Law of the Sea*. Tech. rep. DOI: 10.1093/acprof:oso/9780199299614.003.0002. arXiv: arXiv:1011.1669v3.
- Veers, Paul S (1988). “Simplified fatigue damage and crack growth calculations for wind turbines”. In: *ASME, Gas Turbine and Aeroengine Congress and Exposition*.
- Veers, Paul S and Sandy Butterfield (2001). “Extreme Load Estimation for Wind Turbines : Issues and Opportunities for Improved Practice”. In: *20th ASME Wind Energy Symposium*.
- Veldkamp, Herman Frederik (2006). *Chances in Wind Energy - A probabilistic Approach to Wind Turbine Fatigue Design*. ISBN: 9789076468129.
- Verbruggen, T W (2003). “Wind Turbine Operation & Maintenance based on Condition Monitoring WT- Final report”. In: *Wind Turbine Operation and Maintenance based on Condition Monitoring (WT\_OMEGA) Project Report* April.

- Veritas, Det Norske (2010). *DNV-RP-C205: Environmental conditions and environmental loads*. Tech. rep.
- WAF0 Group (2000). *WAF0-A MATLAB toolbox for analysis of random waves and loads*. Tech. rep.
- Wilkinson, Michael and Garrad Hassan & Partners Ltd (2009). “Reliawind Field Study”. In: *Wind Turbine Reliability Workshop*. Albuquerque, New Mexico.
- Wilkinson, Michael et al. (2010). “Methodology and Results of the Reliawind Reliability Field Study”. In: *European Wind Energy Conference ( EWEC 2010 )*. Ewec, p. 7. ISBN: 9781617823107.
- Wilkinson, Michael et al. (2011). “Measuring wind turbine reliability, results of the reliawind project”. In: *European Wind Energy Association Conference*, pp. 1–8.
- Willsted, Edward A et al. (2017). “Obligations and aspirations: A critical evaluation of offshore wind farm cumulative impact assessments”. In: *Renewable and Sustainable Energy Reviews* 82.September, pp. 2332–2345. ISSN: 1364-0321. DOI: 10.1016/j.rser.2017.08.079. URL: <https://doi.org/10.1016/j.rser.2017.08.079>.
- Wilson, Graeme and David McMillan (2014). “Quantifying the impact of wind speed on wind turbine component failure rates”. In: *European Wind Energy Association 2014 Annual Conference*.
- WindEurope Business Intelligence (2018). *Wind in power 2017 - Annual combined onshore and offshore wind energy statistics*. Tech. rep.
- (2019). *Offshore Wind in Europe - Key trends and statistics 2018*. Tech. rep.
- Yeter, B., Y. Garbatov, and C. Guedes Soares (2014). “Spectral fatigue assessment of an offshore wind turbine structure under wave and wind loading”. In: *Developments in Maritime Transportation and Exploitation of Sea Resources - Proceedings of IMAM 2013, 15th International Congress of the International Maritime Association of the Mediterranean* 1.September, pp. 425–433. DOI: 10.1201/b15813-52.
- Zhu, Pengcheng et al. (2011). “Offshore wind converter reliability evaluation”. In: *8th International Conference on Power Electronics - ECCE Asia: "Green World with Power Electronics", ICPE 2011-ECCE Asia*, pp. 966–971. ISSN: 2150-6078. DOI: 10.1109/ICPE.2011.5944655.

- Ziegler, Lisa (2016). “Fatigue reassessment for lifetime extension of offshore wind monopile substructures”. In: *Journal of Physics: Conference Series* November. DOI: 10.1088/1742-6596/753/9/092010.
- (2018). “Assessment of monopiles for lifetime extension of offshore wind turbines”. PhD thesis. Norwegian University of Science and Technology. ISBN: 9788232632084.
- Ziegler, Lisa et al. (2015). *Sensitivity of wave fatigue loads on offshore wind turbines under varying site conditions*. Vol. 80. Elsevier B.V., pp. 193–200. ISBN: 0378-3839. DOI: 10.1016/j.egypro.2015.11.422. URL: <http://dx.doi.org/10.1016/j.egypro.2015.11.422>.
- Ziegler, Lisa et al. (2017). “Structural monitoring for lifetime extension of offshore wind monopiles: Can strain measurements at one level tell us everything?” In: *Wind Energy Science Discussions*, pp. 1–9. ISSN: 2366-7621. DOI: 10.5194/wes-2017-21. URL: <https://www.wind-energ-sci-discuss.net/wes-2017-21/>.
- Zwick, Daniel (2015). “Simulation and Optimization in Offshore Wind Turbine Structural Analysis”. PhD thesis. ISBN: 9788232608164.





# Appendix A

## Publications

### A.1 Conference publications

Khalid, F., P. R. Thies, and L. Johanning (2015). “Reliability assessment of tidal stream energy : significance for large-scale deployment in the UK”. In: *Proceedings of the 3rd International Conference on Renewable Energies Offshore (RENEW 2018)*. ISBN: 9781138626270.

### A.2 Journal publications

Rinaldi, G. et al. (2018). “Multivariate analysis of the reliability, availability, and maintainability characterizations of a Spar–Buoy wave energy converter farm”. In: *Journal of Ocean Engineering and Marine Energy* 4.3, pp. 199–215. ISSN: 2198-6444. DOI: 10.1007/s40722-018-0116-z. URL: <https://doi.org/10.1007/s40722-018-0116-z>.

# Appendix B

## DLCs

Table B.1: Recommended design load cases for fatigue calculation (British Standards Institution, 2009).

Design situation	DLC	Environmental parameter	Parameter Description
Power production	1.2	1	NTM $V_{in} < V_{hub} < V_{out}$
		2	NSS Joint probability distribution of $H_s$ , $T_p$ , $V_{hub}$
		3	COD, MUL
		4	No currents
		5	NWLR or $\geq$ MSL
Power production plus occurrence of fault	2.4	1	NTM $V_{in} < V_{hub} < V_{out}$
		2	NSS $H_s = E[H_s V_{hub}]$
		3	COD, UNI
		4	No currents
		5	NWLR or $\geq$ MSL
Start up	3.1	1	NTM $V_{in} < V_{hub} < V_{out}$
		2	NSS $H_s = E[H_s V_{hub}]$
		3	COD, UNI
		4	No currents

Table B.1: Recommended design load cases for fatigue calculation (British Standards Institution, 2009).

Design situation	DLC	Environmental parameter	Parameter Description
		5	NWLR or $\geq$ MSL
Normal shut down	4.1	1	NTM $V_{in} < V_{hub} < V_{out}$
		2	NSS $H_s = E[H_s V_{hub}]$
		3	COD, UNI
		4	No currents
		5	NWLR or $\geq$ MSL
Parked (standing still or idling)	6.4	1	NTM $V_{hub} < 0.7V_{ref}$
		2	NSS Joint probability distribution of $H_s$ , $T_p$ , $V_{hub}$
		3	COD, MUL
		4	No currents
		5	NWLR or $\geq$ MSL
Parked and fault conditions	7.2	1	NTM $V_{hub} < 0.7V_1$
		2	NSS Joint probability distribution of $H_s$ , $T_p$ , $V_{hub}$
		3	COD, MUL
		4	No currents
		5	NWLR or $\geq$ MSL
Transport, assembly, maintenance and repair	8.3	1	NTM $V_{hub} < 0.7V_{ref}$
		2	NSS Joint probability distribution of $H_s$ , $T_p$ , $V_{hub}$
		3	COD, MUL
		4	No currents
		5	NWLR or $\geq$ MSL

## Appendix B. DLCs

---

Table B.1: Recommended design load cases for fatigue calculation (British Standards Institution, 2009).

---

Design situation	DLC	Environmental Parameter Description parameter
------------------	-----	--

---

1 = Wind conditions, 2 = Wave conditions, 3 = Wind and wave directionality, 4 = Sea currents, 5 = Water Level

COD = Co-directional, MUL = Multi-directional, NSS = Normal sea state, NTM = Normal turbulence model, NWLR = Normal water level range, UNI = Uni-directional

# Appendix C

## OWT repair times and cost

Table C.1: OWT assembly repair times categorised into subsystems with sub-categorisation based on associated material costs (Carroll et al., 2015).

Assembly	Repair times [hours]			
	Replacement	Major repair	Minor repair	No cost data
Rotor module				
Blades	288	21	9	28
Pitch/Hydraulics	25	19	9	17
Hub	298	40	10	8
Nacelle				
Yaw system	49	20	5	9
Control module				
Controls	12	14	8	17
Sensors	0	6	8	8
Drivetrain Module				
Gearbox	231	22	8	7
Generator	81	24	7	13
Power Module				
Electrical components	18	14	5	7
Contactors/ breaker	Relay/Circuit 150	19	4	5
Power supply/ Transformer	Converter 1	14	7	10
		26	7	19

## Appendix C. OWT repair times and cost

Auxiliary System				
Grease/Oil/Cooling liquid	0	18	4	3
Pumps/Motors	0	10	4	7
Safety	0	7	2	2
Heaters/Coolers	0	14	5	5
Service items	0	10	7	9
Other components	36	21	5	8
Structure				
Tower/Foundation	0	2	5	6

Table C.2: OWT assembly material costs for repair categorised into major replacement, major and minor repairs (Carroll et al., 2015).

Assembly	Repair Cost [€]		
	Replacement [ $\times 10^3$ ]	Major repair [ $\times 10^3$ ]	Minor repair [ $\times 10^2$ ]
Rotor module			
Blades	901.5	1.7	
Pitch/Hydraulics	14	1.9	2.1
Hub	95	1.5	1.6
Nacelle			
Yaw system	12.5	3	1.4
Control module			
Controls	13	2	2
Sensors	0	2.5	1.5
Power Module			
Gearbox	230	2.5	1.25
Generator	603.5	1.6	
Power Module			
Electrical components	12	2	1
Contactors/ Relay/Circuit breaker	13.5	2.3	2.6
Power supply/ Converter	13	5.3	2.4
Transformer	70	2.3	1
Auxiliary System			

---

Grease/Oil/Cooling liquid	0	2	1.6
Pumps/Motors	0	2	3.3
Safety	0	2.4	1.3
Heaters/Coolers	0	1.3	4.7
Service items	0	1.2	0.8
Other components	10	2.4	1.1
Structure			
Tower/Foundation	0	1.1	1.4

---

# Appendix D

## Variables of interest

Table D.1: Considered output parameters from the FAST simulation for fatigue calculation of structural subsystems.

Parameter	Units	Description
InflowWind		
Wind $\beta$ VelX	m/s	Wind velocity in the inertial horizontal Xi-, Yi-axes and the vertical Zi-axis at $\beta = (0,0,90)$ .
Wind $\beta$ VelY		
Wind $\beta$ VelZ		
AeroDyn		
BaN $\beta$ Vrel	m/s	Relative wind speed at Node $\beta$ of Blade $\alpha$ , for $\alpha = 1$ and $\beta = (1-5)$ .
BaN $\beta$ Fx	N/m	Normal and tangential forces (to plane) per unit length at Node $\beta$ of Blade $\alpha$ , for $\alpha = 1$ and $\beta = (1-5)$ .
BaN $\beta$ Fy		
TwN $\beta$ Vrel	m/s	Relative wind speed at tower Node $\beta$ , for $\beta = (1-5)$ .
TwN $\beta$ Fdx	N/m	x- and y-component of drag forces per unit length at tower Node $\beta$ , for $\beta = (1-5)$ in the local tower coordinate system.
TwN $\beta$ Fdy		
HydroDyn		
Wave1Elev	m	Total (first- plus second-order) wave elevations at the coordinates still water level (SWL).
Wave1Elv1	m	First order wave elevation at the coordinates still water level.
Wave1Elv2	m	Second order wave elevation at the coordinates still water level.
HydroFxi	N	Total integrated hydrodynamic loads from both potential flow and strip theory at the WAMIT Reference Point in the inertial frame coordinate system.
HydroFyi		
HydroFzi		
ElastoDyn		



TwHt $\beta$ FLxt TwHt $\beta$ FLyt TwHt $\beta$ FLzt	kN	Local tower roll (fore-aft), pitch (side-to-side) and yaw (torsional) forces at tower gauge $\beta$ for $\beta = (1-5)$ in the tower base coordinate system.
TwHt $\beta$ MLxt TwHt $\beta$ MLyt TwHt $\beta$ MLzt	kN.m	Local tower roll (side-to-side), pitch (fore-aft) and yaw (torsional) moments at tower gauge $\beta$ for $\beta = (1-5)$ in the tower base coordinate system.
Spn $\beta$ MLx $\beta\alpha$ Spn $\beta$ MLy $\beta\alpha$ Spn $\beta$ MLz $\beta\alpha$	kN.m	Local edgewise, flapwise and pitching moments at span station $\beta$ for blade $\alpha$ for $\alpha=1$ and $\beta = (1-5)$ in the blade coordinate system.
Spn $\beta$ FLx $\beta\alpha$ Spn $\beta$ FLy $\beta\alpha$ Spn $\beta$ FLz $\beta\alpha$	kN	Local flapwise, edgewise and axial shear force at span station $\beta$ for blade $\alpha$ for $\alpha=1$ and $\beta = (1-5)$ in the blade coordinate system.
RootFx $\alpha$ RootFy $\alpha$ RootFz $\alpha$	kN	Out-of-plane, in-plane shear and axial forces at the blade root in the coned coordinate system for $\alpha = 1$ .
RootMx $\alpha$ RootMy $\alpha$ RootMz $\alpha$	kN.m	In-plane, out-of-plane and pitching bending moment at the blade root in the coned coordinate system for $\alpha = 1$ .
YawBrFxp YawBrFyp YawBrFzp	kN	Non-rotating tower-top/yaw bearing fore-aft and side-to-side shear forces and axial force defined in the tower-top/base-plate coordinate system.
YawBrMxp YawBrMyp YawBrMzp	kN.m	Non-rotating tower-top/yaw bearing roll, pitch and yaw moments defined in the tower-top/base-plate coordinate system.
RtAeroF $\beta$ xh RtAeroF $\beta$ yh RtAeroF $\beta$ zh	N	Total rotor aerodynamic forces in x-, y- and z-direction in the hub coordinate system.
RtAeroM $\beta$ xh RtAeroM $\beta$ yh RtAeroM $\beta$ zh	N.m	Total rotor aerodynamic moment in x-, y- and z-direction in the hub coordinate system.
SubDyn		
ReactFXss ReactFYss ReactFZss	N	Total base reaction forces at the mudline (0,0, -Water Depth) location in the global inertial- frame coordinate system.
ReactMXss ReactMYss ReactMZss	Nm	Total base reaction moments at the mudline (0,0, -Water Depth) location in the global inertial- frame coordinate system.
IntfFXss IntfFYss	N	Total interface reaction forces at the transition piece reference point (platform reference point) location in the global inertial- frame coordinate system.

## Appendix D. Variables of interest

---

IntfZss		
IntfMXss	Nm	Total interface reaction moments at the transition piece reference point (platform reference point) location in the global inertial- frame coordinate system.
IntfMYss		
IntfMZss		

---

# Appendix E

## Damage Sensitivity to Wind and Wave Seeds

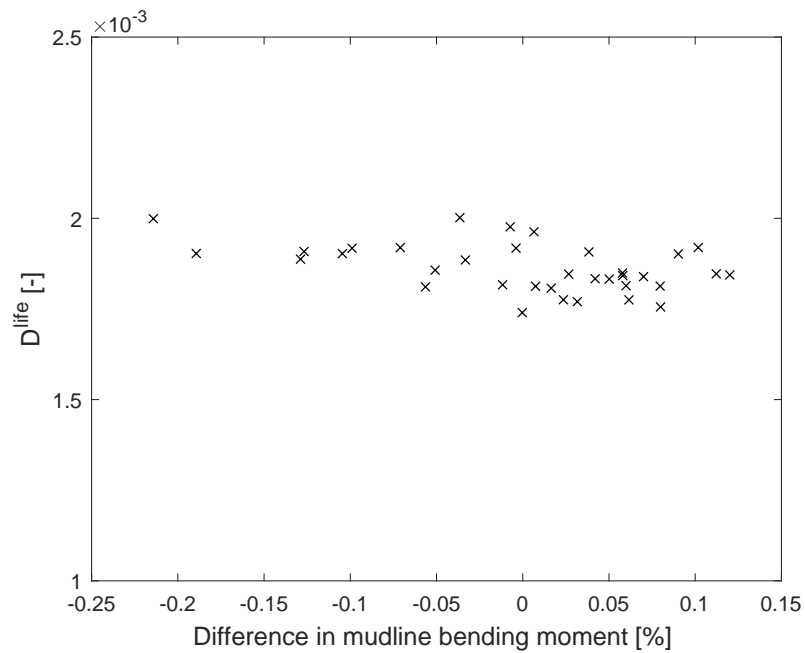


Figure E.1: Comparison between the influence of the choice of wind seed on the percentage difference from the mean of the bending moment of 36 seeds and associated fatigue damage for LLC01.

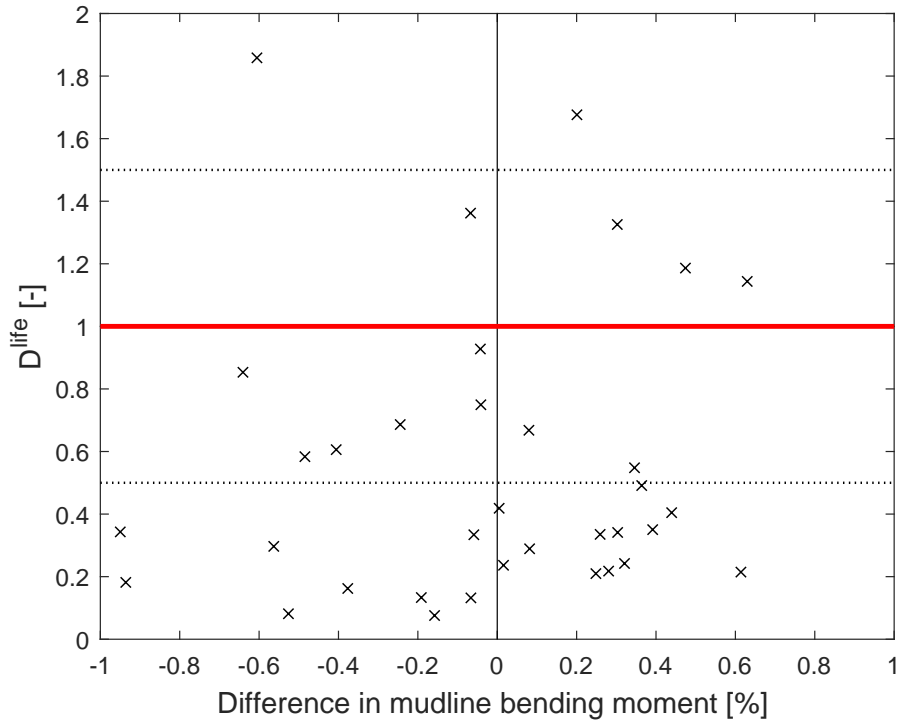


Figure E.2: Comparison between the influence of the choice of wave seed on the percentage difference from the mean of the bending moment of 36 seeds and associated fatigue damage for LLC01.

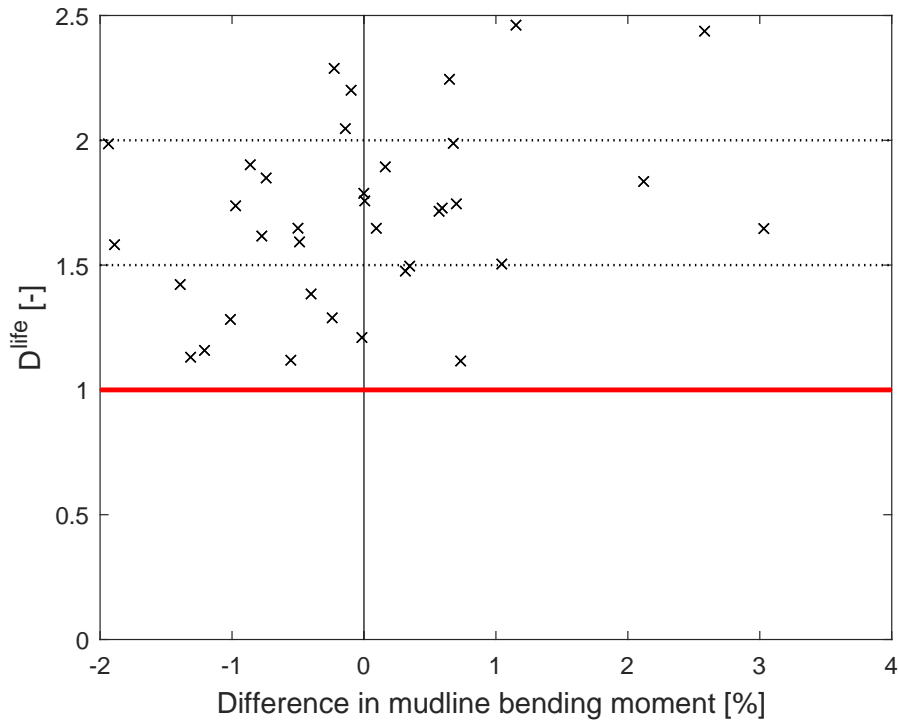


Figure E.3: Comparison between the influence of the choice of wind seed on the percentage difference from the mean of the bending moment of 36 seeds and associated fatigue damage for LLC01.

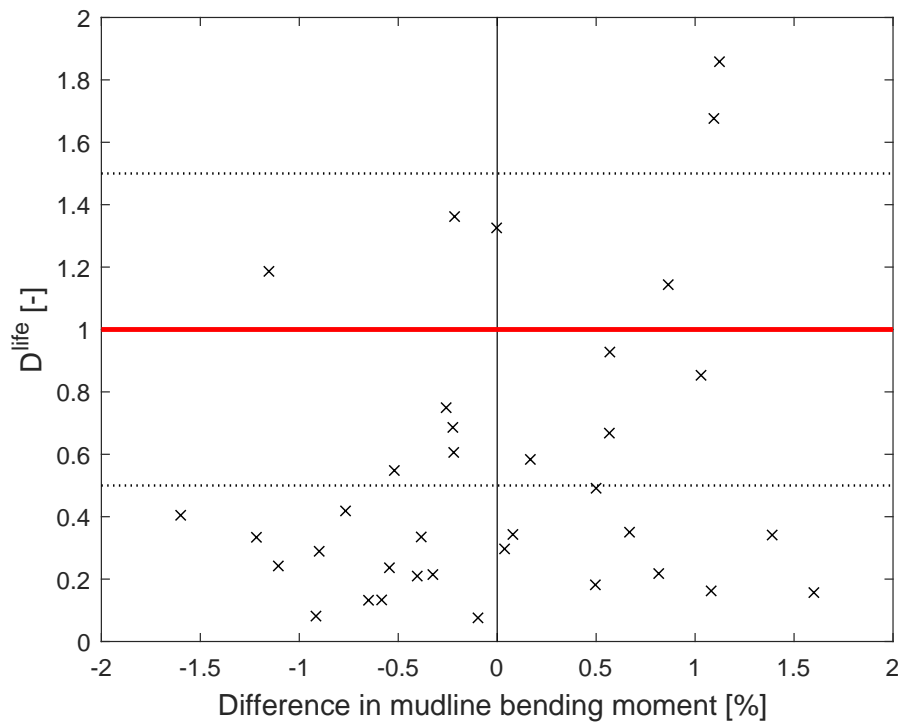


Figure E.4: Comparison between the influence of the choice of wave seed on the percentage difference from the mean of the bending moment of 36 seeds and associated fatigue damage for LLC07.

# Appendix F

## Sensitivity of sub-regional damage

Table F.1: Details of MLife input parameters for which the fatigue analysis is performed at the NEXT GPs.

Parameter	Units	Best-case scenario	Mean-scenario	Worst-case scenario
$m$	-	5	4	3
$ULF$	-	20	5	1.25
$DesLife$	years	5	15	30

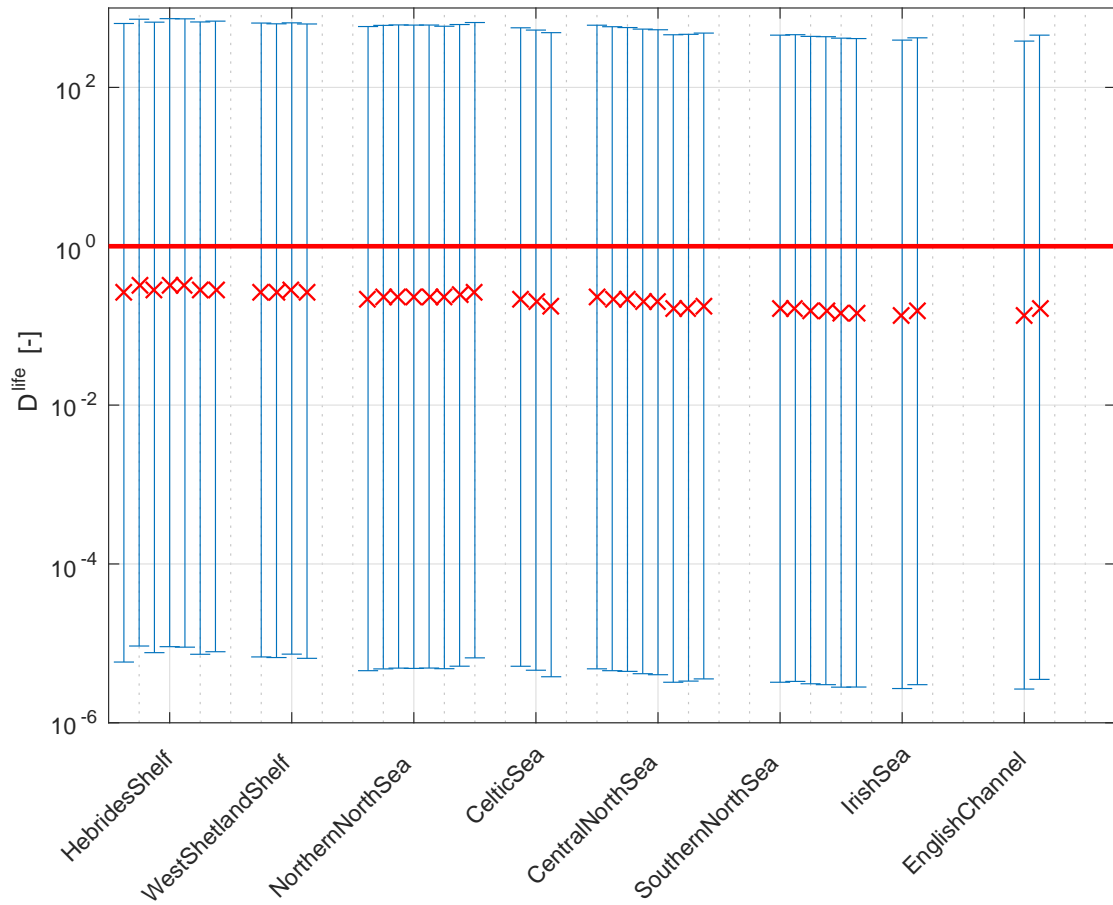


Figure F.1: Comparison of the best-, worst- and mean-case scenario using fatigue-influencing variable inputs from F.1 for all NEXT GPs.

# Appendix G

$K^{DP}$  residuals



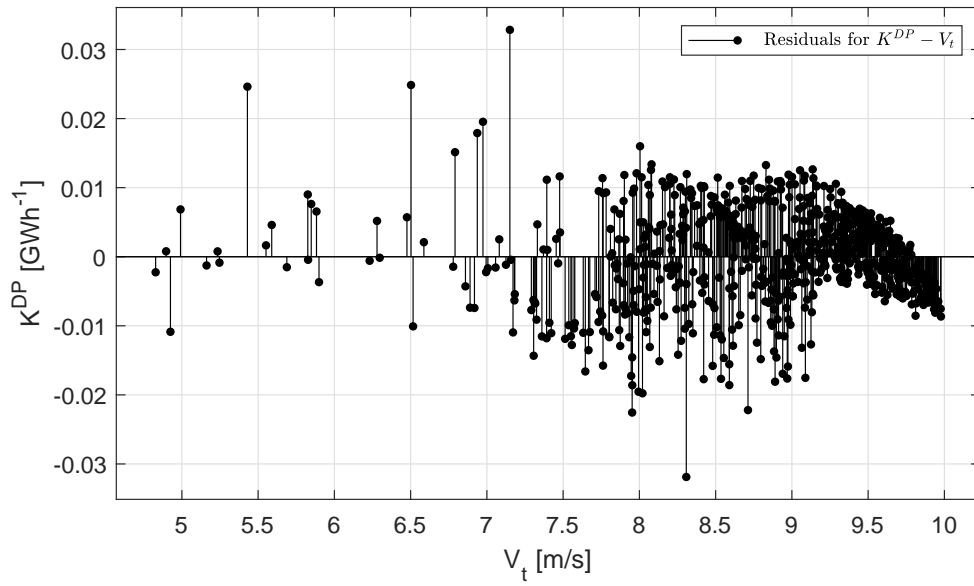


Figure G.1: Residuals for the  $K^{DP} - V_t$  model fit.

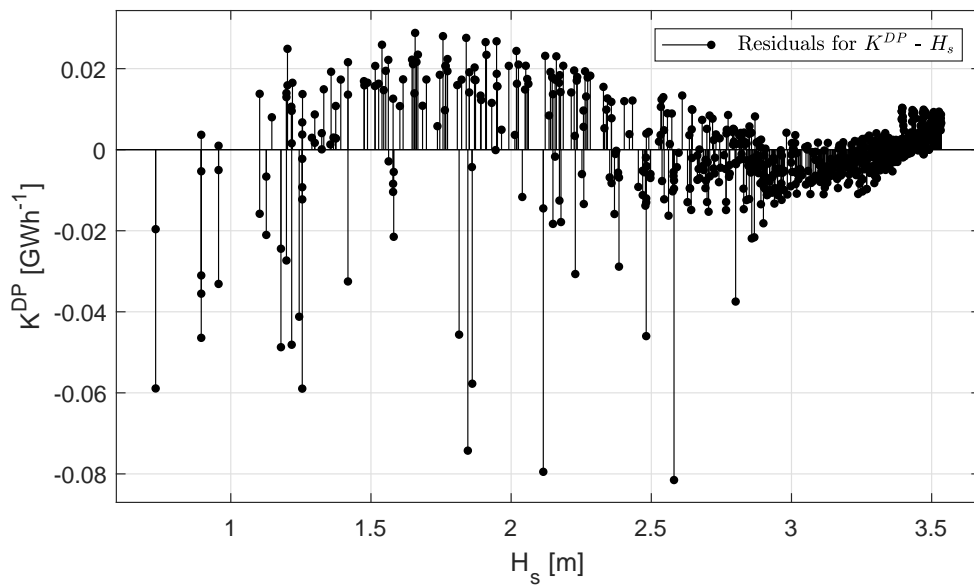


Figure G.2: Residuals for the  $K^{DP} - H_s$  model fit.